Impacts of Hydromodification and Sediment Supply Alterations on Bedload Transport and Bed Morphology in Urbanizing Gravel-bed Rivers

by

Benjamin Douglas Plumb

A thesis
presented to the University of Waterloo
in fulfillment of the
thesis requirement for the degree of
Doctor of Philosophy
in
Civil Engineering

Waterloo, Ontario, Canada, 2017

Examining Committee Membership

The following served on the Examining Committee for this thesis. The decision of the Examining Committee is by majority vote.

External Examiner	Colin Rennie Professor
Supervisor(s)	William K. Annable Associate Professor
Internal Member	Don Burn Professor
Internal Member	Bruce MacVicar Associate Professor
Internal-external Member	Mike Stone Professor

Author's Declaration

This thesis consists of material all of which I authored or co-authored: see Statement of Contributions included in the thesis. This is a true copy of the thesis, including any required final revisions, as accepted by my examiners.

I understand that my thesis may be made electronically available to the public.

Statement of Contributions

Chapter 3 was prepared in collaboration with Peter Thompson of EarthFX Inc. and Dr. Marwan Hassan of the Department of Geography, University of British Columbia. Peter assisted by modifying computer code to extract and process hydrometric gauge data. Dr. Hassan provided guidance on analysis methods and manuscript revisions. Their inputs were paramount in analyzing and synthesizing the data and results presented in this chapter.

Chapter 4 was prepared in collaboration with Chris McKie of the Department of Civil & Environmental Engineering, University of Waterloo, Dr. Mário Franca and Dr. Carmelo Juez, both of the Laboratory of Hydraulic Constructions at École polytechnique fédérale de Lausanne (EPFL). Dr. Franca and Dr. Juez provided fundamental guidance on experimental design and assisted in interpreting results and manuscript revisions. Chris assisted in completing laboratory experiments after I sustained a serious injury and performed the photographic analyses to determine surface grain size distributions.

I certify, with the above qualifications, that this thesis and the research to which it refers is the product of my own work.

Abstract

Urbanization is known to change the hydrologic and sediment supply regimes of rivers, causing more frequent, flashier flood events (hydromodification) and a reduction and redistribution of sediment sources. Presently, the impact that these changes have on bedload transport in gravel-bed channels and the resulting impact on bed morphology remains largely unknown due to a lack of process based studies. A better understanding of how riverbed form and processes evolve with urbanization is critical as they are a primary factor in controlling stream stability, providing habitat for aquatic species and influencing flood elevations. Additionally, stream rehabilitation is becoming increasingly common in urban rivers and an understanding of how sediment transport dynamics change with the alterations common to urbanization is critical for a successful design.

This thesis explores the impact of urbanization, which is the combination of hydromodification and alterations to sediment supply, on the morphodynamics (linkages between channel form and process) of bedforms in gravel-bed rivers. Specific objectives are: 1) to determine if detectable differences in bed morphology exist between rural and urban rivers in the same hydrophysiographic region; 2) to characterize the sediment transport dynamics of a highly urbanized channel; 3) to investigate the differences in geomorphically significant flows and sediment transport characteristics for different levels of watershed urbanization; and 4) to generalize field specific results using a mobile-bed laboratory flume to investigate the sediment transport characteristics for different levels of watershed hydromodification.

Longitudinal profiles of 11 rural and 9 urban watercourses with pool-riffle dominated morphologies in the same hydrophysiographic region (Southern Ontario, Canada) were investigated using three objective bedform identification methods; zero-crossing analysis, bedform differencing technique and residual pool depth analysis, as well as visual field identification. Results indicate that urban rivers possess deeper pools and a more topographically variable bed.

A field investigation was undertaken to characterize event-based sediment transport dynamics of a highly urbanized gravel-bed river over a three year period. Mimico Creek, located in Toronto, Ontario, Canada, is nearly fully urbanized and lacks significant stormwater management controls, therefore making it a

representative study reach. Bedload transport was measured using both active and passive sampling methods to characterize the mobility and transport dynamics of the entire range of surface particles. During this time, over 10 floods were sampled ranging from the approximate threshold discharge to well over the bankfull discharge. Coarse particle mobility differed from that previously reported in literature for rivers with more natural flow regimes. A strong link was found between coarse particle mobility and the transport dynamics of finer material which tends to dominate the bedload.

The measured bedload transport data were also used to calibrate a fractional sediment transport model which was combined with hydrometric data corresponding to different levels of watershed urbanization to perform a geomorphic work analysis. Urbanization is increasing the frequency, volume and time of competent discharge events (capable of performing work on the channel). Greater increases of intermediate discharge events were observed. Less urban streams are more influenced by larger discharge events, while urbanization is shifting the geomorphic significance to lower (but still competent) discharges.

Inspired from the field observations, an unsteady flow laboratory experiment was conducted to provide more generalized results. Three land-use scenarios representing different levels of watershed urbanization were developed from measured hydrometric data. Results show that both unsteady bedload transport dynamics and resulting bed morphology change with different levels of urbanization. Shorter duration hydrographs (corresponding to urban conditions) possess higher transport rates, less pronounced bedload hysteresis loops and more topographic variability of the bed. A proposed parameter for evaluating the degree of hysteresis shows sediment transport is closely linked with falling limb dynamics.

The key conclusion from the field, modeling and laboratory studies is that bedforms in gravel-bed rivers appear to be evolving to a state with more topographic variability. This variability is hypothesized to be additional form roughness to dissipate energy introduced due to hydromodification. These results are unique in literature and further our understanding of urban river processes.

Key words: urbanization, hydromodification, gravel-bed, bedforms, pool-riffle, fluvial geomorphology, sediment transport, geomorphic work, unsteady flow, bedload hysteresis, river rehabilitation.

Acknowledgements

This research project would not have been possible without the guidance, support and mentorship of my supervisor, Dr. William Annable. Bill has been a mentor since I was a 3rd year undergraduate student, and introduced me to river research. He provided guidance and resources throughout this long journey, all the while giving me the freedom to explore many different avenues related to my research. Bill's philosophy on river research is "if you want to understand it, get out in the field and measure it", which can sometimes result in much more work and time than initially anticipated. However, this philosophy has given me a unique appreciation of the steps involved in understanding how rivers behave. It has also instilled values which extend well beyond the world of river research. For this I am grateful.

Special thanks are extended to Dr. Anton Schleiss of the Laboratory of Hydraulic Constructions at École polytechnique fédérale de Lausanne (EPFL). He graciously provided me with resources and laboratory equipment in the world class research facility at LCH. Dr. Mário Franca and Dr. Carmelo Juez provided me with daily motivation and a tremendous amount of guidance during my stay at EPFL. They motivated me to "go steep" with the rather ambitious experimental design I arrived with, and helped me turn it into the final product in this thesis. The technical staff at LCH are thanked for helping with laboratory installations, equipment and sensors. I am forever thankful to Dr. Schleiss, Dr. Franca and Dr. Juez for working to find a solution to complete my remaining experiments after I suffered a serious injury which resulted in an earlier than expected departure from Switzerland.

I would like to thank Dr. Marwan Hassan for providing guidance and inspiration. He helped me turn an abundance of field data into a story. I would also like to thank my PhD Examining Committee for much needed direction in the early stages of this research and helpful comments and revisions in this manuscript.

Those who have done field research in bedload transport know that, at times, it can be highly stressful, labor intensive and require a lot of help. My colleagues in the Department of Civil & Environmental Engineering and at GeoProcess Research Associates spent countless days (and sometimes nights) in the field with me "hunting rocks" and "filling bags", as well offering support during the various rough periods encountered throughout a PhD. Thanks to Cailey McCutcheon, Lorenzo Brignoli, Brad Burrows, Chris

McKie, James Ehrman, Jeff Hirvonen, Pete Thompson, Jeff Muirhead, Ken Glasbergen, Christina Bright and Vernon Bevan. A special mention goes to Brad Burrows who was always keen to rally out for bedload sampling, even overnight in an ice storm. Chris McKie helped both with field work and my laboratory experiments at EPFL, and I could not have asked for a better person for the job. In addition to plenty of field help, James Ehrman helped automate the workflow for tracer particle analysis. Pete Thompson used his free time to modify his MASc code to suit my specific analyses. Jeff Hirvonen and I shared many inspiring conversations about our similar research projects, general river science and how to integrate what we were learning in practice through our consulting at GeoProcess Research Associates.

Terry Ridgway deserves a special acknowledgement. His knowledge set is extensive; field methods in fluvial geomorphology, environmental sensors, pump systems, electrical systems, mechanical fabrication and experimental design, just to name a few. He truly is a jack of all trades. Terry's help and companionship throughout the years in the field, lab and office will always be remembered.

My whitewater kayaking friends and community deserve some credit. Completing a PhD can sometimes be difficult, and kayaking has provided a much needed break, while still fueling my passion for understanding how rivers work. Hydraulic engineers and geomorphologists often study concepts pertaining to the momentum of moving water. My opinion is that one does not truly appreciate the power of a river until they have been continuously recirculated in a powerful hydraulic or launched completely airborne from a wave in a high volume river.

I would like to thank John Beebe (JTB Environmental Systems), the Natural Sciences and Engineering Research Council of Canada (NSERC) (IPS and Discoveries Grant), the Department of Civil & Environmental Engineering, R&M Construction and Water Regime Investigations and Simulations for providing funding for this project.

Finally, a very special acknowledgement to my Chocolate Lab and partner in crime, Rocky. He got me out of the house and away from my computer and has been a much needed companion throughout the final years of this doctorate, especially during these final months.

Dedication

This manuscript is dedicated to my parents. Thank you for your love and support throughout this adventure.

Table of Contents

Examining Committee Membership ii
Author's Declaration iii
Statement of Contributions iv
Abstract v
Acknowledgements vii
Dedication ix
Table of Contents x
List of Figures xiii
List of Tables xvii
List of Equations xviii
List of Abbreviations xix
List of Symbols xx
Chapter 1 Introduction 1
1.1 Objectives 6
1.2 Thesis Organization 7
Chapter 2 Pool-Riffle Metamorphosis in Urbanizing Gravel-bed Rivers of Southern Ontario, Canada 8
2.1 Introduction 8
2.2 Field Sites 9
2.3 Methods 12
2.3.1 Zero-Crossing Analysis 12
2.3.2 Bedform Differencing 12
2.3.3 Residual Pool Depth Analysis 12
2.3.4 Visual Field Identification 13
2.4 Results 13
2.4.1 Comparison Between Objective Methods 13
2.4.2 Pool-Riffle Frequency and Riffle Lengths 16
2.4.3 Pool Depths and Bedform Variability 17
2.4.4 Comparison with Visual Field Identification 19
2.5 Discussion 20
2.6 Conclusions 23

Chapter 3 The Impact of Urbanization on Temporal Changes in Sediment Transport in a Gravel-bed Channel in Southern Ontario, Canada 26
3.1 Introduction 26
3.2 Field Sites 28
3.3 Field Methods 31
3.3.1 Bed Material Sampling 31
3.3.2 Sediment Transport Measurements 31
3.4 Data and Analysis 32
3.4.1 Fractional Transport Analysis 32
3.4.2 Tracer Recovery, Mobility and Transport Distances 33
3.4.3 Hydraulic Modeling and Hydrologic Analysis 34
3.4.4 Sediment Transport Modeling 35
3.4.5 Geomorphic Work Analysis and Effective Discharge (Q_{eff}) Estimation 36
3.5 Results 36
3.5.1 Fractional Transport 36
3.5.2 Tracer Mobility 40
3.5.3 Temporal Changes in Geomorphically Significant Discharges 42
3.6 Discussion 47
3.6.1 The Relationship Between the Mobility of Coarse Particles and Fine Surface Material and Urban Bed Structures 47
3.6.2 Geomorphically Significant Discharges in Urban Streams 48
3.7 Conclusions 51
Chapter 4 The Impact of Hydrograph Variability and Frequency Associated with Urbanization on the Morphodynamics of Gravel-bed Channels 54
4.1 Introduction 54
4.2 Background 55
4.3 Methods 56
4.3.1 Hydrologic Scenario Development 56
4.3.2 Experimental Design 58
4.3.3 Experimental Channel and Measurements 61
4.3.4 Experimental Procedure 63
4.4 Results 64

4.4.1 Bedload Transport Rates and Yields 64
4.4.2 Fractional Transport 68
4.4.3 Bedload Percentiles 71
4.4.4 Bed Surface Texture 75
4.4.5 Topographic Variability 76
4.5 Discussion 80
4.5.1 Hydrograph Unsteadiness on Bedload Transport, Hysteresis and Surface Texture 80
4.5.2 Comparison with Observations in Urbanized Rivers 84
4.5.3 Impacts on the Evolution of Urban Rivers and Implications to Stream Rehabilitation and Stormwater Management 84
4.6 Conclusions 85
Chapter 5 General Conclusions 87
5.1 Introduction 87
5.2 Summary of Results 87
5.3 Implications of Results on Engineering Practices 88
5.4 Future Research 89
References 91
Appendix A Additional Results from Chapter 2 101
Appendix B Additional Results from Chapter 3 142
Appendix C Additional Results from Chapter 4 147

List of Figures

Figure 1.1: *Lane's* [1955] balance scale diagram illustrating the proportionality between channel form and process [from *Rosgen*, 1996]. 2

Figure 1.2: Common land-use progression from unaltered through agricultural to urban with commonly associated point, reach and watershed scale disturbances (watershed scale disturbances indicated in bold italics). 4

Figure 2.1: Reach locations in Southern Ontario, Canada. Shaded region near Toronto represents limits of urban development..... 10

Figure 2.2: Normalized riffle spacing for the rural (left) and urban (right) datasets for a,f) zero-crossing linear regression, b,g) zero crossing nonlinear regression, c,h) bedform differencing with $E_T = (1/N_S)S_D$ tolerance, d,i) bedform differencing with $E_T = 0.75S_D$ tolerance, e,j) residual pool depths. See text for details on methods. Note: f and h are truncated at 30 (#14 and #18 extend beyond)... 14

Figure 2.3: Examples of linear regression error for 02HC033..... 15

Figure 2.4: Point Density vs riffle spacing for; ZC1 zero-crossing linear regression, ZC2 zero crossing nonlinear regression, BD1 bedform differencing with $E_T = (1/N_S)S_D$ tolerance, BD2 bedform differencing with $E_T = 0.75S_D$ tolerance, and RPD residual pool depths. 16

Figure 2.5: Riffle spacing vs percent urban land-use for a) zero crossing nonlinear regression, b) bedform differencing with $0.75S_D$ tolerance, c) residual pool depths. See text for details on methods..... 17

Figure 2.6: a) Mean normalized residual pool depths and b) standard deviation of normalized pool depths for each study reach vs percent urban land-use (residual pool depth method). 18

Figure 2.7: a) NRMSE of linear regression and b) NRMSE of nonlinear regression for each study reach vs percent urban land-use. 19

Figure 2.8: Comparison between objective methods and visual field identification for a) normalized riffle spacing and b) normalized riffle lengths..... 20

Figure 2.9: Average annual frequency of bankfull discharge events for each study reach [modified from *Annable et al.*, 2012]. Error bars represent annual range throughout the study period [*Annable et al.*, 2012]. 22

Figure 3.1: a) Mimico and Etobicoke Creek watersheds and b) Mimico Creek study reach..... 29

Figure 3.2: Grain size distributions of subsurface, surface and bulk mixture (combination of surface and subsurface) for Mimico Creek. 30

Figure 3.3: Dimensionless bedload rating curve for Mimico Creek. Shaded area represents the envelope encompassing several theoretical bedload flux equations [*Meyer-Peter and Muller*, 1948; *Brown*, 1950; *Parker*, 1978]. Solid line represents the calibrated dimensionless *Wilcock-Crowe* [2003] model for each grain fraction joined together in a single line. 37

Figure 3.4: Scaled fractional sediment transport rates ($q_{bi}p_i/f_i$) for all sampled transport events b) Scaled fractional sediment transport rates ($q_{bi}p_i/f_i$) for averaged transport events. Error bars represent the relative standard error. See text for discharge class averaging. Solid and dashed lines included to differentiate approximate boundaries between different transport conditions..... 40

Figure 3.5: a) Fractional transport distances of half-phi grain classes for events less than and greater than Q_{bf}. b) Average event-based percentage of mobility (P_{mevb}) of each grain class for events less than and greater than Q_{bf}, with error bars representing the standard error. 41

Figure 3.6: Scaled transport distances of each particle, half-phi grain class mean and medians based on Equations (3.2) and (3.3). 42

Figure 3.7: Geomorphic work plots for the complete hydrometric series of Mimico Creek (a,b) and Etobicoke Creek (c,d). 43

Figure 3.8: Geomorphic work plots for the land-use scenarios. See text for land-use scenario development and details. 44

Figure 3.9: Geomorphic work characteristics for indicator discharges as a function of urban land-use; a) average number of events per year equaling or exceeding each discharge b) average time each discharge is equaled or exceeded each year c) average fraction of total volume above each discharge for each scenario d) cumulative fraction of total sediment load transported by each discharge. 46

Figure 3.10: Relative proportions of sand and gravel in the bedload for each discharge. 47

Figure 4.1: Summary of observed bedload hysteresis in both field and laboratory studies..... 56

Figure 4.2: Schematic of parameters extracted from field hydrometric data for the development of the laboratory hydrographs corresponding to the land-use scenarios. Q_{peak} and Q_{thres} are peak discharge and threshold discharge, respectively. TTP is time-to-peak and t_h is the threshold duration. See text for details on hydrograph development. 58

Figure 4.3: Schematic of laboratory experiments illustrating the experimental stepped hydrographs (grey line), stepped sediment feed rates (grey patches) and bedload transport rates collected from the bedload trap (black dots). 9, 16 and 33 hydrographs were conducted for LU1, LU2 and LU3, respectively. 60

Figure 4.4: Schematic of experimental channel (top) and photos illustrating the sediment feeder (left), the channel during experiments (middle) and the downstream sediment trap (right). 62

Figure 4.5: Sediment transport rates corresponding to the peak discharge of each hydrograph in a) LU1, b) LU2 and c) LU3. Solid and hollow symbols represent hydrographs exhibiting clockwise hysteresis and counterclockwise hysteresis, respectively. Note: No counterclockwise hysteresis was observed for LU1. 65

Figure 4.6: Phase plots for select hydrographs from each experiment (LU1 top row, LU2 middle row, LU3 bottom row) illustrating the different phases of bedload hysteresis present. Hi denotes the hydrograph number of that specific experiment. 66

Figure 4.7: Sediment yield ratios (Y_{out} / Y_{in}) of each hydrograph for the total yield, rising limb yield and falling limb yield for a) LU1, b) LU2 and c) LU3 and the hysteresis ratio (H_r) (ratio of the rising limb yield and falling limb yield) for d) LU1, e) LU2 and f) LU3. Horizontal line serves as a threshold for: equal input and output sediment yields (top) and clockwise or counter clockwise nature of the hysteresis loops (bottom). 68

Figure 4.8: Transport ratios of each grain class, i, p_i/f_i, where p_i is the proportion of that class in the bedload transported out of the channel and f_i is the proportion of that grain class in the bulk mixture. Hi denotes the hydrograph number of that specific experiment. 70

Figure 4.9: 90th percentile of the bedload transported out of the channel (D_{90load}) at peak discharge for each hydrograph for a) LU1, b) LU2 and c) LU3. 50th percentile of the bedload (D_{50load}) at peak discharge for each hydrograph for d) LU1, e) LU2 and f) LU3. 30th percentile of the bedload (D_{30load}) at peak discharge for each hydrograph for g) LU1, h) LU2 and i) LU3. Solid and hollow symbols represent hydrographs exhibiting clockwise hysteresis and counterclockwise hysteresis, respectively. Note: No counterclockwise hysteresis was exhibited in LU1. 71

Figure 4.10: Bedload percentile phase plots of D_{90load} for select hydrographs from each experiment (LU1 top row, LU2 middle row, LU3 bottom row). D_{90bulk} indicated by horizontal line. Hi denotes the hydrograph number of that specific experiment. 73

Figure 4.11: Bedload percentile phase plots of D_{50load} for select hydrographs from each experiment (LU1 top row, LU2 middle row, LU3 bottom row). D_{50bulk} indicated by horizontal line. Hi denotes the hydrograph number of that specific experiment. 74

Figure 4.12: Bedload percentile phase plots of D_{30load} for select hydrographs from each experiment (LU1 top row, LU2 middle row, LU3 bottom row). D_{30bulk} indicated by horizontal line. Hi denotes the hydrograph number of that specific experiment. 75

Figure 4.13: 90th percentile of the surface (D_{90surf}) after each hydrograph for a) LU1, b) LU2 and c) LU3. 50th percentile of the surface (D_{50surf}) after each hydrograph for d) LU1, e) LU2 and f) LU3. 30th percentile of the surface (D_{30surf}) at peak discharge for each hydrograph for g) LU1, h) LU2 and i) LU3. Solid and hollow symbols represent hydrographs exhibiting clockwise hysteresis and counterclockwise hysteresis, respectively. Bulk percentiles indicated by horizontal lines. Note: No counterclockwise hysteresis was exhibited in LU1. 76

Figure 4.14: Normalized erosion and deposition depths and the proportion of the bed undergoing erosion and deposition for a,b) LU1, c,d) LU2 and e,f) LU3. Median RMSE of the 20 profiles in ($RMSE_{50}$) each bed scan, where the error bars represent one standard deviation of the RMSE values (σ_{RMSE}). See text for details. Solid and hollow symbols in b, d and f represent hydrographs exhibiting clockwise hysteresis and counterclockwise hysteresis, respectively. Grey patches depict the range of bed variability for each experiment. 78

Figure 4.15: LU1 (a) LU2 (b) and LU3 (c) hydrographs scenario (grey patches) with all the bedload transport rates collected during each experiment (black dots). Note: the bedload transport rates from the first hydrograph of each experiment are not included. 81

Figure 4.16: Normalized yield (Y_{out}/Y_{in}) for total yield (combination of rising and falling limbs), rising limb yield and falling limb yield for all hydrographs in each experiment, excluding the first hydrograph. 83

List of Tables

Table 2.1: Selected riffle-pool morphology study reach characteristics 11

Table 3.1: Mimico Creek general characteristics. D_{isurf} and D_{isub} define the i^{th} percentile for the bed surface and subsurface, respectively. 30

Table 3.2: Hydrologic land-use scenario details. 35

Table 4.1: Land-use scenario descriptions and data sources 57

Table 4.2: Experimental hydrograph variables and associated unsteady flow parameters derived from gauge data 59

List of Equations

(2.1) 12
(3.1) 32
(3.2) 33
(3.3) 34
(4.1) 61
(4.2) 61
(4.3) 77

List of Abbreviations

Abbreviation	Description
GPS	global positioning system
GSD	grain size distribution
NRMSE	normalized root-mean-square error
RFID	radio-frequency identification
RMSE	root-mean-square error
SWM	stormwater management
TTP	time-to-peak

List of Symbols

Symbol	Description
A_d	area of bed experiencing deposition [L^2]
A_e	area of bed experiencing erosion [L^2]
A_T	total planar area of the channel bed [L^2]
A_w	watershed area [L^2]
B	channel bottom width [L]
D_{gi}	geometric mean of the i^{th} particle class [L]
D_i	particle diameter of the i^{th} particle (or particle class) [L]
D_{ibulk}	particle diameter of percentile i of the bulk bed mixture [L]
D_{iload}	particle diameter of percentile i of the bedload [L]
D_{isub}	particle diameter of percentile i of the bed subsurface [L]
D_{isurf}	particle diameter of percentile i of the bed surface [L]
E_T	elevation tolerance parameter [L]
f_i	fraction of i^{th} grain class in the bulk bed material [-]
F_i	fraction of i^{th} grain class in the surface bed material [-]
g	gravitational acceleration [LT^{-2}]
h_0	flow depth at base flow [L]
Δh	change in flow depth [L]
h_{bf}	average bankfull depth [L]
H_r	hysteresis ratio [-]
L^*	scaled transport distance for particle i [-]
L_i	discrete transport distance for particle i [L]
L_{D50}	mean particle travel distance of the grain class that contains the D_{50} size [L]
$L_{D50surf}$	mean particle travel distance of the grain class that contains the D_{50surf} size [L]
L_{mevb}	mean event-based transport distance of each tracer survey [L]

$RMSE_{50}$	median root-mean-square error [L]
N_f	total number of recovered tracer particles [-]
N_{fevb}	event-based number of recovered tracer particles [-]
N_L	normalized length of surveyed longitudinal profile [-]
N_S	normalized mean survey point spacing [-]
N_t	total number of seeded tracer particles [-]
N_m	total number of particles found to be mobile [-]
N_{mevb}	event-based number of particles found to be mobile [-]
P	unsteadiness parameter [-]
p_i	fraction of i^{th} grain class in the bedload [-]
P_{mevb}	percent of event-based particles found to be mobile [-]
P_m	percent of total particles found to be mobile [-]
P_r	total tracer recovery rate [-]
P_{revb}	event-based tracer recovery rate [-]
q	unit water discharge [L^2T^{-1}]
q_{bi}	unit bedload flux of the i^{th} particle class [L^2T^{-1}]
$q_{s,in}$	unit sediment input rate [$MT^{-1}L^{-1}$]
q^*_{bi}	dimensionless unit bedload flux of the i^{th} particle class [-]
q_{peak}	unit peak discharge [L^2T^{-1}]
q_s	unit sediment output rate [$MT^{-1}L^{-1}$]
q_{thres}	unit threshold discharge [L^2T^{-1}]
Q_{bf}	bankfull discharge [L^3T^{-1}]
Q_{eff}	effective discharge [L^3T^{-1}]
Q_{half}	half-load discharge [L^3T^{-1}]
Q_{peak}	peak discharge [L^3T^{-1}]
Q_{thres}	threshold discharge [L^3T^{-1}]

S_D standard deviation of differenced elevations [L]

t_h threshold duration of hydrograph [T]

t_{tot} total experiment duration [T]

u_{*0} shear velocity at base flow [LT^{-1}]

V_d net volume of deposited material [L^3]

V_e net volume of eroded material [L^3]

V_h hydrograph volume [L^3]

V_{tot} total volume [L^3]

W_{bf} average bankfull width [L]

W_k total work flow index [T]

Y_{in} sediment input yield [M]

Y_f sediment output yield for falling limb [M]

Y_{out} sediment output yield [M]

Y_r sediment output yield for rising limb [M]

Greek symbols

τ_0	channel bed shear stress [$ML^{-1}T^{-2}$]
τ_c	critical shear stress [$ML^{-1}T^{-2}$]
τ_{ri}	reference shear stress for the i^{th} particle class [$ML^{-1}T^{-2}$]
τ_c	critical shear stress [$ML^{-1}T^{-2}$]
$\Delta_{z,e}$	normalized erosion depth [L]
$\Delta_{z,d}$	normalized deposition depth [L]
ρ_w	mass density of water [ML^{-3}]
ρ_s	mass density of sediment [ML^{-3}]
σ_{RMSE}	standard deviation of root-mean-square error values [L]

"The river has a way of carrying all it touches downstream, around the next bend and off into the unknown. The river does not discriminate as to its passengers and will gladly take anything its powerful flow can persuade to accompany it. Putting in, I began a relationship with the river, an understanding that acknowledged the bond that I was about to make."

-Jonathan Bowler

Chapter 1
Introduction

River forms and the processes that continually alter their states are interrelated in an ongoing feedback loop. The shape of the cross section and bed profile, often referred to as channel form, is a function of the processes occurring through it, namely flow and the quantity and composition of sediment being transported [*Leopold et al.*, 1964; *Knighton*, 1998]. These processes, in turn, are influenced by the channel shape and the composition of sediment composing the bed and banks of the channel. A "quasi-stable" channel is considered to be one that the average shape of the cross section remains relatively constant, although the channel may migrate due to bank erosion and deposition associated with meandering. Thus, channel form can remain relatively constant over long periods of time, although the position of the channel may not [*Leopold et al.*, 1964].

Bedforms are an inherent physical expression of a given river system. These form elements add additional complexity to the feedback loop between form and process as their formation is governed by flow mechanics and sediment movement [*Leeder*, 1983], but in turn bedforms influence flow through additional form resistance [*Simons and Richardson*, 1966; *Millar*, 1999] as well as sediment transport along the channel [e.g. *Sear*, 1996]. Bedforms exist in sand-bed channels as ripples, dunes and anti-dunes, depending on flow strength and flow regime [*Simons and Richardson*, 1966]. In gravel-bed rivers, bedforms exist at different spatial scales from micro-scale features such as particle clusters [*Martini*, 1977; *Brayshaw et al.*, 1983] and stone cells [*Church et al.*, 1998] to macro-scale forms such as pools, steps, riffles and bars [*Leopold et al.*, 1964; *Montgomery and Buffington*, 1997]. The adjustment of these macro-scale form elements is the focus of this work.

Pool-riffle morphologies commonly occur in moderate channel slopes (<1.5%) [*Montgomery and Buffington*, 1997] and in rivers where median particle sizes exceed 2 mm in bedload material [*Richards*, 1976]. They consist of a series of deeps (pools) and shallows (riffles) which are rhythmically expanding and contracting; inter-spaced at approximate distances of 5 to 7 times the channel width from the previous form of the same type [*Leopold et al.*, 1964; *Keller and Melhorn*, 1978]. Surface material on riffles tends to be coarser than that of pools [*Leopold et al.*, 1964], however, this is dependent on antecedent flood conditions as pools can be filled in during extended low-flow periods while being swept clean of the finer (sand) material during large floods [*Keller*, 1971; *Richards*, 1976]. Pool-riffle development and

maintenance has been suggested to occur due to different velocity gradients with increasing discharge in pools and riffles [*Keller*, 1971] or the minimization of potential energy expenditure [*Yang*, 1971]. These bedforms also provide critical spawning habitat [*Kondolf and Wolman*, 1993] and energy dissipation through flow resistance [*Yang*, 1971; *Millar*, 1999].

The self-organizing, self-adjusting nature of rivers and the interrelation between river form and processes implies that alterations to boundary conditions that control processes such as flow and sediment input will result in systematic changes to channel form. The proportionality between form and process, and the resulting direction of change due to an adjustment was conceptualized by *Lane* [1955] and is illustrated in the popular balance scale diagram (Figure 1.1).

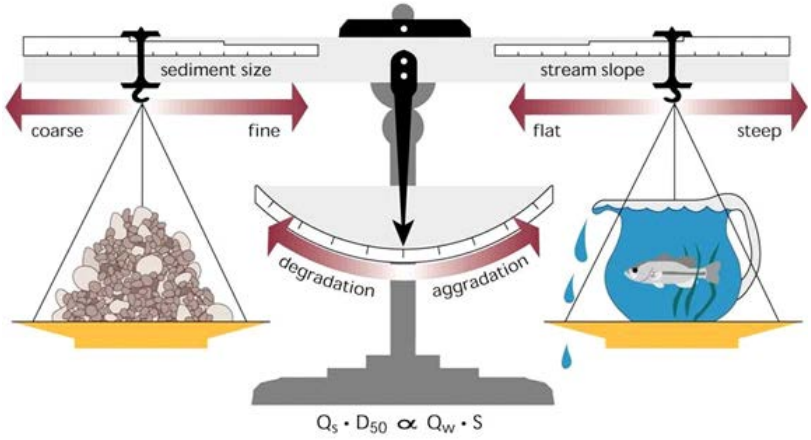

Figure 1.1: *Lane's* [1955] balance scale diagram illustrating the proportionality between channel form and process [from *Rosgen*, 1996].

This concept describes that the sediment load (amount) and caliber (size) is proportional to the water discharge (amount) and the channel slope (ability of the river to transport the water and sediment). Changes to any of these variables will result in either channel degradation or aggradation, depending on the variable and direction of change. This proportionality has been used as the basis of a number of channel evolution models to document channel change in varying hydrophysiographic regions [e.g. *Schumm*, 1969; *Schumm et al.*, 1984; *Julien*, 2002; *Hawley and Bledsoe.*, 2013].

Disturbances to river systems can occur on multiple spatial and temporal scales. Spatial scales include point scale, reach scale and watershed scale. Examples of point and reach scale disturbances are; dam construction, channelization, gravel bar mining, influx of sediment from a landslide or a local diversion of

water for agriculture. Watershed scale disturbances are commonly associated with large-scale forest fires and changes in land-use practices, where a watershed is developed for agricultural or urban purposes. While reach scale disturbances have been well documented to have impacts on channel morphology, watershed scale disturbances have tended to result in greater impacts as they commonly include various point or reach scale disturbances, in addition to the larger scale alterations [*Gregory*, 2006]. Watershed scale disturbances associated with land-use change commonly begin with a transition from an unaltered condition to agricultural land-use conditions, consisting of deforestation, the construction of drainage canals (channelization), tile drains, and water harvesting through irrigation practices. From here, the watershed may become urbanized, resulting in increases to impervious surfaces (reduction in infiltration capacity) and drainage densities through the construction of buildings, roads, parking lots and storm sewer networks (Figure 1.2). Of the different types of watershed scale disturbances due to with land-use change, changes associated with urbanization have resulted in the most extreme changes to watershed hydrology and channel morphology [*Leopold*, 1968; *Gregory*, 2006].

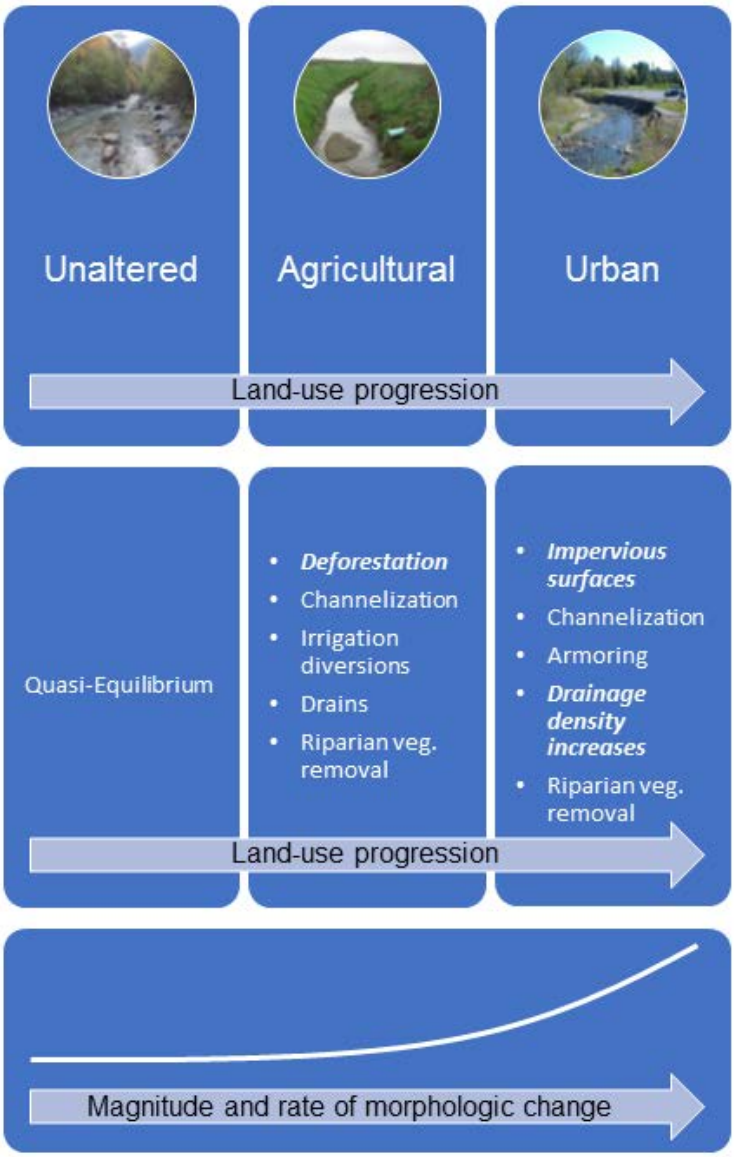

Figure 1.2: Common land-use progression from unaltered through agricultural to urban with commonly associated point, reach and watershed scale disturbances (watershed scale disturbances indicated in bold italics).

Urbanization is known to alter the hydrologic response of a watershed, often referred to as hydromodification, changing the spatial and temporal delivery of how water enters a channel; with documented increases in flood frequency, flood peaks and flashiness and corresponding decreases in flood durations [*Leopold*, 1968; *Hollis*, 1975; *Hawley and Bledsoe*, 2011; *Annable et al.*, 2012]. Urbanization

can also alter the sediment sources and supply (bed material, suspended or washload) to a river, including increases during active construction phases [*Wolman*, 1967] and the redistribution of locations of sediment sources within a watershed from upland sources to predominantly in-channel sources [*Trimble*, 1997; *Nelson and Booth*, 2002]. It is unclear how bed material supply is changed as a watershed approaches build-out (its maximum possible state of urbanization), however, a space-for-time substitution conducted on watersheds with varying degrees of urbanization in southern Ontario by *Annable et al.* [2012] suggests that bed material supply decreases with increasing urban land-use. These changes ultimately "tip the scale", and result in alterations to channel form in urbanized channels.

The systematic channel response associated with urbanization has primarily been documented as channel enlargement [*Hammer*, 1972; *Booth*, 1990; *Pizzuto et al.*, 2000; *Chin*, 2006; *Hawley and Bledsoe*, 2013], which often coincides with excessive erosion and/or deposition, resulting in the ecological degradation of the channel [*Walsh et al.*, 2005]. Some studies have contradicted this, concluding that urban channels do not increase in size [*Annable et al.*, 2012]. The impact that urbanization may have on channel bed morphology has been less documented, with the primary observation being bed coarsening [*Finkenbine et al.*, 2000; *Pizzuto et al.*, 2000; *Annable et al.*, 2012; *Hawley et al.*, 2013]; however, there is a lack of knowledge on how channel bedforms and the sediment transport characteristics maintaining them evolve under urbanizing flow and sediment routing regimes (both form and process), especially pertaining to gravel-bed channels.

Historical engineering measures in urban channels have been channelization, channel armoring and "peak flow shaving" through stormwater management practices. While these proved effective as short-term solutions, their long-term impacts have generally contributed to the morphologic and ecologic degradation already observed in these channels [*MacRae*, 1997; *Walsh et al.*, 2005]. This degradation common to urban channels has resulted in an increase in urban river rehabilitation projects [*Bernhardt et al.*, 2005; *Roni et al.*, 2008; *Kenney et al.*, 2012]. A common practice has been to reintroduce pool-riffle morphologies to enhance channel stability and augment aquatic habitat diversity [*Newbury and Gaboury*, 1993; *Harper et al.*, 1998; *Booth*, 2005; *Schwartz et al.*, 2015], but this activity has been documented to be difficult to achieve in urban settings [*Harper et al.*, 1998; *Schwartz et al.*, 2015]. Integral to the successful implementation of river rehabilitation projects is an understanding of the sediment transport characteristics of both the existing and desired channel outcomes [*Kellerhals and Miles*, 1996; *Shields Jr. et al.*, 2003], however, due to the lack of process based studies in urban rivers and long-term sediment data sets, indirect

methods such as sediment budgets [e.g. *Allmendinger et al.*, 2007] and numerical modelling [*Schwartz and Neff*, 2011] are often employed without field calibration. There is thus a need to better understand how a) bed morphology and b) sediment transport processes are changing at the field-scale due to watershed urbanization in gravel-bed channels.

1.1 Objectives

The overall objective of this thesis is to explore the impact of urbanization, which is the combination of hydromodification and alterations to sediment supply, on bed morphology in gravel-bed rivers. Due to existing data and the proximity to field sites, the field data encompass rivers located in Southern Ontario, Canada. Specific objectives are as follows:

1. Determine if detectable differences in bed morphology exist between rural and urban rivers in the same hydrophysiographic region;
2. Characterize the sediment transport dynamics of a highly urbanized channel;
3. Investigate the differences in geomorphically significant flows and sediment transport characteristics for different levels of watershed urbanization; and
4. Generalize field specific results using a mobile-bed laboratory flume to investigate the sediment transport characteristics for different levels of watershed hydromodification.

The overall contribution of this thesis work is a better understanding of how the morphodynamics (the linkage between channel form and process) of gravel-bed channels is changing with watershed urbanization. This is of particular importance for water resources engineers, watershed managers, fluvial geomorphologists and aquatic biologists/ecologists involved in:

- Flood control: Evolving bedforms may result in a change in form roughness which can have notable impacts on measured and estimated water levels [*Millar*, 1999];
- Aquatic habitat management: Evolving bedforms may result in a change in bed variability and composition which can have positive or negative impacts (depending on the direction and magnitude of change) on the species that occupy those habitat niches [*Kellerhals and Miles*, 1996];
- River restoration/rehabilitation activities: As understanding the sediment transport dynamics of the restoration reach is a crucial factor in a successful design [*Kellerhals and Miles*, 1996; *Shields Jr. et al.*, 2003], more process based studies will further our knowledge of the impacts of urbanization on sediment transport in gravel-bed channels. Moreover, current prescribed river rehabilitation

metrics have been derived from rivers with relatively unaltered hydrologic regimes [*Leopold et al.*, 1964; *Newbury and Gaboury*, 1993; *Annable*, 1996b; *Rosgen*, 1996] and it is possible that these metrics are not adequate for rivers with altered hydrologic and sediment regimes.

1.2 Thesis Organization

The format of this thesis introduces Chapters 2, 3 and 4 as distinct topics, or manuscripts, which have been, or will be, submitted to scientific journals. There may be slight repetition amongst the literature reviews within each chapter, which is necessary for each chapter to flow independently of each other. To facilitate the linkage between these distinct topics, a transition paragraph is included between Chapters 2 and 3, and Chapters 3 and 4.

Chapter 2 addresses objective one. Measured longitudinal profiles from datasets of rural and urban rivers are compared using multiple objective bedform identification methods. The methods and results from this study are presented and discussed.

Chapter 3 addresses objectives two and three. Results from the multi-year bedload transport sampling campaign on Mimico Creek are presented, discussed and compared to existing literature. The methods and results from the fractional bedload transport modelling and magnitude-frequency analysis are also presented and discussed.

Chapter 4 addresses objective four. The methods and results from the mobile-bed laboratory study are presented and discussed. This includes the development of hydrologic scenarios used to simulate different levels of watershed hydromodification. The results are compared to existing field studies in literature and potential applications to field-scale engineering solutions.

Chapter 5 combines the major conclusions from the three distinct manuscripts presented in Chapters 2, 3 and 4, highlighting their significance to water-resources engineering, aquatic habitat management and river rehabilitation and ties them back to the study objectives. Additionally, recommendations for future research are discussed.

Cited references and appendices follow Chapter 5. Appendices include additional results and supporting information pertaining to Chapters 2, 3 and 4.

Chapter 2
Pool-Riffle Metamorphosis in Urbanizing Gravel-bed Rivers of Southern Ontario, Canada

2.1 Introduction

Rivers adjust their form based on the spatial and temporal inputs of water and sediment that they receive. Departure from a quasi-equilibrium form of a given watercourse may occur when the state variables deviate from long-term trends resulting in channel adjustments which depend upon the type and magnitude of disturbance [*Leopold et al.*, 1964; *Schumm*, 1969]. Urbanization is known to alter hydrologic responses of a watershed, changing spatial and temporal routing characteristics of how and when water enters a watercourse [*Leopold*, 1968; *Hollis*, 1975; *Hawley and Bledsoe*, 2011]. Sediment sources and supply (bed material, suspended or washload) may also change or be redistributed during and after the period of urbanization from upland to predominantly in-channel sources [*Wolman*, 1967; *Trimble*, 1997; *Nelson and Booth*, 2002]. It is unclear how bed material supply changes as a watershed approaches build-out, however, a space-for-time substitution conducted on watersheds with varying degrees of urbanization in southern Ontario, Canada by *Annable et al.*, [2012] suggests that bed material supply decreases with increasing urban land-use.

Channel enlargement resulting from urbanization is a common morphologic adjustment [*Hammer*, 1972; *Booth*, 1990; *Pizzuto et al.*, 2000; *Chin*, 2006; *Hawley and Bledsoe*, 2013]. Impacts to channel bed morphology during the corresponding period have been less documented, however, bed coarsening has been a common observation [*Finkenbine et al.*, 2000; *Pizzuto et al.*, 2000; *Annable et al.*, 2012; *Hawley et al.*, 2013]. In riffle-pool dominated morphologies, a shortening of riffles and a corresponding lengthening and deepening of pools was observed for watersheds of increasing urbanization [*Annable*, 2010; *Hawley et al.*, 2013]. *Annable* [2010] also documented an increase in meander wavelength in urban gravel-bed channels without a corresponding increase in pool-riffle spacing, which effectively increase the frequency of riffles and pools with respect to the meander geometry.

The changing frequency of bedforms is similar to the spatial transition between lower-slope to higher-slope morphologies (i.e. riffle-pool to step-pool), where the bedform frequency and corresponding spatial variability adjusts in response to changing erosive energy resulting from channel gradient [*Montgomery*

and Buffington, 1997]. Deeper pools act in similar ways to scour-pools below hydraulic structures, which are known to dissipate energy [*Bormann and Julien*, 1991]. Pool-riffle development and maintenance has been suggested to occur due different velocity gradients with increasing discharge in pools and riffles [*Keller*, 1971] or the minimization of potential energy expenditure [*Yang*, 1971]. It is hypothesized that pool-riffle frequency changes may be temporally occurring with the increasing erosive energy, where the channel gradient may not change considerably [*Annable*, 2010; *Hawley et al.*, 2013]. Knowing the ultimate morphologic adjustment due to urbanization is important for stream ecology, flood control and target morphologies in stream restoration design.

Existing studies on gravel-bedform evolution arising from urbanization have all employed field based characterizations of riffles and pools and, as such, can be biased due to operator preference in the definition of where riffles and pools begin or end [*Richards*, 1976; *Hayward*, 1980; *O' Neill and Abrahams*, 1984; *Wooldridge and Hickin*, 2002]. The objective of this study is to employ objective bedform identification methods on datasets of rural [*Annable*, 1996a] and urban [*Annable et al.*, 2012] gravel-bed, pool-riffle watercourses in the same hydrophysiographic region to determine if any differences exist in a) pool-riffle sequence frequencies and b) topographic variability of bed profiles between the two datasets. The objective bedform identification methods employed here are 1) zero-crossing analysis [*Richards*, 1976], 2) bedform differencing technique [*O'Neill and Abrahams*, 1984] and, 3) residual pool depths [*Lisle*, 1987]. Each method offers different measures of bedform geometry and topographic variability. These methods are also compared to visual field identification to assess if any major differences are present.

2.2 Field Sites

River data sets from *Annable* [1996a] and *Annable et al.* [2012] for rural and urban watersheds, respectively, were initially screened based upon a number of criteria to ensure that selected watercourses were representative of pool-riffle morphologies [*Montgomery and Buffington*, 1997] and that the surveyed longitudinal profiles were sufficient for representative comparisons. *Leopold et al.* [1964] suggest a minimum of two meander wavelengths to adequately characterize the morphologic characteristics of the river. As such, the normalized longitudinal length of the surveys (N_L), which is the longitudinal distance normalized by the average bankfull width (W_{bf}), was chosen to a minimum of 24 (assumes an average pool-riffle sequence of 6 channel widths) wherever possible (in all cases but one). Density of field-surveyed points along each longitudinal profile was also considered. Certain objective bedform identification methods require that an even spacing of points be employed, for example, one point every bankfull width

[*O'Neill and Abrahams*, 1984]. This method, however, may omit some of the "minor patterns", characterized as smaller steps and topographic variations observed throughout riffles and pools [*Hayward*, 1980]. The longitudinal survey methods employed by *Annable* [1996b] and *Annable et al.* [2012] characterize every major break in slope and, at a maximum spacing, every channel width. The normalized mean spacing (N_S), which is the mean distance between points normalized by the average bankfull width (W_{bf}), ranged in this study between $0.48 \leq N_S \leq 1.30$. Logistics of field surveys will inherently introduce variability into this metric as it is difficult to obtain measurements at precise intervals, and four of the selected reaches have an N_S slightly greater than 1. The percentage of urban land-use was identified for the same approximate time period as the channels were surveyed using a combination of land-use classification maps [*OMNR*, 2006] and historical aerial photograph inspection [*Thompson*, 2013]. While there is some overlap between urban and rural datasets, the urban land-use in the rural datasets was more distributed throughout the watershed, which acts to attenuate the hydrologic impacts associated with urbanization. Surficial geology of the reaches is primarily till, with some overlying glaciofluvial deposits. The final selected reaches and associated characteristics are presented in Table 2.1. A map of their locations is illustrated in Figure 2.1.

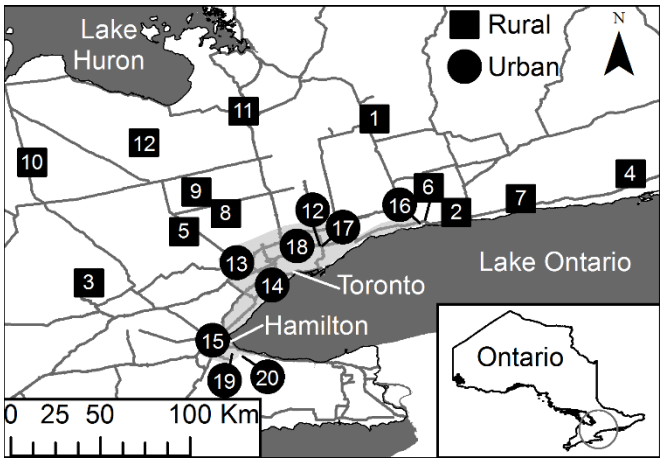

Figure 2.1: Reach locations in Southern Ontario, Canada. Shaded region near Toronto represents limits of urban development.

Table 2.1: Selected riffle-pool morphology study reach characteristics

Map Ref. #	Name	EC Gauge	Land-Use	A_w (km^2)	% Urban Land-Use	Avg. Slope (m/m)	Avg. W_{bf} (m)	Avg. h_{bf} (m)	N_L (W_{bf})	N_S (m/W_{bf})
1	BEAVER RIVER NEAR BEAVERTON	02EC011	R	282	4	4.10E-03	27.6	1.36	29.2	0.86
2	BOWMANVILLE CREEK AT BOWMANVILLE	02HD006	R	82.9	6	7.70E-03	15.8	0.60	78.6	1.21
3	CANAGAGIGUE CREEK NEAR ELMIRA	02GA023	R	118	7	3.80E-03	27.6	0.74	55.9	0.70
4	COLD CREEK AT ORLAND	02HK007	R	159	3	8.00E-04	22.3	1.22	32.0	0.76
5	CREDIT RIVER NEAR CATARACT	02HB001	R	82.3	4	1.40E-03	17.8	0.84	54.6	0.88
6	FAREWELL CREEK AT OSHAWA	02HD014	R	58.5	14	8.70E-03	19.2	0.54	43.7	0.75
7	GANARASKA RIVER ABOVE DALE	02HD012	R	232	2	1.90E-03	27.6	1.30	48.6	0.82
8	HUMBER RIVER NEAR PALGRAVE	02HC047	R	117	6	2.20E-03	15.2	0.84	60.1	0.96
9	NOTTAWASAGA RIVER AT HOCKLEY	02ED026	R	172.9	4	3.20E-03	14.3	0.92	27.0	1.00
10	SAUGEEN RIVER ABOVE DURHAM	02FC016	R	329	2	1.40E-03	41.7	0.92	26.2	0.57
11	WILLOW CREEK AT MIDHURST	02ED010	R	127	11	1.20E-03	15.7	0.78	41.9	0.60
12	DON RIVER AT YORK MILLS	02HC005	U	95.5	72	2.10E-03	14.9	0.93	87.5	0.68
13	ETOBICOKE CREEK AT BRAMPTON	02HC017	U	67.7	24	4.40E-03	13.0	0.43	66.0	0.48
14	ETOBICOKE CREEK BELOW QEW	02HC030	U	215.4	62	5.10E-03	19.1	0.83	106.2	1.30
15	GRINDSTONE CREEK NEAR ALDERSHOT	02HB012	U	83.9	13	5.00E-03	11.7	0.47	13.6	0.80
16	HARMONY CREEK AT OSHAWA	02HD013	U	43	44	2.60E-03	9.7	0.77	69.7	0.94
17	LITTLE DON RIVER AT DON MILLS	02HC029	U	135.1	70	2.10E-03	14.1	1.10	53.9	1.00
18	MIMICO CREEK AT ISLINGTON	02HC033	U	73.8	87	5.50E-03	11.7	0.90	170.0	0.63
19	REDHILL CREEK AT HAMILTON	02HA014	U	56.3	66	2.70E-03	13.1	0.57	104.0	1.33
20	STONEY CREEK AT STONEY CREEK	02HA022	U	19.2	15	1.00E-02	8.7	0.76	25.6	1.28

Notes: R = rural land-use, U = urban land-use, W_{bf} = bankfull width, h_{bf} = bankfull depth, N_L = normalized reach length, N_S = normalized survey point spacing.

2.3 Methods

2.3.1 Zero-Crossing Analysis

Zero-crossing analysis involves fitting a regression model to each measured bed profile in order to detrend the profile, and the corresponding residuals are used to identify riffles (as positive residuals) and pools (as negative residuals) [*Richards*, 1976]. Both linear and second-order polynomials were fitted to the profiles with all regressions being significant at a confidence level of 95%. The root-mean-square error (RMSE) of the regressions results in a measure of absolute fit of the model, or how much the residuals deviate from a planar bed. Given that channels of different sizes will have inherently different magnitudes of residuals, a scaling parameter is required to compare the RMSE values obtained from different channels. The normalized root-mean-square error (NRMSE) is proposed here, which is defined as:

$$NRMSE = RMSE/h_{bf} \quad \textbf{(2.1)}$$

where h_{bf} is the average bankfull depth.

2.3.2 Bedform Differencing

Bedform differencing involves differencing successive elevations in the downstream direction along a given profile [*O'Neill and Abrahams*, 1984]. An uninterrupted sequence of differences with the same sign (i.e. positive or negative) is defined as a series, and the sum of each series is referred to as a series elevation change. The series elevation changes are then summed to obtain a cumulative elevation change. If the cumulative elevation change exceeds a specified tolerance, a new bedform is identified and the cumulative elevation change is reset to zero. This process is then repeated for the entire profile length. The ability to adequately represent bedforms using this technique is strongly dependent upon the appropriate selection of an elevation tolerance parameter (E_{T}) [*O'Neill and Abrahams*, 1984; *Wooldridge and Hickin*, 2002; *Hanrahan*, 2007]. It has been suggested that $E_{\mathrm{T}} = 0.75S_D$, where $\mathrm{S_D}$ represents the standard deviation of the differenced elevations, be adopted for survey point spacings of approximately one channel width [*O'Neill and Abrahams*, 1984]. When spacing of field-sampled points varies greatly, *Hanrahan* [2007] suggested a tolerance of $E_{\mathrm{T}} = (1/N_S)S_D$. Both tolerances were tested in this study.

2.3.3 Residual Pool Depth Analysis

Residual pool depth analysis was introduced by *Lisle* [1987] as a metric to evaluate pool depths independent of discharge. In pool-riffle dominated morphologies, the residual depth of a point is the difference between the thalweg elevation and the downstream riffle crest. Correspondingly, the residual depths of riffles are

by definition equal to zero. This method has been used to investigate the temporal changes in longitudinal profiles due to large sediment pulses [*Madej*, 1999] and due to the removal of large woody debris [*Lisle*, 1995a], but has not been used to investigate the bed response due to watershed urbanization. Both the mean and standard deviation of residual pool values give a measure of the bed variability in the longitudinal direction. Similar to the zero-crossing analysis, a scaling parameter is required as the magnitude of residual pool values will be different for different sized channels. Average bankfull depth (h_{bf}) has been suggested as an appropriate scaling factor as it remains relatively constant throughout the reach [*Madej*, 1999].

2.3.4 Visual Field Identification

As an additional validation of the objective bedform identification methods, results were compared to the field identified bedform geometries in both datasets [*Annable 1996a*; *Annable et al.*, 2012]. Riffles were characterized as regions of shallow, fast moving water which has a relatively constant flow depth [*Annable*, 1996b] and by changes in substrate coarseness, since the surface layer of riffles is known to be coarser than that of pools [*Leopold et al.*, 1964; *Lisle and Hilton*, 1992]. Conversely, pools were characterized as relatively deep regions with a near horizontal water surface profile (at low discharges) [*Leopold et al.*, 1964]. Field identification methods allow substrate to be considered in addition to geometry, but may introduce possible operator bias as the indicators listed above can vary temporally with stage, with higher stages tending to equalize the water surface slope, making the discrimination between riffles and pools difficult [*Leopold et al.*, 1964]. Substrate indicators can be dependent on flood history, which can cause differences in riffle-pool sedimentation coupling [*Keller*, 1971; *Chartrand et al.*, 2015]. Even without these factors, two different operators may not have the same definition of the beginning and end of a riffle. Nonetheless, visual methods serve as a comparison to the objective method results used here [*Wooldridge and Hickin*, 2002].

2.4 Results

2.4.1 Comparison Between Objective Methods

To compare the different methods, normalized mean riffle spacing (mean spacing between riffles normalized by W_{bf}) and the distribution of normalized riffle spacing for each rural and urban reach are examined (Figure 2.2). Although not presented, similar relative trends are exhibited for the normalized pool spacing.

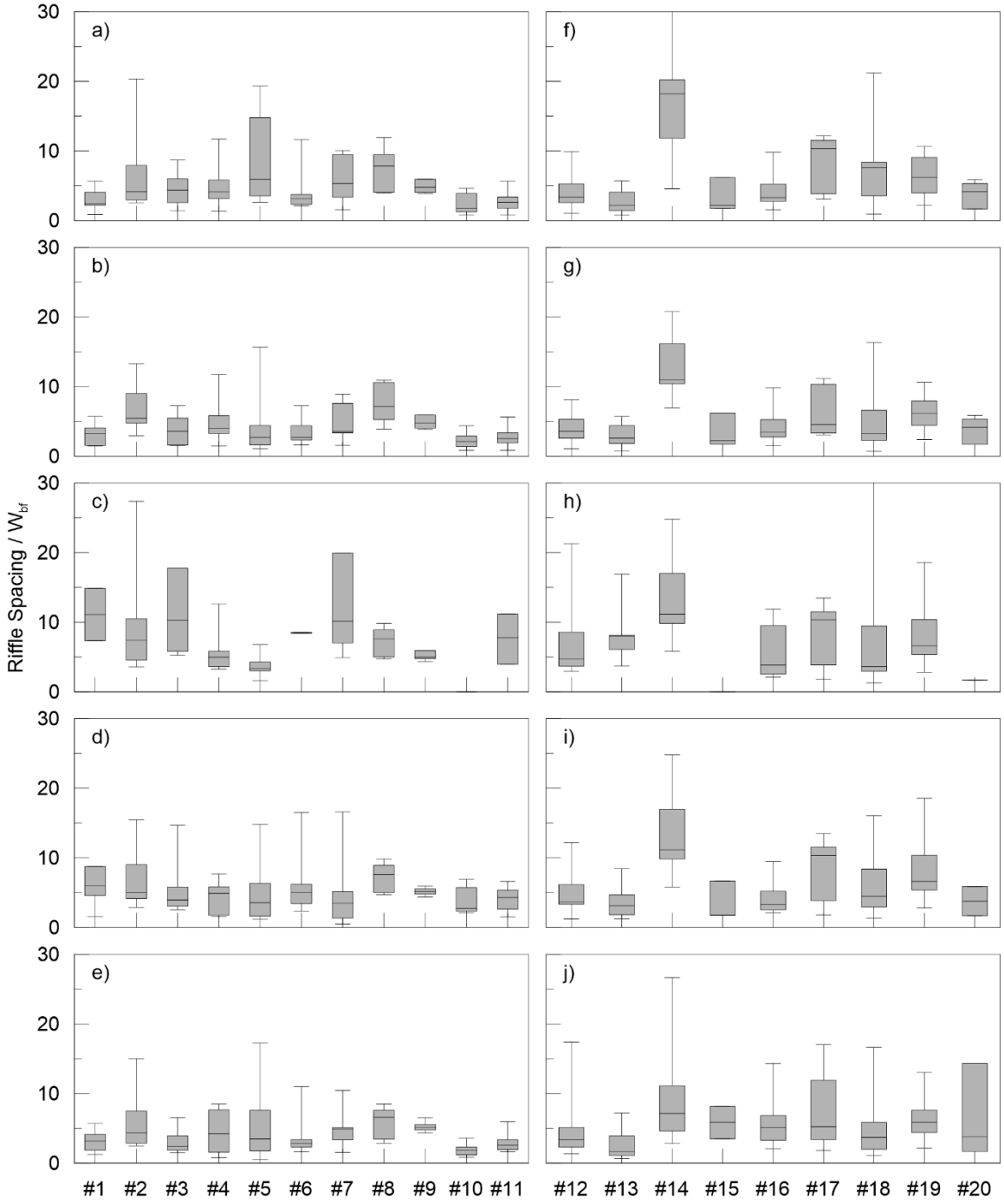

Figure 2.2: Normalized riffle spacing for the rural (left) and urban (right) datasets for a,f) zero-crossing linear regression, b,g) zero crossing nonlinear regression, c,h) bedform differencing with $E_T = (1/N_S)S_D$ tolerance, d,i) bedform differencing with $E_T = 0.75S_D$ tolerance, e,j) residual pool depths. See text for details on methods. Note: f and h are truncated at 30 (#14 and #18 extend beyond).

In general, the bedform differencing method using the $E_T = (1/N_S)S_D$ tolerance (Figures 2.2c and 2.2h) deviates the greatest relative to other methods, arising from several reaches having low N_S values and resulting in a high tolerance unable to capture many of the bedforms present in these reaches. As N_S increases to a value greater than 1.0, results from this method begin to converge on the other tolerance employed ($E_T = 0.75S_D$) (Figures 2.2d and 2.2i), which better aligns with the other methods. The zero-crossing method using linear regression (Figures 2.2a and 2.2f) also results in spacings that often deviate from the other methods. Inspection of the profiles fitted with linear models (Appendix A) reveals that there are certain cases when the linear model missed pools or riffles due to localized reaches of higher or lower elevations relative to the mean downward trend of the channel (Figure 2.3). Especially present in surveys of longer length, longitudinal profiles often exhibit concave shapes which the linear model is unable to characterize. The nonlinear regression model performs as good or better than the linear regression model (Figures 2.2b and 2.2g) as it often captures sub-reaches of different elevations and better fits concave profiles (Figure 2.3). The residual pool depth method (Figures 2.2e and 2.2j) often yields larger riffle spacings as some of the bedforms identified with the other methods are in the pool regions upstream of a large riffle crest. However, the deviations are not as great as the $E_T = (1/N_S)S_D$ tolerance bedform differencing or the zero-crossing linear models.

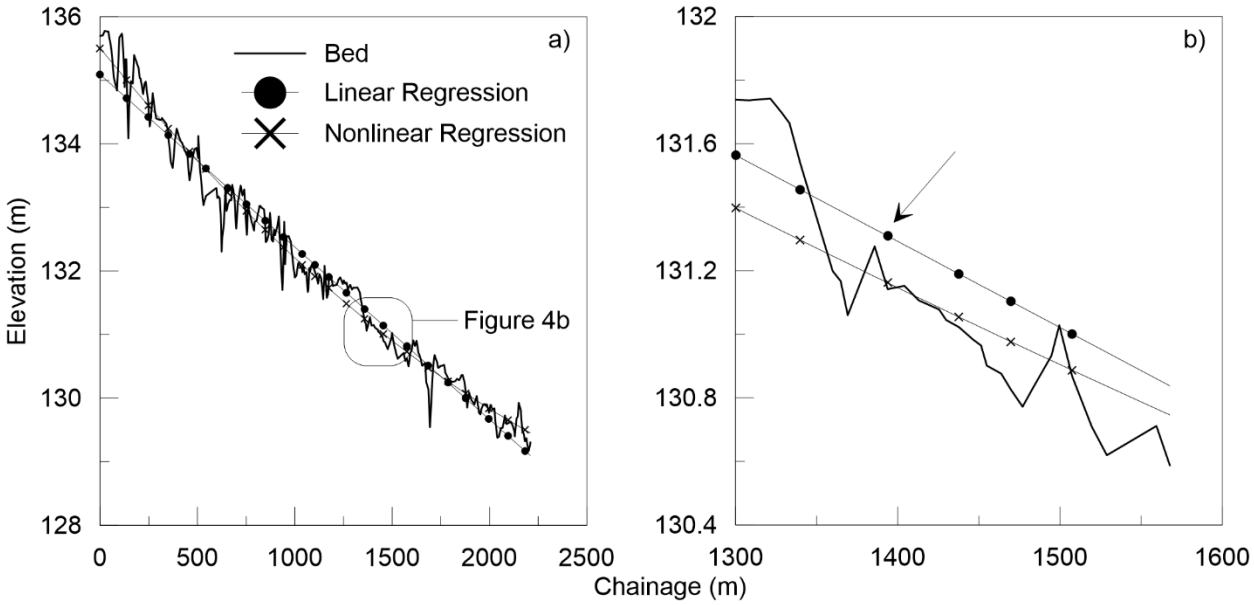

Figure 2.3: Examples of linear regression error for 02HC033.

To examine if longitudinal sample point spacing impacted the resulting bedform frequencies, normalized mean riffle spacings are plotted against normalized survey point spacing (N_S) for each method employed

(Figure 2.4). For all methods except $E_T = (1/N_S)S_D$ tolerance bedform differencing (which already considers N_S in the method), there is a significant ($p < 0.05$) increasing trend, although considerable scatter is still exhibited. However, as previously mentioned, the survey methods considered every significant break in slope and morphologic feature and it was difficult to conclude if the correlation between sample point spacing and riffle spacing is an artifact of the methods involved or simply a consequence of reaches surveyed with higher point densities where increased frequencies in bedform features were observed.

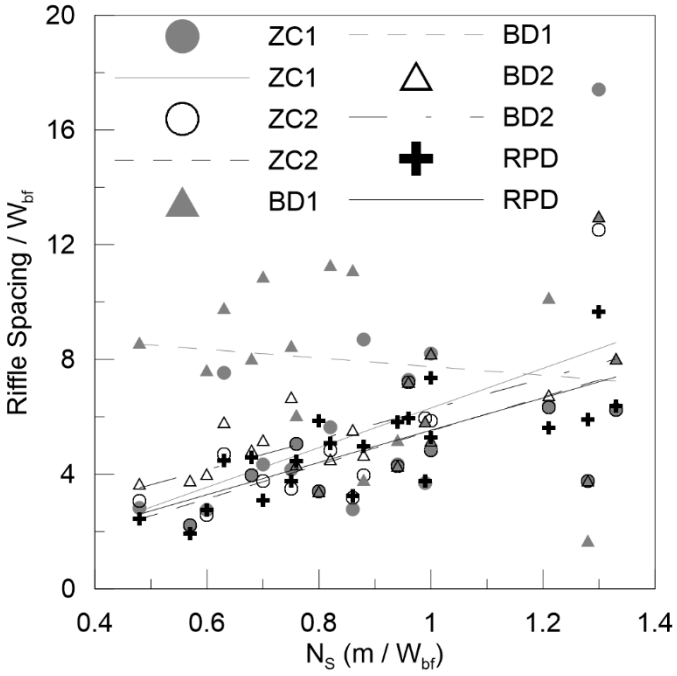

Figure 2.4: Point Density vs riffle spacing for; ZC1 zero-crossing linear regression, ZC2 zero crossing nonlinear regression, BD1 bedform differencing with $E_T = (1/N_S)S_D$ tolerance, BD2 bedform differencing with $E_T = 0.75S_D$ tolerance, and RPD residual pool depths.

Given these comparisons, zero-crossing nonlinear models, $E_T = 0.75S_D$ tolerance bedform differencing and residual pool methods were chosen to examine any trends present between the urban and rural datasets. These methods are referred to hereafter as the zero-crossing, bedform difference and residual pool methods. Detailed results from each objective method are located in Appendix A.

2.4.2 Pool-Riffle Frequency and Riffle Lengths

Normalized riffle spacing from the three selected methods are compared to the percent urban land-use (as determined by *Annable et al.*, [2012]) in Figure 2.5. Considerable scatter is visible with no significant trends (verified with linear regression models, not shown). The three methods were averaged for each

dataset resulting in a mean spacing of 4.6 ± 1.2 and 5.7 ± 2.6 channel widths for rural and urban channels, respectively. A two-tailed t-test fails to reject the null hypothesis of statistical similarity (p=0.24), indicating that there are no significant differences between rural and urban mean riffle frequencies. This is true even when the visible outlier (02HC030) is removed (which decreases the mean riffle spacing for the urban reaches to 4.9 ± 1.4 channel widths), as this is the only point to fall outside the 95% confidence limits in the linear regressions (not shown). The outlier represents an urban reach with different surficial geology (interbedded limestone and shale) which has resulted in a more planar bed with larger spacing between major morphologic units.

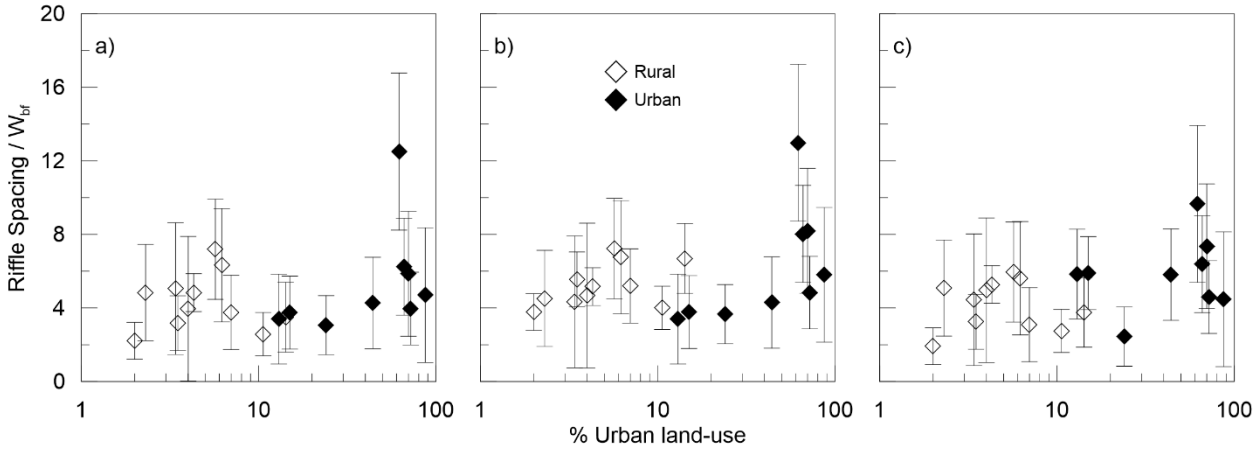

Figure 2.5: Riffle spacing vs percent urban land-use for a) zero crossing nonlinear regression, b) bedform differencing with $0.75S_D$ tolerance, c) residual pool depths. See text for details on methods.

Although not shown, similar results are obtained for riffle lengths. Mean riffle lengths are 2.6 ± 0.8 and 2.4 ± 1.1 channel widths for rural and urban channels, respectively. A two-tailed t-test also fails to reject the null hypothesis of statistical similarity (p=0.31) indicating there is no difference in mean riffle lengths between the rural and urban channels.

2.4.3 Pool Depths and Bedform Variability

Pool depths between urban and rural datasets are evaluated by comparing the normalized mean residual pool depths obtained for each channel (Figure 2.6a). Mean normalized residual pool depths are 0.34 ± 0.13 and 0.49 ± 0.15 for the rural and urban datasets, respectively. A two-tailed t-test determined these two means to be statistically different (p = 0.03), indicating that pool depths are, on average, deeper in urban watercourses. No correlation was found between the normalized mean residual pool depth and the percent urban land-use.

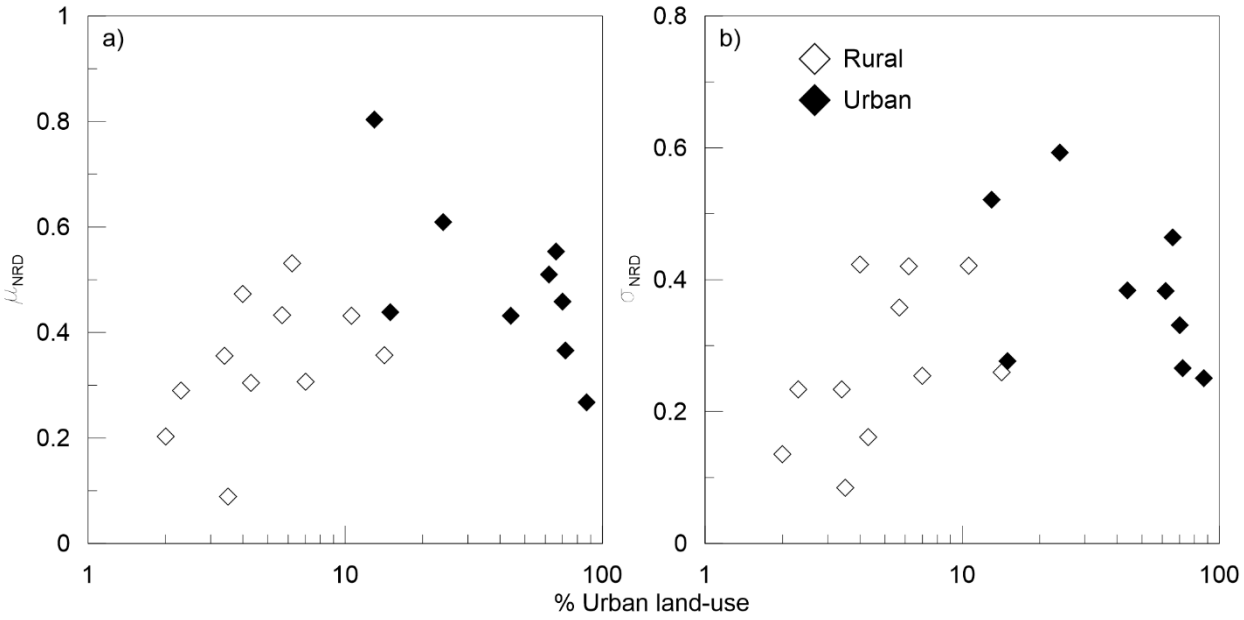

Figure 2.6: a) Mean normalized residual pool depths and b) standard deviation of normalized pool depths for each study reach vs percent urban land-use (residual pool depth method).

Bed variability is assessed using both the standard deviation of normalized residual depths (Figure 2.6b) and the NRMSE for both linear and nonlinear zero-crossing methods (Figure 2.7). A two-tailed t-test found standard deviations of normalized residual depths to be significantly different ($p = 0.05$) between the rural and urban datasets with means of 0.27 ± 0.12 and 0.39 ± 0.12, respectively. A weak correlation was found between the standard deviation of normalized residual pool depths and the percent urban land-use ($p = 0.08$) with a linear-log regression, however, considerable variability exists with the model explaining only 16% of the variability (not shown). The linear regression zero-crossing method yields mean NRMSE values of 0.36 ± 0.15 and 0.45 ± 0.18 for the rural and urban datasets, respectively, while the nonlinear regression yields mean NRMSE values of 0.33 ± 0.12 and 0.43 ± 0.16 for the rural and urban datasets, respectively. While mean NRMSE values for the urban datasets are higher, implying more variability, two-sided t-tests are unable to reject the null hypothesis at the 95% confidence level ($p = 0.22$ and $p = 0.13$ for linear and nonlinear methods, respectively).

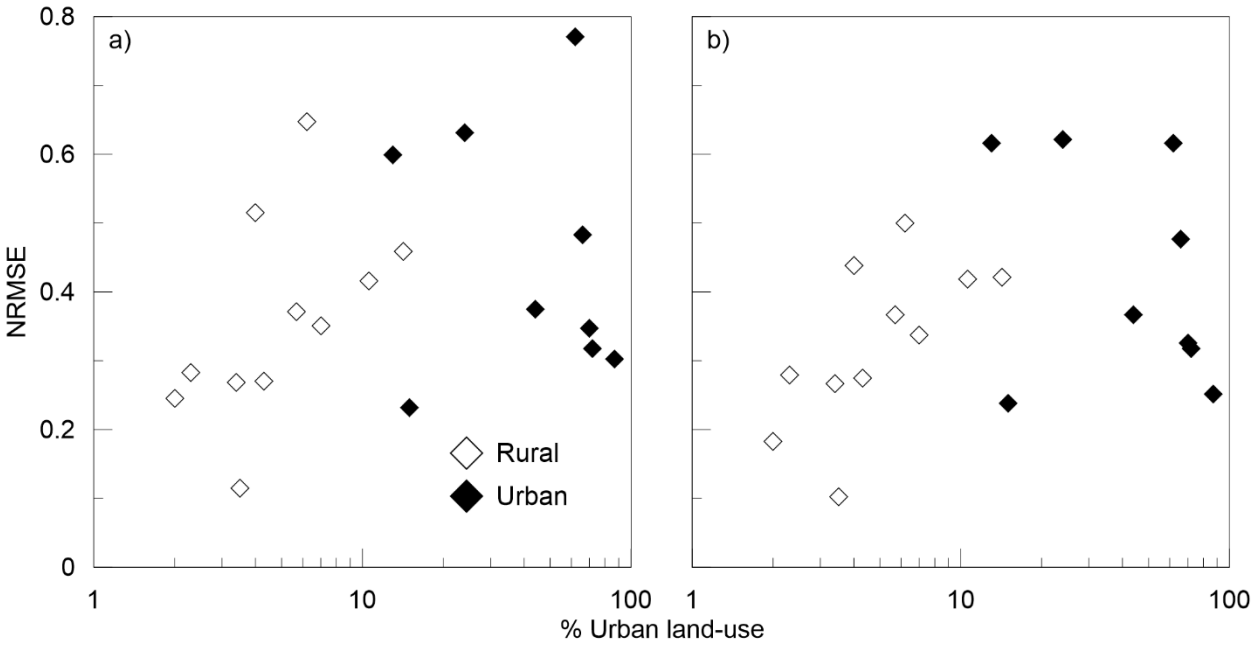

Figure 2.7: a) NRMSE of linear regression and b) NRMSE of nonlinear regression for each study reach vs percent urban land-use.

2.4.4 Comparison with Visual Field Identification

Normalized riffle spacings from field identification are 4.8 ± 1.5 and 6.4 ± 2.2 channel widths for rural and urban channels, respectively. Correspondingly, normalized mean riffle lengths are 2.3 ± 1.0 and 2.1 ± 1.1 channel widths for rural and urban channels, respectively. Comparing the field identified results to riffle spacings and lengths obtained with the objective identification methods reveals no statistical differences between the methods. In both cases, two-sided t-tests fail to reject the null hypothesis of statistical similarity at a 95% confidence level, implying that both field and objective methods yield similar results. Both field and objective methods arrive at similar results for riffle spacing in rural channels, with more scatter present for urban channels (Figure 2.8a). In general, objective methods result in shorter riffle spacings than field methods, especially for urban channels. More scatter exists between these methods for riffle lengths, with objective methods resulting in longer riffle lengths than field methods (Figure 2.8b). A possible explanation for the increased scatter in lengths is that the objective methods do not differentiate between riffles and runs, which are separated in the field methods.

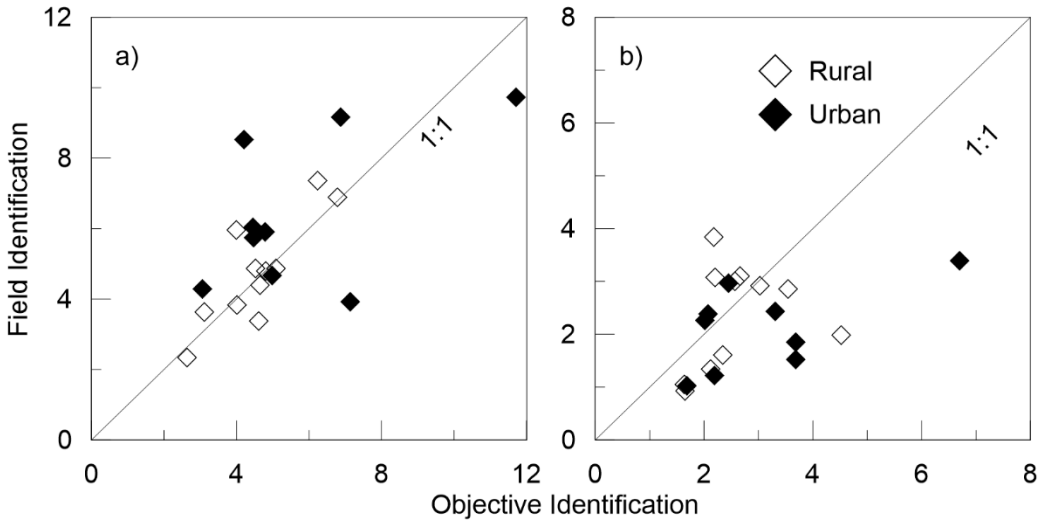

Figure 2.8: Comparison between objective methods and visual field identification for a) normalized riffle spacing and b) normalized riffle lengths.

2.5 Discussion

The similarities in pool-riffle spacing between urban and rural datasets are not surprising. Although *Annable* [2010] commented on an increased pool-riffle frequency for urban channels, this was due to a reported increase in meander wavelength, and not a decrease in the spacing relative to channel width. This can be interpreted as an increase in pool-riffle frequency relative to the common relationships associated with meander geometry [*Leopold et al.*, 1964]. Further, although the common pool (or riffle) spacing is 5-7 channel widths [*Leopold et al.*, 1964; *Keller and Melhorn*, 1978], considerable natural variability can still exist within free forming pool-riffle morphology [*Keller and Melhorn*, 1978]. Variability in pool-riffle sequences can also arise from forcing features such as large woody debris or channel obstructions [*Lisle*, 1986; *Montgomery et al.*, 1995]. Regardless of watershed land-use, pool-riffle sequences are known to be relatively stationary once developed, unlike bedforms in sand bed streams [*Leopold et al.*, 1964], further enforcing that major rearrangements (detectable using statistical methods with a relatively small sample size) of these large bed features would not likely occur.

Although the watercourses evaluated here are within a similar hydrophysiographic region, local variations in geology and valley morphology can also influence this sequence, but in general pool-riffle sequences tend to develop with similar patterns independent of bed geology [*Keller and Melhorn*, 1978], although this was not evaluated in this study. Forcing elements can considerably alter pool-riffle sequences [*Lisle*, 1986;

Montgomery et al., 1995]. In urban streams, these may be bridge abutments, storm sewer outfalls, grade control structures or other anthropogenically introduced material. Large anthropogenically introduced material, such as rip-rap commonly used for bank protection or traditional revetments, was observed in many of the bedforms present in the urban streams (arising from failed channel works) resulting in a bed armoring layer disproportionately large in size to the naturally derived bed and bank material supply. These combined factors could be resulting in the larger standard deviation associated with mean riffle spacing of urban channels studied here (confirmed with both objective and field methods), however, the methods used in this study did not differentiate between naturally forming pool-riffle sequences or forced sequences so no conclusive evidence can be drawn.

The increased topographic variability identified in urban reaches, although subtle, supports the field observations of *Annable* [2010] who observed additional "in-line pools" which did not correspond to pools associated with the outside of bends, which are a common characteristic of pool-riffle morphologies. These in-line pools were described as having a shallower depth relative to bend pools, which supports why these were not identified in the objective bedform identification methods, which are only suited for identifying major bedform units [*Wooldridge and Hickin*, 2002]. These shallower pools would, however, correspondingly increase the bed variability, which is indicated by the results presented in this study (Figures 2.6b, 2.7a and 2.7b).

Increased pool depths are also consistent with observations made in urbanizing pool-riffle morphologies of the Eastern United States [*Hawley et al.*, 2013]. As a primary response to urbanization is known to be channel incision [*Schumm et al.*, 1984; *Booth*, 1990], it follows that deeper pools would be expected as a form of channel response to the urban hydrologic and sediment supply regimes. Deeper pools would also serve as an extra form of energy dissipation, much like a plunge pool below a hydraulic structure, such as those common in stream restoration [*Scurlock et al.*, 2012]. Pools are known to scour at flows above bankfull and begin to fill as the stage drops below this threshold [*Leopold et al.*, 1964; *Lisle*, 1979]. However, an increase in flood events above this threshold could result in additional scour relative to fill. Urban streams in this study have been documented to have an increased average annual frequency of bankfull discharge events relative to rural streams (Figure 2.9), supporting the observed deeper pools. Increased flood events of the urban channels also supports the theory of additional energy dissipation. Bed material supply has been documented to be a controlling factor for pool depths [*Whittaker and Davies*, 1982; *Buffington et al.*, 2002], erosion rates and bed surface texture [*Pfeiffer et al.*, 2017]. In a flume study

with forced steps, maximum pool depths corresponded to the lowest bed material supply rate [*Whittaker and Davies*, 1982]. Bed material supply has been suggested to decrease with urbanization [*Annable et al.*, 2012], which could also be a contributing factor to the observed differences. A higher frequency of channel obstructions in urban channels (storm sewer outfalls, bridge abutments and grade control structures) could also contribute to greater pool depths [*Buffington et al.*, 2002].

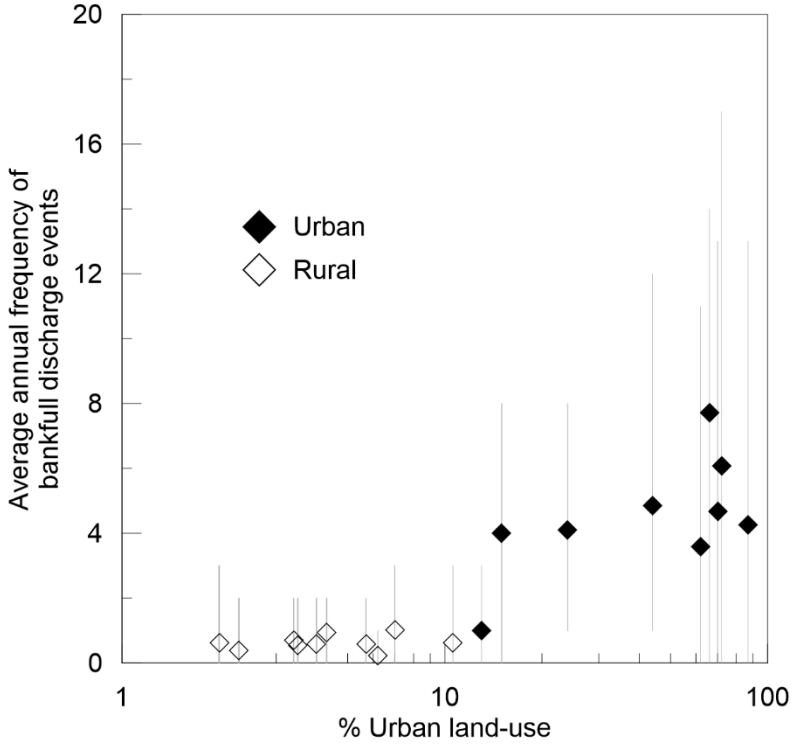

Figure 2.9: Average annual frequency of bankfull discharge events for each study reach [modified from *Annable et al.*, 2012]. Error bars represent annual range throughout the study period [*Annable et al.*, 2012].

Urbanization is known to change the hydrologic regime of a watershed by increasing flood peaks and frequencies, while decreasing lag-times and event durations [*Leopold*, 1968; *Hollis*, 1975; *Hawley and Bledsoe*, 2011; *Annable et al.*, 2012]. These changes in hydrology introduce additional erosive energy into the river system, and consequently channels undergoing watershed urbanization have been documented to depart from their previous morphologies towards a new quasi-equilibrium condition in balance with the new hydrologic and sediment regimes [*Hammer*, 1972; *Booth*, 1990; *Pizzuto et al.*, 2000; *Chin*, 2006; *Hawley and Bledsoe*, 2013]. Evidence from this study suggests that riverbeds in gravel-bed, pool-riffle morphology dominated watercourses are becoming more topographically variable as a manifestation of this

increased erosive energy. Increased topographic variability is suggested to act as additional form roughness to compensate for the increase in small to intermediate discharge events common to urbanization [*Hollis*, 1975; *Booth*, 1990]. Form roughness has been documented to be more significant at low to medium flows before it becomes drowned out [*Parker and Peterson*, 1980]. However, evidence also exists which suggests that form roughness can still dominate at bankfull flows [*Millar*, 1999]. Additional form roughness due to increased topographic variability, whether they be from in-line pools (discussed in the previous paragraph) or simply deeper bend pools could be the subtle development of a new quasi-equilibrium characteristic in urban gravel-bed watercourses.

The limited number of watercourses studied here presents a sample size limitation which can decrease the power of the statistical tests used in the analysis. It is possible that an increased sample size would yield different results, although it would require a dataset which extends to different hydrologic and physiologic regions, which would further confound the results. Moreover, the different survey lengths of the study reaches may be providing bias to the overall results since some reaches will inherently include more bedforms than others. A standardized reach length could be used to reduce this possible bias, although in order for all reaches to be included, this standardized reach would need to be small (Table 2.1). It is desirable to have the longest possible survey reach to include the most bedforms and variability. As such, the total surveyed lengths of each reach were used.

These results have implications on the prediction of flood elevations, as additional form roughness may cause elevated water levels. This is particularly important in urban areas due to the increased potential for infrastructure damage and human risk. Additionally, increased topographic variability has implications for the design of stream restoration projects in urban channels. Many of the common techniques are based on relationships derived from forested streams [*Newbury and Gaboury*, 1993; *Rosgen*, 1996] and may not be representative for systems with altered hydrologic and sediment regimes.

2.6 Conclusions

Longitudinal profiles of 11 rural and 9 urban watercourses with pool-riffle dominated morphologies in the same hydrophysiographic region of southern Ontario, Canada were investigated using three objective bedform identification methods; zero-crossing analysis, bedform differencing technique and residual pool analysis in addition to visual field identification. Objective and field methods both produced comparable results. Results revealed considerable scatter in the pool-riffle spacing, with no differences found between

rural and urban channels. A significant difference was found for average pool depths and topographic variability, with urban watercourses possessing both deeper pools, and more topographic variability. Deeper pools in the urban channels are considered to result from a reduced bed material supply and an increased frequency of channel obstructions. Additionally, they are speculated to be a means of dissipating additional energy due to the increased erosive potential of the altered hydrologic regime. Additional topographic variability is suggested to be a manifestation of the increased energy introduced through watershed urbanization, which effectively increases the form resistance of the channel. These results have implications for the prediction of flood elevations, as additional form roughness may cause elevated water levels. This condition is particularly important in urban areas due to the increased potential for infrastructure damage and human safety. Additionally, the increased topographic variability of bedforms demonstrated here has implications for the design of urban stream restoration projects as they may differ from rural watershed conditions.

Transition Paragraph A

Urbanization has commonly resulted in alterations to channel morphology. While changes associated with gravel bedforms have been less documented, currently available literature reports similar trends. In the previous chapter we documented differences in longitudinal profile characteristics and bedforms between rural and urban rivers. These documented changes align with existing research and are hypothesized to result from alterations to hydrology and sediment supply commensurate with urbanization. Our current understanding of the channel processes influencing these changes (namely bedload transport) is limited due to the lack of process based field studies conducted in urban rivers. The objective of this chapter[1] is to characterize bedload transport processes in a highly urbanized river. We used multiple methods to measure both coarse and fine non-cohesive particles comprising the transported bedload. A fractional bedload transport dataset spanning most of the range of particles present on the bed (from sand to large cobble keystones) in an urban river has not been documented in published literature to this date, and the results are significant as they can be compared to other datasets from rivers with more natural flow regimes. A strong link was found between coarse particle mobility and the dynamics of finer material which tends to dominate the bedload. Coarse particle mobility is very low and particles transport at much shorter distances than those reported in literature. Finer bed material is more variable when coarse particles are less mobile. Another objective of this chapter is to investigate how changes in hydrology common to urbanization change geomorphically significant discharges. Measured transport data were used to calibrate a fractional sediment transport model which was combined with hydrometric data corresponding to different levels of watershed urbanization to perform a geomorphic work analysis. Urbanization is increasing the frequency, volume and time of competent discharge events (capable of performing work on the channel). Greater increases of intermediate discharge events are observed. Less urban streams are more influenced by larger discharge events, while urbanization is shifting the geomorphic significance to lower (but still competent) discharges.

[1]Plumb, B. D., W. K. Annable, P. J. Thompson and M. A. Hassan (*in review*), The impact of urbanization on temporal changes in sediment transport in a gravel-bed channel in Southern Ontario, Canada, *Water Resources Research*.

Chapter 3

The Impact of Urbanization on Temporal Changes in Sediment Transport in a Gravel-bed Channel in Southern Ontario, Canada

3.1 Introduction

Land-use change alters both the spatial and temporal distribution of how water is delivered to channels, often referred to as hydromodification. Urbanization, a cause of hydromodification, has been documented to change the amount of runoff generated from a rainfall event, resulting in a change to event-based hydrograph characteristics by increasing flood peaks, decreasing lag-times and decreasing event durations [*Leopold*, 1968; *Hollis*, 1975; *Hawley and Bledsoe*, 2011]. Increases in runoff and drainage density common to urbanization also results in an increased frequency of small-to-intermediate discharge events [*Booth*, 1990], which can alter the frequency and duration of potential channel maintaining or channel forming flows observed in a given watershed [*Annable et al.*, 2011].

Hydromodification combined with spatial and temporal changes in sediment supply to urbanizing streams have resulted in historically observed alterations to channel morphology. Increases in sediment loading from the release of construction (suspended) sediment during the early phases of urbanization [*Wolman*, 1967] were historically documented to result in channel deposition and bed fining [e.g. *Leopold*, 1973]. After the construction phase, a frequently observed change is channel enlargement, either through incision, widening, or a combination thereof [*Hammer*, 1972; *Booth*, 1990; *Pizzuto et al.*, 2000; *Chin*, 2006; *Hawley and Bledsoe*, 2013]. The long-term impact that urbanization has on channel bed structure has been less documented than changes to the overall channel cross-section. Bed coarsening has been observed in gravel-bed streams undergoing urbanization [*Finkenbine et al.*, 2000; *Pizzuto et al.*, 2000; *Annable et al.*, 2012; *Hawley et al.*, 2013]; however, there is a lack of knowledge on how channel bedforms and bed morphology have evolved under a hydromodified regime, especially pertaining to gravel-bed channels. In riffle-pool dominated morphologies, a shortening of riffles and corresponding lengthening and deepening of pools in channels were found to be consistent with increasing watershed urbanization [*Annable*, 2010; *Hawley et al.*, 2013]. *Annable* [2010] also found a greater frequency of riffle-pool sequences in a study of 12 urban gravel-bed streams in Southern Ontario which have undergone significant hydromodification.

Since urbanization is known to increase the frequency of low-to-intermediate magnitude floods [*Konrad et al.*, 2005; *Chin*, 2006; *Thompson*, 2013], applying this observation to the geomorphic effectiveness hypothesis of *Wolman and Miller* [1960] suggests that urbanization should change the frequency at which the effective discharge occurs. This hypothesis combines the frequency of flows and the corresponding work performed by each of the flows to arrive at a discharge that transports the maximum amount of sediment in the long term, commonly referred to as the effective discharge. It has been applied to gravel-bed channels using both bedload transport models [*Andrews*, 1980; *Torizzo and Pitlick*, 2004] and measured bedload rating curves [*Emmett and Wolman*, 2001].

The effective discharge has been suggested to equal the channel-forming discharge in floodplain dominated morphologies, also commonly referred to as the bankfull discharge [*Wolman and Miller*, 1960; *Leopold et al.*, 1964; *Andrews*, 1980]. Effective and bankfull discharges have also been shown to be different, with effective discharges being commonly less than the respective bankfull discharge [*Benson and Thomas*, 1966; *Pickup and Warner*, 1976; *Lenzi et al.*, 2006; *Hassan et al.*, 2014].

The general concept of a single channel-forming discharge has also been challenged, notably in gravel-bed rivers. Instead, multiple effective discharges have been suggested with lower, more frequent, discharges corresponding to channel maintaining discharges (e.g. low bars, pool scouring, sediment redistribution) and higher, less frequent, discharges corresponding to channel-forming discharges (e.g. channel cross-section, planform, macro-scale bedforms) [*Lenzi et al.*, 2006; *Surian et al.*, 2009; *Hassan et al.*, 2014]. Additionally, effective discharge analyses in gravel-bed rivers have suggested that only bedload transport is important when considering channel-forming processes [*Lenzi et al.*, 2006].

Little emphasis has been placed on quantifying the geomorphic significance of the increase in small to intermediate events common in urbanizing watersheds. Effective discharge is often used as a surrogate for the channel forming discharge in stream rehabilitation projects, which are becoming increasingly common in urban areas [*Bernhardt et al.*, 2005; *Kenney et al.*, 2012]. It is of interest to know how the geomorphic work accomplished by different discharges (the fraction of sediment moved by each discharge class) changes with increasing urbanization, so that this can be accounted for when performing channel rehabilitation designs in these conditions. The geomorphic work analysis is a suitable method for assessing the relative changes in flood magnitude and frequency of the bedload transport characteristics of a gravel-bed river. The strength of this approach is that it can be calibrated with field measurements. Specific

objectives of this study are: 1) to characterize the bedload transport dynamics in an existing highly urbanized stream; and 2) to use magnitude-frequency concepts (geomorphic work) to investigate how the hydromodification resulting from urbanization has impacted the temporal sediment transport characteristics of the same stream.

This study addresses the first question using field sediment transport measurements (both direct pressure-difference sampler and indirect tracer particle methods) collected from a highly urbanized gravel-bed stream taken over a three-year period. To address the second question, the sediment transport measurements are used to calibrate a fractional bedload transport model which is combined with hydrometric gauge data from Environment Canada for two streams to create four hydrologic scenarios representing four different land-use conditions. For each scenario, the magnitude-frequency and cumulative time, water volume and sediment transport exceedance characteristics are evaluated for a set of commonly employed geomorphic indicator discharges, including the threshold discharge, bankfull discharge, effective discharge and half-load discharge. We expected to see an increase of the relative portion of sediment transported by discharges corresponding to intermediate floods, as those commonly increase with urbanization. Additionally, we expected to see less transport of the coarse particles due to the highly armored nature of the study reach.

3.2 Field Sites

The majority of the study focuses on Mimico Creek, where all field measurements were conducted. Hydrometric data from the upper watershed of Etobicoke Creek were used to supplement the magnitude-frequency analysis, which is further explained in the methodology sections.

Mimico Creek is located in Toronto, Ontario, Canada and discharges directly into Lake Ontario (Figure 3.1). A large portion of the upper watershed consists of glaciolacustrine deposits which transition to Halton till, resulting from the late Wisconsinin period [*OGS*, 2010]. The majority of the watershed is urbanized (85% total developed area) with the headwaters dominated by industrial and residential land-use, the mid-region dominated by industrial land-use and the lower portion of the watershed dominated by residential uses. Stormwater management (SWM) controls (e.g. SWM ponds) within the watershed are lacking, with less than 30% of the urban area having any stormwater management control and only 10% having stormwater controls pertaining to erosion control (e.g. specific volume capture and not just peak-flow shaving) [*TRCA*, 2010]. Inspection of aerial photographs of the watershed indicates that the non-urban land

consists of golf courses, meadows, parkland and riparian corridor, with little forest. These areas are well vegetated and are not likely major sediment sources for the channel. Inspection of the stream and tributaries upstream suggests that the dominant sediment source is derived through bank erosion, which has been suggested as being the major contributor to long-term sediment yield in urban streams [*Trimble*, 1997; *Nelson and Booth*, 2002]. Two in-line flood control structures (detention basins) located in the upper portion of the watershed (upstream of the study reach) are acting as sediment sinks, however the exact extent to which they disrupt the sediment continuity is unknown.

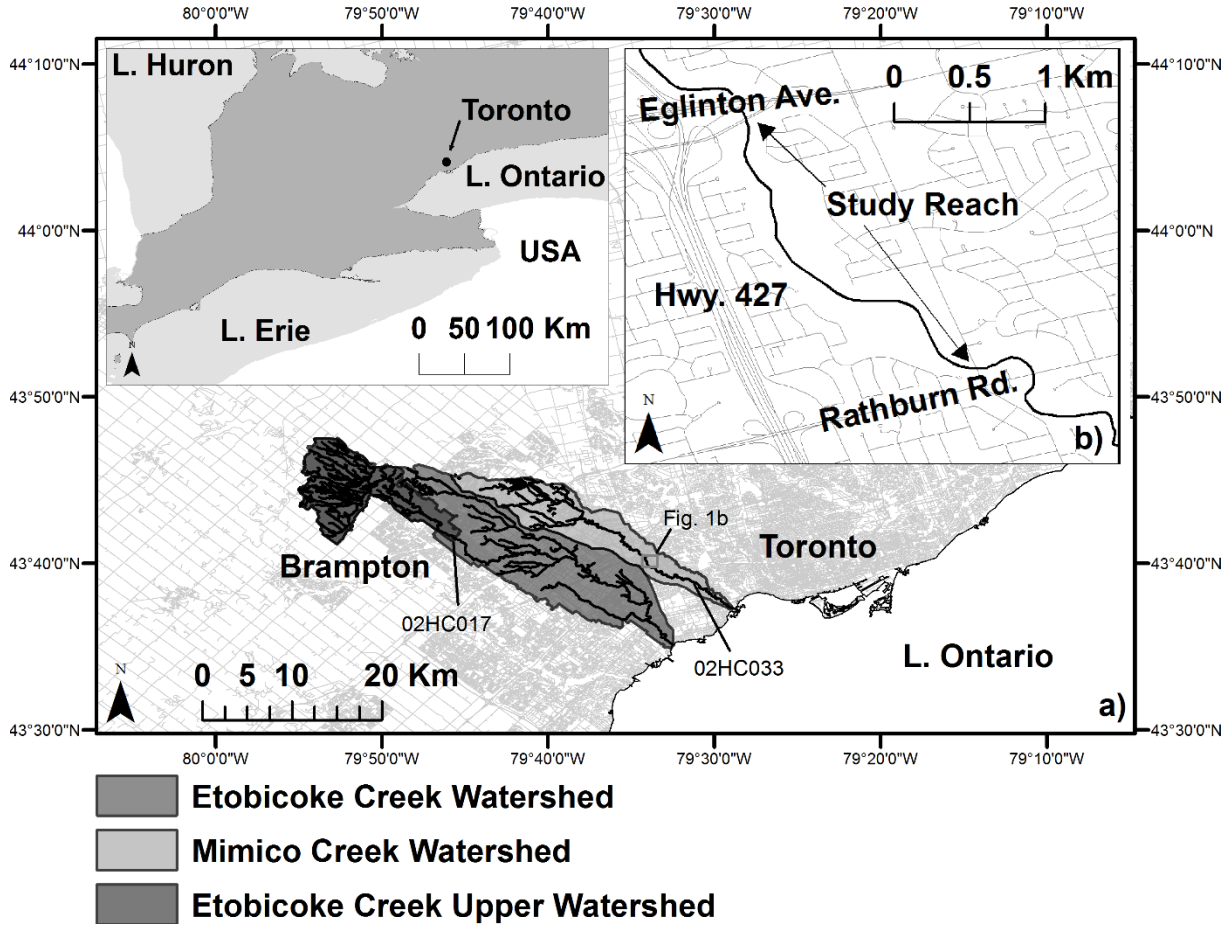

Figure 3.1: a) Mimico and Etobicoke Creek watersheds and b) Mimico Creek study reach.

The 1.8 km study reach is located in the lower portion of the watershed (Figure 3.1). The dominant morphology of the reach is a single-thread riffle-pool morphology [*Montgomery and Buffington*, 1997] with an average gradient of 0.4%, average bankfull width of 13 m (Table 3.1) and 25 riffle-pool sequences. The grain size distributions are consistent with other gravel-bed rivers, exhibiting a bimodal distribution with a

secondary peak in the sand fraction (Figure 3.2). A hydrometric gauge station (02HC033) with a 50-year record, operated by Environment Canada, is located a short distance downstream with no major tributaries entering the stream between the study reach and gauge such that continuity of flow can be assumed. This gauge provides 15-minute discharge data using the stage-discharge rating curve method.

Table 3.1: Mimico Creek general characteristics. D_{isurf} and D_{isub} define the ith percentile for the bed surface and subsurface, respectively.

Effective watershed area (km^2)*	73.8
Current percent urban land-use*	87
Study reach slope (%)	0.4
Study reach length (km)	1.8
Study reach average width (m)	13.0
D_{16surf} / D_{50surf} / D_{84surf} (mm)	8 / 48 / 183
D_{16sub} / D_{50sub} / D_{84sub} (mm)	0.9 / 7 / 35

*Annable et al. (2012)

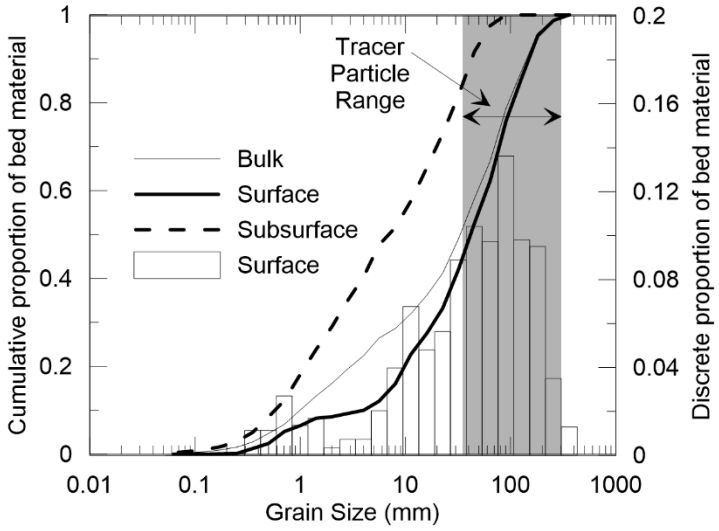

Figure 3.2: Grain size distributions of subsurface, surface and bulk mixture (combination of surface and subsurface) for Mimico Creek.

Etobicoke Creek is located immediately west of Mimico Creek (Figure 3.1). While the entire watershed is larger than Mimico Creek, the upper watershed (Environment Canada Gauge 02HC017) has a similar watershed size (67.7 km^2), geology and channel morphology to Mimico Creek [*Annable et al.*, 2012]. The

major difference is the land-use conditions, with the upper portion of Etobicoke Creek only having approximately 24% urban land-use [*Annable et al.*, 2012].

3.3 Field Methods

3.3.1 Bed Material Sampling

Bed material was characterized by a combination of modified *Wolman* [1954] pebble counts, and diagnostic volumetric sampling [cf. *Church et al.*, 1987; *Bunte and Abt*, 2001]. Approximately 1300 pebbles were measured along the riffles throughout the reach. Four large representative volumetric samples (~300kg in total) were obtained, separating surface and subsurface samples. The surface layer was determined as the depth of the largest particle present on the surface and the sub-surface was sampled to the same layer thickness [*Church et al.*, 1987; *Bunte and Abt*, 2001]. The large number of pebble count samples were merged with the surface fraction of the volumetric samples [cf. *Bunte and Abt*, 2001]. This was done to account for the shortcomings of both methods; pebble counts being unable to adequately represent finer material present on the bed [*Rice and Church*, 1996] and the very large volume of sediment required to adequately represent the large particles present on the bed [*Church et al.*, 1987].

3.3.2 Sediment Transport Measurements

Bedload transport sampling was segregated into two major components in order to capture the mobility characteristics of both the coarse particles (less frequently mobile) and the finer (non-cohesive) particles (which typically constitute the majority of the frequently transported bedload). Sampling of the coarse particle transport was conducted using tracer particles embedded with unique radio-frequency identification (RFID) tags [*Nichols*, 2004; *Lamarre et al.*, 2005]. A total of 550 tracer particles were seeded in November 2011 on riffles throughout the reach. The grain-size distribution of tracer particles spanned between D_{40surf} and ~D_{max} (largest grain class present on the bed) (Figure 3.2), with the smallest tracer size set due to the physical limitations of drilling RFID tags into the particles. Particle mass and a, b and c axis dimensions were recorded prior to seeding. Tracer surveys occurred after every competent flood and were performed using an Aquartis Leone system with a 0.5 m diameter detection loop and spatially referenced using a differential GPS.

Bedload sampling was conducted during competent floods using a modified single width increment method [*Edwards and Glysson*, 1988] with 0.076 m Helley-Smith samplers [*Helley and Smith*, 1971]. This method involves dividing the channel into equal-width "panels" and obtaining a bedload sample at the mid-point

of each panel. Due to the rapidly fluctuating hydrographs characteristic of Mimico Creek (with between 500% and 7000% increases in discharge in 2-7 hours), it was difficult to obtain the recommended 20 samples along the channel width while assuming quasi-steady state discharge, as outlined by *Emmett* [1980]. The number of sampling points (between 4 and 8), and corresponding panel widths (between 0.5 m and 2 m), were varied based on the flashiness of each specific hydrograph, which was verified in the field based on frequent stage measurements using a staff gauge located at the bedload sampling site. The percent difference in discharge for a single transect ranged from 3% to 33%, with the larger differences corresponding to the lower discharge samples (e.g. a change of 2 m^3/s, from 7 m^3/s to 9 m^3/s throughout the transect). Samples were dry sieved in the laboratory at a half-phi scale.

3.4 Data and Analysis

3.4.1 Fractional Transport Analysis

A dimensionless bedload rating curve was developed following the methods of *Parker et al.* [1982]. The weighted dimensionless bedload flux for each grain fraction, i (q^*_{bi}), was computed as:

$$q^*_{bi} = \frac{q_{bi} F_i^{-1}}{\left\{[(\rho_s/\rho_w) - 1] g D_{gi}\right\}^{0.5} D_{gi}} \quad \textbf{(3.1)}$$

where ρ_s is the sediment density (assumed to be 2650 kg/m^3), ρ_w is water density (assumed to be 1000 kg/m^3), D_{gi} is the geometric mean of the i^{th} grain class, F_i is the fraction of the i^{th} grain class in the bed surface material, and q_{bi} is the volumetric bedload flux of the i^{th} grain class, computed from the measured bedload samples. Similar to other studies [Ashworth and Ferguson, 1989; Whiting and King, 2003], several sediment bedload flux equations were also plotted for reference [Meyer-Peter and Muller, 1948; Brown, 1950; Parker, 1978].

Fractional transport rates ($p_i q_{bi}$), where p_i is the fraction of transported material for particle class i, were also weighted by each particle class's respective fraction of the bulk sediment mixture, f_i. In this study, the bulk sediment fraction was chosen as it is more representative of material being transported over the bed, which includes material derived from bank erosion and not just material derived from the bed surface [*Church and Hassan*, 2002]. Similar to *Church and Hassan* [2002], the surface material was characterized using pebble counts, and as such, may be biased towards larger sizes. Using the bulk fraction eliminates this bias.

3.4.2 Tracer Recovery, Mobility and Transport Distances

Total and event-based recovery and mobility percentages were obtained using relationships consistent with previous tracer studies in order to characterize the total and event-based mobility of coarse particles [*Einstein*, 1937; *Ashworth and Ferguson*, 1989; *Church and Hassan*, 1992; *MacVicar and Roy*, 2011; *Schneider et al.*, 2014]. Total recovery rates (P_r) for each tracer survey were calculated by $P_r = N_f/N_t$, where N_f and N_t are the number of particles found in each survey and the total number of seeded particles, respectively. Event-based recovery rates (P_{revb}) were determined for the i^{th} survey by $P_{revb(i)} = N_{fevb(i)}/N_{f(i-1)}$, where $N_{fevb(i)}$ is the number of tracers found in each survey that were also found in the previous survey. The percentage of mobile particles (P_m) was determined using $P_m = N_m/N_f$, where N_m is the number of mobile particles in a given survey. Correspondingly, the event-based percentage of mobile particles (P_{mevb}) was determined by $P_{mevb} = N_{mevb}/N_{fevb}$, where N_{mevb} is the number of mobile particles which were also found in the previous survey.

Individual transport distances (path lengths) were computed from measured coordinates of a given tracer between two successive tracer surveys, and assigned as the net travel distance relative to the channel thalweg. Mean transport distances were computed considering both total particles found in a survey and only mobile particles found in a survey by taking the arithmetic mean of both datasets. Additionally, tracer particles were binned in half-phi grain classes, and the mean transport distance determined for each.

In order to compare the relative travel distance of particles in this system to others reported in literature, scaled transport distances (L^*) were calculated and compared to the empirical relationship of *Church and Hassan* [1992], expressed as the following:

$$L^* = L_i/L_{D50surf} = 1.77[1 - \log_{10}(D_i/D_{50sub})]^{1.35} \quad \textbf{(3.2)}$$

where L_i is the transport distance for a specific particle with diameter D_i, $L_{D50surf}$ is the mean path length of the median surface particle class and D_{50sub} is the median particle diameter of the bed material subsurface. For this study, $L_{D50surf}$ was obtained as the mean transport distances of all particles that fell into the half-phi class which contained the D_{50surf} particle size. D_{50sub} was replaced with D_{50bulk} (median grain size of entire bed mixture, including surface and subsurface) due to the highly armored nature of Mimico Creek (D_{50surf}/D_{50sub}, defined as the armor ratio, of 5.6). Equation (3.2) has been suggested to describe a path length distribution where the largest fractions are only partially mobile [*Wilcock*, 1997]. *MacVicar and Roy* [2011] found the following equation to better describe particle path lengths of unconstrained clasts:

$$L^* = L_i/L_{D50} = (D_i/D_{50})^{-2.0} \quad \textbf{(3.3)}$$

where L_{D50} was replaced with $L_{D50surf}$ and D_{50} was replaced with D_{50bulk} to facilitate comparison between Equations (3.2) and (3.3). Comparing the path length distributions to these two relationships will facilitate in the overall characterization of the transport type and whether the coarse particles behave as unconstrained stones or are influenced by other particles on the bed.

3.4.3 Hydraulic Modeling and Hydrologic Analysis

Hydraulic modeling using HEC-RAS [*USACE*, 2004] was performed to obtain reach averaged shear stress required for sediment transport modeling. A calibrated model using a quasi-steady approximation resulted in a relationship between shear stress and discharge which was combined with the sediment transport model (discussed in Section 3.4.4).

Two field calibrated discharges were established to differentiate between low and high magnitude discharge events. The bankfull discharge (Q_{bf}) of ≈ 20 m^3/s was identified as the stage corresponding to the crests of point bars and cross-sectional break indicators such as depositional benches in straight sections of the reach, which were all in general agreement of each other [cf. *Annable et al.*, 2011]. Discharge was calibrated during several floods by noting the time at which the stage reached the bankfull indicators along the reach and reconciling the time with the discharge estimated at the gauge. This value is further supported by a 15-year study on a reach located a short distance downstream, which yielded a bankfull discharge of 18.4 m^3/s [*Annable et al.*, 2012]. The threshold discharge (Q_{thres}) of ≈ 8 m^3/s is defined as the discharge at which any sediment entrainment occurs. This was verified during the Helley-Smith bedload sampling campaign during several flood events as the discharge below which no (or very little) sediment was collected in the samplers over a long sampling duration (> 1 hour).

Hydrometric gauge data (15-minute instantaneous) were used for the geomorphic work analysis. To assess the incremental impacts of urbanization, the Mimico Creek streamflow records were augmented with records from the upper watershed of Etobicoke Creek in a space-for-time substitution. The streamflow records for Etobicoke Creek begin in an unaltered watershed condition (rural agriculture land-use but not urban), while Mimico Creek was already approximately 40% urban at the beginning of the hydrometric record (1969 for both sites). Etobicoke Creek and Mimico Creek (Figure 3.1) have similar effective watershed areas (defined as the watershed area including anthropogenic modifications such as storm sewer networks) (67.7 km^2 and 73.8 km^2, respectively), channel morphologies (both pool-riffle with bankfull

widths ranging between 11 and 13 m) and slopes (both 0.04 m/m). Moreover, the watersheds are within 5 km and therefore receive similar precipitation amounts (Figure 3.1). Land-use characteristics were estimated in GIS using historical aerial photos [*Thompson*, 2013]. Hydrometric data from the two watersheds were used in a space-for-time substitution to create four hydrologic land-use scenarios representing different degrees of watershed hydromodification (Table 3.2). Each scenario has a period of record between 10 and 20 years (average of 14 years), which is within the recommended length for effective discharge estimation [*Biedenharn et al.*, 2000], one of the geomorphic indicator discharges chosen for the study. These record lengths were chosen to adequately characterize the change in low to intermediate floods while still maintaining scenarios that were as stationary as possible (i.e. short enough that the amount of urbanization increase within each scenario is minimized). Additional information on the land-use scenarios can be found in Appendix B (Figure B.1, Table B.1).

Table 3.2: Hydrologic land-use scenario details.

Land-Use Scenario	Percent Urban Land-use	Data Source	Period
LU1 - Pre-Development	5	02HC017	1969-1985
LU2 - Moderately Urbanized	17	02HC017	1987-2012
LU3 - Urbanized	54	02HC033	1969-1985
LU4 - Highly Urbanized	76	02HC033	1987-2012

3.4.4 Sediment Transport Modeling

Sediment transport modeling was completed for each half-phi fraction measured with the Helley-Smith samplers. The method used is based on the approach discussed by *Wilcock* [2001a], and applied by *Chartrand et al.* [2015], where a fractional transport model is calibrated to a number of sediment transport measurements. The *Wilcock-Crowe* [2003] model was calibrated to each fraction by adjusting the reference shear stress, τ_{ri}, for each fraction through the use of a calibration coefficient. This model was chosen as it is widely used to model sediment transport in heterogeneous sand-gravel mixtures, and can be calibrated to field measured sediment transport rates [*Wilcock*, 2001a]. Particles smaller than 0.5 mm and larger than 32 mm were not used for calibration due to sampling biases associated with the Helley-Smith [*Emmett*, 1980; *Lisle*, 1995b; *Whiting and King*, 2003]. Calibration factors were averaged for sand sized and gravel sized particles, resulting in values of 1.29 and 1.04 for sand and gravel (and larger) sized particles, respectively. This model was applied to the shear stress rating curve developed from the hydraulic modeling, thus obtaining fractional transport rates for each half-phi grain class for the entire range of discharges.

3.4.5 Geomorphic Work Analysis and Effective Discharge (Q_{eff}) Estimation

A critical step in estimating Q_{eff} is determining the appropriate bin width for the flow classes of the hydrometric data [*Sichingabula, 1999*; *Biedenharn et al.*, 2000; *Lenzi et al.*, 2006; *Hassan et al.*, 2014]. Currently, there is no generally accepted method for selecting the number of flow classes [*Lenzi et al.*, 2006]. For this study, the fixed-width method was employed which determines the bin width based on the largest discharge on record and has been shown to preserve the geomorphic significance of both the lower and upper ranges of flows within the series [*Hassan et al.*, 2014]. Since both watersheds have maximum discharges of approximately 60 m^3/s, a bin width of 0.1 m^3/s was chosen such that there were over 100 discharge classes for each hydrologic scenario.

The median discharge within each discharge class was then combined with the fractional sediment transport model and multiplied by the discharge frequency of occurrence to obtain the proportion of the total load transported by each discharge class, with the largest corresponding to the effective discharge. Additionally, cumulative sediment-water-time curves were developed [cf. *Schmidt and Potyondy*, 2004]. These curves show the cumulative percentage of time, water volume and sediment transport for each discharge class and were used to identify another geomorphically significant metric, the half-load discharge, Q_{half}, which is defined as the discharge that transports half of the total load over the entire period of record, and has been argued to be a more appropriate metric over effective discharge as it is not influenced by the division of hydrometric data [*Klonsky and Vogel*, 2011; *Sholtes and Bledsoe*, 2016].

3.5 Results

3.5.1 Fractional Transport

Twelve events were sampled between 2012 and 2013, with discharges ranging between 8.0 m^3/s and 26.5 m^3/s. In general, the dimensionless bedload flux for each grain fraction increases with dimensionless shear stress, with variability expected for bedload transport measurements in gravel-bed rivers (Figure 3.3). Measured fractional transport rates are lower than those predicted by the bedload flux models for all grain sizes except the largest. The difference for each grain size class becomes less with higher shear stress (Figure 3.3).

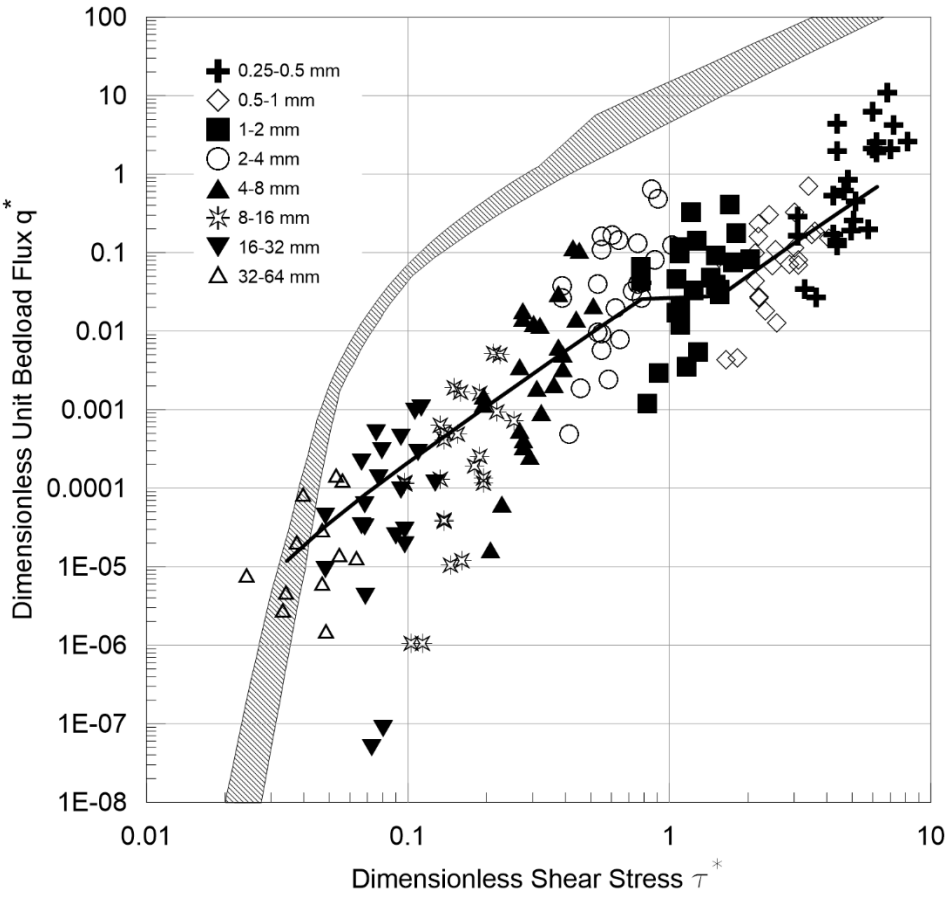

Figure 3.3: Dimensionless bedload rating curve for Mimico Creek. Shaded area represents the envelope encompassing several theoretical bedload flux equations [*Meyer-Peter and Muller*, 1948; *Brown*, 1950; *Parker*, 1978]. Solid line represents the calibrated dimensionless *Wilcock-Crowe* [2003] model for each grain fraction joined together in a single line.

Fractional transport rates exhibit a large amount of variability, specifically at lower discharges (Figure 3.4a). Scaled transport rates ($q_{bi}p_i/f_i$) exhibit a "similarity range" of nearly constant values bound between the solid and dashed lines in Figure 3.4a and 3.4b [*Church and Hassan*, 2002]. Fractions finer than this range (< 0.5 mm) are underrepresented in the bedload as a portion is travelling in suspension. Fractions larger than this range (to the right of the dashed line in Figures 3.4a and 3.4b) are considered only partially mobile [*Wilcock and McArdell*, 1997]. Consistent with *Church and Hassan* [2002], the similarity ranges decrease with lower discharge events, implying that particles larger than fine sand are only partially mobile. When the scaled fractional rates are averaged into discharge classes, representing low (~Q_{thres}), medium

(1.5-2Q_{thres}) and high discharges (>Q_{bf}) (Figure 3.4b), the relative standard errors (standard error divided by the mean, illustrated by the error bars) illustrate the larger variability of the low discharge class (averages of 0.50, 0.43 and 0.42 for low, medium and high, respectively). Additionally, there is little difference between the similarity ranges of the low and medium classes, spanning between 0.5 mm and approximately 6 mm. The grain classes in the partial transport domain exhibit increased variability (average relative standard error of 0.61) compared to the overpassing and equally mobile particles (average relative standard error of 0.40). At discharges > Q_{bf} , the similarity range spans between 0.5 mm to approximately 10 - 20 mm (Figure 3.4b), and the standard errors are generally constant for all grain classes, regardless of the transport domain.

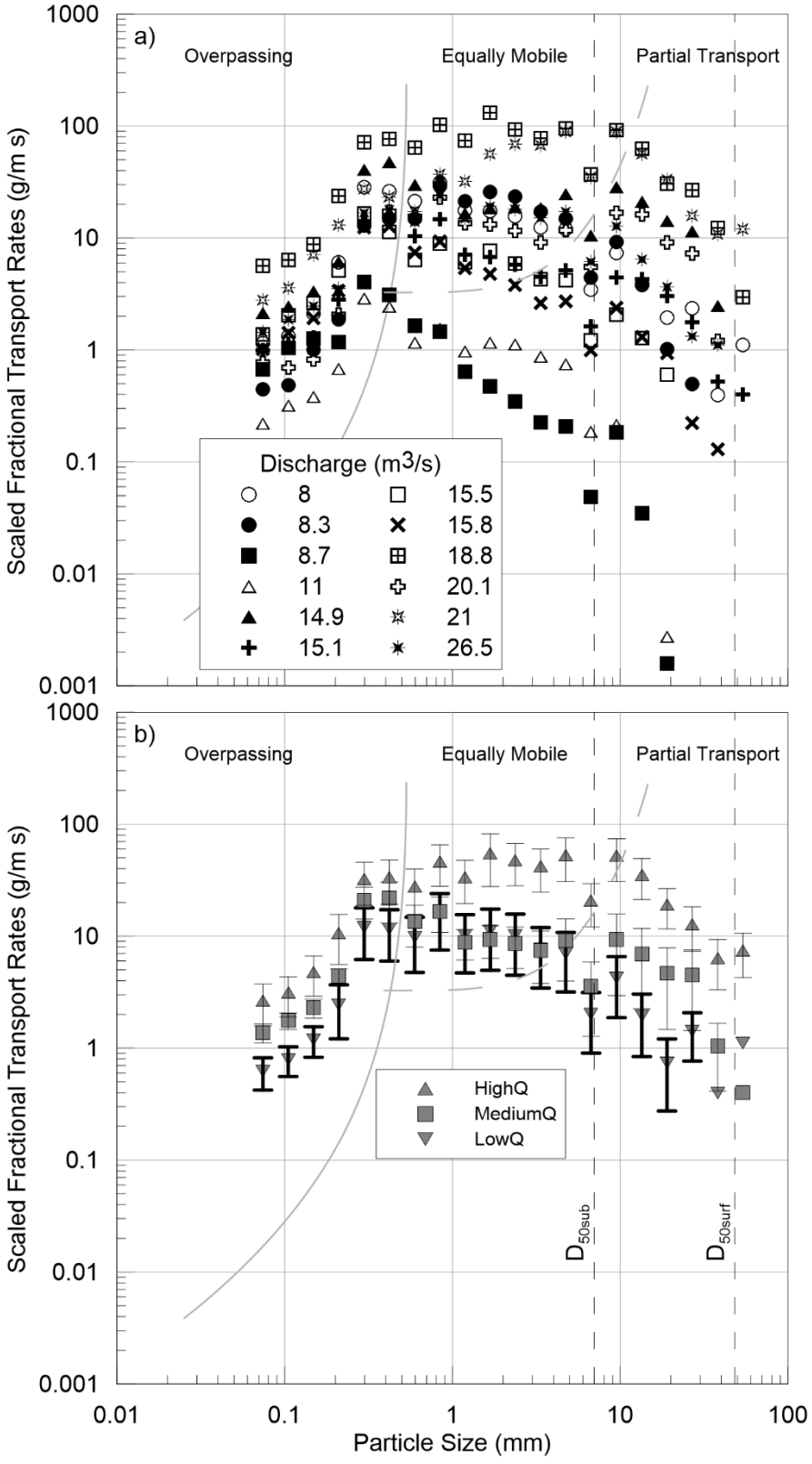
a)
Overpassing
Equally Mobile
Partial Transport
Scaled Fractional Transport Rates (g/m s)
1000
100
10
1
0.1
0.01
0.001
Discharge (m3/s)
8
8.3
8.7
11
14.9
15.1
15.5
15.8
18.8
20.1
21
26.5
b)
Overpassing
Equally Mobile
Partial Transport
Scaled Fractional Transport Rates (g/m s)
HighQ
MediumQ
LowQ
D50sub
D50surf
0.01
0.1
1
10
100
Particle Size (mm)

Figure 3.4: Scaled fractional sediment transport rates ($q_{bi}p_i/f_i$) for all sampled transport events b) Scaled fractional sediment transport rates ($q_{bi}p_i/f_i$) for averaged transport events. Error bars represent the relative standard error. See text for discharge class averaging. Solid and dashed lines included to differentiate approximate boundaries between different transport conditions.

3.5.2 Tracer Mobility

A total of thirteen tracer surveys were conducted between 2011 and 2013 with peak discharges between each tracer survey event ranging from 11 m^3/s ($0.55Q_{bf}$) to 45 m^3/s ($2.25Q_{bf}$). The number of competent discharge events (events > Q_{thres}) between successive surveys ranged from one to six. Six of the surveys were truly event-based, meaning that only one discharge event above Q_{thres} occurred between successive surveys. Of the successive pairs which were not event-based, only one had two discharge events greater than Q_{bf}. Recovery rates were generally high, with average total and event-based recovery rates of 81% and 86%, respectively. Event-based mobility ranged from 2% to 24%, with an average of 11%. When considering both mobile and immobile particles, average event-based transport distances (L_{mevb}) ranged between 0.1 m < L_{mevb} < 3.5 m. In the remainder of analyses which consider transport distances, only the mobile particles were considered, which ranged from 2.8 m < L_{mevb} < 16.2 m. The first survey was not used for the event-based analysis due to the low sample size of mobile particles (N=9). A summary of the results is located in Appendix B (Figure B.2 and Table B.2)

No relationships were found between mean tracer transport distance (L_{mevb}) and peak discharge or cumulative stream energy [cf. *Haschenburger and Church*, 1998]. Results are presented in Appendix B (Figure B.3).

The mean transport distance of each half-phi grain fraction shows no differences for events greater or less than Q_{bf} (Figure 3.5a). In both cases, some particles in all grain size classes were mobile. Both power-fit relationships between mean transport distance and grain size for events greater than (R^2=0.76) and less than (R^2=0.49) Q_{bf} have statistically similar slopes and intercepts at a 95% confidence level. This similarity implies that the coarse particles travel similar distances independent of the peak discharge, which is supported by the previous finding between L_{mevb} and peak discharge. However, the smaller sample size of mobile particles below Q_{bf} and the weaker R^2 is likely influencing this result. Scaled transport distances (L^*) of the mean fractions plot below Equation (3.2), but fall within the 95% confidence limits given by *Church and Hassan* [1992] for all fractions except one (Figure 3.6). The scaled median transport distance

for each fraction falls well below the 95% confidence limits of Equation (3.2), and closely approximates the relationship describing unconstrained particles (Equation (3.3)). The largest two class medians show no difference between scaled transport distance and grain size (Figure 3.6).

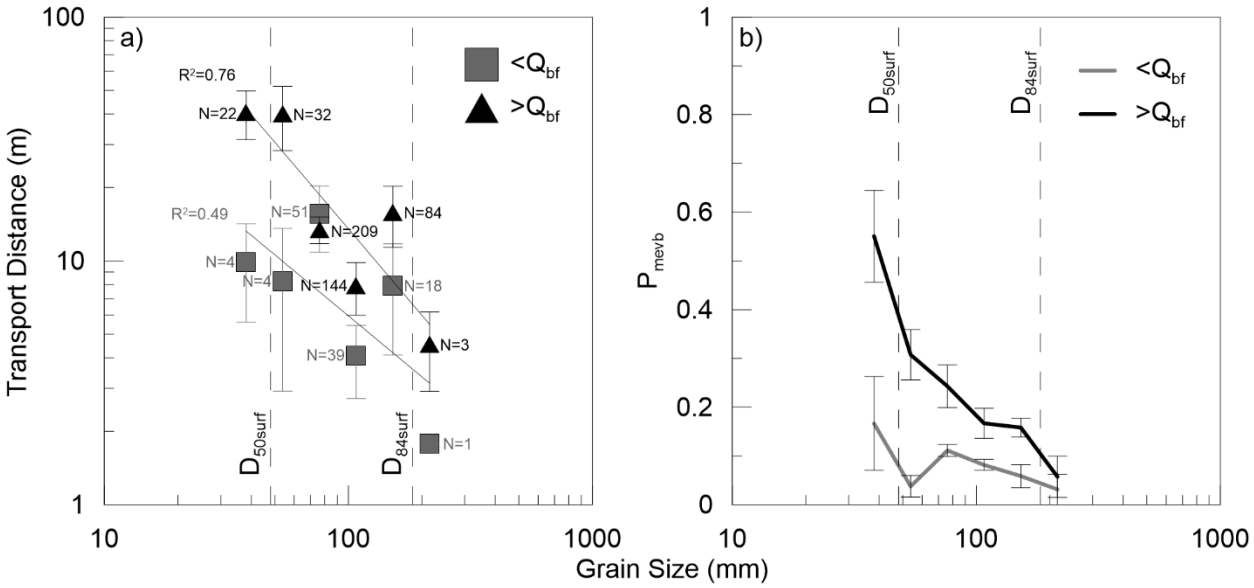

Figure 3.5: a) Fractional transport distances of half-phi grain classes for events less than and greater than Q_{bf}. b) Average event-based percentage of mobility (P_{mevb}) of each grain class for events less than and greater than Q_{bf}, with error bars representing the standard error.

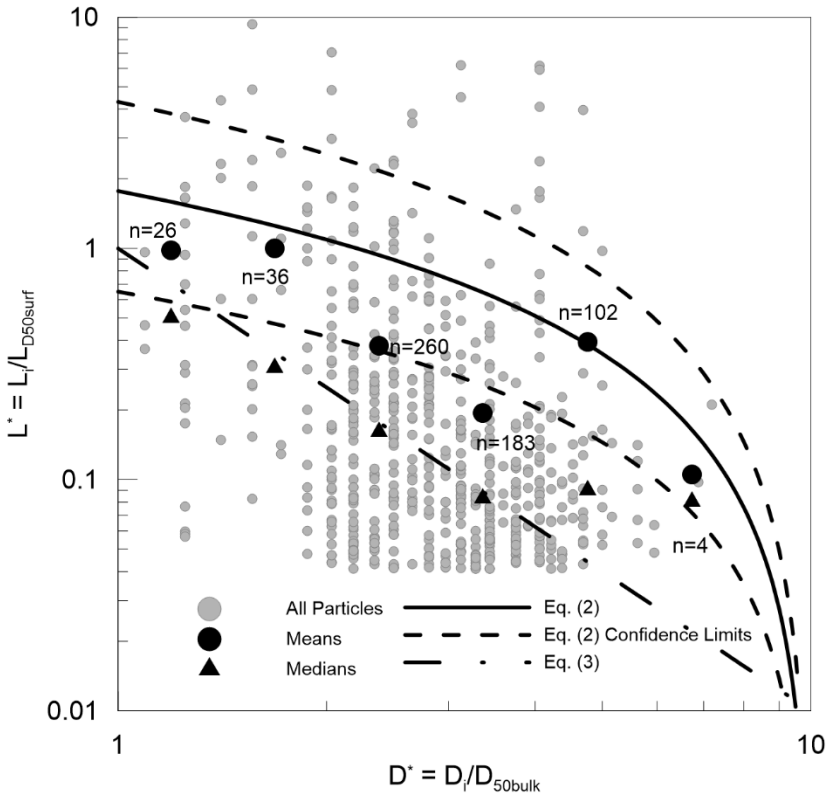

Figure 3.6: Scaled transport distances of each particle, half-phi grain class mean and medians based on Equations (3.2) and (3.3).

The major difference in tracer mobility for events exceeding Q_{bf} is the percentage of particles mobilized. The average mobility of each grain fraction for events below Q_{bf} ranges from almost 0% to 20%, with little variation between grain sizes (Figure 3.5b). Conversely, the average mobility for events exceeding Q_{bf} ranges between 10% and 60%, with a continuous downward trend between mobility and grain size, which is indicative of partial transport [*Church and Hassan,* 2002; *Haschenburger and Wilcock,* 2003].

3.5.3 Temporal Changes in Geomorphically Significant Discharges

Effective and half-load discharges were obtained from both total time series for Mimico Creek and Etobicoke Creek (Figure 3.7). Effective discharges of 22.9 m^3/s and 25.9 m^3/s and half-load discharges of 28.0 m^3/s and 27.7 m^3/s were obtained for Mimico Creek and Etobicoke Creek, respectively. The similarity of the discharges between watersheds further validates the space-for-time substitution to evaluate the evolution of these discharges with increasing urban land-use. The respective Q_{eff} and Q_{half} from both watersheds were averaged for the temporal analysis. The geomorphic work analysis was performed on the four land-use scenarios (Figure 3.8) and using the cumulative sediment-water-time curves, pertinent

characteristics pertaining to event frequencies, durations, volumes and sediment transport were quantified for the four indicator discharges previously mentioned (Q_{thres} = 8.0 m^3/s, Q_{bf} = 20.0 m^3/s, Q_{eff} = 24.4 m^3/s, Q_{half} = 27.8 m^3/s) (Figure 3.9). The relative proportion of sand and gravel in the bedload for each discharge was also computed using the fractional transport bedload model combined with the hydrometric record (Figure 3.10).

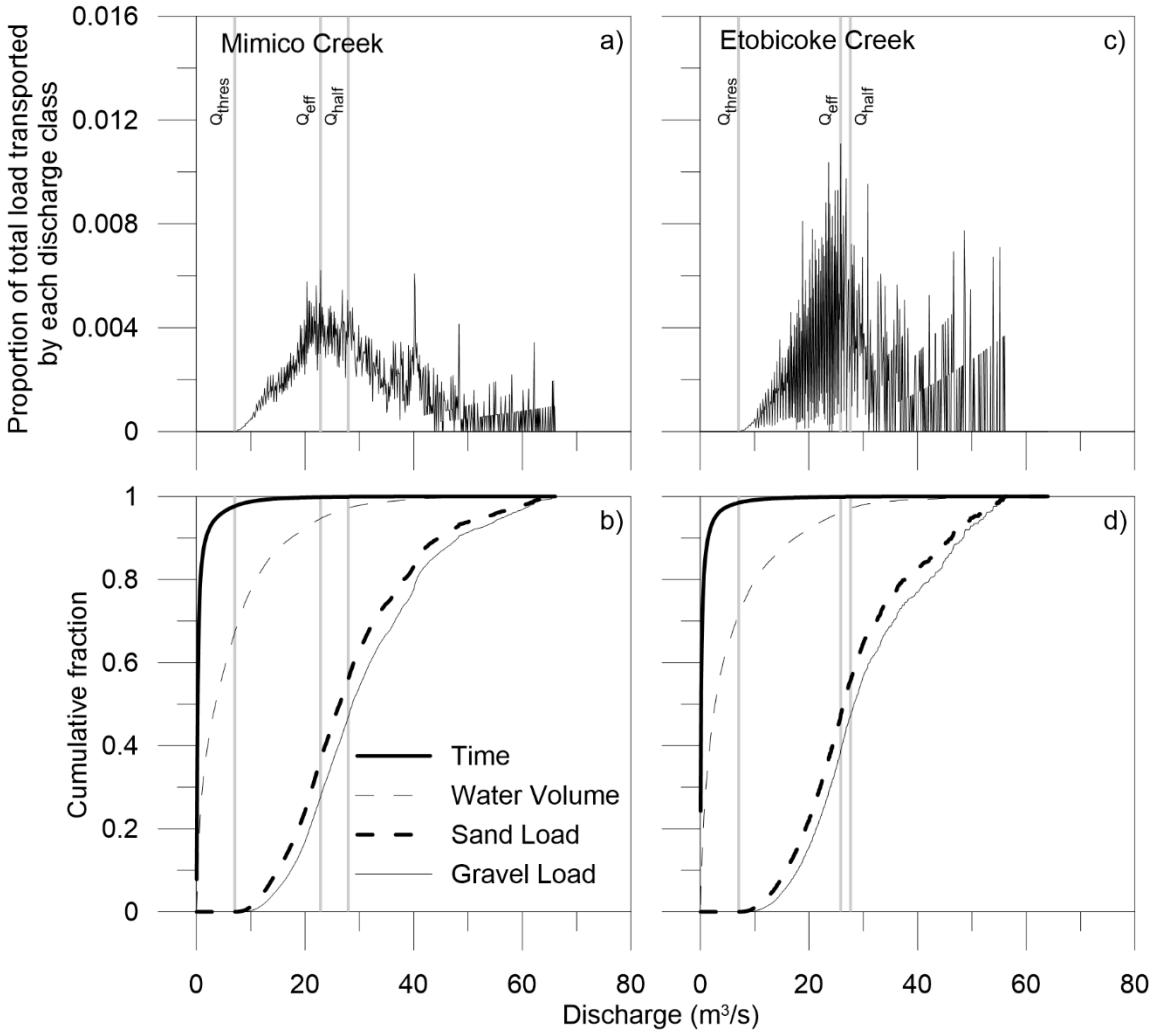

Figure 3.7: Geomorphic work plots for the complete hydrometric series of Mimico Creek (a,b) and Etobicoke Creek (c,d).

Q_{eff} for each individual land-use scenario varies significantly, ranging between 26.9 m^3/s and 55.2 m^3/s (Figure 3.8). These two extremes occur in the lower urban scenarios, while the two higher urban scenarios have similar Q_{eff} values (40.2 m^3/s and 40.3 m^3/s). In all land-use scenarios, the Q_{half} values are similar, ranging between 24.4 m^3/s and 29.5 m^3/s. The variation in Q_{eff} for these scenarios is attributed to the

occurrence of two large flood events which skewed the estimation of Q_{eff} using the event-based division method that inherently preserves the geomorphic significance of low frequency, high magnitude events [*Hassan et al.*, 2014].

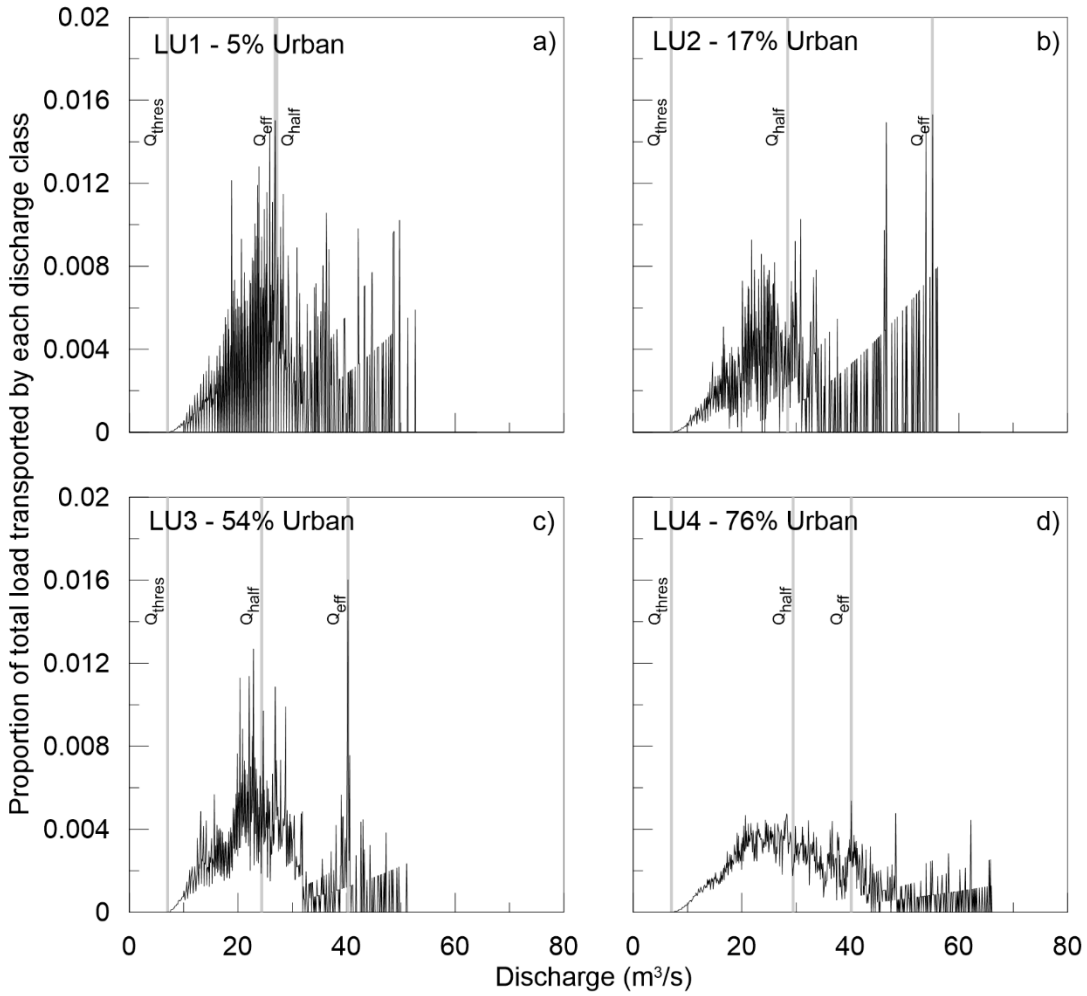

Figure 3.8: Geomorphic work plots for the land-use scenarios. See text for land-use scenario development and details.

For all four indicator discharges, there is a clear increase in their average annual frequency of occurrence (Figure 3.9a). For example, events exceeding Q_{thres} and Q_{half} increase from approximately 7 to 22 and 1 to 2 events per year, respectively. Smaller magnitude events increase at a greater percentage than larger magnitude events (approximately 250% increase for Q_{thres} and Q_{bf} and approximately 200% increase for Q_{eff} and Q_{half}). The time each discharge is equaled or exceeded is greater for the non-urban condition, decreases with slight urbanization (LU2 and LU3), and increases to its maximum for the highest urbanized

scenario (Figure 3.9b). This initial drop is attributed to a switch between less frequent but longer duration snowmelt dominated floods to warm weather flood events caused by convective storms which has been shown for some urbanizing streams in Southern Ontario [*Thompson*, 2013]. Correspondingly, the total fraction of volume above these four indicator discharges behaves in a similar fashion (Figure 3.9c). The cumulative fraction of sediment transported by each discharge shows little difference between land-use conditions (Figure 3.9d). The deviation in LU3 (56% urban land-use) can be explained due to that time period having fewer larger magnitude events than the other three (75^{th} percentile discharge for LU3 is 15.6 m^3/s versus between 19.4 and 20.9 m^3/s for the other three) (Figure B.1), which would result in the intermediate discharges transporting a proportionally larger amount of sediment relative to the other scenarios. When considering the other three scenarios, there is very little variation in the cumulative fraction of sediment transported for the lower magnitude discharges (Q_{thres} and Q_{bf}), which correspond to more sand dominated transport (Figure 3.10). For the larger geomorphic discharges (Q_{eff} and Q_{half}), where gravel transport is dominant (Figure 3.10), there is a slight reduction in the cumulative sediment transported with increasing urban land-use, which is indicative of the increase in frequency for these geomorphically significant discharges as is typical with urbanization [*Hollis*, 1975; *Booth*, 1990]. This observation suggests that the geomorphic significance is being shifted to the more frequent, lower magnitude events. However, in general, the relative cumulative sediment transport proportions do not change significantly with urban land-use, as has also been documented for other streams in the same hydrophysiographic area [*Annable et al.*, 2012]. The average annual yield increases approximately 150% between LU1 and LU4, with similar increases in both sand and gravel yield (not shown).

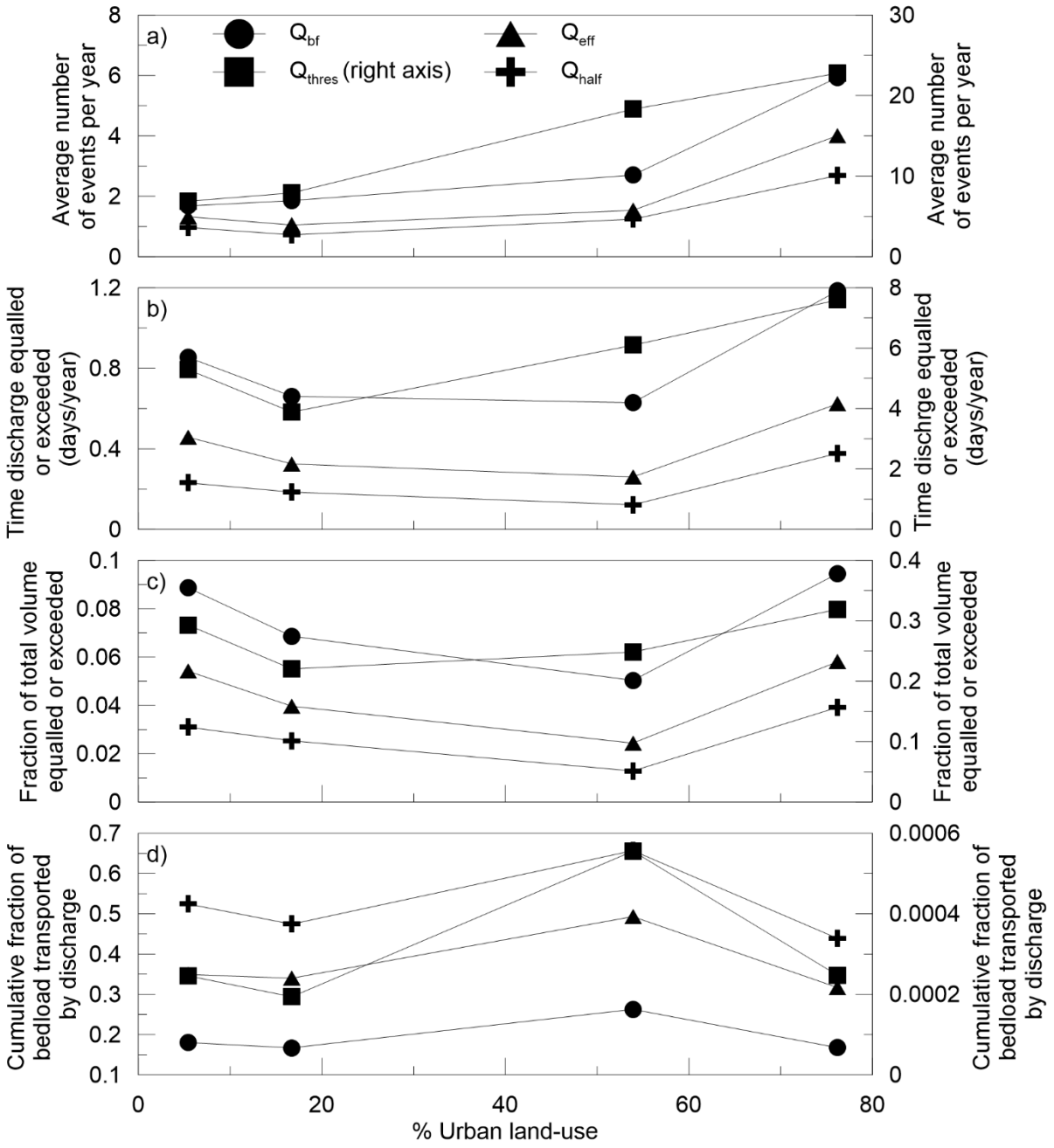

Figure 3.9: Geomorphic work characteristics for indicator discharges as a function of urban land-use; a) average number of events per year equaling or exceeding each discharge b) average time each discharge is equaled or exceeded each year c) average fraction of total volume above each discharge for each scenario d) cumulative fraction of total sediment load transported by each discharge.

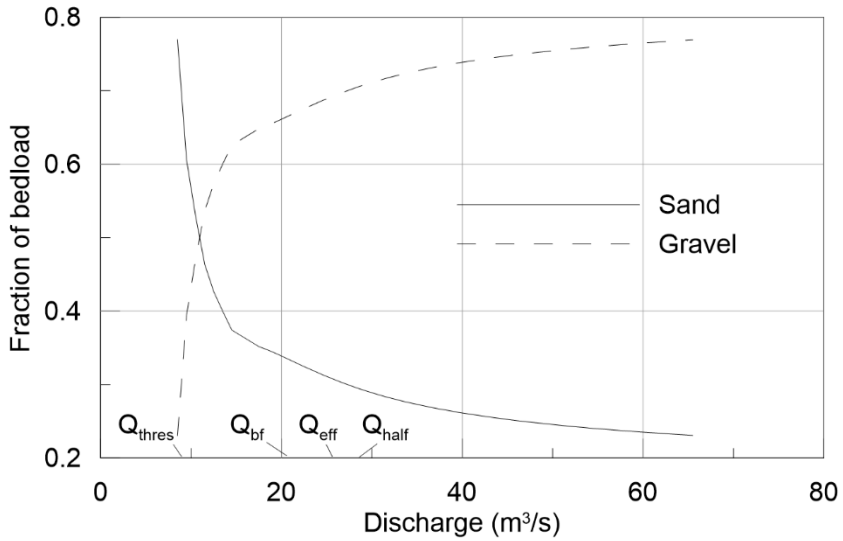

Figure 3.10: Relative proportions of sand and gravel in the bedload for each discharge.

3.6 Discussion

3.6.1 The Relationship Between the Mobility of Coarse Particles and Fine Surface Material and Urban Bed Structures

The dimensionless sediment rating curve for Mimico Creek (Figure 3.3) suggests that the finer bed material (between coarse gravel and coarse sand, approximately 32 mm – 0.5 mm) is underrepresented in the load when compared to traditional bedload flux models. This can be explained by either particle interactions on the bed (e.g. larger particles influencing smaller ones by shielding them from entrainment or by arresting their transport) [*Ashworth and Ferguson*, 1989] or the reduction of these grain sizes in the bed material supply [*Whiting and King*, 2003]. Additionally, the high degree of bed armoring (armor ratio of 5.6) is a likely contributor to the reduced fraction of finer material present in the bedload. The possible particle interactions are also validated by the *Wilcock-Crowe* [2003] model calibration, with the sand fraction having a larger calibration factor than the gravel fraction, indicating a shift towards equal mobility of sand relative to gravel [*Parker et al.*, 1982]. Possible particle interactions at small and intermediate discharge events are also evident in the scaled fractional transport rates (Figures 3.4a-b), which exhibit more variability than the rates corresponding to larger discharge events. At these lower yet still geomorphically significant discharges, the mobility of coarse particles is diminished (Figure 3.5b), suggesting the episodic entrainment of the coarse particles ($>D_{50surf}$) is a controlling factor in the higher variability seen in the finer bed fractions ($<D_{50surf}$) at these discharges. At larger discharges ($>Q_{bf}$), where 200% increases in frequency

and time, as well as slight increases in volume have been documented with increasing urbanization (Figure 3.9a-c), the mobility rate of the coarse particles is increased relative to the lower discharges (Figure 3.5b). Correspondingly, the variability in the scaled fractional transport rates of the finer bed material is lower (Figure 3.4b), further enforcing the relationship between the different mobility characteristics of the coarse ($>D_{50surf}$) and fine ($<D_{50surf}$) material that constitutes the bedload.

For all discharges, coarse material travels shorter distances (Figure 3.6) than the average travel distance for rivers which possess a wide range of hydrologic regimes and channel characteristics [*Church and Hassan*, 1992]. This short transport distance is attributed to the higher flashiness and shorter event duration, a hydrograph characteristic common to both urban rivers [*Annable et al.*, 2012] and the desert rivers outlined in *Church and Hassan* [1992] (see Figure 1 of their work), which also tend to have shorter transport distances than the average. When mobilized, the coarse particles follow a relationship that suggests unconstrained movement, indicating their transport distance depends mainly on particle size [*Church and Hassan*, 1992; *MacVicar and Roy*, 2011]. Frequent mobility yet short transport distances of coarse bed material (Figure 3.6) may be acting to increase topographic variability of the channel bed, thus providing more resistance to flow through additional form roughness [*Millar*, 1999] to compensate for additional energy added to the system due to the greater frequency, time and volume above the geomorphically significant discharges reported in this study. Increased topographic variability in urban rivers has been observed in field studies through increased riffle-pool frequencies and intermediate pools (shallower pools located within riffles) in urban rivers throughout Southern Ontario [*Annable*, 2010] and through the systematic shortening of riffles and deepening of pools observed in urbanizing streams in northern Kentucky [*Hawley et al.*, 2013], both of which were attributed to excess energy dissipation caused by altered hydrologic regimes.

3.6.2 Geomorphically Significant Discharges in Urban Streams

The space-for-time substitution performed in this study confirms the general hydrologic response common to urbanization: increased frequency of intermediate discharge events (Figure 3.9a) [*Chin*, 2006; *Annable et al.*, 2012] and increased time and slight increases to volume of competent discharges (Figures 3.9b and 3.9c) [*Annable et al.*, 2012]. The smallest of the indicator discharges, Q_{thres}, is increased from approximately 7 to 22 events per year. At this discharge, the bedload is approximately 75% sand (Figure 3.10) and is considered to be in the phase 1 transport regime, characterized by sand moving over a relatively immobile bed (Figure 3.5b) [*Jackson and Beschta*, 1982]. The remaining three indicator discharges

correspond to phase 2 transport, where gravel is dominant (Figure 3.10) [*Jackson and Beschta*, 1982; *Wilcock and McArdell*, 1997]. The greater increase in Q_{thres} relative to the others would suggest that the time spent in phase 1 transport is increased and therefore a larger amount of sand would be transported relative to a non-urbanized stream, which is supported by the approximate 150% increase in average annual yield between LU1 and LU4.

Although the average annual yield increases, the relative fraction of cumulative sediment load is not changing considerably with increasing urbanization (Figure 3.9d). This is a surprising result as it was expected that the relative contribution of sediment transported would increase, especially for the lower competent discharges which increase in frequency, volume and time. The fractional transport model used in this study only considers sediment mobilized from the bed surface and does not consider other sediment inputs such as bank erosion. Mimico Creek possesses a high armor ratio, suggesting that the bed has likely coarsened, a common documented geomorphic response to urbanization [*Finkenbine et al.*, 2000; *Pizzuto et al.*, 2000; *Annable et al.*, 2012; *Hawley et al.*, 2013]. Sand and fine gravel, which dominate the bedload at low competent discharges (Figure 3.10) are therefore underrepresented on the bed surface, but likely contribute additionally through bank erosion (observed in both the study reach and upper reaches of Mimico Creek), another common geomorphic response to urbanization [*Trimble*, 1997; *Nelson and Booth*, 2002]. Considering bank erosion as a sediment source would likely change the relative fractions of sediment transported by each discharge, especially for the lower competent discharge where sand transport is dominant. This emphasizes the importance of characterizing sediment sources for urban streams using methods such as sediment budgets [*Reid and Dunne*, 2002; *Allmendinger et al.*, 2007].

Differences in Q_{eff} for each scenario can be explained by a combination of the event-based methodology employed and the division of hydrometric data to create the scenarios. The event-based methodology employed preserves the significance of less frequent, large flood events [*Hassan et al.*, 2014], which have been suggested to be significant in the formation of macro-scale channel morphology in gravel-bed channels [*Lenzi et al.*, 2006]. However, inherent natural variability of precipitation patterns and corresponding streamflow records could confound the trends in Q_{eff} as some of the observed differences may be caused by different trends in rainfall and not due to watershed urbanization. To isolate the impact of urbanization on Q_{eff}, LU2 and LU4 are compared as they are both based on the same period of record (LU2 corresponding to Etobicoke Creek and LU4 corresponding to Mimico Creek). LU2 has a large Q_{eff} (55.2 m^3/s) which is caused by two large flood events over 50 m^3/s (Figures 3.8b and B.1).

Correspondingly, these same two discharge events produced peak discharges of over 60 m^3/s for LU4 (Figure B.1), however, the resulting Q_{eff} is much lower (40.2 m^3/s) (Figure 3.8d). Given the two large discharges are higher for LU4, it would be plausible that the resulting Q_{eff} would reflect these large events, similar to LU2. However, the increase in more frequent lower magnitude events, resulting in more volume above Q_{thres} (Figure 3.9a, 3.9b and 3.9c), is offsetting the impact of the less frequent, higher magnitude events. This comparison suggests that both more frequent, low magnitude events and less frequent, high magnitude events have geomorphic significance in the temporal evolution of gravel-bed streams similar to those in this study, as has been documented for gravel-bed rivers in other regions [*Lenzi et al.*, 2006; *Surian et al.*, 2009; *Hassan et al.*, 2014]. However, it appears that the increase in frequent, low magnitude events due to urbanization is shifting more geomorphic importance to these events.

The design of this study includes some assumptions because complete datasets (including hydrometric, geomorphic and sediment transport data) representing the evolution of a watershed from rural to highly urbanized are lacking in literature. As such, this study was supplemented using a paired watershed space-for-time substitution. Paired watershed studies and space-for-time substitutions are a common method of analysis in urban hydrology and geomorphology [*Chin*, 2006] and forest hydrology [*Grant et al.*, 2008; *Alila et al.*, 2009] to evaluate the impact of an intervention (such as urbanization or deforestation) on watershed processes. However, this method has been challenged, specifically when comparing how flood peak magnitudes change after an impact, as it does not consider how the frequency of these events change [*Alila et al.*, 2009]. Since urbanization changes both the magnitude and frequency of flood events [*Leopold*, 1968; *Hollis*, 1975; *Booth*, 1990; *Hawley and Bledsoe*, 2011; *Annable et al.*, 2012], the magnitude-frequency, or geomorphic work, approach [*Wolman and Miller*, 1960] is well suited as it takes into account the entire range of discharges capable of performing work on the channel, not just the flood peaks. This analysis method inherently considers changes in both magnitude and frequency, and their corresponding impact on the sediment transport characteristics of the channel. The similar physical characteristics and resulting effective discharges (Figure 3.7) of both watersheds further supports the use of a space-for-time substitution. This similarity is interesting, considering both have such different land-use characteristics. However, differences are evident in the proportion of the total load transported by the larger discharges (observed in the right-hand "tails" in Figures 3.7a and 3.7c). Etobicoke Creek (Figure 3.7c) is influenced more by less frequent, high magnitude events relative to the more urbanized Mimico Creek (Figure 3.7a). This difference further emphasizes the concept that the geomorphic change in these streams is not governed by a single discharge, but a range, considering both less frequent, high magnitude and more frequent, low

magnitude events. The lesser significance of large events for Mimico Creek further suggests that urbanization is putting more geomorphic significance in the more frequent, smaller events.

Fractional sediment transport measurements for model calibration were only available for recent years of Mimico Creek, which represents the highest urban scenario. It is acknowledged that the sediment transport dynamics will likely change with different levels of urbanization. Specifically, the bed surface would likely coarsen reducing the availability of sands and fine gravels on the bed (as discussed above). However, the use of the same model for each scenario isolates the change in hydrology associated with urbanization. If an uncalibrated sediment transport capacity model was used for each scenario (such as the ones compared in Figure 3.3), the relative trends between scenarios would not change, as the sediment transport rates would shift accordingly for each scenario. However, a calibrated sediment transport model is still considered more representative to use over an uncalibrated model [*Wilcock,* 2001a].

3.7 Conclusions

This study identified that sediment transport in an urban gravel-bed channel appears to be impacted by the altered hydrologic regime. Transport of the finer bed material is highly variable at discharges between the threshold for motion and the bankfull discharge. Correspondingly, mobility of the coarse material is very low at these discharges, and when mobilized the particle path lengths are short relative to those reported in literature and follow a relationship characteristic of unconstrained particle movement. At higher discharges, the finer bedload fractions become less variable, with a corresponding increase in coarse particle mobility. Coarse particle path lengths do not change considerably at higher discharges. These short path lengths, combined with the mobility differences at varying discharges appears to be a controlling factor in the transport of the finer material which dominates the bedload. This is more prevalent at lower discharges (still sediment mobilizing) which are known to increase proportionally more due to urbanization.

The frequency and time of discharge above Q_{thres}, Q_{bf}, Q_{eff} and Q_{half} all increase with urbanization, with a less pronounced increase in volume. Correspondingly, the average annual bedload yield increases approximately 150% from an unurbanized to highly urbanized condition. Little change in the relative cumulative sediment load transported by each discharge are attributed to the underrepresentation of sand and fine gravel on the bed surface and the surface-based fractional transport model not considering additional sediment sources such as bank erosion, emphasizing the importance of sediment budgeting in urban streams.

The geomorphic significance of the indicator discharges evaluated in this study reveal considerable variability, enforcing that these gravel-bed streams are influenced by a range of discharges, spanning between frequent, low magnitude events to less frequent, high magnitude events. The less urban scenarios are influenced more by less frequent, high magnitude events, suggesting that the increase in frequent lower magnitude events due to urbanization is shifting the geomorphic significance towards these frequent events.

Transition Paragraph B

The previous two chapters documented changes in both channel form and process associated with urbanization. Despite the high-resolution and novelty of the field data and analysis methods, field results only document form changes in one hydrophysiographic region, with detailed bedload transport data for only one river. As such, a laboratory experiment was developed in this chapter[1], inspired from the field data and observations in the previous chapters, but designed such that more general characteristics associated with gravel-bed morphology and corresponding sediment transport dynamics could be assessed. Three unsteady flow experiments representing different levels of watershed urbanization were conducted in a mobile-bed flume. Both bedload transport and bed morphology were measured throughout the experiments. Results show that both unsteady bedload transport dynamics and resulting bed morphology change with different levels of urbanization, with similarities observed between laboratory results and field results observed in the previous chapters and in published literature. Shorter duration hydrographs (corresponding to urban conditions) possess higher transport rates, less pronounced bedload hysteresis loops and more topographic variability of the bed. A proposed parameter for evaluating the degree of hysteresis shows sediment transport is closely linked with falling limb dynamics, which has implications on stormwater management practices.

[1]Plumb, B. D., W. K. Annable, C. Juez, C. W. McKie and M. J. Franca (*in review*), The impact of hydrograph variability and frequency associated with urbanization on the morphodynamics of gravel-bed channels, *Journal of Geophysical Research: Earth Surface*.

Chapter 4

The Impact of Hydrograph Variability and Frequency Associated with Urbanization on the Morphodynamics of Gravel-bed Channels

4.1 Introduction

The rate of morphologic change in a gravel-bed channel is concordant with the magnitude and frequency of discharges capable of transporting that channel's bed material [*Wolman and Miller*, 1960; *Poff et al.*, 1997]. Although it is commonplace to characterize fluvial changes by a single representative threshold discharge approach [*Leopold et al.*, 1964], a channel is ultimately formed by the range in competent flows capable of performing work on the erodible boundaries, defined as the natural flow regime [*Poff et al.*, 1997; *Lenzi et al.*, 2006; *Surian et al.*, 2009]. These competent flows, combined with the amount and texture of transported sediment, interact with the existing bed surface to determine an equilibrium condition in terms of hydraulic resistance and amount of sediment transported. When this magnitude and frequency relationship (the natural flow regime) is altered, the channel morphology will adjust to the new boundary conditions [ex. *Lane*, 1955; *Schumm et al.*, 1987].

The natural flow regime has been characterized by five components; magnitude, frequency, duration, timing and flashiness [*Poff et al.*, 1997]. Although this characterization is based upon processes that regulate the ecological integrity of a watercourse, these five metrics also influence sediment transport and the resulting morphology of a channel. The process of watershed urbanization has been documented to change the natural flow regime by altering individual hydrograph characteristics such as increasing flood peaks, decreasing lag-times (time-to-peak) and decreasing overall event durations [*Leopold*, 1968; *Hollis*, 1975; *Hawley and Bledsoe*, 2011] as well as increasing the frequency of small-to-intermediate discharge events [*Booth*, 1990; *Konrad et al.*, 2005]. The overall result is more frequent "flashier" competent hydrographs.

Here we investigate the questions of how hydrological changes associated with urbanization impact bedload transport rates and sizes, bedload hysteresis, bed surface textures and bed topographic variability. Many field studies have focused on changes in morphology arising from urbanization, with the dominant channel response being channel enlargement and bed coarsening [*Hammer*, 1972; *Leopold*, 1973; *Booth*, 1990; *Pizzuto et al.*, 2000; *Chin*, 2006; *Annable et al.*, 2012; *Hawley and Bledsoe*, 2013; *Hawley et al.*, 2013]. Most of these field studies investigate form-based parameters, with little to no measurements on channel

processes (such as bedload transport). Little emphasis has been placed to date on isolating the impact of the hydrologic component of urban land-use change on bedload transport dynamics.

To address these questions, a series of unsteady flow laboratory experiments were designed to represent different stages of watershed urbanization, ranging from rural (non-urban land-use) to highly urbanized. Hydrograph parameters (flashiness and duration) and average annual frequency of events corresponding to a specific return-period were derived from hydrometric gauge stations of two urbanizing watersheds, collectively spanning the entire land-use transformation from rural to urban. Specific objectives of this study were to characterize the bedload transport responses (rates, yields, sizes and hysteresis) to differing hydrographs as well as investigate how differing hydrograph characteristics impact the resulting bed texture and topographic variability. The experimental channel conditions are inspired by field data; however, the general nature of the experiments allow for more general interpretations towards the impacts of urbanization on gravel-bed morphodynamics.

4.2 Background

Unsteady flow is known to produce bedload hysteresis, generating a lag between discharge and bedload transport rates [*Williams, 1989*]. Common classes of sediment hysteresis are 1) single value, indicating no difference in sediment transport rate between the rising and falling limbs of a hydrograph; 2) clockwise, indicating a greater sediment transport rate on the rising limb of hydrographs; 3) counterclockwise, indicating a greater sediment transport rate on the falling limb of hydrographs; 4) single value plus a loop, a combination of 1 and either 2 or 3; and 5) figure eight, a combination of 2 and 3 [*Williams, 1989*]. Although these classes were originally characterized for suspended sediment concentrations, they have also been observed for bedload transport under unsteady flow conditions in both field [*Reid et al*, 1985; *Sidle*, 1988; *Kuhnle*, 1992; *Hassan and Church*; 2001] and laboratory studies [*Lee et al.*, 2004; *Mao*, 2012; *Humphries et al.*, 2012; *Waters and Curran*, 2015; *Wang et al.*, 2015; *Mrokowska et al.*, 2016]. Clockwise hysteresis has been attributed to a lag in the formation of roughness elements to arrest sediment transport [*Kuhnle*, 1992] or to an initially loose bed due to antecedent floods [*Reid et al.*, 1985]. Counterclockwise hysteresis is commonly attributed to bedform lag [*Lee at al.*, 2004] as well as bed stabilization due to antecedent periods of low flow [*Reid et al.*, 1985; *Waters and Curran*, 2015].

Bedload and surface grain size hysteresis have been documented in laboratory settings. *Hassan et al.* [2006] reported gradual coarsening of bedload during rising limbs of experiments, whereas fining was observed

through falling limbs for symmetrical and asymmetrical hydrographs; indicating a clockwise trend. Bed surface textures for hydrographs, specifically those of shorter duration, did not change considerably from the initial bulk mixtures which was attributed to less time for winnowing or settling processes to occur due to the short durations of the hydrographs [*Hassan et al.*, 2006]. When longer duration hydrographs were studied, channel beds showed a gradual coarsening during the falling limbs of experiments, indicating that sufficient time for particle winnowing and settling had been achieved [*Hassan et al.*, 2006]. Similar surface texture trends were obtained by *Mao* [2012], with hydrographs corresponding to lower peak discharges showing greater degrees of bed coarsening on falling limbs. Bedload percentiles, however, exhibited a counterclockwise trend with coarser bedload observed on the falling limb [*Mao*, 2012]. Conversely, *Wang et al.* [2015] reported bed surface fining for hydrographs with a shorter rising limb, and little change in bed surface texture for hydrographs with a longer rising limb for both unimodal and bimodal sediment mixtures. Key results from these studies are summarized in Figure 4.1.

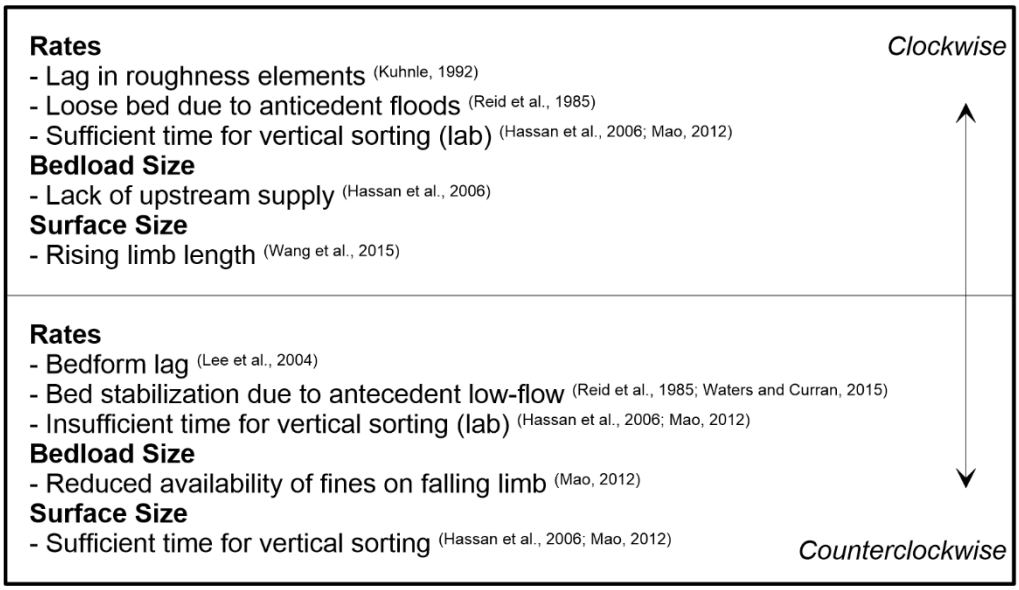

Figure 4.1: Summary of observed bedload hysteresis in both field and laboratory studies.

4.3 Methods

4.3.1 Hydrologic Scenario Development

Hydrological inputs for the laboratory experiments were designed based upon combining the temporal land-use trends of two urbanizing rivers located in Toronto, Ontario, Canada: Etobicoke Creek (67.7 km^2) and Mimico Creek (73.8 km^2). Both watersheds have approximately 45 years of instantaneous (15 min)

discharge data with similar watershed areas (<10% difference), channel morphologies and, due to their proximity, similar rainfall [*Annable et al.*, 2012; *Thompson*, 2013]. Their principal physical difference is the amount of land-use change that has occurred in the period of record, verified by temporal aerial photo analysis [*Thompson*, 2013]. Etobicoke Creek has evolved from rural to 20% urban land-use, while Mimico Creek has transformed from 45% to 88% urban land-use during the same period of hydrometric record. A space-for-time substitution was undertaken with the objective of combining the time-series stream gauge data for both reaches to construct an approximate 70-year hydrologic record representing the evolution of a watershed ranging from rural (≈ 0% urban land-use) to nearly fully urbanized. From this series, three land-use scenarios were established, each representing a different range of urban land-use (Table 4.1).

Table 4.1: Land-use scenario descriptions and data sources.

Hydrology Scenario	Percent Urban Land-use	Study Reach	Environment Canada Gauge ID	Period
Pre-Development (LU1)	<10%	Etobicoke	02HC017	1969-1985
Urbanized (LU2)	40-60%	Mimico	02HC033	1969-1985
Highly Urbanized (LU3)	>60%	Mimico	02HC033	1986-2012

The 1-year return period of the undeveloped prototype [*Thompson*, 2013] watershed was chosen to capture the change in intermediate, competent discharge events due to urbanization which have been shown to change more than larger magnitude events [*Hollis*, 1975; *Booth*, 1990; *Annable et al.*, 2012]. The events with peak discharges falling within ±10% of this discharge were used to populate the event database for each land-use scenario investigated.

For each event; peak discharge, total volume, total time-to-peak, total duration, threshold volume, threshold time-to-peak and threshold duration were extracted using an algorithm developed by *Thompson* [2013]. Threshold parameters were defined based upon a field observed discharge that was found to mobilize the D_{50} particle in one of the prototype streams during a multi-year bedload transport sampling campaign (Chapter 3). The average of each aforementioned event parameter was used to construct characteristic triangular hydrographs, representing average hydrograph characteristics for each land-use scenario (Figure 4.2). Thus, the impacts of progressive hydromodification can be evaluated systematically across different experiments.

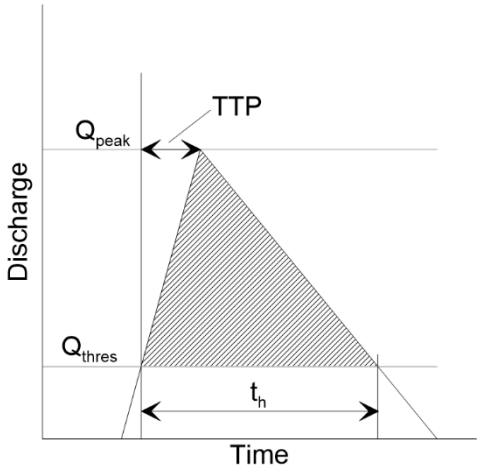

Figure 4.2: Schematic of parameters extracted from field hydrometric data for the development of the laboratory hydrographs corresponding to the land-use scenarios. Q_{peak} and Q_{thres} are peak discharge and threshold discharge, respectively. TTP is time-to-peak and t_h is the threshold duration. See text for details on hydrograph development.

The number of hydrographs chosen for each experiment represented 10 years of time in the prototype condition. This duration was chosen as a trade-off between ensuring a representative timescale to observe changes in bed morphology and sediment transport characteristics, and the overall length of each experiment. Timescales of bed adjustments in gravel-bed channels are highly variable and are dependent upon a number of factors including; type of disturbance, magnitude of disturbance, timescale of the disturbance, and the resilience of the channel. In terms of spatial scales of adjustment, local grain scale-adjustments and micro-scale bedforms tend to occur on the smallest timescales, followed by macro-scale bedforms (such as riffles, bars and pools), changes to the channel cross section and finally changes to the channel planform and gradient [*Knighton*, 1998; *Buffington*, 2012]. *Knighton* [1998] provides an estimated range for the adjustment period of gravel-bed streams ranging between 5 and 100 years. The focuses of these experiments are on changes in bedload transport characteristics (rates, textures and hysteresis) and changes in bed texture (grain-scale changes), and not on macro-scale morphology. The chosen timescale, considered as sufficient, was within the lower end of this range. The experiments were designed as one-dimensional (no channel meandering), and as such, no bars or "large-scale" bedforms were expected.

4.3.2 Experimental Design

Hydraulic and sediment parameters have been roughly scaled to an experimental flume by means of Froude scaling for one of the prototype rivers (Mimico Creek, at a scale of 1:24). A poorly sorted bimodal sand-

gravel mixture with bulk material characteristics for D_{30bulk}, D_{50bulk}, D_{84bulk}, D_{90bulk} and $D_{maxbulk}$ of 0.5 mm, 2 mm, 6.5 mm, 7 mm and 10 mm, respectively, was used (all of which was non-cohesive). For each hydrologic scenario (experiment), peak discharge was held constant and only flashiness (time-to-peak), duration and frequency were altered (Figure 4.3). The peak discharge (Q_{peak}) was established such that the mobility ratio of applied bed shear (estimated using the depth-slope product method) to critical bed shear (estimated using methods outlined by Komar [1987]) (τ_0 / τ_c) for the D_{84bulk} particle size was approximately equal to 1. Each triangular hydrograph was approximated in a series of short steps, as has been done in previous experiments simulating unsteady flow [*Hassan et al.*, 2006; *Mao*, 2012; *Martin and Jerolmack*, 2013; *Waters and Curran*, 2015]. The Froude number in the experiments ranged from 0.4 to 0.8, which is within range of the prototype streams and previous experiments studying unsteady flow [*Lee et al.*, 2004; *Mao*, 2012; *Waters and Curran*, 2015]. Sediment input rates were established based on measured bedload transport rates in Mimico Creek [*Annable et al.*, 2012] (Chapter 3). The sediment input rating curve was approximated into two input rates, such that the input rate was increased partway through the rising limb (at $0.7Q_{peak}$) and then decreased part way through the falling limb. This two-step sediment input was done to simplify the experimental procedure as the sediment input rate required manual adjustment. The difference in total input using this two-step method and adjusting during every discharge step was less than 5%, confirmed through analytical computation of the total load transported using the scaled bedload rating curve and the two-step method. A summary of the experimental boundary conditions is provided in Table 4.2 and Figure 4.3.

Table 4.2: Experimental hydrograph variables and associated unsteady flow parameters derived from gauge data.

Exp	q_{thres} (L/s m)	q_{peak} (L/s m)	$q_{s,in}$ (low) (g/s m)	$q_{s,in}$ (high) (g/s m)	TTP (min)	t_h (min)	V_h (m^3)	Freq. (#/yr.)	No. Hyd.	t_{tot} (hr.)	V_{tot} (m^3)	P	W_k	W_{ktot}
LU1	12.0	32.0	8.0	14.0	42.0	82.0	52.0	0.9	9.0	12.3	468	7.39E-05	748	6732
LU2	12.0	32.0	8.0	14.0	21.0	45.0	28.5	1.6	16.0	12.0	456	1.35E-04	410	6559
LU3	12.0	32.0	8.0	14.0	21.0	37.0	23.5	3.3	33.0	20.4	776	1.64E-04	338	11155

Notes: q_{thres} is unit threshold discharge, q_{peak} is unit peak discharge, $q_{s,in}$ is unit sediment input rate, TTP is time-to-peak, t_h is threshold hydrograph duration, V_h is hydrograph volume, t_{tot} is total experimental time, V_{tot} is total volume of water, P is unsteadiness parameter, W_k is total flow work index for each hydrograph and W_{ktot} is the total flow work index for each experiment.

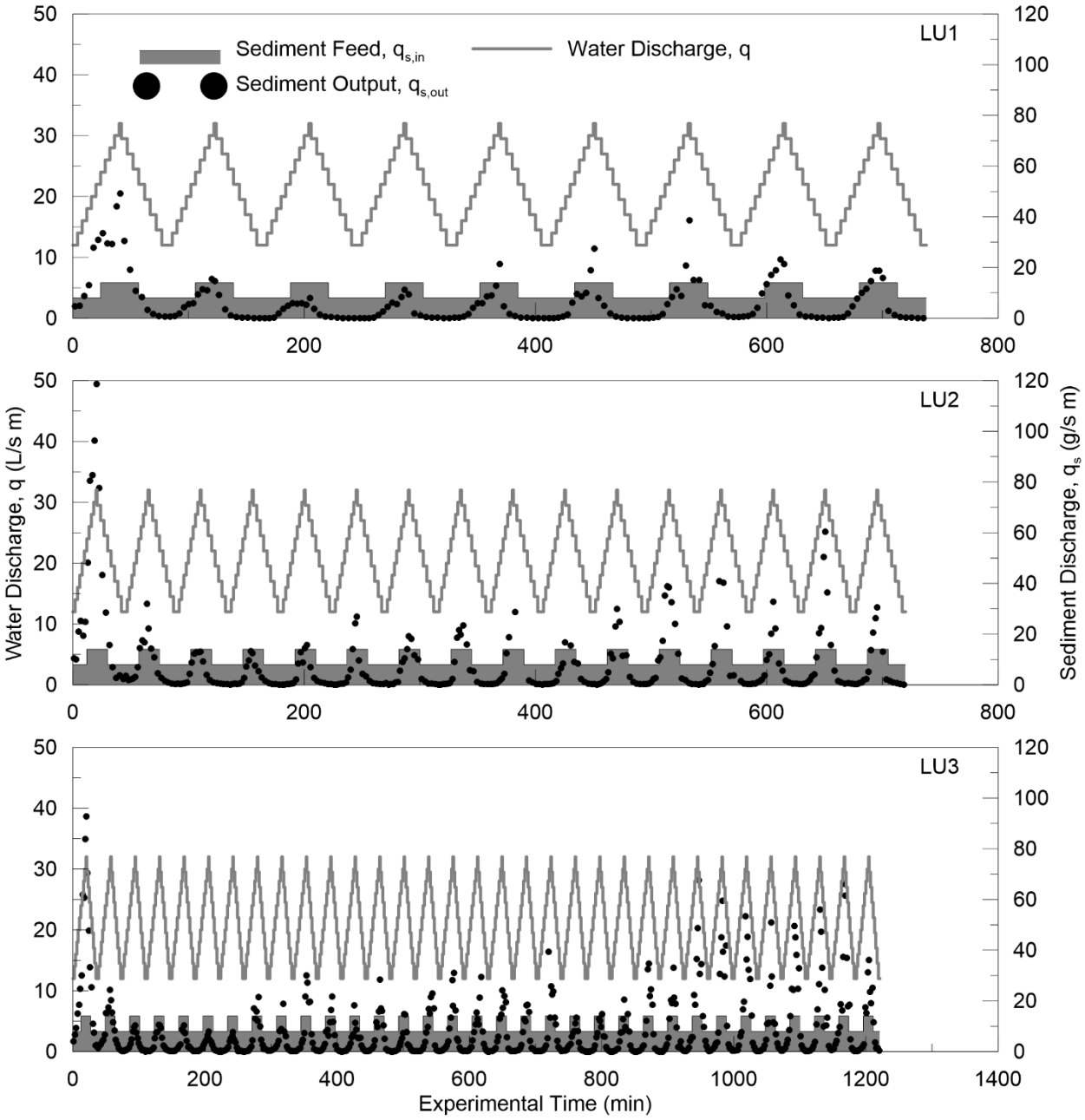

Figure 4.3: Schematic of laboratory experiments illustrating the experimental stepped hydrographs (grey line), stepped sediment feed rates (grey patches) and bedload transport rates collected from the bedload trap (black dots). 9, 16 and 33 hydrographs were conducted for LU1, LU2 and LU3, respectively.

Also shown in Table 4.2 are unsteadiness parameters which have been previously derived to characterize sediment yield in unsteady flow hydrographs. The unsteadiness parameter (*P*) of *Graf and Suszka* [1985]

characterizes the unsteadiness of flow by the ratio of the change in flow depth (Δh) and the hydrograph duration (t_h),

$$P = \frac{\Delta h}{u_{*0} t_h} \tag{4.1}$$

where u_{*0} is the shear velocity at base flow and calculated assuming quasi-uniform conditions. The total flow work index (W_k) [*Yen and Lee*, 1995] represents the total work performed by the hydrograph,

$$W_k = \frac{u_{*0}^2 V_h}{g {h_0}^3 B} \tag{4.2}$$

where V_h is the hydrograph volume, h_0 is the flow depth at base flow and B is the channel width.

4.3.3 Experimental Channel and Measurements

Experiments were conducted at the Laboratoire de Constructions Hydrauliques (LCH), at the École polytechnique fédérale de Lausanne (EPFL), using a 9 m long by 0.5 m wide flume with sediment being supplied at the upstream end by an Archimedes screw sediment feeder (Figure 4.4). A calibrated valve-discharge relationship, which was tested to be ±10% accurate for each discharge step, was used to simulate the experimental hydrographs. Discharge was continuously measured at the channel inlet using a V-notch weir and ultrasonic sensor. Bedload transport was measured by a bedload trap located at the downstream end of the flume where the sediment routed through a valve and into a 0.125 mm collection bin which was emptied between each discharge step, such that individual rates and textures could be obtained throughout the rising limb, peak and falling limb of each hydrograph (Figure 4.4). Sediment samples were subsequently dried, weighed and sieved at the half-phi scale.

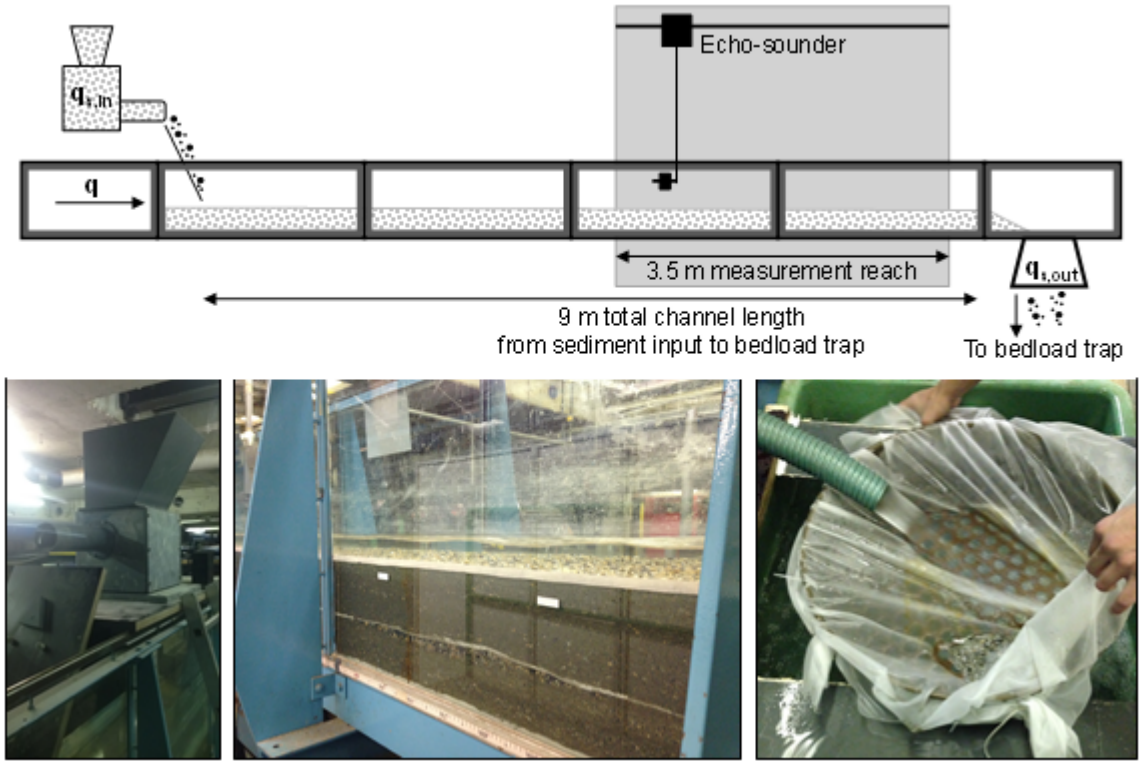

Figure 4.4: Schematic of experimental channel (top) and photos illustrating the sediment feeder (left), the channel during experiments (middle) and the downstream sediment trap (right).

Throughout each hydrograph, flow depth was continuously measured using a series of ultrasonic sensors placed throughout the channel, and verified by measurements with a ruler against the clear channel walls. After each hydrograph, topographic scans were conducted using a mini-echo-sounder, with an accuracy of ±1 mm, along a 3.5 m long reach of the channel at the downstream end. This 3.5 m long reach was chosen at the downstream end to ensure that the sediment transport rates and resulting bed texture was not influenced by the upstream boundary conditions of the channel (i.e. the sediment feeder). A series of 20 longitudinal profiles spaced every 0.02 m along the channel width were conducted with the echo-sounder, obtaining measurements every 0.01 m in the stream-wise direction. Due to physical limitations of the instrument, 0.06 m closest to the sidewalls could not be scanned. The grain size distribution (GSD) of the bed was also obtained in this 3.5 m measurement reach using high resolution (12 MP) photos. Similar to methods used by *Mao* [2012], a 0.3 m by 0.3 m grid was imposed over each photo using CAD software. The b axis (intermediate axis) was digitized for the 64 particles located at each node of the grid (grid spacing of 4.3 cm), resulting in up to 768 particles for each GSD estimate. It should be noted that some photos (<

3% of total) and nodes (< 1% of total) were not suitable for the analysis due to lighting and/or blurriness. These photos and nodes were subsequently removed from the analysis.

4.3.4 Experimental Procedure

A pilot test was conducted with the objective of determining the equilibrium slope of the channel. The initial slope was set at 0.005 m/m and the LU1 hydrograph (and corresponding sediment feed) was continuously cycled until an equilibrium slope of 0.01 m/m was achieved after six hydrographs, or approximately 10 hours of testing.

Each experiment began with identical initial conditions. The sediment mixture was placed in the channel and screeded to the initial 0.01 m/m slope. The bed was then slowly saturated and drained to promote initial settlement of the freshly placed sediment. A period of low flow, enough to mobilize sand fractions, with no sediment feed was then initialized to provide the channel with a flow history [*Waters and Curran*, 2015]. This period lasted for approximately 8 hours, and was considered complete when the sand particles had rearranged such that their mobility was limited in the channel (through visual observation) and there was negligible sediment appearing in the bedload trap. Flow was then stopped and the bed slowly drained for initial bed photos. After the photo inventory, the tailgate was raised and the channel filled with water to a depth of approximately 0.3 m for the mini-echo-sounder to be submerged throughout the measurement reach (used in measuring the bed morphology).

Once echo-soundings were completed, the bed was slowly drained by lowering the tailgate and a low-flow condition initialized. Flow was subsequently increased monotonically to the first step in the hydrograph (12 L/s/m), thereupon the downstream bedload trap was opened and the hydrograph was simulated. After the current hydrograph was completed, flow was quickly reduced (within 5 – 10 seconds) to arrest sediment transport and the tailgate slowly raised for the post-hydrograph scan using the echo-sounder. Upon the completion of the scan, the channel was slowly drained and post-hydrograph photos acquired of the bed. This process was then repeated for the remaining hydrographs in the experiment. It should be noted that the raising and lowering of the tailgate, draining of the channel and the reinitialization of hydrographs did not cause any significant impact to the bed between experiments (visually verified) with the impacts limited to a few instances of particles rolling or shifting. The overall experimental time for the experiments, including the flow history periods, was approximately 70 hours. This time does not include the time taken to prepare the bed, conduct the scans or take the bed photos.

4.4 Results

4.4.1 Bedload Transport Rates and Yields

In each experiment, sediment transport rates and corresponding yields for the first hydrograph were much higher than remaining hydrographs (Figure 4.3). This has been observed in other sediment-feed laboratory studies [*Ferrer-Boix and Hassan*, 2014] and is interpreted to be influenced by the initial bed configuration, such that the bed contained a higher content of fine material and had not established sufficient sedimentary structure to resist the imposed flow conditions, both of which can cause increased bedload transport [*Papanicolaou and Schuyler*, 2003; *Curran and Wilcock*, 2005]. As such, the first hydrograph eroded a significant amount of material from the bed. This was followed by a period of lower transport (and yields), where the sediment lost in the first hydrograph flush was replenished and the bed gained some structure to resist the flow regime. During this period, very small transport rates were observed during the lower discharges in both the rising and falling limbs, and any considerable transport occurred near the peak. After this period, the sediment transport rates gradually increased and approached a state where, over a cycle of hydrographs, the sediment input equaled the sediment output (on a hydrograph basis).

For the LU1 experiment, overall transport rates were lower than those of LU2 and LU3. This included both initial higher rates observed in the first hydrograph, and subsequent rates as the experiments progressed. Transport rates corresponding to the peak discharge of each hydrograph are shown in Figure 4.5. It should be noted that normalized time for each hydrograph is the ratio between the number of that specific hydrograph and the total number of hydrographs in the experiment (expressed as a percent). Excluding the first hydrograph in each experiment, the maximum transport rate for LU1 at peak discharge was approximately 40 g/s/m, whereas LU2 and LU3 both have transport rates above 60 g/s/m. LU2 and LU3 exhibit similar trends, they both have longer periods of low sediment transport rates, followed by an increase until the rates appear to stabilize, although with considerable variability inherent in bedload transport. This final period of relatively stable transport rates is more pronounced in LU3, as the rates appear to stabilize at approximately 50 g/s/m, with the variability being ±14 g/s/m (Figure 4.5c).

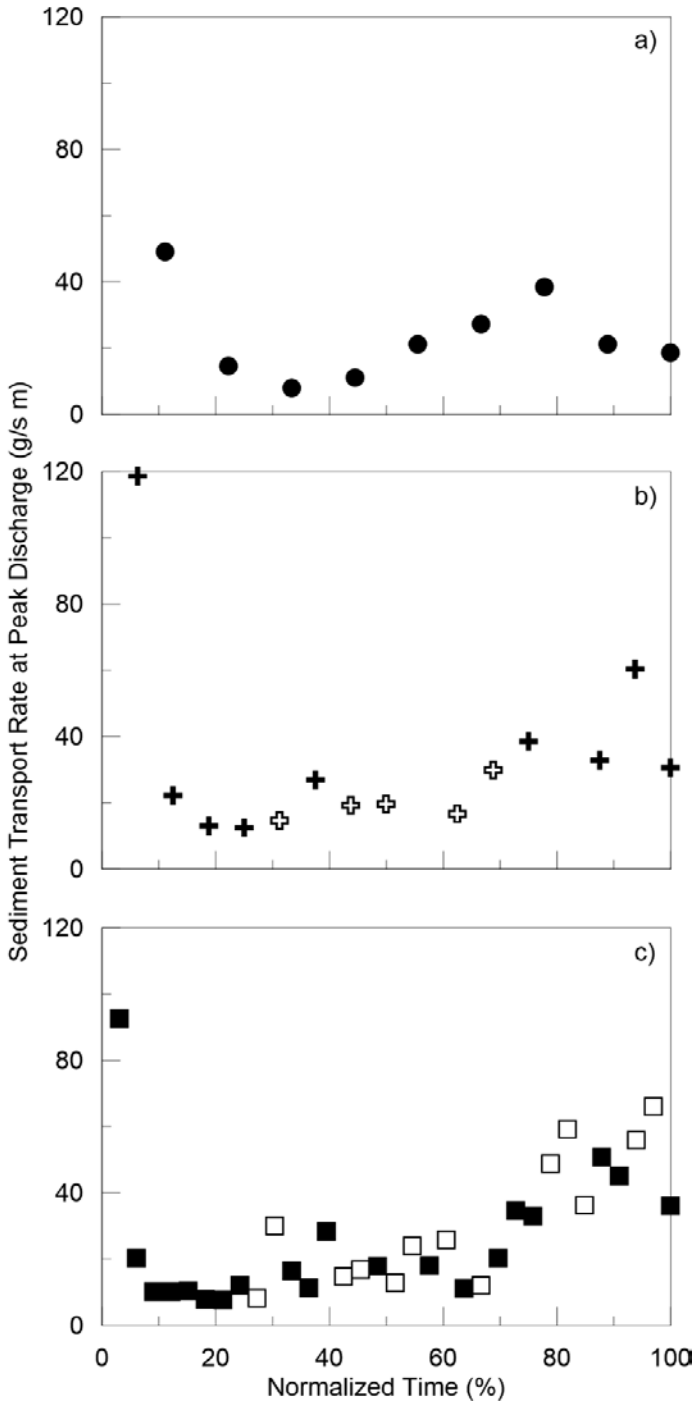

Figure 4.5: Sediment transport rates corresponding to the peak discharge of each hydrograph in a) LU1, b) LU2 and c) LU3. Solid and hollow symbols represent hydrographs exhibiting clockwise hysteresis and counterclockwise hysteresis, respectively. Note: No counterclockwise hysteresis was observed for LU1.

Notable bedload hysteresis was observed during the hydrographs. A selection from each experiment is presented in Figure 4.6 with hydrographs chosen near the beginning, middle and end of each experiment to illustrate the evolution of bedload hysteresis throughout experiment. For example, LU1-H5 refers to the fifth hydrograph in the LU1 experiment. Clockwise hysteresis or a combination of single value plus clockwise loop is observed for all hydrographs in LU1 (Figure 4.6, top row). For LU2 (Figure 4.6, middle row) and LU3 (Figure 4.6, bottom row), the hysteresis is much more varied, with all five of the common classes being exhibited as the experiments progress. However, in general, the hysteresis loops are much tighter for these shorter flashier hydrographs, resembling a more single value hysteresis with occasional small loops. The higher transport rates of LU2 and LU3 relative to LU1 are further illustrated in Figure 4.6.

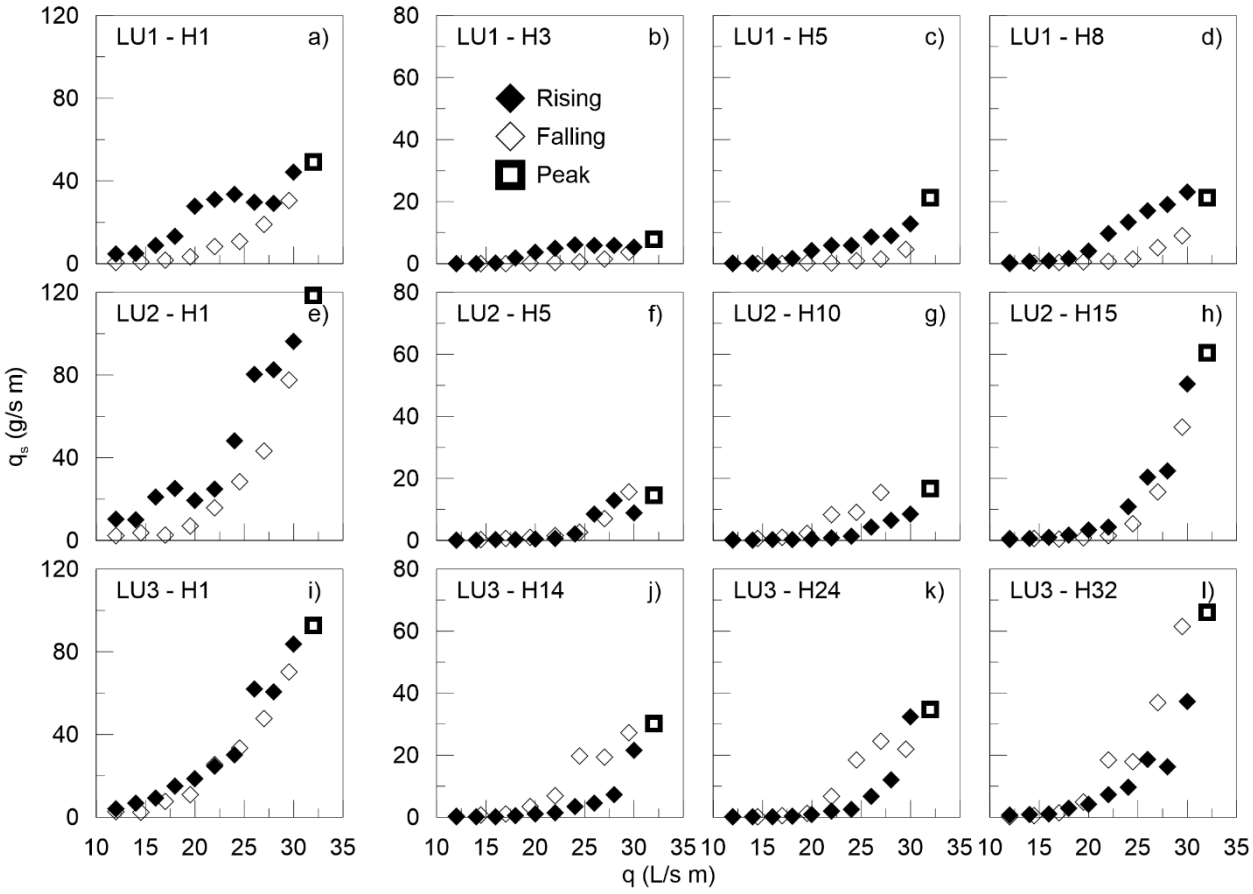

Figure 4.6: Phase plots for select hydrographs from each experiment (LU1 top row, LU2 middle row, LU3 bottom row) illustrating the different phases of bedload hysteresis present. Hi denotes the hydrograph number of that specific experiment.

In all experiments, the output yield (Y_{out}), which is the total mass of sediment collected in the bedload trap for each hydrograph, is much higher for the initial hydrograph than the input yield (Y_{in}), which is the total mass of sediment input during each hydrograph. Subsequent hydrographs in each experiment observed lower yields, averaging outputs between 25% and 30% of their respective inputs, and slowly increasing until the output approximately equaled the input, which also corresponds to the stabilization of the transport rates previously noted (Figure 4.5). LU1 never achieves a quasi-steady state in transport, with a maximum Y_{out}/Y_{in} ratio of approximately 0.6 (Figure 4.7a). Both LU2 and LU3 progresses to a $Y_{out}/Y_{in} \approx 1.0$ after 12 and 25 hydrographs, respectively, and oscillates about this condition for the duration of each experiment (Figures 4.7b and 4.7c). A major difference between LU1 and either LU2 or LU3 are the yields derived from the rising and falling limbs of the hydrographs. Figures 4.7d, 4.7e and 4.7f illustrate the ratio of the rising limb output yield (Y_r) to the falling limb output yield (Y_f), or herein referred to as the hysteresis ratio (H_r). $H_r = 1.0$ indicates yields are balanced between the rising and falling limbs of the hydrograph whereas $H_r > 1.0$ and $H_r < 1.0$ correspond to clockwise and counterclockwise hysteresis, respectively. For all experiments, $H_r > 1.0$ for the first few hydrographs of each test. For LU2 and LU3, $H_r \rightarrow 1.0$ after 7 and 9 hydrographs, respectively, and subsequently oscillates about $H_r \cong 1.0$ (ranging between $0.6 \leq H_r \leq 1.4$). The observed exception is in the final two hydrographs of LU2 which shows a strong clockwise hysteresis. H_r for LU1 remains high, never departing below 1.0 and only tending below 2.0 on one occasion (H_r averaging 3.6), whereas LU2 and LU3 averages remain close to unity (1.4 and 1.2 respectively). Greater variability is also observed with the hysteresis of experiment LU1, with a range in H_r of 4.9, compared to ranges of 2.5 and 1.9 for LU2 and LU3, respectively. It is interesting to note that once equilibrium between sediment input and output is achieved, H_r approaches 1.0.

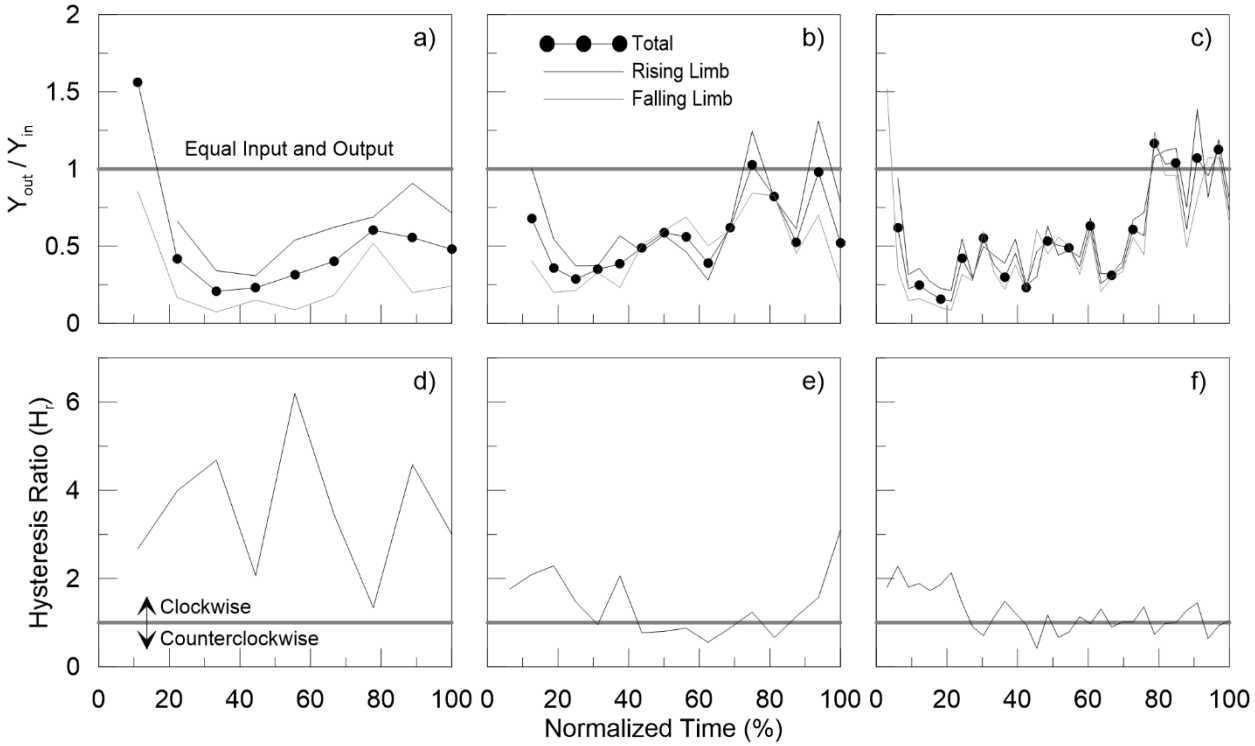

Figure 4.7: Sediment yield ratios (Y_{out} / Y_{in}) of each hydrograph for the total yield, rising limb yield and falling limb yield for a) LU1, b) LU2 and c) LU3 and the hysteresis ratio (H_r) (ratio of the rising limb yield and falling limb yield) for d) LU1, e) LU2 and f) LU3. Horizontal line serves as a threshold for: equal input and output sediment yields (top) and clockwise or counter clockwise nature of the hysteresis loops (bottom).

4.4.2 Fractional Transport

The transport ratio, p_i / f_i [*Parker et al.*, 1982], was computed for all hydrographs of each experiment, with a select number shown to illustrate observed trends (Figure 4.8). Here, p_i is the fraction of transported material for particle class *i*, and f_i is the fraction of particle class i in the bulk sediment mixture. A transport ratio equaling 1, greater than 1 or less than one indicates that the specific grain class is in a state of equal mobility, overrepresented in the bedload relative to the bed mixture or underrepresented in the bedload relative to the bed mixture, respectively.

In all experiments, the transport ratio for all particle sizes trends towards a value of 1 with successive hydrographs in each experiment. This is attributed to the direct feed nature of the experimental setup, which does not allow for partial transport over long periods of time [*Wilcock*, 2001b]. However, the relative trends

between experiments and likewise the rising and falling limb trends can still be compared. For LU1 and LU2, there is a tendency for coarser fractions to be more mobile on the rising limb than on the falling limb, with the opposite holding true for finer fractions. LU1 and LU2 generally have higher transport ratios for finer fractions relative to LU3. There is considerably more scatter in the observed transport ratios of LU3, with only some of the hydrographs exhibiting similar trends to LU1 and LU2. Coarse particle transport ratios are generally higher for LU3, with values approaching and exceeding 2 - higher values corresponding to the rising limb. The transport ratio of finer material reduces in both rising and falling limbs of later hydrographs of LU3; infrequently exceeding 1.0. In general, the finer material of LU3 is still more abundant on the falling limb, similar to LU1 and LU2.

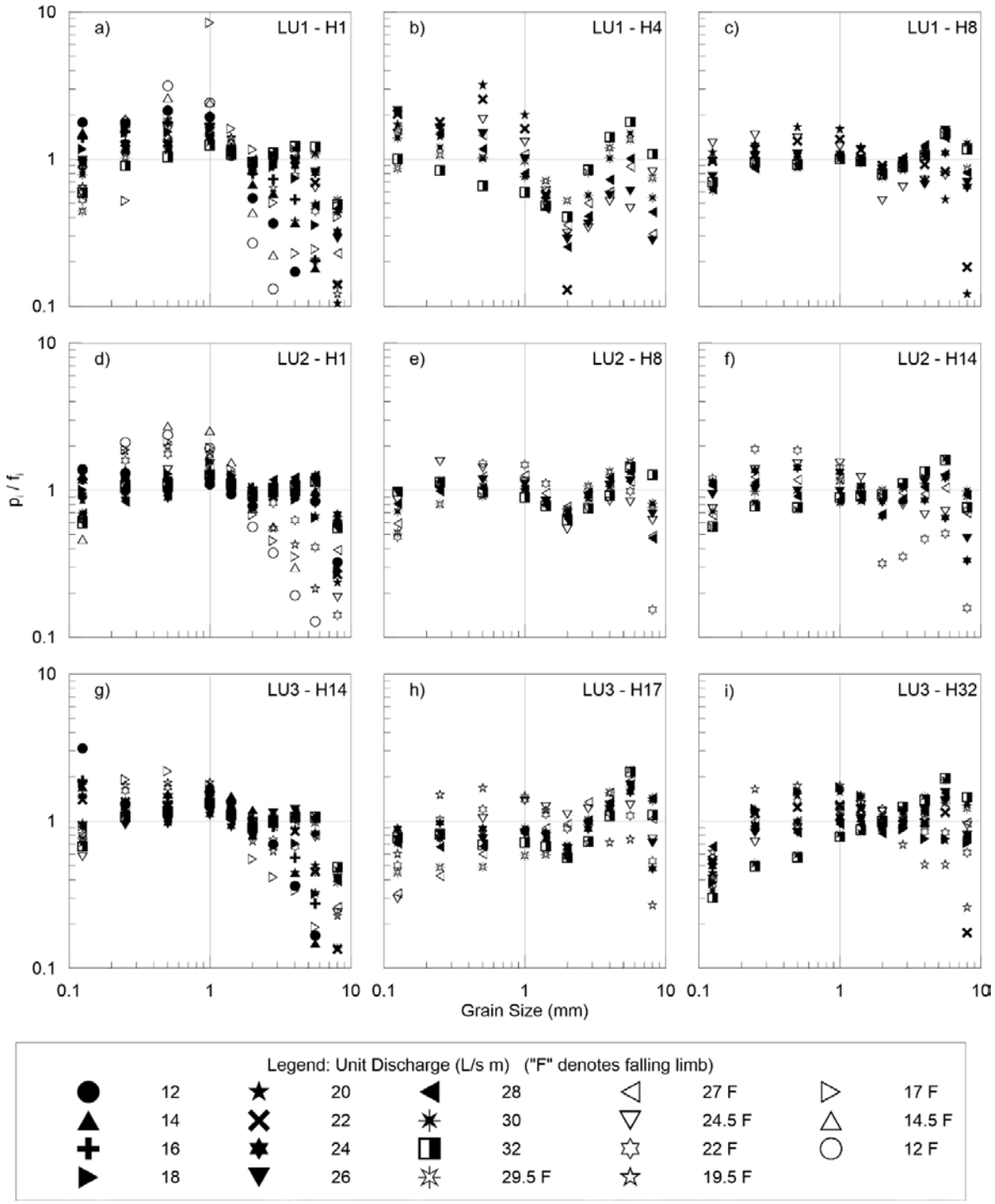

Figure 4.8: Transport ratios of each grain class, *i*, p_i/f_i, where p_i is the proportion of that class in the bedload transported out of the channel and f_i is the proportion of that grain class in the bulk mixture. Hi denotes the hydrograph number of that specific experiment.

4.4.3 Bedload Percentiles

The D_{30load}, D_{50load} and D_{90load} percentiles were chosen to characterize the lower, median and larger particle sizes of the bedload transported through the channel, respectively. Figure 4.9 illustrates particle percentiles for bedload samples corresponding to Q_{peak}. Similar trends for all experiments are observed for the coarsest particles in the bedload (D_{90load}), where D_{90load} for the first few hydrographs (only the first in the case of LU1) are finer than the D_{90bulk} of 7.0 mm (Figure 4.9a, 4.9b, 4.9c). Grain sizes gradually increase to values coarser than the D_{90bulk} and stabilize at values of approximately 7.5 mm.

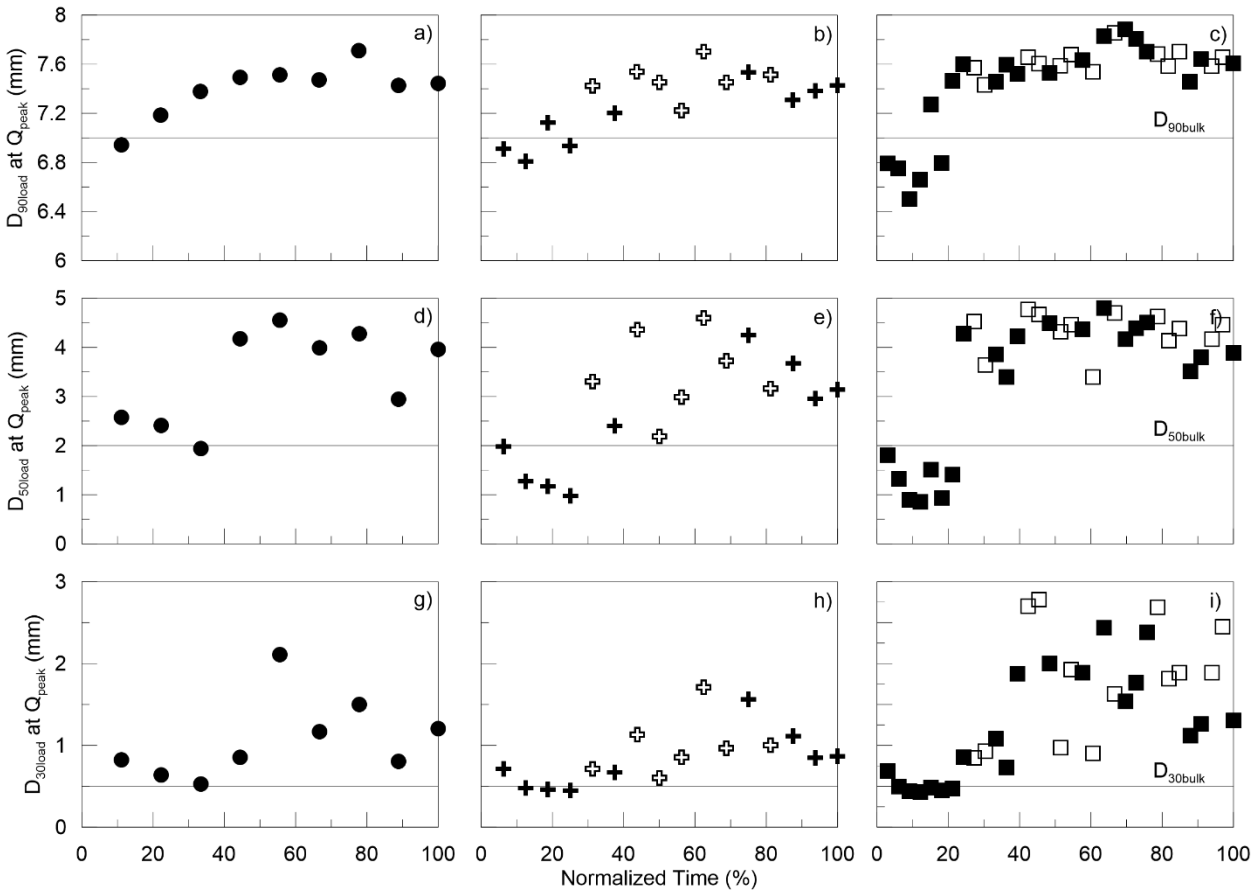

Figure 4.9: 90th percentile of the bedload transported out of the channel (D_{90load}) at peak discharge for each hydrograph for a) LU1, b) LU2 and c) LU3. 50th percentile of the bedload (D_{50load}) at peak discharge for each hydrograph for d) LU1, e) LU2 and f) LU3. 30th percentile of the bedload (D_{30load}) at peak discharge for each hydrograph for g) LU1, h) LU2 and i) LU3. Solid and hollow symbols represent hydrographs exhibiting clockwise hysteresis and counterclockwise hysteresis, respectively. Note: No counterclockwise hysteresis was exhibited in LU1.

D_{50load} for LU1 begins slightly coarser than the D_{50bulk} of 2.0 mm but coarsens abruptly to approximately 4.0 mm after the third hydrograph (Figure 4.9d). A similar trend is observed for LU2, with the exception that a brief period of fining of D_{50load} occurs after the first hydrograph, with a less abrupt increase (Figure 4.9e). Also, there is a noted gradual fining of the final six hydrographs in LU2, with $D_{50load} \rightarrow D_{50bulk}$. D_{50load} of LU3 similarly begins finer than the D_{50bulk} which abruptly increases, similar to the other experiments, here averaging 4.0 mm (Figure 4.9f). There is less of a downward trend noted in grain size of LU3 as the experiment progresses (relative to the other experiments), indicating that the median size remains relatively constant at peak discharge for LU3.

LU1 and LU2 exhibit similar trends in D_{30load}. The experiments begin with $D_{30load} \approx D_{30bulk} \approx 0.5$ mm which gradually increase to $D_{30load} \approx 1.5$ mm (with the exception of hydrograph 5 in LU1) and then trend back towards the D_{30bulk} (Figures 4.9g and 4.9h). LU3 exhibits a much different trend (Figure 4.9i); the first several hydrographs remain similar to D_{30bulk}; however, the mean and variance notably increase as the experiment progresses, with the latter hydrographs possessing a range between 1.0 mm and 2.8 mm. This change occurs when bedload hysteresis patterns begin to fluctuate between clockwise and counterclockwise modes of transport.

Bedload percentiles also exhibit hysteresis effects with the rising and falling limb of each hydrograph. In general, bedload is coarser on the rising limbs (Figures 4.10, 4.11 and 4.12); although much more variable than the hysteresis patterns observed for discharge. Exceptions to this are noted in Figure 4.10g and 4.11a. Similar to the observations in Figure 4.6, Figures 4.10 - 4.12 illustrate select bedload percentiles for hydrographs near the beginning, middle and end of each experiment, such that the evolution of the bedload percentile hysteresis can be observed. Hysteresis trends in all experiments for D_{90load} exhibit similar trends, exhibiting a gradual coarsening as each experiment progressed, with mostly single value hysteresis trends ($H_r \approx 1.0$) or having slight clockwise trends (Figure 4.10). Hysteresis patterns of D_{50load} are more variable than the previously noted grain sizes and tend to steepen as each experiment progressed, indicating a more abrupt change in D_{50load} with increasing or decreasing discharge (Figure 4.11). Hysteresis trends of D_{30load} remain similar for LU1 (Figure 4.12 a – d), become slightly steeper for LU2 (Figure 4.11 e – h) and notably steeper and coarser for LU3 (Figure 4.12 i – l), further enforcing the higher variability observed in Figure 4.9i. It is noted that samples obtained that were smaller than approximately 200 g were not sieved nor included in these figures as meaningful grainsize analysis on such small sample size could not be reliably obtained.

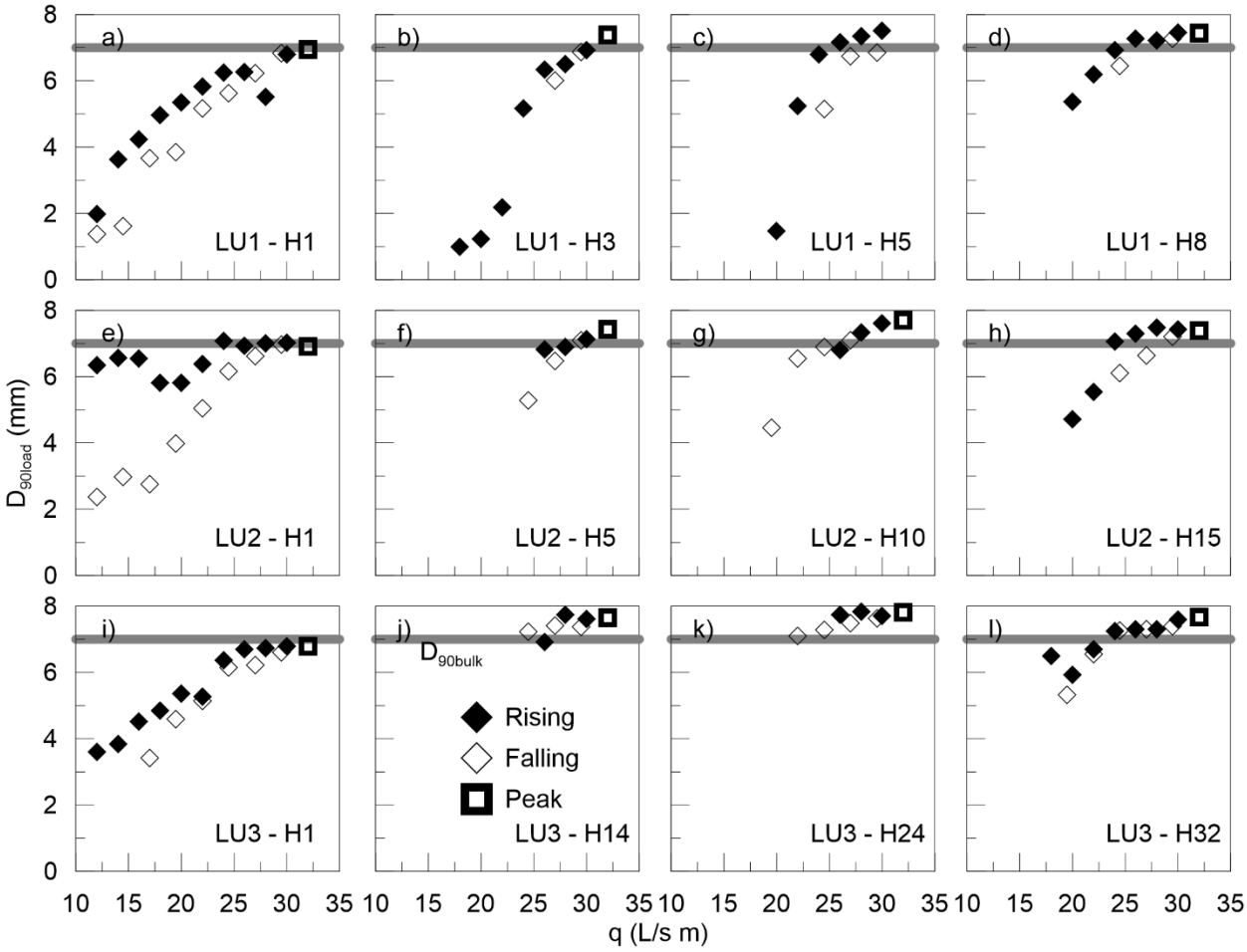

Figure 4.10: Bedload percentile phase plots of D_{90load} for select hydrographs from each experiment (LU1 top row, LU2 middle row, LU3 bottom row). D_{90bulk} indicated by horizontal line. Hi denotes the hydrograph number of that specific experiment.

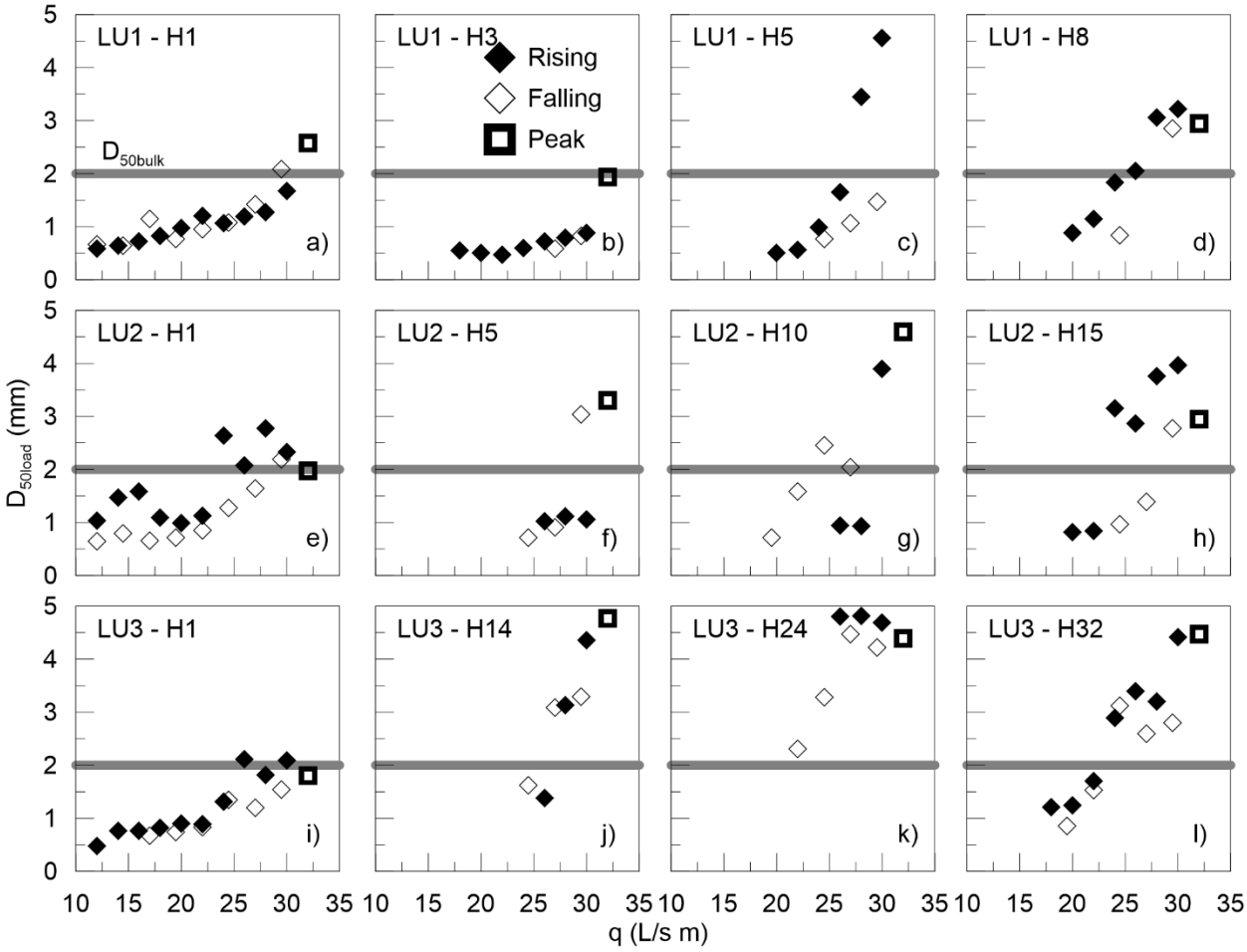

Figure 4.11: Bedload percentile phase plots of D_{50load} for select hydrographs from each experiment (LU1 top row, LU2 middle row, LU3 bottom row). D_{50bulk} indicated by horizontal line. Hi denotes the hydrograph number of that specific experiment.

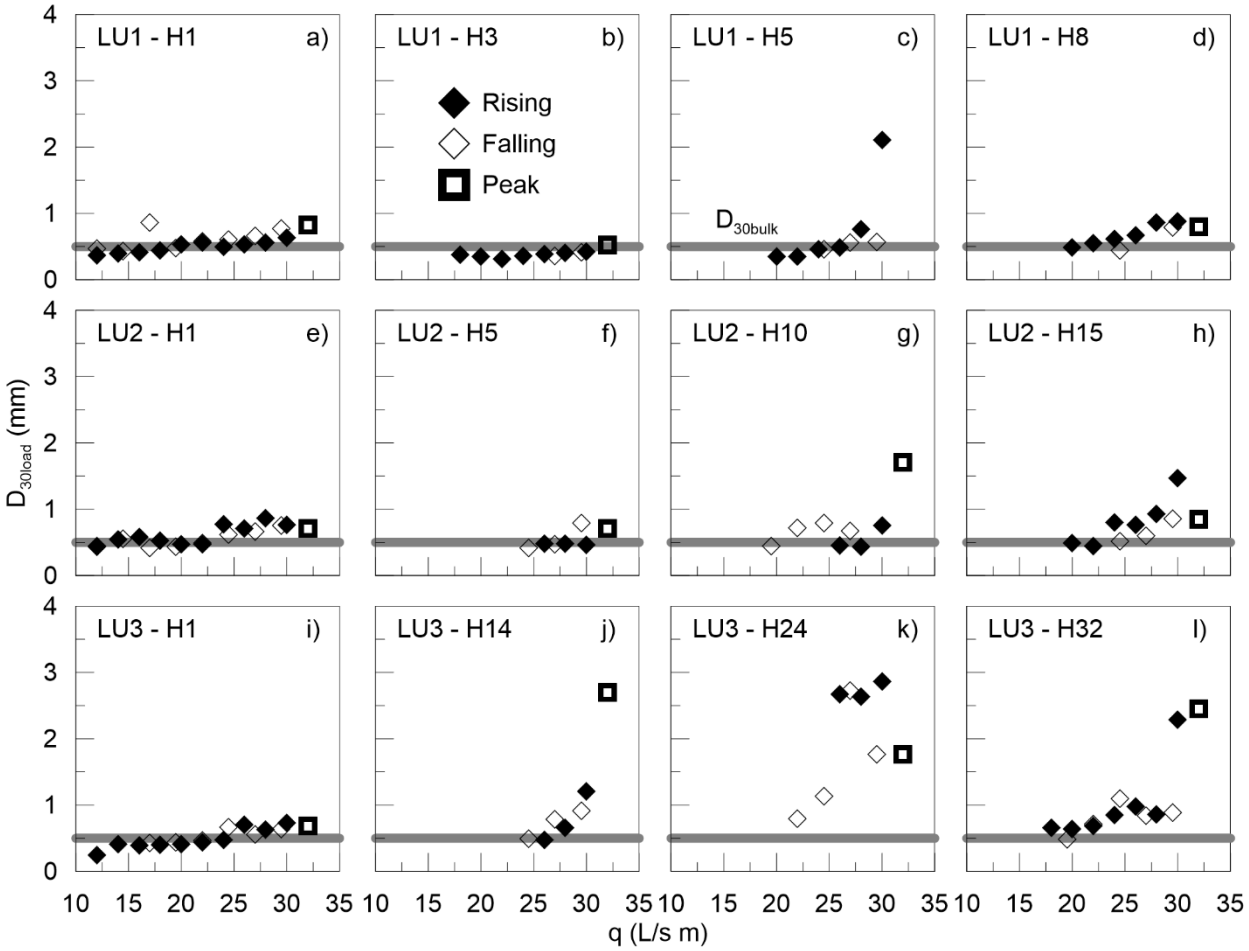

Figure 4.12: Bedload percentile phase plots of D_{30load} for select hydrographs from each experiment (LU1 top row, LU2 middle row, LU3 bottom row). D_{30bulk} indicated by horizontal line. Hi denotes the hydrograph number of that specific experiment.

4.4.4 Bed Surface Texture

In all experiments, armor layers developed on the channel bed, with surface percentiles D_{90surf}, D_{50surf} and D_{30surf} all coarser than their respective bulk mixture values (Figure 4.13). The experiments all begin with a slightly coarser bed than their bulk mixtures which is attributed to the period of water working to establish flow histories. D_{90surf} for all experiments shows more scatter than the smaller percentiles. LU2 and LU3 both have similar average surface textures throughout the experiments, with average $D_{90surf} \approx 8.5$ mm, $D_{50surf} \approx 4.5$ mm, $D_{30surf} \approx 3.5$ mm. LU1 coarsens to a greater extent until approximately midway through the experiment, when it exhibits a period of fining and approaches the equilibrium values of LU2 and LU3, although still slightly coarser. For LU2 and LU3, the most abrupt changes in surface texture

correspond to hydrographs which exhibited a counterclockwise bedload hysteresis. It should be noted that these results differ from those obtained in other studies as the surface texture here is measured between hydrographs, not throughout [*Hassan et al.*, 2006; *Mao*, 2012; *Wang et al.*, 2015].

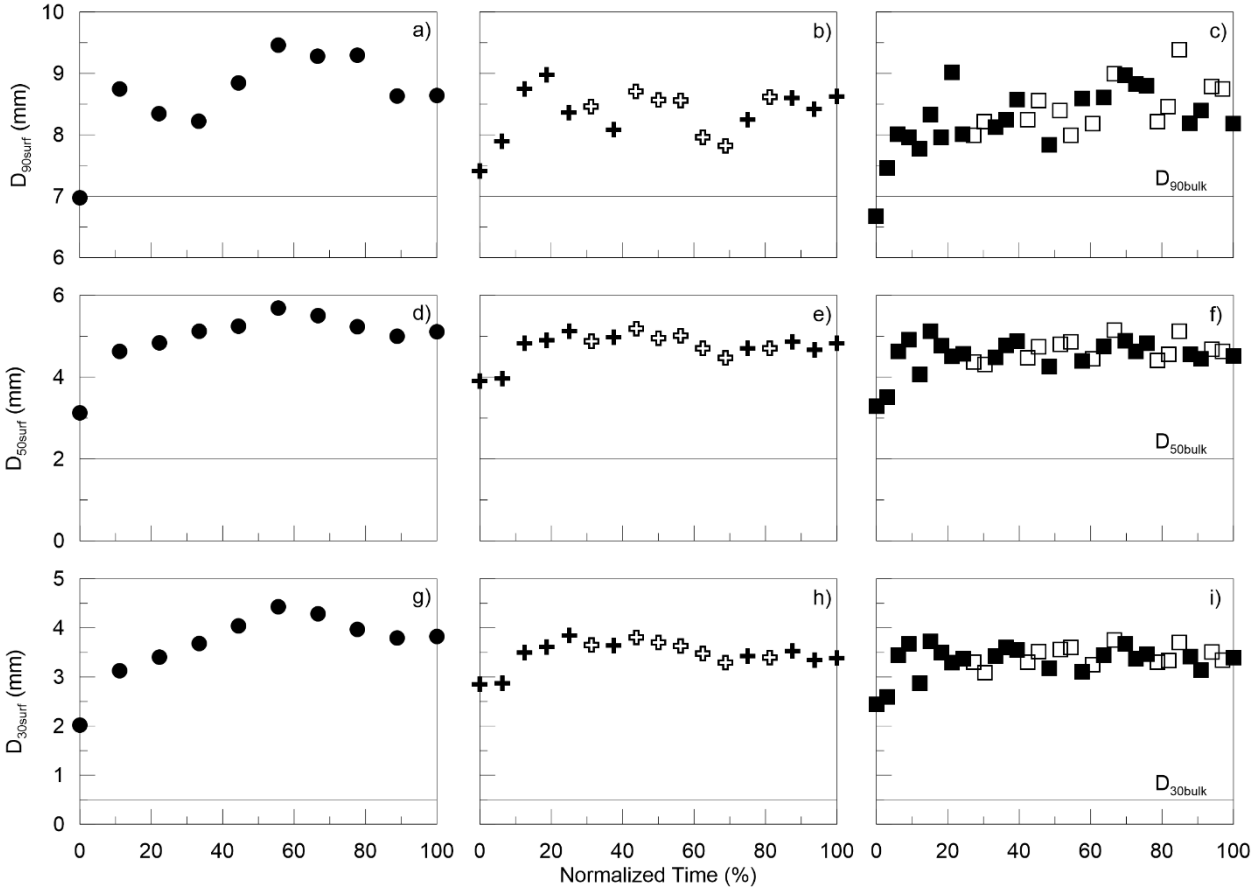

Figure 4.13: 90th percentile of the surface (D_{90surf}) after each hydrograph for a) LU1, b) LU2 and c) LU3. 50th percentile of the surface (D_{50surf}) after each hydrograph for d) LU1, e) LU2 and f) LU3. 30th percentile of the surface (D_{30surf}) at peak discharge for each hydrograph for g) LU1, h) LU2 and i) LU3. Solid and hollow symbols represent hydrographs exhibiting clockwise hysteresis and counterclockwise hysteresis, respectively. Bulk percentiles indicated by horizontal lines. Note: No counterclockwise hysteresis was exhibited in LU1.

4.4.5 Topographic Variability

For each scan, the 20 longitudinal profiles were merged together to create a digital elevation model (DEM), representing the bed topography after each hydrograph. Successive DEMs were compared using DEM

differencing and the net volumes of both erosion (V_e) and deposition (V_d) were determined. Normalized erosion ($\Delta_{z,e}$) depth was calculated as:

$$\Delta_{z,e} = \frac{V_e}{A_e} \quad \textbf{(4.3)}$$

where A_e is the planar area of the bed which experienced erosion. Similar calculations were undertaken for the normalized deposition ($\Delta_{z,d}$) depth, using V_d and A_d. Additionally, A_e and A_d were compared against the total planar area (A_T), which is the full area of the 3.5 m long study reach, to determine the relative fraction of the bed which experienced erosion and deposition. These analyses allow an additional assessment of when the channel reaches an equilibrium condition between hydrographs. Normalized experiment time versus erosion/deposition for experiments LU1, LU2 and LU3 are illustrated in Figures 4.14a, 4.14c, and 4.14e respectively; where maximum scour depths of 5.0 mm, 8.0 mm and 3.0 mm respectively were observed (all corresponding to the initial hydrograph of each experiment).

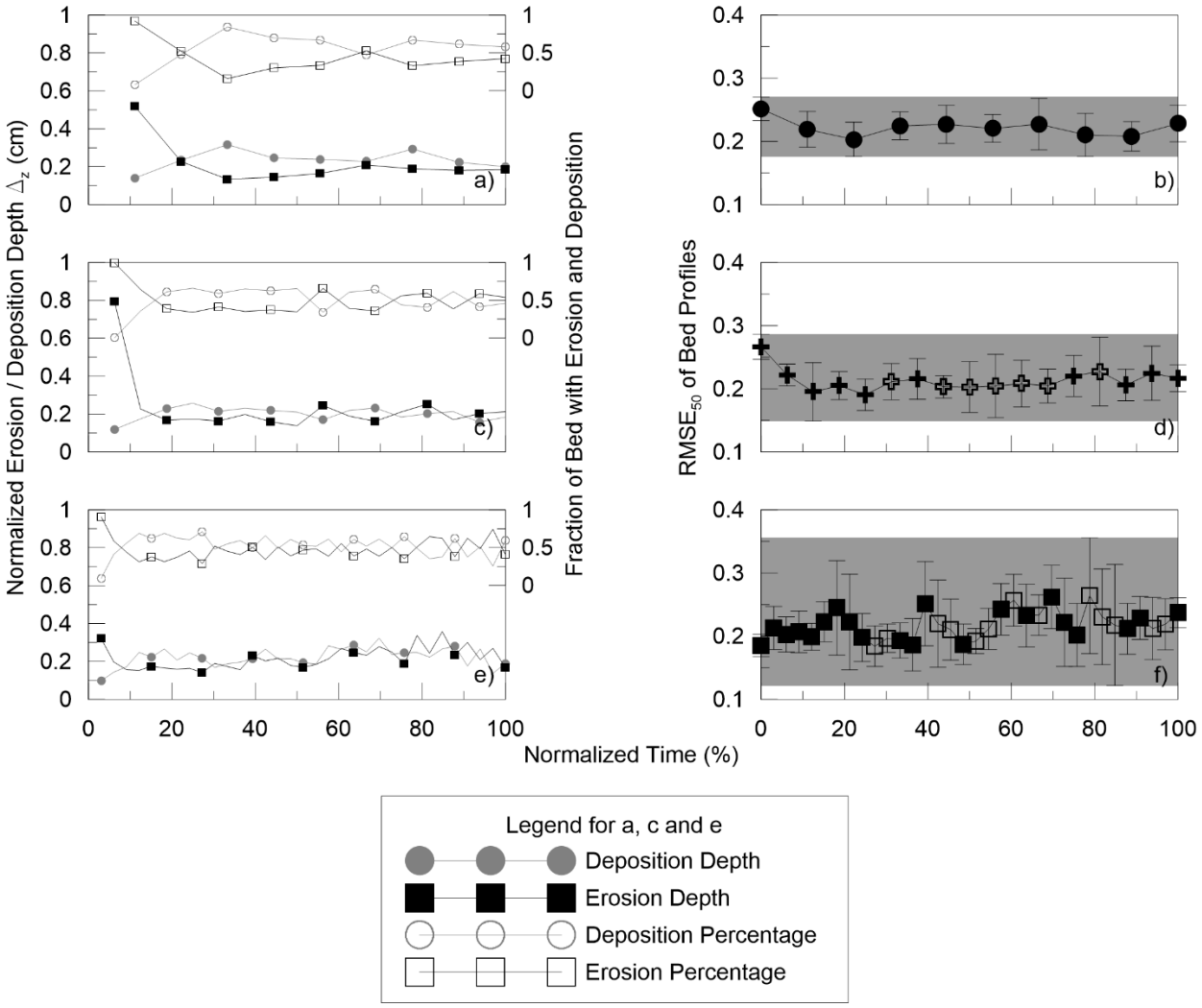

Figure 4.14: Normalized erosion and deposition depths and the proportion of the bed undergoing erosion and deposition for a,b) LU1, c,d) LU2 and e,f) LU3. Median RMSE of the 20 profiles in ($RMSE_{50}$) each bed scan, where the error bars represent one standard deviation of the RMSE values (σ_{RMSE}). See text for details. Solid and hollow symbols in b, d and f represent hydrographs exhibiting clockwise hysteresis and counterclockwise hysteresis, respectively. Grey patches depict the range of bed variability for each experiment.

Consistent with the high yields and transport rates observed after the first hydrograph of each experiment, nearly 100% of the bed in the 3.5 m long study reach exhibited erosion during this period. In subsequent events, deposition trends dominate, which were eventually replaced by alternating erosion and deposition trends in later hydrographs (indicating an approximate balance between erosion and depositional areas).

Normalized erosion and deposition depths trend towards a value of approximately 2.0 mm, which corresponds to D_{50bulk}. As the frequency of hydrographs increases from LU1 to LU3, oscillations between erosion and deposition occur earlier in each experiment. LU1 does not reach an equilibrium condition, but it is clearly trending in that particular direction (Figure 4.14a).

To assess the change in surface structure and micro-scale bedforms, a bed variability analysis was conducted. Linear regressions were fitted to each of the 20 longitudinal profile scans per hydrograph [*Richards*, 1976], and the residual values from the regressions used as a metric of bed variability for each specific longitudinal profile. The metric chosen was the root-mean-square error (RMSE) for each regression, which represents the square-root of the residual variance. The median RMSE ($RMSE_{50}$) for the 20 profiles was calculated from the median of the 20 RMSE values from the linear regressions after each hydrograph. This $RMSE_{50}$ parameter represents the overall variability of the bed after each hydrograph. Correspondingly, the standard deviation of the 20 RMSE (σ_{RMSE}) values for each scan were also computed, thus providing a metric for the intra-bed variability (how different the variability of the 20 different profiles is relative to each other) from each scan. All linear regressions for this analysis are statistically significant at the 95% confidence level, with correspondingly high R^2 values ($R^2 \geq 0.95$). Second-order polynomials were also tested, and yielded similar results to the linear models, as such, the linear models were used [*Chayes*, 1970].

All three experiments have similar average $RMSE_{50}$ values throughout the entire experiment, with $RMSE_{50}$ values of 0.222, 0.213 and 0.218 for LU1, LU2 and LU3 respectively. Variability in $RMSE_{50}$ increases with each experiment (increasing hydrograph frequency), with $RMSE_{50}$ standard deviations of 0.014, 0.017 and 0.022 for LU1, LU2 and LU3, respectively, although this increase from LU1 to LU3 was not found to be statistically different ($p=0.12$).

Figures 4.14b, 4.14d and 4.14f illustrate the $RMSE_{50}$ values for each scan, as well as the σ_{RMSE} of the 20 RMSE values for each hydrograph (shown by the error bars as $\pm\sigma_{RMSE}$). The increased variability of $RMSE_{50}$ values is visible in LU3. Correspondingly, increases in σ_{RMSE} for LU3 (Figure 4.14f) - indicating greater topographic variability (higher σ_{RMSE}) are also visible, which also increases with each subsequent hydrograph (higher standard deviation of $RMSE_{50}$ values). Increased topographic variability with increasing hydrograph frequency and decreasing duration is further accentuated in Figures 4.14b, 4.14d, and 4.14f denoted by the vertical limits of the shaded regions.

4.5 Discussion

4.5.1 Hydrograph Unsteadiness on Bedload Transport, Hysteresis and Surface Texture

Hydrograph unsteadiness has been shown here to impact bedload transport rates, percentiles, hysteresis and the resulting surface composition (texture and structure). The decreasing event durations, and flashier hydrographs of experiments LU2 and LU3, relative to experiment LU1, resulted in higher bedload transport rates (Figure 4.15) and tighter hysteresis loops (Figure 4.6). Conversely, the longer duration hydrographs of experiment LU1 yielded lower bedload transport rates which notably decreased during the falling limb of each event resulting in strong clockwise hysteresis patterns. Similar trends were observed by *Mao* [2012], where particle rearrangements and bed surface restructuring during the falling hydrograph limbs gave rise to an increased critical shear stress and consequently, a reduction in sediment transport rates.

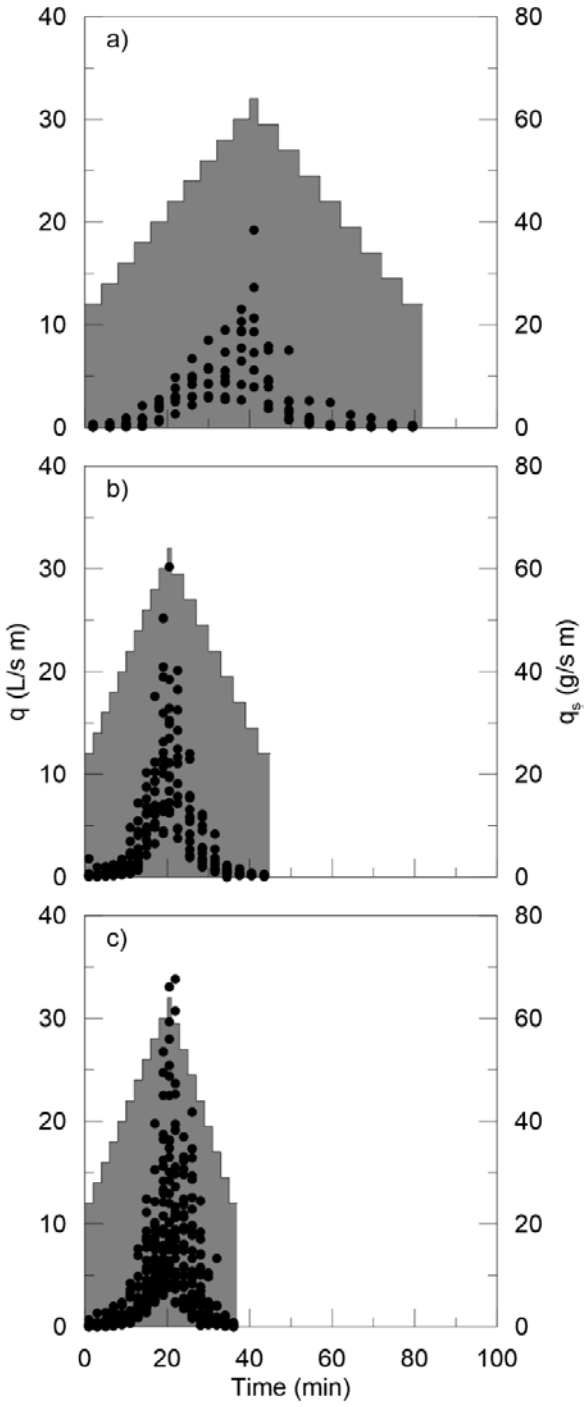

Figure 4.15: LU1 (a) LU2 (b) and LU3 (c) hydrographs scenario (grey patches) with all the bedload transport rates collected during each experiment (black dots). Note: the bedload transport rates from the first hydrograph of each experiment are not included.

Trends in fractional transport ratios reported here are consistent with those reported in other unsteady flow experiments with an overrepresentation of coarse material on the rising limb, an overrepresentation of fine material on the falling limb, and a clockwise hysteresis pattern in the bedload percentiles [*Hassan et al.*, 2006; *Wang et al.*, 2015]. With decreasing duration (increasing flashiness), the bedload percentiles became much more variable (Figure 4.9), with steeper hysteresis loops for the median and finer particles in the bedload (Figures 4.11 and 4.12). Bedload hysteresis trends also appear to influence this variability in bedload percentiles, as the bedload percentiles in LU2 and LU3 begin to depart from the bulk values when the hysteresis trends begin to switch between clockwise and counterclockwise (Figure 4.9e, 4.9f, 4.9h, 4.9i).

Likely the largest impact of the shorter duration, flashier hydrographs is in the bedload hysteresis direction and resulting sediment yields, characterized by H_r. Longer duration hydrographs (LU1) exhibited hysteresis ratios greater than 1, with significantly less material being transported on the falling limbs. Shorter duration hydrographs exhibited hysteresis ratios close to 1.0 which oscillate about unity, in either clockwise or counterclockwise trends. As mentioned above, this oscillation also corresponds to a departure from bulk values of the bedload percentiles (Figure 4.9e, 4.9f, 4.9h, 4.9i) and a steepening of the bedload size hysteresis (Figures 4.10 – 4.12).

Figure 4.16 illustrates the normalized sediment yields (Y_{out}/Y_{in}) for i) all hydrographs (combination of both rising and falling limbs), ii) the rising limbs of all hydrographs, and iii) the falling limbs of all hydrographs for each experiment. The yield from the first hydrograph of each experiment was not included due to the much higher rates (previously discussed). Although LU2 and LU3 have flashier rising limbs than LU1, the normalized yield for the rising limb is similar for all the experiments (ranging from 0.59 to 0.67). The major difference in experiment results are in the falling limbs. The falling limb flow durations of LU2 and LU3 are 60% and 40% of LU1, respectively. Therefore, the flashiness of the falling limb largely controlled the amount of sediment being transported; with LU1 only having a falling limb yield ratio of 0.20, while LU3 has a falling yield ratio of 0.70. Observations on falling limb duration had been hypothesized by *Hassan et al.* [2006] to be a critical factor governing the amount of vertical sorting of the bed, with shorter durations resulting in insufficient time for the sorting process to occur. *Hassan et al.* [2006] also attributed observed clockwise hysteresis to the sediment starved nature of the experimental channel, as their experiments were conducted with no sediment supply. In this study, experiments had identical sediment supply rates with only the duration of sediment supply varied (derived from the differing hydrograph durations). The slightly coarser bed texture corresponding to the longer duration hydrographs (Figure 4.13)

supports the possibility of vertical sorting being a contributing factor for the observed differences in transport rates.

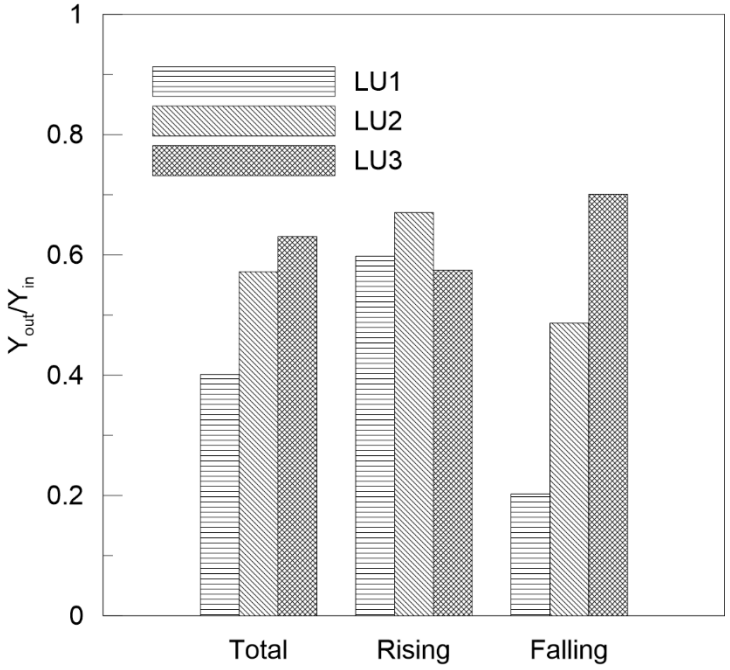

Figure 4.16: Normalized yield (Y_{out}/Y_{in}) for total yield (combination of rising and falling limbs), rising limb yield and falling limb yield for all hydrographs in each experiment, excluding the first hydrograph.

Another notable difference between hydrographs of each experiment was in the variability of bed topography. The shorter duration hydrographs resulted in larger changes in bed variability after successive hydrographs and greater intra-bed variability between the hydrographs. While the exact reason for this increased bed variability remains unknown, there are a number of possible contributing factors. The shorter falling hydrograph limbs of experiment LU3 may allow less time for the bed to reorganize after the peak, which is also supported by the higher transport rates observed on the falling limbs, relative to LU1. Although not physically quantified, a number of microform clusters were observed to develop on the bed, and the increased variability could be clusters forming as an additional energy dissipation mechanism [*Papanicolaou and Schuyler*, 2003] to account for the flashy, frequent events in LU3. This more variable bed structure is hypothesized to be diminishing the entrainment rate of the sand grains by sheltering them from the flow, which is supported by the transport ratios trending towards equal mobility (Figure 4.8), the increased variability of D_{30load} for LU3 (Figure 4.9i) and the slightly finer bed texture of LU3 relative to LU1 (Figure 4.13).

4.5.2 Comparison with Observations in Urbanized Rivers

Although no field study has documented bedload transport rate as detailed as this lab study in urban settings, a number of similarities exist between results shown in this study and documented characteristics of urban watercourses. *Annable et al.* [2012] documented decreasing scatter in bedload rating curves with increasing urbanization. While they hypothesized these decreases were due to a reduced and more longitudinally evenly dispersed bed material supply sources, it could also be in part due to the flashier hydrographs consistent with their study reaches, which could be exhibiting less hysteresis effects ($H_r \approx 1$).

Increased topographic variability has been documented in urban streams with shorter, steeper riffles and correspondingly deeper pools [*Hawley et al.*, 2013] and more topographically variable riffles [*Annable*, 2010]. In both cases, this was hypothesized to be additional form roughness to account for the additional energy introduced through flashier, more frequent floods, an observation that directly supports the increased topographic variability observed in the flashier hydrographs of this laboratory study.

One of the most documented traits in gravel-bed streams undergoing urbanization is bed coarsening [*Finkenbine et al.*, 2000; *Pizzuto et al.*, 2000; *Annable et al.*, 2012; *Hawley et al.*, 2013]. The results from this study show the opposite, in that the hydrographs corresponding to a non-urban watershed resulted in a coarser surface layer. This is attributed to the fact that the sediment supplies were identical for all the experiments in this study. Armoring has been strongly associated with reductions in sediment supply [*Dietrich et al.*, 1989; *Buffington and Montgomery*, 1999], which are believed to occur after the initial urban build-out period [*Wolman*, 1967; *Chin*, 2006; *Annable et al.*, 2012]. While the objective of this study was to evaluate the change in sediment transport dynamics and bed morphology associated with the hydrologic changes of urbanization, this result enforces the complex interaction exhibited between changes in both hydrology and sediment supply and their respective influences on bed morphology at the field-scale.

4.5.3 Impacts on the Evolution of Urban Rivers and Implications to Stream Rehabilitation and Stormwater Management

The most frequently observed change to channel morphology due to urbanization has been channel enlargement, either through incision, widening, or a combination thereof [*Hammer*, 1972; *Booth*, 1990; *Pizzuto et al.*, 2000; *Chin*, 2006; *Hawley and Bledsoe*, 2013]. Since urbanization increases the frequency of competent floods, it follows that the total flow work index, W_k, (Equation 4.2) would also increase over the long-term due to a greater volume of water performing work on the channel [*Annable et al.*, 2012;

Plumb et al., Chapter 3]. An increase in channel width (B) would reduce W_k thus attempting to return the channel to a quasi-equilibrium condition. Correspondingly, an increase in form roughness would increase the flow depth, in turn reducing the flow velocity, energy gradient and shear velocity, also serving to decrease W_k. In this study, the channel sidewalls were non-erodible, and as such, the topographic variability adjusted to reduce W_k. *Annable et al.* [2012] reported little changes in bankfull channel width, but more frequent floodplain inundation thereby increasing B, as well as increased topographic variability [*Annable*, 2010]. *Hawley et al.* [2013] reported a combination of channel widening and increases in topographic variability. These trajectories of change may be important factors to consider for stream restoration projects in urban or urbanizing watersheds. If channel width is a constraint, for example, a more variable bed profile may be a sufficient and necessary measure (in combination with floodplain connectivity, if possible) to account for the changing boundary conditions associated with watershed urbanization. The strong tie between falling limb durations and bedload transport properties also has implications on stormwater management, which causes changes to the falling limbs of events, impacting sediment transport and erosion in channels [*McCuen and Moglen*, 1989; *MacRae*, 1997]. In reaches below dams where aquatic habitat is often improved through controlled water releases to mobilize sediment [*Battisacco et al.*, 2016; *Juez et al.*, 2016], a controlled flood with a shorter falling limb may result in the additional desired morphological variability.

4.6 Conclusions

Laboratory experiments were conducted to investigate how common hydrologic changes associated with watershed urbanization impact bedload transport rates and channel morphology in a gravel-bed channel. Three hydrologic conditions (experiments) representing different levels of watershed urbanization were derived from hydrometric gauge data of urbanizing watersheds in Ontario, Canada. Each experiment consisted of a series of hydrographs with equal peak discharge and varying duration and flashiness.

Longer duration hydrographs resulted in lower sediment transport rates, clockwise hysteresis loops and less topographic variability in the channel bed. Conversely, shorter duration hydrographs resulted in higher transport rates, more variable hysteresis, but generally closer to single value, and more topographic bed variability. A hysteresis ratio metric was introduced to quantify the bedload hysteresis. The mentioned variable hysteresis was attributed to vertical sorting and additional sheltering from larger grains and micro-scale structures, which is supported by the coarser bed of the longer duration hydrographs, fractional transport ratios, and topography scans. This hysteresis ratio was used to show that hydrographs where bed

material supply and transport is in disequilibrium result in clockwise hysteresis, whereas hydrographs that have equilibrium bed material supply and transport do not possess strong hysteresis characteristics.

The previously mentioned results confirm other research conducted on unsteady flow bedload transport in gravel-bed channels. Observations made here also relate to field scale observations made on urban river bedload transport dynamics and morphology. These observations have implications on stream restoration and stormwater management practices in urban or urbanizing watersheds.

Chapter 5
General Conclusions

5.1 Introduction

This thesis investigates the impacts of urbanization on bedforms in gravel-bed rivers. Changes to both channel form and process (bedload transport) are of interest. These changes are investigated at both field and laboratory scales and supplemented with sediment transport modeling and geomorphic work analyses. These approaches are complementary as the field results are limited to rivers in the same hydrophysiographic region, with detailed bedload transport measurements only available for one river. The laboratory and modeling studies allow more generalized interpretations of the alterations to channel processes due to urbanization. Key findings from each chapter are presented in the following section.

5.2 Summary of Results

Longitudinal profiles of 20 rivers in Southern Ontario were examined to determine if changes in bedforms exist between rural and urban rivers in Chapter 2. Both visual field identification and objective bedform identification methods were employed to eliminate bias associated with operator error. Results reveal that urban rivers possess deeper pools and more topographically variable longitudinal profiles. This increased topographic variability is hypothesized to be a manifestation of increased form roughness due to increased energy introduced due to more frequent competent discharge events. Increased form roughness acts as an additional energy dissipation mechanism.

Chapter 3 presents results from the field bedload transport campaign on a highly urbanized river. We used multiple methods to measure both coarse and fine particles comprising the transported bedload. A strong link was found between coarse particle mobility and the transport dynamics of finer material which tends to dominate the bedload. Coarse particle mobility is very low and particles transport at much shorter distances than those reported in literature. Finer bed material transport is more variable when coarse particles are less mobile. The limited mobility and short transport distances of coarse particles may be a contributing factor in the observed topographic variability documented in the previous chapter. Measured transport data were also used to calibrate a fractional sediment transport model which was combined with hydrometric data corresponding to different levels of watershed urbanization to perform a geomorphic work analysis. Urbanization is increasing the frequency, volume and time of competent discharge events

(capable of performing work on the channel), which supports the observations made in the previous chapter. Greater increases of intermediate discharge events were observed. Less urban streams are more influenced by larger discharge events, while urbanization is shifting the geomorphic significance to lower (but still competent) discharges.

Observations and results from the field study were used to develop a more general unsteady flow laboratory experiment presented in Chapter 4. Similar to Chapter 3, a number of land-use scenarios representing different levels of watershed urbanization were developed from measured hydrometric data. Results show that both unsteady bedload transport dynamics and resulting bed morphology change with different levels of urbanization, with similarities between laboratory results and field results observed in the previous chapters and in published literature. Shorter duration hydrographs (corresponding to urban conditions) possess higher transport rates, less pronounced bedload hysteresis loops and more topographic variability of the bed. These results align with field results presented in previous chapters, as well as existing field studies in urban rivers. A proposed parameter for evaluating the degree of hysteresis shows sediment transport is closely linked with falling limb dynamics.

5.3 Implications of Results on Engineering Practices

Results presented in this thesis indicate that urban rivers are evolving to a state of more topographic variability, although it is unknown if this is a final quasi-equilibrium state. Nonetheless, additional roughness results in higher flow depths for a given discharge. This has a direct impact on the prediction of flood elevations, which is particularly important in urban areas due to the close proximity of built infrastructure and increased risk to human safety. Results in this study confirm previous research that the magnitude and frequency of flood events in urban rivers are increasing, which further emphasizes the importance of accurate flood elevation predictions.

Results presented in this thesis also have implications on river rehabilitation techniques. If a more topographically variable channel is a long-term state for urban rivers, this will need to be considered when performing channel rehabilitation designs. A common technique in urban stream rehabilitation is to alter channel bedforms through the construction of riffles and pools. Current guidelines informing practitioners are generally derived from relationships made in more natural rivers. The insight gained from Chapter 2 of this thesis can be used to better inform engineers, geomorphologists and ecologists on target

morphologies when performing these designs, in addition to the current tools available, specifically that a more topographically variable bed may be necessary in highly hydromodified watersheds. An understanding of bedload transport is important in the success of a stream rehabilitation design. The bedload transport data collected in this thesis is unique as datasets of this caliber in urban rivers are lacking in literature. Data and results presented in this thesis is an important contribution to further our understanding of how channel processes are evolving in urbanizing rivers.

Results from the laboratory study indicate bedload transport is closely linked to falling limb characteristics of hydrographs. Stormwater management (SWM) is known to impact the falling limb of flood events, and results from this thesis can be used to better assess the impacts of different SWM alternatives on sediment transport and channel erosion. Additionally, controlled floods downstream of dams are becoming increasingly common to augment aquatic habitat by increasing morphological diversity. Results from this thesis (Chapter 4) can be expanded on and used to assist in the design of hydrograph characteristics of the flood to target specific sediment transport objectives.

5.4 Future Research

The results and methods presented in this thesis create many opportunities for further research to build upon them. Future research is possible for both form and process studies at the field scale as well as modeling, geomorphic work analyses and laboratory studies.

While more labor and time intensive to obtain, process based field studies in urban rivers are paramount to furthering our understanding on how these rivers have evolved due to anthropogenic modification. The methods presented in Chapter 3 provide a framework to evaluate the impacts of urbanization relative to unaltered rivers, or throughout the urbanization process of a single river. Due to the lack of long-term datasets spanning the entire period of urbanization, assumptions of the land-use scenarios were made using a space-for-time substitution with an adjacent watershed. As more hydrometric datasets spanning from unaltered to highly modified become available, this framework can be applied to eliminate the possible biases introduced through the space-for-time substitution conducted here. Another limitation exists in the sediment transport model used for the geomorphic work analysis. This model was calibrated based on only measurements of the most urban scenario, since no sediment transport measurements were available for other periods. Since urbanization is known to change bed surface characteristics, channel width and depth,

which heavily influence sediment transport characteristics [*Wilcock and Crowe*, 2003], it follows that for a more representative characterization of sediment transport characteristics, both detailed morphologic bed surface, and bedload transport measurements are required for each stage of watershed urbanization. Thus, longer term datasets can be collected in urbanizing watersheds collecting hydrometric data, bed surface samples and sediment transport samples at different stages of watershed urbanization. Sediment transport measurements are logistically difficult to obtain, however even a small number at discharges close to the threshold of movement can greatly improve the predictions of sediment transport models [*Wilcock*, 2001a].

Urbanization can lead to different changes depending on hydrophysiographic region [*Chin*, 2006]. Methods and results from the form based field study in Chapter 2 can be extended to other climactic regions to compare if urbanization produces similar changes to channel bedforms, thus further generalizing the results presented in this thesis.

Morphologic changes associated with urbanization are believed to be a combination of both changes in hydrology and changes in sediment supply delivered to the channel. The laboratory experiments in Chapter 4 only investigated the changes associated with hydrology, and it is acknowledged that this is only one contributing factor influencing the morphologic change of rivers. The framework used in the laboratory study can be repeated in combination with alterations to sediment supply and compared to results presented here to attempt to isolate the impacts of both hydrology and sediment supply and assess their combined impacts on sediment transport and bed morphology. Additionally, different hydrologic scenarios representing a range of discharge events could be incorporated to assess the impacts of different flood magnitudes in addition to changing frequencies.

This thesis offers insight in how urbanization is changing channel processes influencing previously observed changes in channel morphology. Both methods and results obtained can be used to guide further research on urban morphodynamics in gravel-bed rivers.

References

Alila, Y., P. K. Kuraś, M. Schnorbus, and R. Hudson (2009), Forests and floods: A new paradigm sheds light on age-old controversies, *Water Resour. Res.*, W08416, doi:10.1029/2008WR007207.

Allmendinger, N. E., J. E. Pizzuto, G. E. Moglen, and M. Lewicki (2007), A Sediment Budget for an Urbanizing Watershed, 1951-1996, Montgomery County, Maryland, U.S.A., *J. Am. Water Resour. Assoc.*, *43*(6), 1483-1498, doi:10.1111/j.1752-1688.2007.00122.x.

Andrews, E. D. (1980), Effective and bankfull discharges of streams in the Yampa River Basin, Colorado and Wyoming, *J. Hydrol.*, *46*, 311-330.

Annable, W. K. (1996a), *Database of morphologic characteristics of watercourses in Southern Ontario*, Ontario Ministry of Natural Resources, ISBN:0-7778-5112-1.

Annable, W. K. (1996b), *Morphological relationships of rural water courses in southwestern Ontario and selected field methods in fluvial geomorphology*, Ontario Ministry of Natural Resources, ISBN:0-7778-5113-X.

Annable, W. K. (2010), Quasi-equilibrium conditions of urban gravel-bed stream channels in southern Ontario, Canada, and their implications for urban-stream restoration, Ph.D. Thesis, Colorado State University, Fort Collins, Colorado, USA.

Annable, W. K., V. G. Lounder, and C. C. Watson (2011), Estimating channel-forming discharge in urban watercourses, *River Res. Appl.*, *27*(6), 738-753, doi:10.1002/rra.1391.

Annable, W. K., C. C. Watson, and P. J. Thompson (2012), Quasi-equilibrium conditions of urban gravel-bed stream channels in southern Ontario, Canada, *River Res. Appl.*, *28*(3), 302-325, doi:10.1002/rra.1457.

Ashworth, P. J., and R. I. Ferguson (1989), Size-selective entrainment of bed load in gravel bed streams, *Water Resour. Res.*, *25*(4), 627-634.

Battisacco, E., M. J. Franca, and A. J. Schleiss (2016), Sediment replenishment: Influence of the geometrical configuration on the morphological evolution of channel-bed, *Water Resour. Res.*, *52*, 8879–8894, doi:10.1002/2016WR019157.

Benson, M. A., and D. M. Thomas (1966), A definition of dominant discharge, *Bull. Int. Assoc. Sci. Hydrol.*, *11*(2), 76-80, doi:10.1080/02626666609493460.

Bernhardt, E. S., et al. (2005), Synthesizing U.S. River Restoration Efforts, *Science*, *308*(5722), 636-637, doi:10.1126/science.1109769.

Biedenharn, D. S., R. R. Copeland, C. R. Thorne, R. D. Hey, and C. C. Watson (2000), Effective Discharge Calculation: A Practical Guide *Rep.*, U.S. Army Corps of Engineers.

Booth, D. B. (1990), Stream-channel incision following drainage-basin urbanization, *J. Am. Water Resour. Assoc.*, *26*(3), 407-417, doi:10.1111/j.1752-1688.1990.tb01380.x.

Booth, D. B. (2005), Challenges and prospects for restoring urban streams: a perspective from the Pacific Northwest of North America, *J. N. Am. Benthol. Soc.*, *24*(3), 724–737, doi:10.1899/04-025.1.

Bormann, N. E., and P. Y. Julien (1991), Scour downstream of grade-control structures, *J. Hydraul. Eng.*, *117*(5), 579-594.

Brayshaw, A. C., L. E. Frostick, and I. Reid (1983), The hydrodynamics of particle clusters and sediment entrapment in coarse alluvial channels, *Sedimentology*, *30*(1), 137-143.

Brown, C. B. (1950), Sediment Transportation, in *Engineering Hydraulics*, edited by H. Rouse, pp. 769-857, John Wiley, New York.

Buffington, J. M. (2012), Changes in Channel Morphology Over Human Time Scales, in *Gravel-bed Rivers: Processes, Tools, Environments*, edited by M. Church, P. M. Biron and A. G. Roy, pp. 435-463, John Wiley & Sons Ltd., UK.

Buffington, J. M., and D. R. Montgomery (1999), Effects of sediment supply on surface textures of gravel-bed rivers, *Water Resour. Res.*, *35*(11), 3523-3530, doi:10.1029/1999WR900232.

Buffington, J. M., T. E. Lisle, R. D. Woodsmith, and S. Hilton (2002), Controls on the size and occurrence of pools in coarse-grained forest rivers, *River Res. Appl.*, *18*(6), 507-531, doi:10.1002/rra.693.

Bunte, K., and S. R. Abt (2001), Sampling surface and subsurface particle-size distributions in wadable gravel-and-cobble-bed streams for analyses in sediment transport, hydraulics, and streambed monitoring, *Gen. Tech. Rep. RMRS-GTR-74*, U.S. Dep. of Agric., For. Serv., Rocky Mt. Res. Stat., Fort Collins, CO.

Chartrand, S. M., M. A. Hassan, and V. Radić (2015), Pool-riffle sedimentation and surface texture trends in a gravel bed stream, *Water Resour. Res.*, *51*, 8704-8728, doi:10.1002/2015WR017840.

Chayes, F. (1970), On Deciding Whether Trend Surfaces of Progressively Higher Order Are Meaningful, *Geol. Soc. of Am. Bull.*, *81*(4), 1273-1278.

Chin, A. (2006), Urban transformation of river landscapes in a global context, *Geomorphology*, *79*, 460-487, doi:10.1016/j.geomorph.2006.06.033.

Church, M., and M. A. Hassan (1992), Size and distance of travel of unconstrained clasts on a streambed, *Water Resour. Res.*, *28*(1), 299-303, doi:10.1029/91WR02523.

Church, M., M. A. Hassan, and J. F. Wolcott (1998), Stabilizing self-organized structures in gravel-bed stream channels: Field and experimental observations, *Water Resour. Res.*, *34*(11), 3169-3179, doi:10.1029/98WR00484.

Church, M., and M. A. Hassan (2002), Mobility of bed material in Harris Creek, *Water Resour. Res.*, *38*(11), 1237, doi:10.1029/.2001WR000753.

Church, M. A., D. G. McLean, and J. F. Wolcott (1987), River bed gravels: sampling and analysis, in *Sediment Transport in Gravel-bed Rivers*, edited by C. R. Thorne, J. C. Bathurst and R. D. Hey, John Wiley & Sons Ltd., New York.

Curran, J. C., and P. R. Wilcock (2005), Effect of Sand Supply on Transport Rates in a Gravel-Bed Channel, *J Hydraul. Eng.*, *131*(11), 961-967, doi:10.1061/(ASCE)0733-9429(2005)131:11(961).

Dietrich, W. E., J. W. Kirchner, H. Ikeda, and F. Iseya (1989), Sediment supply and the development of the

coarse surface layer in gravel-bedded rivers, *Nature*, *340*, 215-217, doi:10.1038/340215a0.

Edwards, T. K., and G. D. Glysson (1988), *Field Methods for Measurement of Fluvial Sediment*, Dep. Of the Inter., U.S. Geol. Surv.

Einstein, H. A. (1937), Bed load transport as a probability problem, Ph.D. Thesis, ETH Zurich, Zurich, Switzerland.

Emmett, W. W. (1980), A field calibration of the sediment-trapping characteristics of the Helley-Smith bedload sampler, *Prof Paper 1139*, U.S. Geol. Surv., 44 pp.

Emmett, W. W., and M. G. Wolman (2001), Effective discharge and gravel-bed rivers, *Earth Surf. Process. and Landforms*, *26*, 1369-1380, doi:10.1002/esp.303.

Finkenbine, J. K., J. W. Atwater, and D. S. Mavinic (2000), Stream health after urbanization, *J. Am. Water Resour. Assoc.*, *36*, 1149-1160, doi:10.1111/j.1752-1688.2000.tb05717.x.

Graf, W. H., and L. Suszka (1985), Unsteady flow and its effect on sediment transport, paper presented at Proceedings of the 21st IAHR Congress (pp. 1–5).

Grant, G. E., S. L. Lewis, J. H. Swanson, J. H. Cissel, and J. J. McDonnell (2008), Effects of Forest Practices on Peak Flow and Consequent Channel Response: A State-of-Science Report for Western Oregon and Washington, *Gen. Tech. Rep. PNW-GTR-760*, U.S. Dep. of Agric., For. Serv., Pac. NW Res. Stat., Corvallis, OR.

Gregory, K. J. (2006), The human role in changing river channels, *Geomorphology*, *79*, 172-191, doi:10.1016/j.geomorph.2006.06.018

Hammer, T. R. (1972), Stream channel enlargement due to urbanization, *Water Resour. Res.*, *8*(6), 1530-1540, doi:10.1029/WR008i006p01530.

Hanrahan, T. P. (2007), Bedform morphology of salmon spawning areas in a large gravel-bed river, *Geomorphology*, *86*(3–4), 529 – 536, doi:10.1016/j.geomorph.2006.09.017.

Harper, D., M. Ebrahimnezhad, and F. Climent I Cot (1998), Artificial riffles in ri7er rehabilitation: setting the goals and measuring the successes, *Aquatic Conser: Mar. Freshw. Ecosyst.*, *8*, 5-16.

Haschenburger, J. K., and M. Church (1998), Bed material transport estimated from the virtual velocity of sediment, *Earth Surf. Process. and Landforms*, *23*, 791-808, doi:10.1002/(SICI)1096-9837(199809)23:9<791::AID-ESP888>3.0.CO;2-X.

Haschenburger, J. K., and P. R. Wilcock (2003), Partial transport in a natural gravel bed channel, *Water Resour. Res.*, *39*(1), 1020, doi:10.1029/2002WR001532.

Hassan, M. A., and M. Church (2001), Sensitivity of bed load transport in Harris Creek: Seasonal and spatial variation over a cobble-gravel bar, *Water Resour. Res.*, *37*(3), 813-825, doi:10.1029/2000WR900346.

Hassan, M. A., D. Brayshaw, Y. Alila, and E. Andrews (2014), Effective discharge in small formerly glaciated mountain streams of British Columbia: Limitations and implications, *Water Resour. Res.*, *50*, 4440-4458, doi:10.1002/2013WR014529.

Hassan, M. A., R. Egozi, and G. Parker (2006), Experiments on the effect of hydrograph characteristics on vertical grain sorting in gravel bed rivers, *Water Resour. Res.*, 42, W09408, doi:10.1029/2005WR004707.

Hawley, R. J., and B. P. Bledsoe (2011), How do flow peaks and durations change in suburbanizing semi-arid watersheds? A southern California case study, *J. Hydrol.*, *405*(1-2), 69-82, doi:10.1016/j.jhydrol.2011.05.011.

Hawley, R. J., and B. P. Bledsoe (2013), Channel enlargement in semiarid suburbanizing watersheds: A southern California case study, *J. Hydrol.*, *496*, 17 – 30, doi:10.1016/j.jhydrol.2013.05.010.

Hawley, R. J., K. R. MacMannis, and M. S. Wooten (2013), Bed coarsening, riffle shortening, and channel enlargement in urbanizing watersheds, northern Kentucky, USA, *Geomorphology*, *201*, 111-126, doi:10.1016/j.geomorph.2013.06.013.

Hayward, J. A. (1980), Hydrology and stream sediments in a mountain catchment, Special Pub. No. 17, Tussock Grasslands & Mountain Lands Institute, Lincoln College, 236 pp., Canterbury, New Zealand.

Helley, E. J., and W. Smith (1971), Development and calibration of a pressure-difference bedload sampler, *Open File Rep. 73-108*, U.S. Geol. Surv. Water Resour. Div., Menlo Park, California.

Hollis, G. E. (1975), The effect of urbanization on floods of different recurrence interval, *Water Resour. Res.*, *11*(3), 431-435, doi:10.1029/WR011i003p00431.

Humphries, R., J. G. Venditti, L. S. Sklar, and J. K. Wooster (2012), Experimental evidence for the effect of hydrographs on sediment pulse dynamics in gravel-bedded rivers, *Water Resour. Res.*, *48*, W01533, doi:10.1029/2011WR010419.

Jackson, W. L., and R. L. Beschta (1982), A model of two-phase bedload transport in an Oregon coast range stream, *Earth Surf. Process. and Landforms*, *7*, 517-527, doi:10.1002/esp.3290070602.

Juez, C., E. Battisacco, A.J. Schleiss, M.J. Franca (2016), Assessment of the performance of numerical modeling in reproducing a replenishment of sediments in a water-worked channel, *Adv. Water Resour.*, *92*, 10-22, doi:10.1016/j.advwatres.2016.03.010.

Julien, P. Y. (2002), *River Mechanics*, Cambridge University Press.

Keller, E. A. (1971), Areal sorting of bed-load material: The hypothesis of velocity reversal, *Geol. Soc. of Am. Bull.*, *82*, 753-756.

Keller, E. A., and W. N. Melhorn (1978), Rhythmic spacing and origin of pools and riffles, *Geol. Soc. of Am. Bull.*, *89*, 723-730.

Kellerhals, R., and M. Miles (1996), Fluvial geomorphology and fish habitat: Implications for river restoration, paper presented at Ecohydraulique 2000.

Kenney, M. A., P. R. Wilcock, B. F. Hobbs, N. E. Flores, and D. C. Martínez (2012), Is Urban Stream Restoration Worth It?, *J. Am. Water Resour. Assoc.*, *48(3)*, 603-615, doi:10.1111/j.1752-1688.2011.00635.x.

Klonsky, L., and R. M. Vogel (2011), Effective Measures of "Effective Discharge", *J. Geol.*, *119(1)*, 1-14,

doi:10.1086/657258.

Knighton, D. (1998), *Fluvial Forms & Processes: A New Perspective*, 383 pp., Oxford University Press Inc., New York.

Komar, P. D. (1987), Selective gravel entrainment and the empirical evaluation of flow competence, *Sedimentology*, *34*(6), 1165-1176, doi:10.1111/j.1365-3091.1987.tb00599.x.

Kondolf, G. M., and M. G. Wolman (1993), The sizes of salmonid spawning gravels, *Water Resour. Res.*, *29*(7), 2275-2285, doi:10.1029/93WR00402.

Konrad, C. P., D. B. Booth, and S. J. Burges (2005), Effects of urban development in the Puget Lowland, Washington, on interannual streamflow patterns: Consequences for channel form and streambed disturbance, *Water Resour. Res.*, *41*(7), 1-15, doi:10.1029/2005WR004097.

Kuhnle, R. A. (1992), Bed load transport during rising and falling stages on two small streams, *Earth Surf. Process. and Landforms*, *17*(2), 191-197, doi:10.1002/esp.3290170206.

Lamarre, H., B. J. MacVicar, and A. G. Roy (2005), Using passive integrated transponder (PIT) tags to investigate sediment transport in gravel-bed rivers, *J. Sediment. Res.*, *75*, 736-741, doi:10.2110/jsr.2005.059.

Lane, E. W. (1955), The importance of fluvial morphology in hydraulic engineering, *Proceedings of the American Society of Civil Engineers*, *81*, 1-17.

Lee, K. T., Y.-L. Liu, and K.-H. Cheng (2004), Experimental investigation of bedload transport processes under unsteady flow conditions, *Hydrol. Process.*, *18*(13), 2439-2454, doi:10.1002/hyp.1473.

Leeder, M. R. (1983), On the Interactions between Turbulent Flow, Sediment Transport and Bedform Mechanics in Channelized Flows, in *Modern and Ancient Fluvial Systems*, edited J. D. Collinson and J. Lewin, pp. 3-18, Blackwell Publishing Ltd.

Lenzi, M. A., L. Mao, and F. Comiti (2006), Effective discharge for sediment transport in a mountain river: Computational approaches and geomorphic effectiveness, *J. Hydrol.*, *326*(1–4), 257-276, doi:10.1016/j.jhydrol.2005.10.031.

Leopold, L. B. (1968), Hydrology for Urban Land Planning - A Guidebook on the Hydrologic Effects of Urban Land Use, *U.S. Geol. Surv. Circular No. 554.*, Washington, D.C.

Leopold, L. B. (1973), River Channel Change with Time: An Example: Address as Retiring President of The Geological Society of America, Minneapolis, Minnesota, November 1972, *Geol. Soc. of Am. Bull.*, *84*(6), 1845-1860.

Leopold, L. B., M. G. Wolman, and J. P. Miller (1964), *Fluvial Processes in Geomorphology*, 522 pp., Dover Publications Inc., New York.

Lisle, T. E. (1979), A sorting mechanism for a riffle-pool sequence: Summary, *Geol. Soc. of Am. Bull.*, *90*(7), 616-617.

Lisle, T. E. (1986), Stabilization of a gravel channel by large streamside obstructions and bedrock bends, Jacoby Creek, northwestern California, *GSA Bull.*, *97*(8), 999-1011.

Lisle, T. E. (1987), Using "residual depths" to monitor pool depths independently of discharge, *Res. Note PSW-RN-394*, U.S. Dep. of Agric., For. Serv., Pacific SW Forest and Range Experiment Station, Berkeley, CA.

Lisle, T. E. (1995a), Effects of Coarse Woody Debris and its Removal on a Channel Affected by the 1980 Eruption of Mount St. Helens, Washington, *Water Resour. Res.*, *31*(7), 1797-1808, doi:10.1029/95WR00734.

Lisle, T. E. (1995b), Particle Size Variations Between Bed Load and Bed Material in Natural Gravel Bed Channels, *Water Resour. Res.*, *31*(4), 1107-1118, doi:10.1029/94WR02526.

Lisle, T. E., and S. Hilton (1992), The Volume of Fine Sediment in Pools: An Index of Sediment Supply in Gravel-Bed Streams, *J. Am. Water Resour. Assoc.*, *28*(2), 371-383, doi:10.1111/j.1752-1688.1992.tb04003.x.

MacRae, C. R. (1997), Experience from Morphological Research on Canadian Streams: Is Control of the Two-year Frequency Runoff Event the Best Basis for Stream Channel Protection?, paper presented at Effects of Watershed Development and Management on Aquatic Ecosystems, Proceedings of an Engineering Conference, ASCE.

MacVicar, B. J., and A. G. Roy (2011), Sediment mobility in a forced riffle-pool, *Geomorphology*, *125(3)*, 445-456, doi:10.1016/j.geomorph.2010.10.031.

Madej, M. A. (1999), Temporal and spatial variability in thalweg profiles of a gravel-bed river, *Earth Surf. Process. and Landforms*, *24*(12), 1153-1169.

Mao, L. (2012), The effect of hydrographs on bed load transport and bed sediment spatial arrangement, *J. Geophys. Res.*, *117*, F03024, doi:10.1029/2012JF002428.

Martin, R. L., and D. J. Jerolmack (2013), Origin of hysteresis in bed form response to unsteady flows, *Water Resour. Res.*, *49*(3), 1314-1333, doi:10.1002/wrcr.20093.

Martini, I. P. (1977), Gravelly flood deposits of Irvine Creek, Ontario, Canada, *Sedimentology*, *24*(5), 603-622.

McCuen, R. H., and G. E. Moglen (1988), Multicriterion stormwater management methods, *J. Water Resour. Plan. and Manage.*, *114*(4), 414-431, doi:10.1061/(ASCE)0733-9496(1988)114:4(414).

Meyer-Peter, E., and R. Muller (1948), Formulas for bed-load transport, Proceedings 2nd Meeting, Int. Assoc. of Hydraul. Res., Stockholm, 39-64.

Millar, R. G. (1999), Grain and form resistance in gravel-bed rivers, *J. Hydraul. Res.*, *37*(3), 303-312, doi:10.1080/00221686.1999.9628249.

Montgomery, D. R., and J. M. Buffington (1997), Channel-reach morphology in mountain drainage basins, *Geol. Soc. of Am. Bull.*, *109*(5), 596-611.

Montgomery, D. R., J. M. Buffington, R. D. Smith, K. M. Schmidt, and G. Pess (1995), Pool Spacing in Forest Channels, *Water Resour. Res.*, *31*(4), 1097-1105, doi:10.1029/94WR03285.

Mrokowska, M. M., P. M. Rowinski, L. Ksiazek, A. Struzynski, M. Wyrebek, and A. Radecki-Pawlik

(2016), Flume Experiments on Gravel Bed Load Transport in Unsteady Flow---Preliminary Results, in *Hydrodynamic and Mass Transport at Freshwater Aquatic Interfaces: 34th International School of Hydraulics*, edited by P. M. Rowinski and A. Marion, pp. 221-233, Springer International Publishing, Switzerland.

Nelson, E. J., and D. B. Booth (2002), Sediment sources in an urbanizing, mixed land-use watershed, *J. Hydrol.*, *264*(1–4), 51-68, doi:10.1016/S0022-1694(02)00059-8.

Newbury, R. W., and M. N. Gaboury (1993), *Stream Analysis and Fish Habitat Design: A Field Manual*, 2 ed., 262 pp., Newbury Hydraulics, Gibsons, BC.

Nichols, M. H. (2004), A radio frequency identification system for monitoring coarse sediment particle displacement, *Appl. Eng. Agric.*, *20*(6), 783-787.

OGS (2010), Surficial geology of Southern Ontario, *Miscellaneous Release--Data Rep. 128-REV*, Ontario Geological Survey.

O'Neill, M. P., and A. D. Abrahams (1984), Objective Identification of Pools and Riffles, *Water Resour. Res.*, *20*(7), 921-926, doi:10.1029/WR020i007p00921.

Parker, G. (1978), Self-formed straight rivers with equilibrium banks and mobile bed. Part 2. The gravel river, *J. Fluid Mech.*, *89*(1), 127-146.

Parker, G., and A. W. Peterson (1980), Bar resistance of gravel-bed streams, *J. Hydraul. Div.*, *106*(HY10, Proc. Paper, 15733), 1559-1575.

Parker, G., P. C. Klingeman, and D. G. McLean (1982), Bedload and size distribution in paved gravel-bed streams, *J. Hydraul. Div.*, *108*(4), 544-571.

Pfeiffer, A. M., N. J. Finnegan, and J. K. Willenbring (2017), Sediment supply controls equilibrium channel geometry in gravel rivers, *PNAS*, *114*(13), 3346-3351, doi:10.1073/pnas.1612907114.

Pickup, G., and R. F. Warner (1976), Effects of hydrologic regime on magnitude and frequency of dominant discharge, *J. Hydrol.*, *29*(1), 51-75.

Pizzuto, J. E., W. C. Hession, and M. McBride (2000), Comparing gravel-bed rivers in paired urban and rural catchments of southeastern Pennsylvania, *Geology*, *28*(1), 79-82.

Poff, N. L., J. D. Allan, M. B. Bain, J. R. Karr, K. L. Prestegaard, B. D. Richter, R. E. Sparks, and J. C. Stromberg (1997), The Natural Flow Regime, *BioScience*, *47*(11), 769-784, doi:10.2307/1313099.

Reid, I., L. E. Frostick, and J. T. Layman (1985), The incidence and nature of bedload transport during flood flows in coarse-grained alluvial channels, *Earth Surf. Process. and Landforms*, *10*, 33-44, doi:10.1002/esp.3290100107.

Reid, L. M., and T. Dunne (2002), Sediment budgets as an organizing framework in fluvial geomorphology, in *Tools in Fluvial Geomorphology*, edited by G. M. Kondolf and H. Piegay, pp. 1-38, John Wiley and Sons, Ltd.

Rice, S., and M. A. Church (1996), Sampling surficial fluvial gravels: the precision of size distribution percentile estimates, *J. Sediment. Res.*, *66*(3), 654-665.

Richards, K. S. (1976), The morphology of riffle-pool sequences, *Earth Surf. Process.*, *1*, 71-88, doi:10.1002/esp.3290010108.

Roni, P., K. Hanson, and T. Beechie (2008), Global Review of the Physical and Biological Effectiveness of Stream Habitat Rehabilitation Techniques, *N. Am. J. Fisheries Manage.*, *28*(3), 856-890, doi:10.1577/M06-169.1.

Rosgen, D. L. (1996), *Applied River Morphology*, 385 pp., Wildland Hydrology, Pagosa Springs, CO.

Schmidt, L. J., and J. P. Potyondy (2004), Quantifying Channel Maintenance Instream Flows: An Approach for Gravel-Bed Streams in the Western United States, *Gen. Tech. Rep. RMRS-GTR-128*, U.S. Dep. of Agric., For. Serv., Rocky Mt. Res. Stat., Fort Collins, CO.

Schneider, J. M., J. M. Turowski, D. Rickenmann, R. Hegglin, S. Arrigo, L. Mao, and J. W. Kirchner (2014), Scaling relationships between bed load volumes, transport distances, and stream power in steep mountain channels, *J. Geophys. Res. Earth Surf.*, *119*(3), 533-549, doi:10.1002/2013JF002874.

Schumm, S. A. (1969), River Metamorphosis, *J. Hydraul. Div.*, *95*(1), 255-274.

Schumm, S. A., M. D. Harvey, and C. C. Watson (1984), *Incised Channels: Morphology, Dynamics and Control*, 200 pp., Water Resources Publications, Colorado.

Schwartz, J. S., and K. J. Neff (2001), Use of River2D Hydrodynamic Model for Stream Restoration Assessment and Design, paper presented at World Environmental and Water Resources Congress 2011.

Schwartz, J. S., K. J. Neff, F. E. Dworak, and R. R. Woockman (2015), Restoring riffle-pool structure in an incised, straightened urban stream channel using an ecohydraulic modeling approach, *Ecological Eng.*, *78*, 112 – 126, doi:10.1016/j.ecoleng.2014.06.002.

Scurlock, S. M., C. I. Thornton, and S. R. Abt (2012), Equilibrium Scour Downstream of Three-Dimensional Grade-Control Structures, *J. Hydraul. Eng.*, *138*(2), 167-176, doi:10.1061/(ASCE)HY.1943-7900.0000493.

Sear, D. A. (1996), Sediment transport processes in pool-riffle sequences, *Earth Surf. Process. Landforms*, *21*, 241-262.

Shields Jr., F. D., R. R. Copeland, P. C. Klingeman, M. W. Doyle, and A. Simon (2003), Design for stream restoration, *J. Hydraul. Eng.*, *129*(8), 575-584.

Sholtes, J. S., and B. P. Bledsoe (2016), Half-Yield Discharge: Process-Based Predictor of Bankfull Discharge, *J. Hydraul. Eng.*, *142*(8), doi:10.1061/(ASCE)HY.1943-7900.0001137.

Sichingabula, H. M. (1999), Magnitude-frequency characteristics of effective discharge for suspended sediment transport, Fraser River, British Columbia, Canada, *Hydrol. Process.*, *13*(9), 1361-1380, doi:10.1002/(SICI)1099-1085(19990630)13:9<1361::AID-HYP808>3.0.CO;2-H.

Sidle, R. C. (1988), Bed load transport regime of a small forest stream, *Water Resour. Res.*, *24*(2), 207-218, doi:10.1029/WR024i002p00207.

Simons, D. B., and E. V. Richardson (1966), Resistance to flow in alluvial channels, *US Geol. Surv. Prof. Paper 422-J*.

Surian, N., L. Mao, M. Giacomin, and L. Ziliani (2009), Morphological effects of different channel-forming discharges in a gravel-bed river, *Earth Surf. Process. and Landforms*, *34*(8), 1093-1107, doi:10.1002/esp.1798.

Thompson, P. J. (2013), Event based characterization of hydrologic change in urbanizing southern Ontario watersheds via high resolution stream gauge data, M.A.Sc., University of Waterloo, Waterloo, Ontario, Canada.

Torizzo, M., and J. Pitlick (2004), Magnitude-frequency of bed load transport in mountain streams in Colorado, *J. Hydrol.*, *290*(1–2), 137-151, doi:10.1016/j.jhydrol.2003.12.001.

TRCA (2010), Etobicoke and Mimico Creeks Watershed Technical Update Report, Toronto and Region Conservation Authority (TRCA), Toronto, Ontario, Canada.

Trimble, S. W. (1997), Contribution of Stream Channel Erosion to Sediment Yield from an Urbanizing Watershed, *Science*, *278*(5342), 1442-1444.

USACE (2004), HEC-RAS River Analysis System - User's Manual, U.S. Army Corps of Engineers (USACE), Davis, CA.

Walsh, C. J., A. H. Roy, J. W. Feminella, P. D. Cottingham, P. M. Groffman, and R. P. Morgan (2005), The urban stream syndrome: current knowledge and the search for a cure, *J. N. Am. Benthol. Soc.*, *24*(3), 706-723, doi:10.1899/04-028.1.

Wang, L., A. J. S. Cuthbertson, G. Pender, and Z. Cao (2015), Experimental investigations of graded sediment transport under unsteady flow hydrographs, *Int. J. Sed. Res.*, *30*(4), 306 – 320, doi:10.1016/j.ijsrc.2015.03.010.

Waters, K. A., and J. C. Curran (2015), Linking bed morphology changes of two sediment mixtures to sediment transport predictions in unsteady flows, *Water Resour. Res.*, *51*(4), 2724-2741, doi:10.1002/2014WR016083.

Whiting, P. J., and J. G. King (2003), Surface particle sizes on armoured gravel streambeds: effects of supply and hydraulics, *Earth Surf. Process. and Landforms*, *28*(13), 1459-1471, doi:10.1002/esp.1049.

Whittaker, J. G., and T. R. H. Davies (1982), Erosion and sediment transport processes in step-pool torrents, in *Recent Developments in the Explanation and Prediction of Erosion and Sediment Yield*, edited by D. E. Walling, pp. 99-104, International Association of Hydrological Sciences, Wallingford.

Wilcock, P. R. (1997), Entrainment, displacement and transport of tracer gravels, *Earth Surf. Process. and Landforms*, *22*(12), 1125-1138, doi:10.1002/(SICI)1096-9837(199712)22:12<1125::AID-ESP811>3.0.CO;2-V.

Wilcock, P. R. (2001a), Toward a practical method for estimating sediment-transport rates in gravel-bed rivers, *Earth Surf. Process. and Landforms*, *26*(13), 1395-1408, doi:10.1002/esp.301.

Wilcock, P. R. (2001b), The Flow, the Bed, and the Transport: Interaction in Flume and Field, in *Gravel-bed Rivers V*, edited by M. P. Mosley, New Zealand Hydrological Society.

Wilcock, P. R., and J. C. Crowe (2003), Surface-based transport model for mixed-size sediment, *J. of Hydraul. Eng.*, *129*(2), 120-128, doi:10.1061/(ASCE)0733-9429(2003)129:2(120).

Wilcock, P. R., and B. W. McArdell (1997), Partial transport of a sand/gravel sediment, *Water Resour. Res.*, *33*(1), 235-245, doi:10.1029/96WR02672.

Williams, G. P. (1989), Sediment concentration versus water discharge during single hydrologic events in rivers, *J. Hydrol.*, *111*(1), 89 – 106.

Wolman, M. G. (1954), A method of sampling coarse river-bed material, *Eos*, *35*(6), 951-956, doi:10.1029/TR035i006p00951.

Wolman, M. G. (1967), A cycle of sedimentation and erosion in urban river channels, *Geografiska Annaler*, *49A*(2-4), 385-395.

Wolman, M. G., and J. P. Miller (1960), Magnitude and frequency of forces in geomorphic processes, *J. Geol.*, *68*(1), 54-74, doi:10.1086/626637.

Wooldridge, C. L., and E. J. Hickin (2002), Step-pool and cascade morphology, Mosquito Creek, British Columbia: a test of four analytical techniques, *Can. J. Earth Sci.*, *39*(4), 493-503, doi:10.1139/e01-087.

Yang, C. T. (1971), Formation of riffles and pools, *Water Resour. Res.*, *7*(6), 1567-1574, doi:10.1029/WR007i006p01567.

Yen, C. L., and K. T. Lee (1995), Bed Topography and Sediment Sorting in Channel Bend with Unsteady Flow, *J. Hydraul. Eng.*, *121*(8), 591-599.

Appendix A

Additional Results from Chapter 2

Notes: Additional results are presented documenting raw outputs of the objective bedform methods for each reach investigated. Results are presented in increasing order according to the Map Reference No. on Figure 2.1 and Table 2.1.

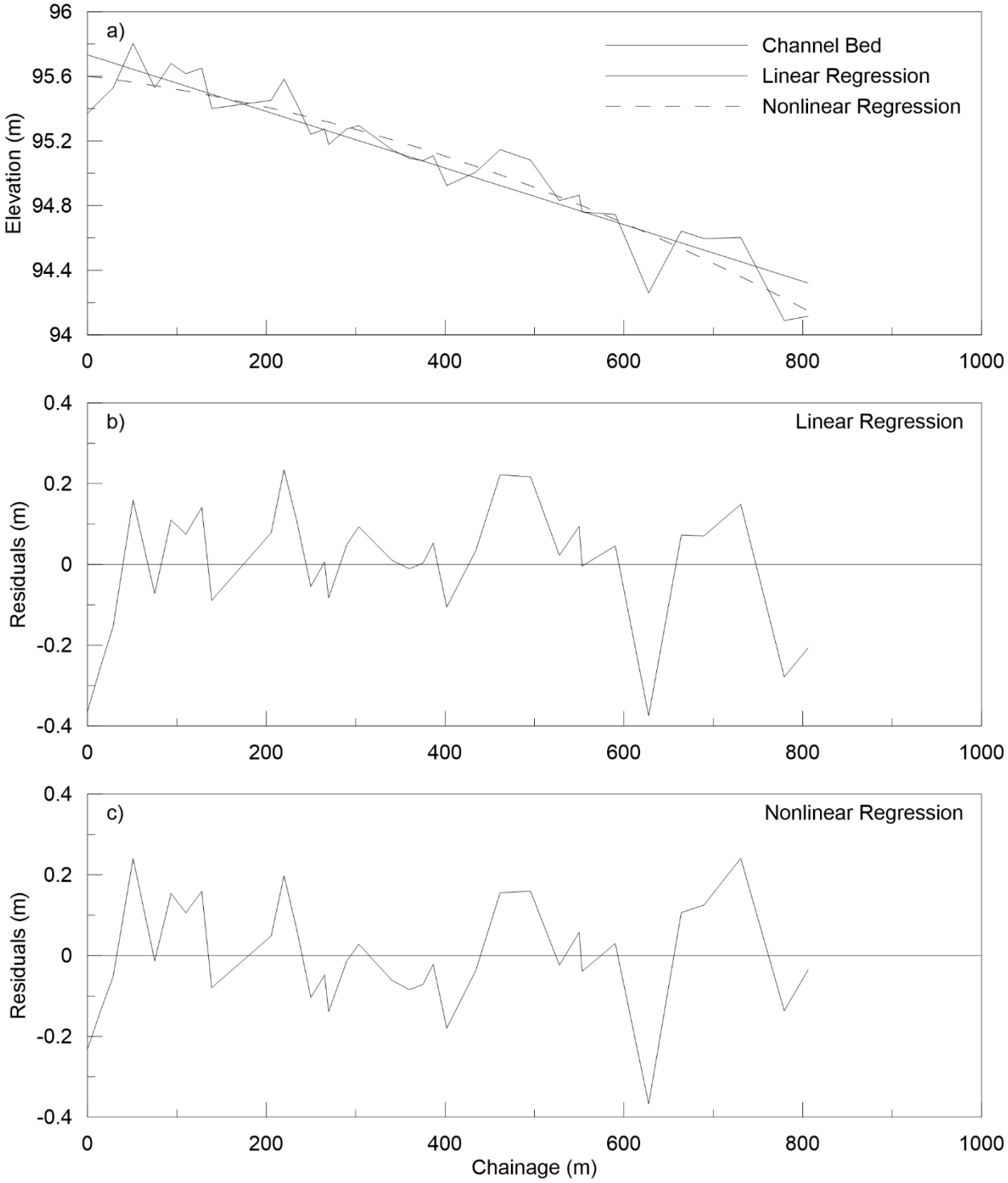

Figure A.1: a) Longitudinal profile with fitted linear and nonlinear regression models, b) residuals from linear regression model and c) residuals from nonlinear regression model for 02EC011.

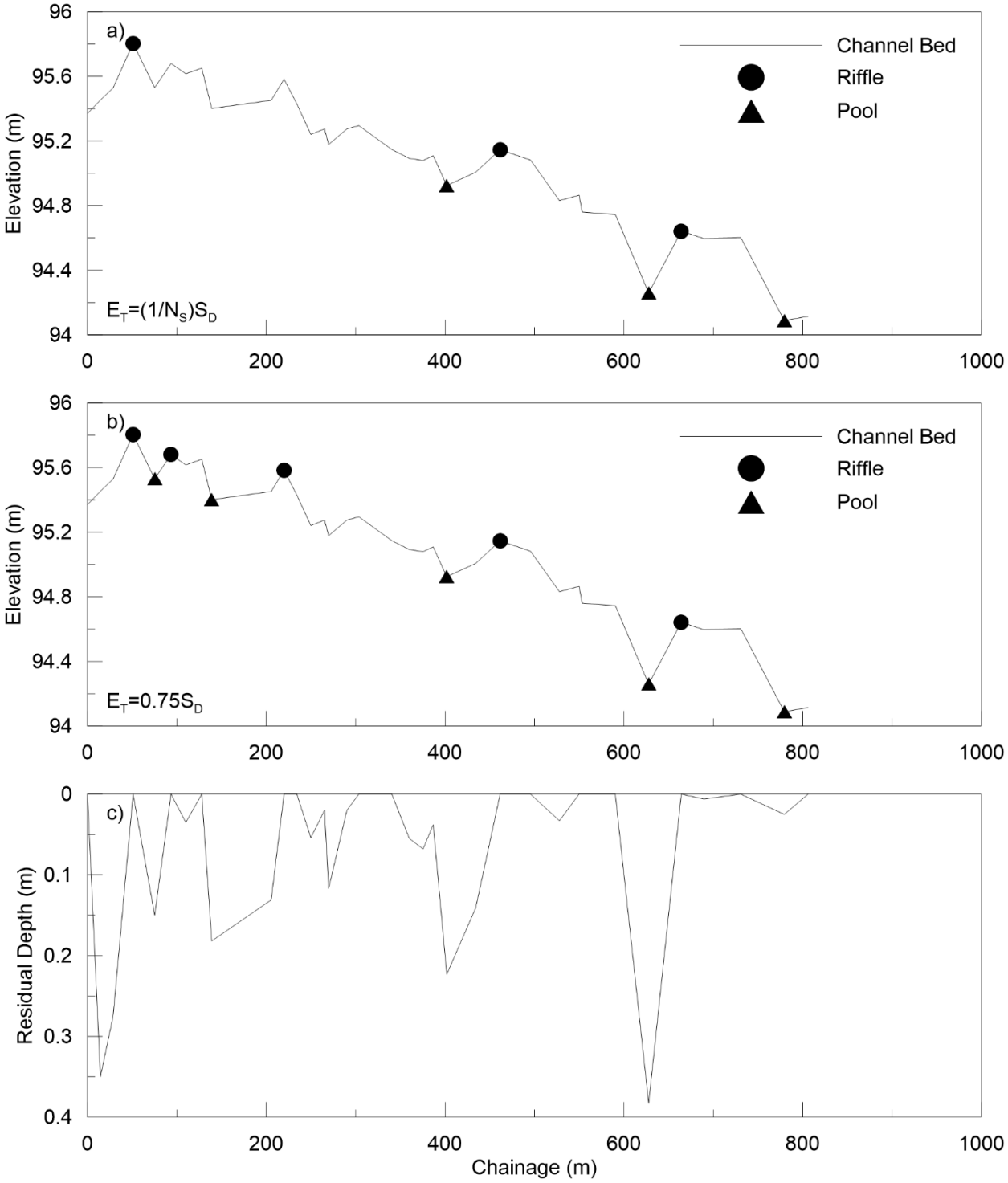

Figure A.2: Longitudinal profile with identified bedforms using bedform differencing with a) $(1/N_S)S_D$ tolerance and b) $0.75S_D$ tolerance and c) residual pool depths for 02EC011.

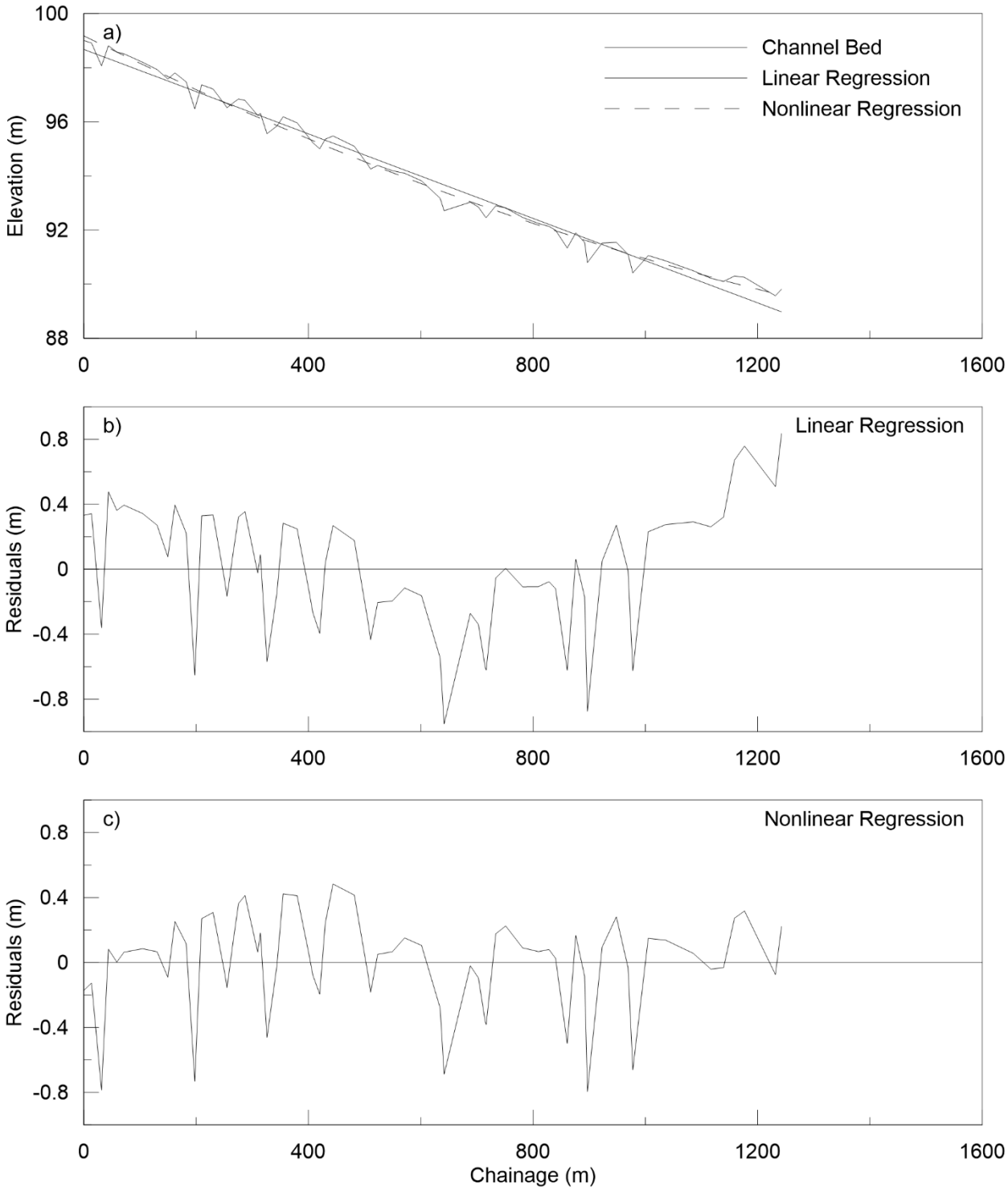

Figure A.3: a) Longitudinal profile with fitted linear and nonlinear regression models, b) residuals from linear regression model and c) residuals from nonlinear regression model for 02ED006.

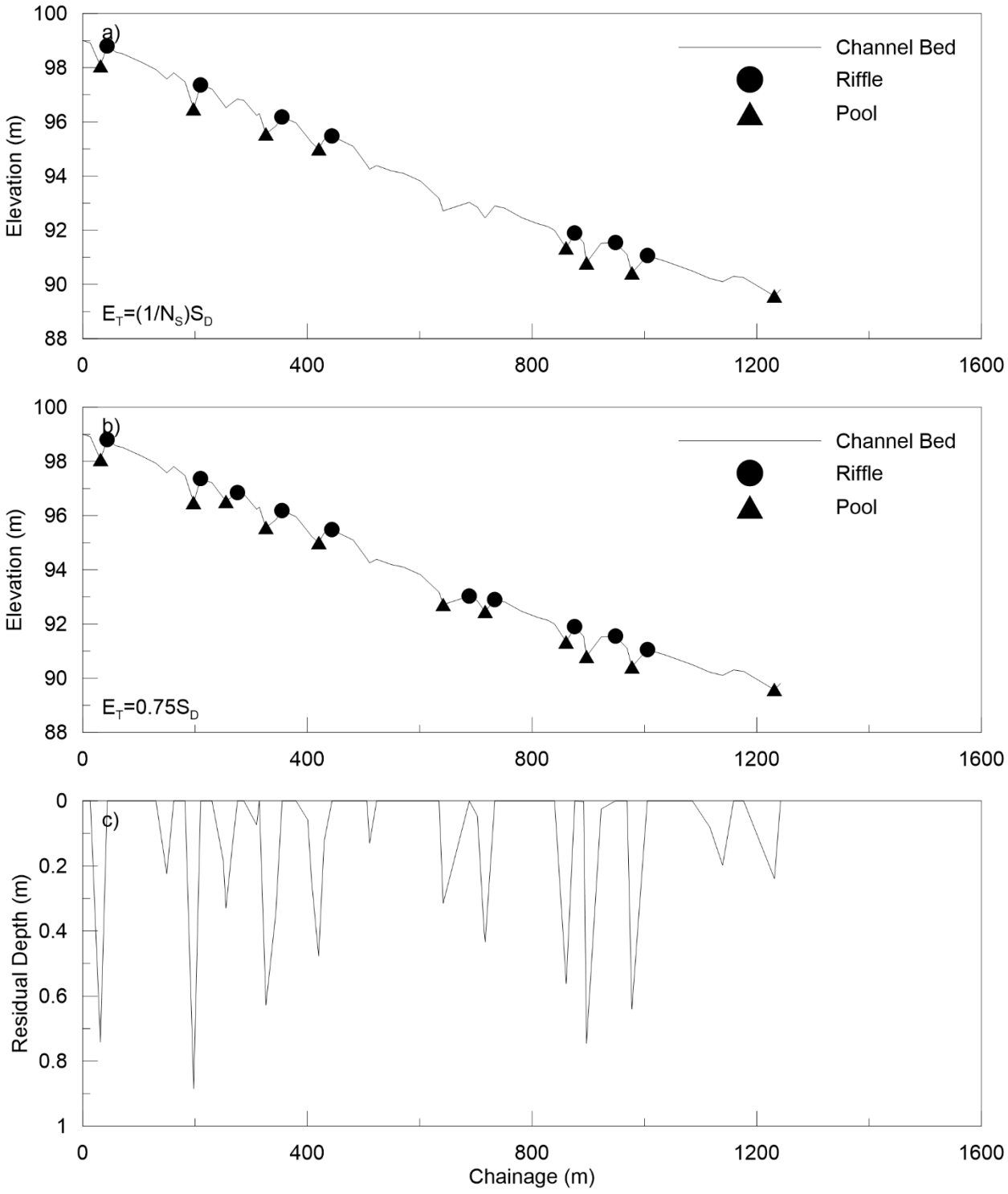

Figure A.4: Longitudinal profile with identified bedforms using bedform differencing with a) $(1/N_S)S_D$ tolerance and b) $0.75S_D$ tolerance and c) residual pool depths for 02ED006.

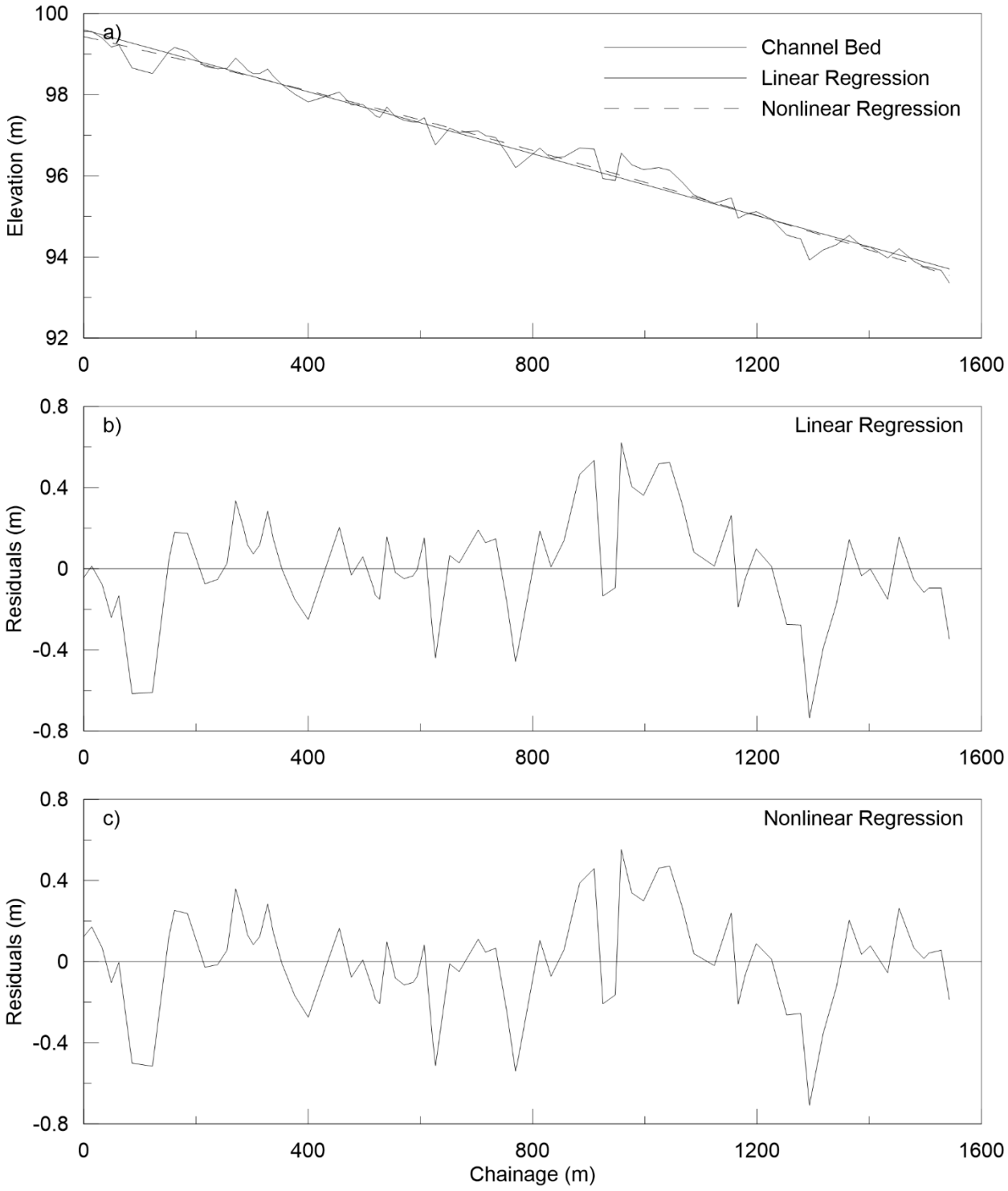

Figure A.5: a) Longitudinal profile with fitted linear and nonlinear regression models, b) residuals from linear regression model and c) residuals from nonlinear regression model for 02GA023.

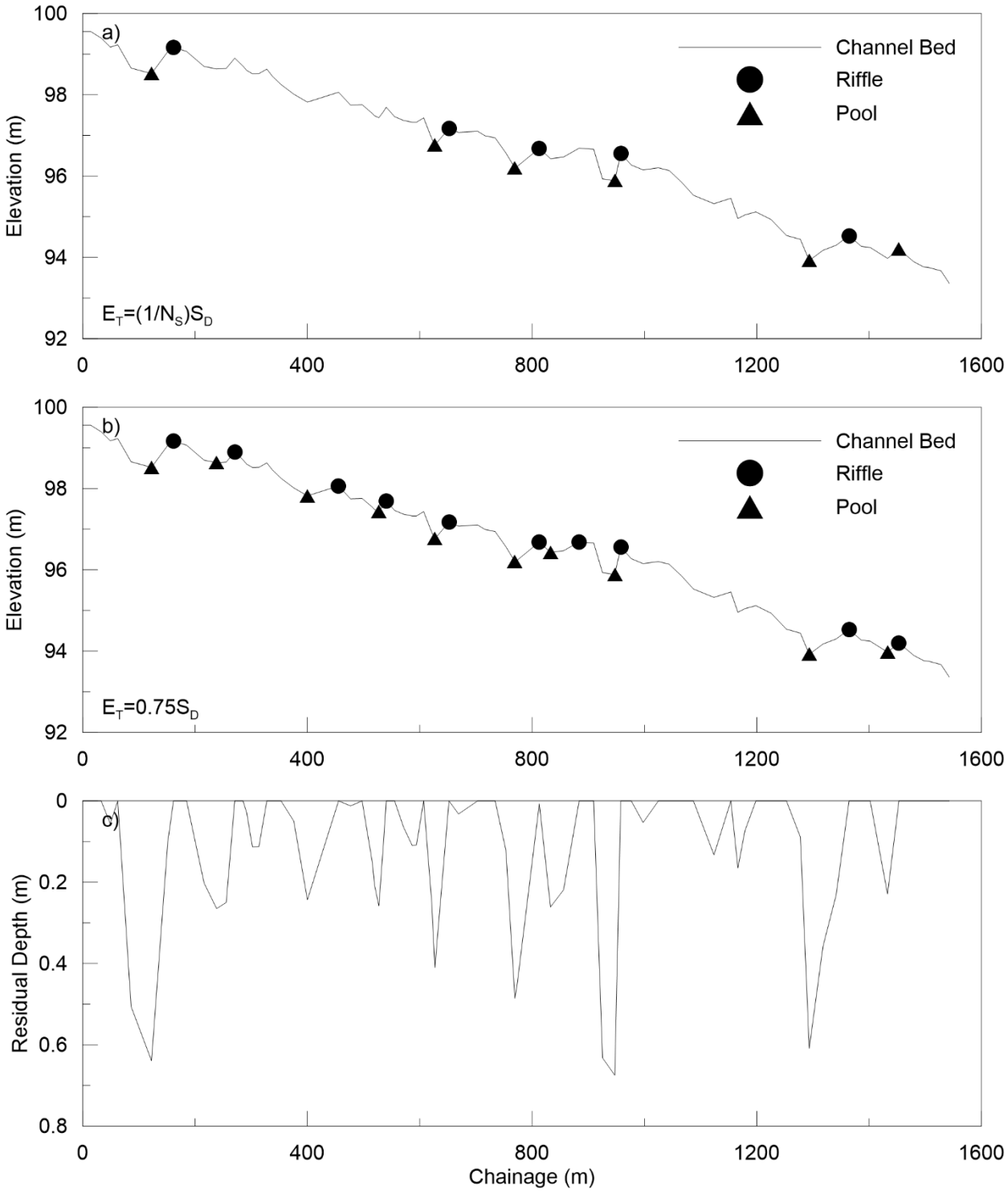

Figure A.6: Longitudinal profile with identified bedforms using bedform differencing with a) $(1/N_S)S_D$ tolerance and b) $0.75S_D$ tolerance and c) residual pool depths for 02GA023.

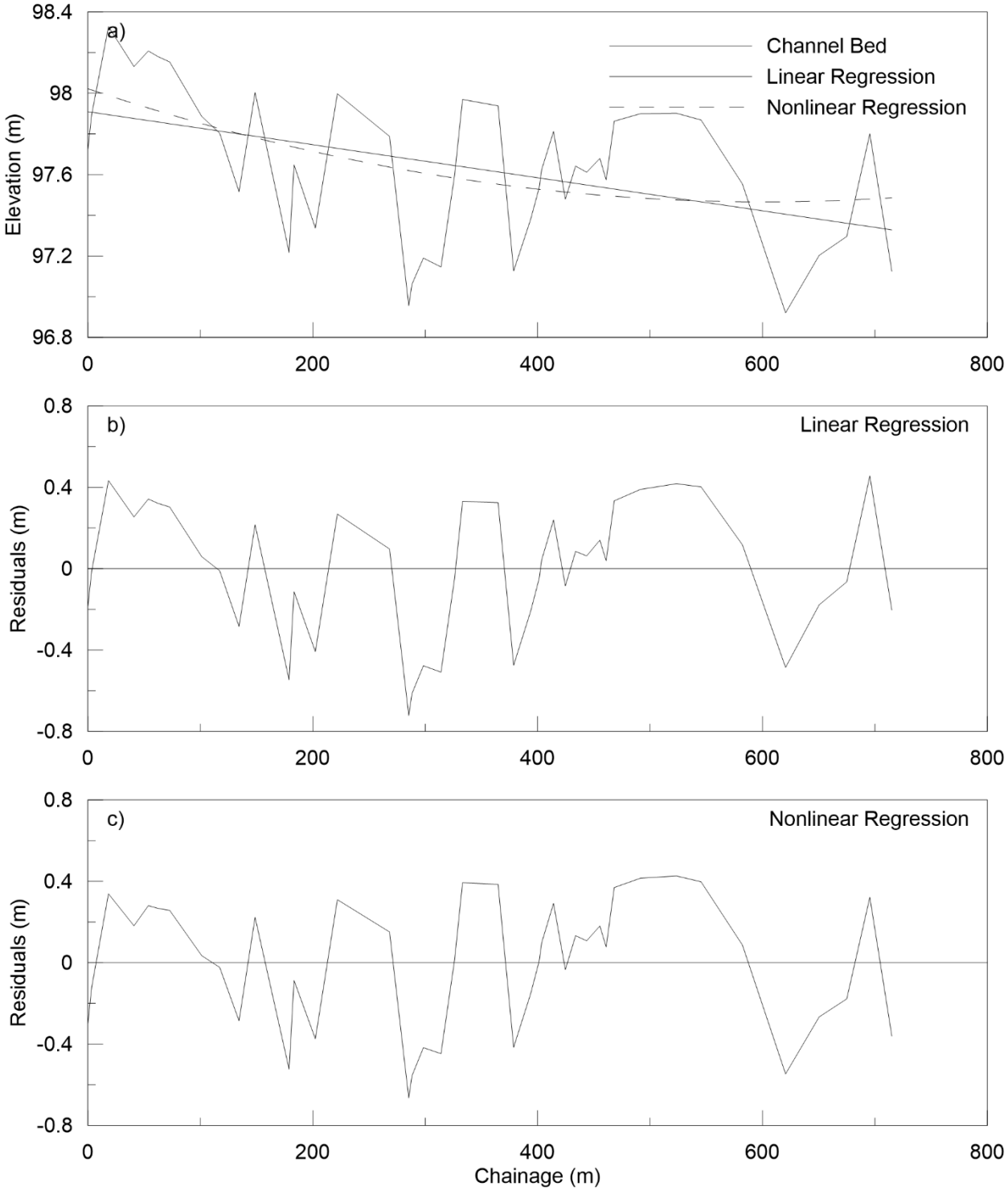

Figure A.7: a) Longitudinal profile with fitted linear and nonlinear regression models, b) residuals from linear regression model and c) residuals from nonlinear regression model for 02HK007.

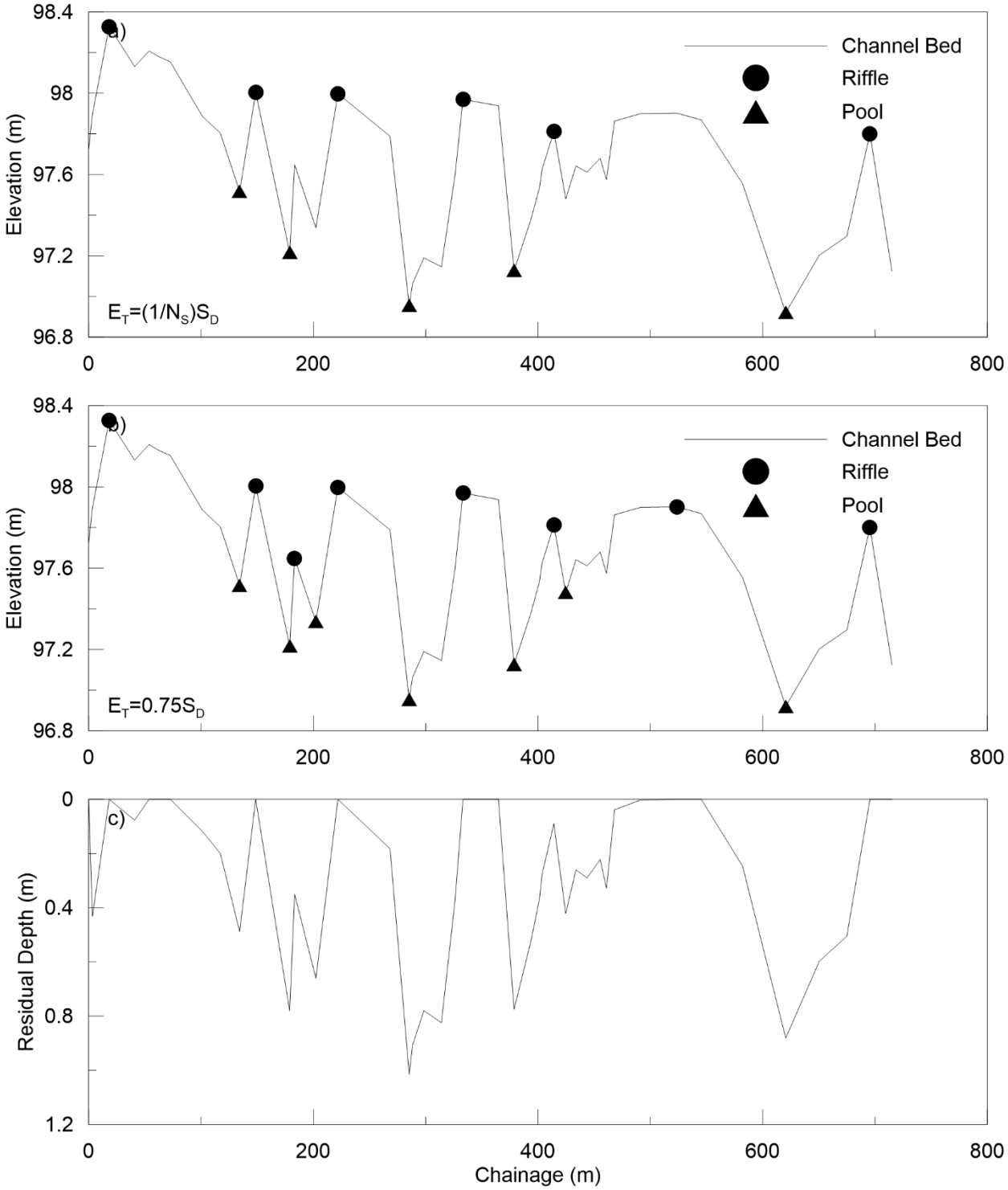

Figure A.8: Longitudinal profile with identified bedforms using bedform differencing with a) $(1/N_S)S_D$ tolerance and b) $0.75S_D$ tolerance and c) residual pool depths for 02HK007.

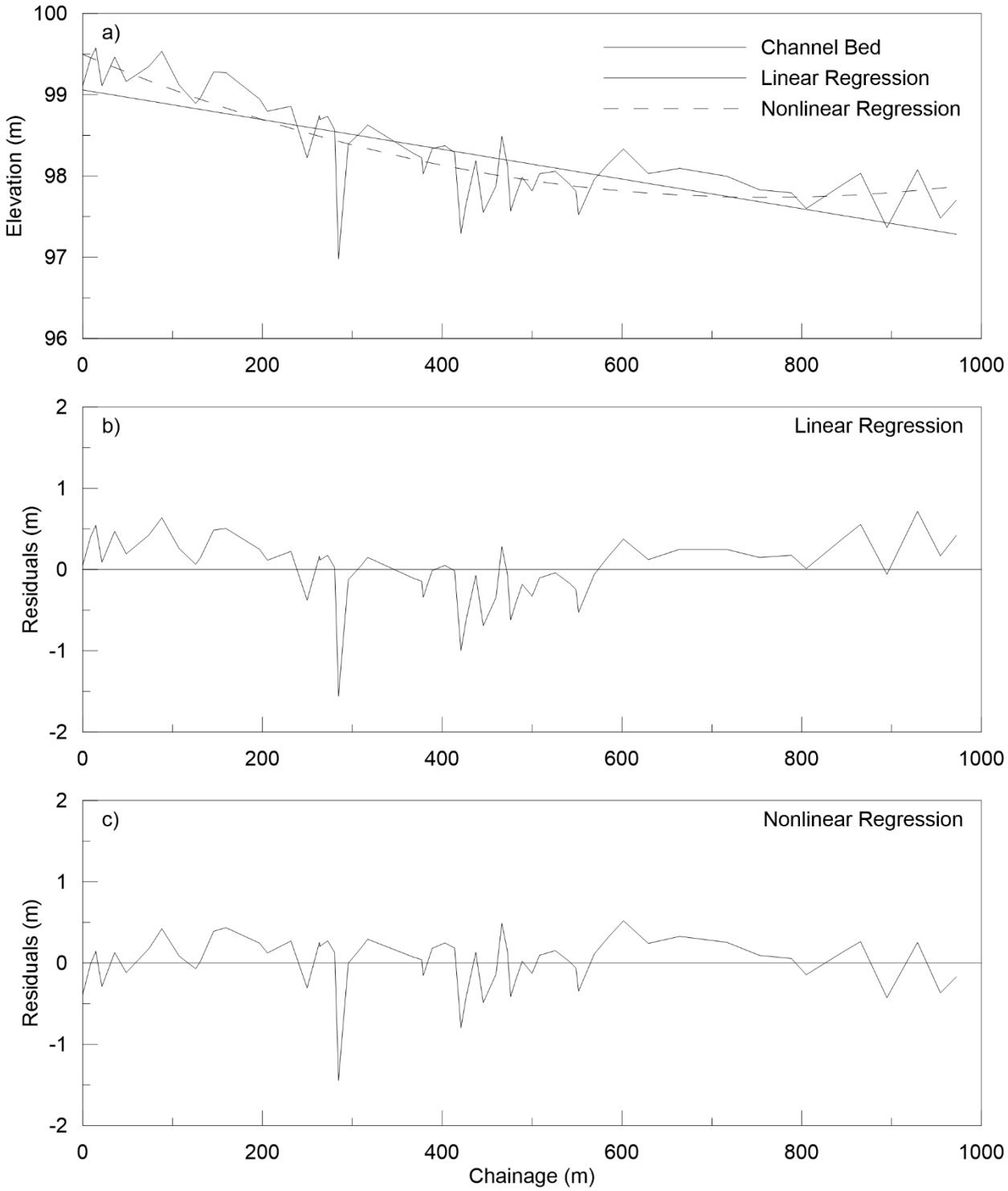

Figure A.9: a) Longitudinal profile with fitted linear and nonlinear regression models, b) residuals from linear regression model and c) residuals from nonlinear regression model for 02HB001.

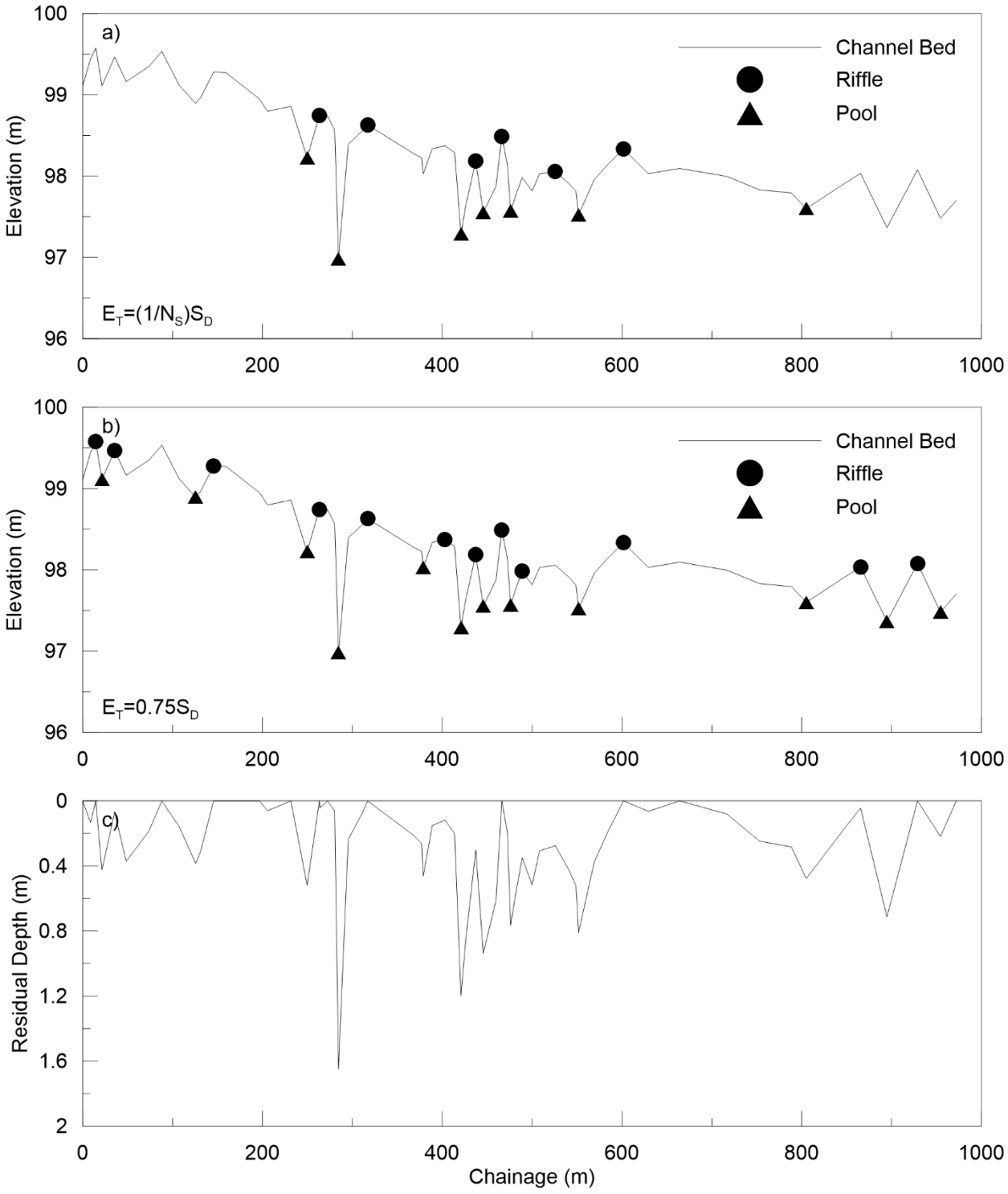

Figure A.10: Longitudinal profile with identified bedforms using bedform differencing with a) $(1/N_S)S_D$ tolerance and b) $0.75S_D$ tolerance and c) residual pool depths for 02HB001.

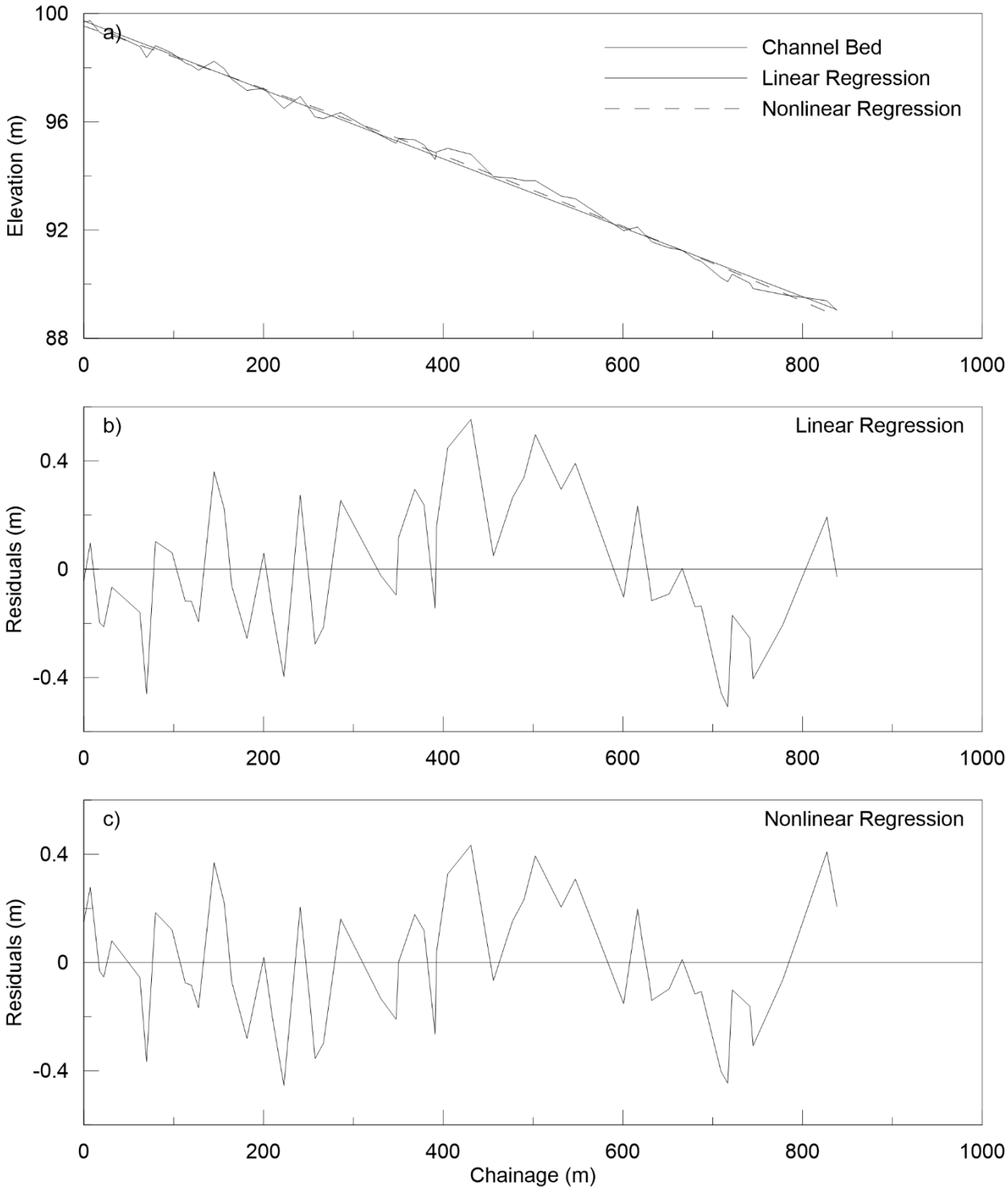

Figure A.11: a) Longitudinal profile with fitted linear and nonlinear regression models, b) residuals from linear regression model and c) residuals from nonlinear regression model for 02HD014.

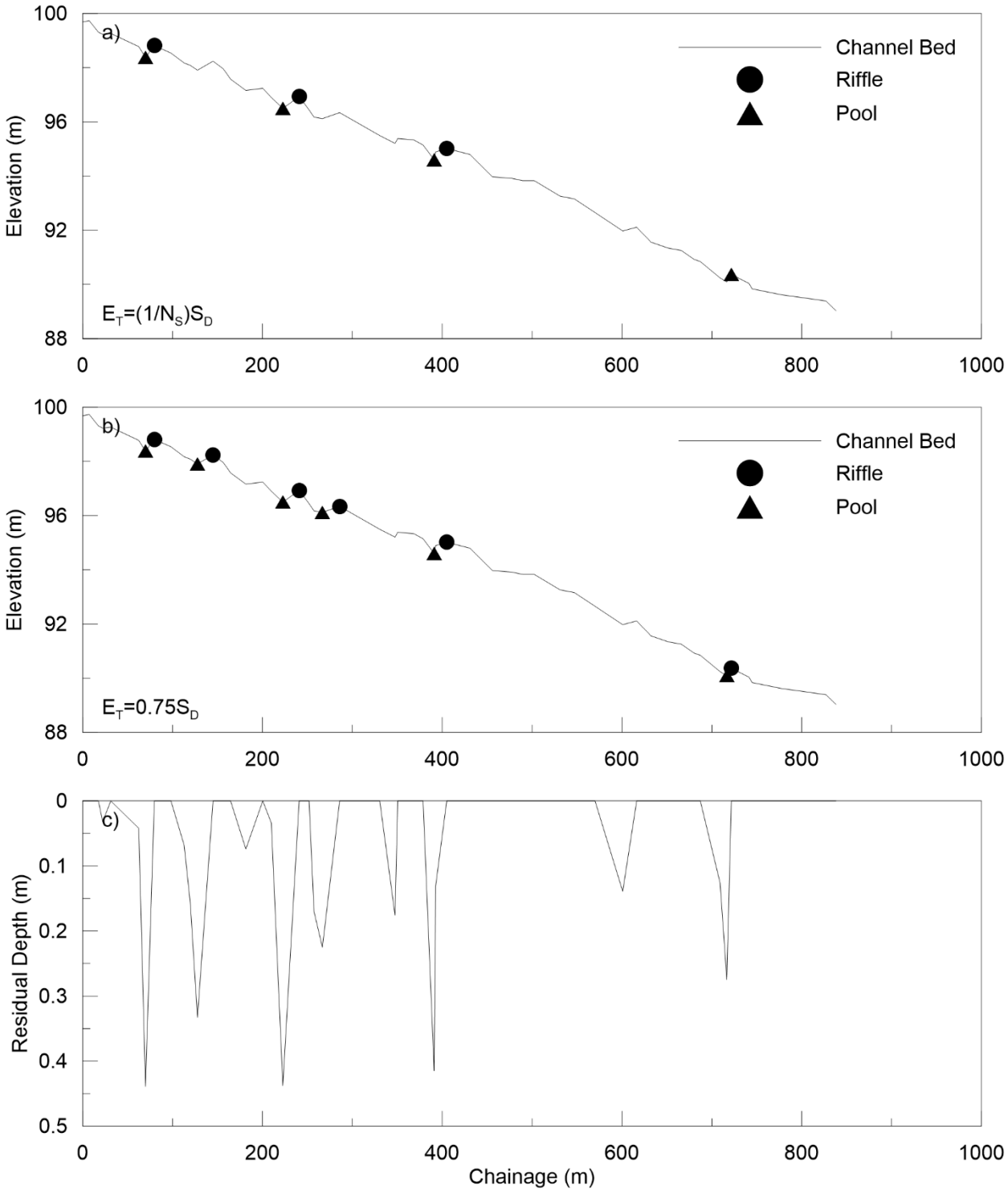

Figure A.12: Longitudinal profile with identified bedforms using bedform differencing with a) $(1/N_S)S_D$ tolerance and b) $0.75S_D$ tolerance and c) residual pool depths for 02HD014.

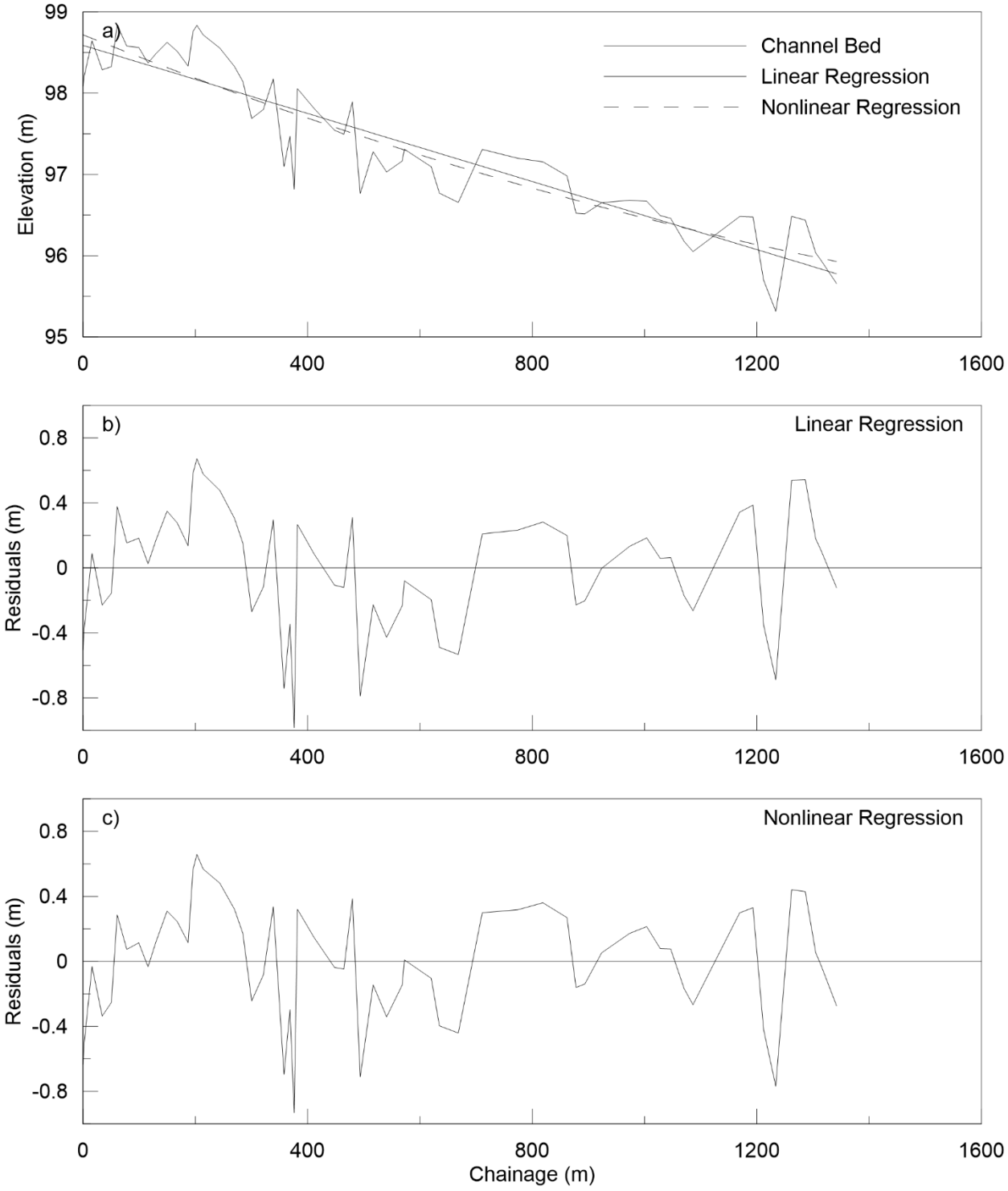

Figure A.13: a) Longitudinal profile with fitted linear and nonlinear regression models, b) residuals from linear regression model and c) residuals from nonlinear regression model for 02HD012.

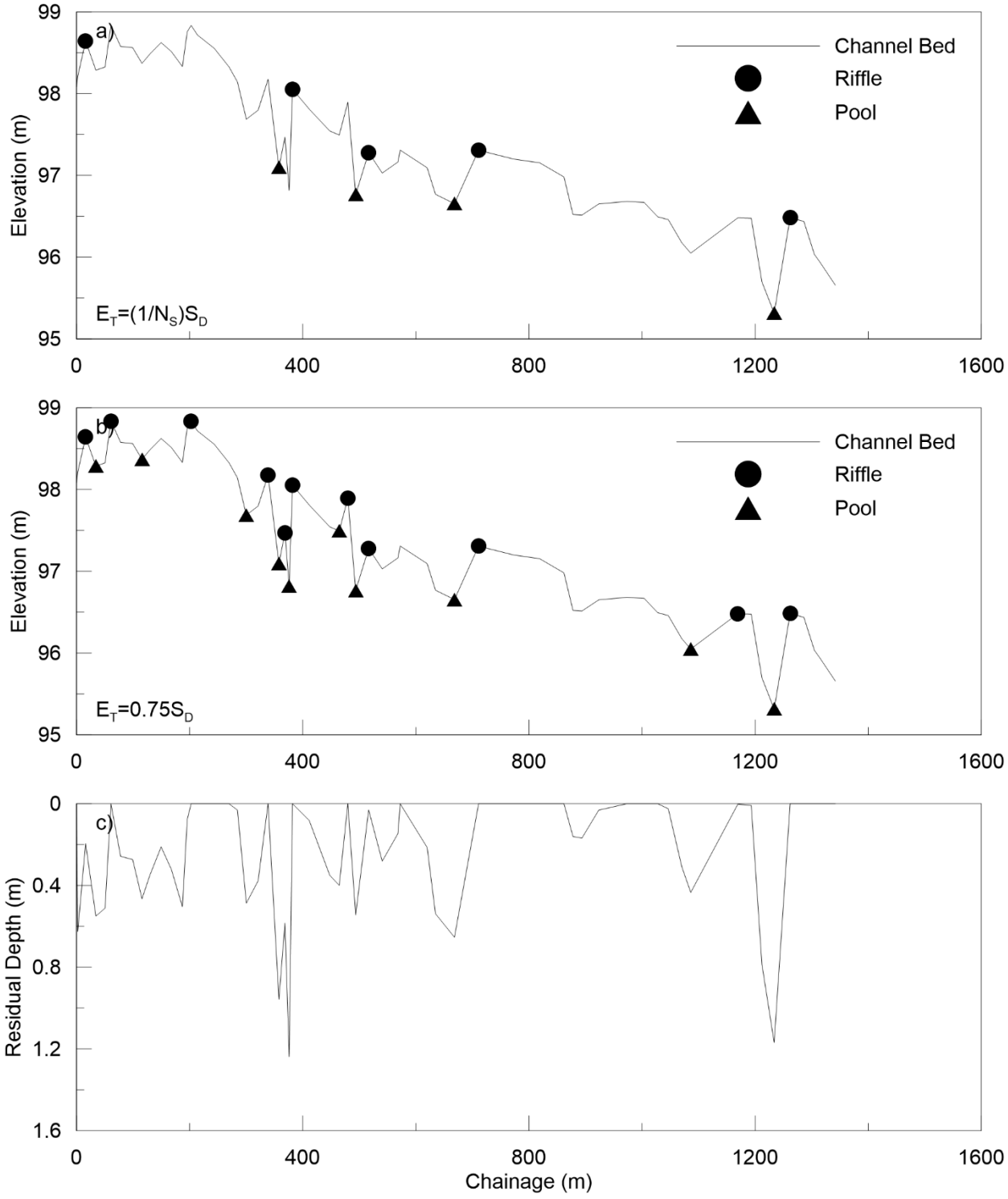

Figure A.14: Longitudinal profile with identified bedforms using bedform differencing with a) $(1/N_S)S_D$ tolerance and b) $0.75S_D$ tolerance and c) residual pool depths for 02HD012.

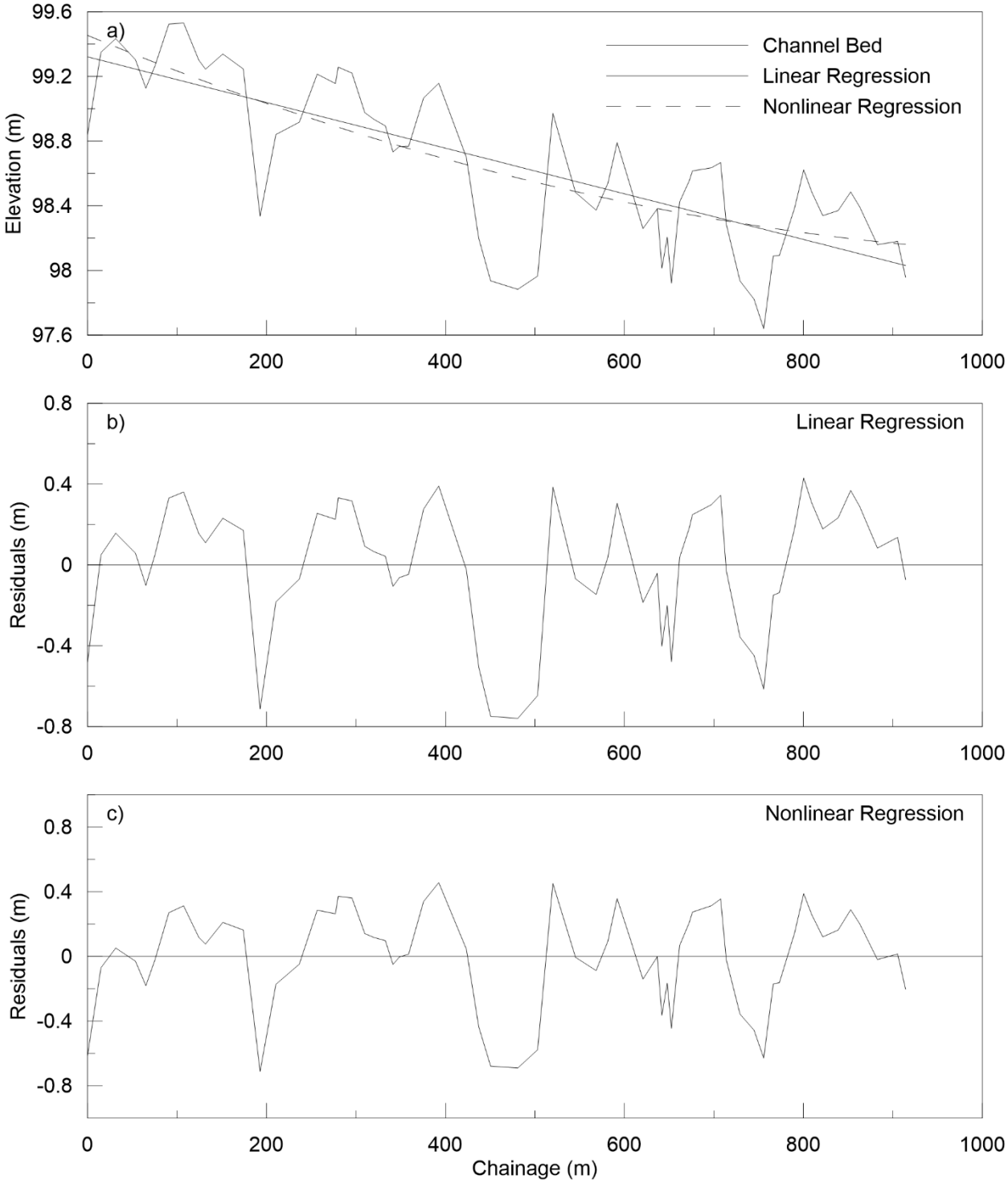

Figure A.15: a) Longitudinal profile with fitted linear and nonlinear regression models, b) residuals from linear regression model and c) residuals from nonlinear regression model for 02HC047.

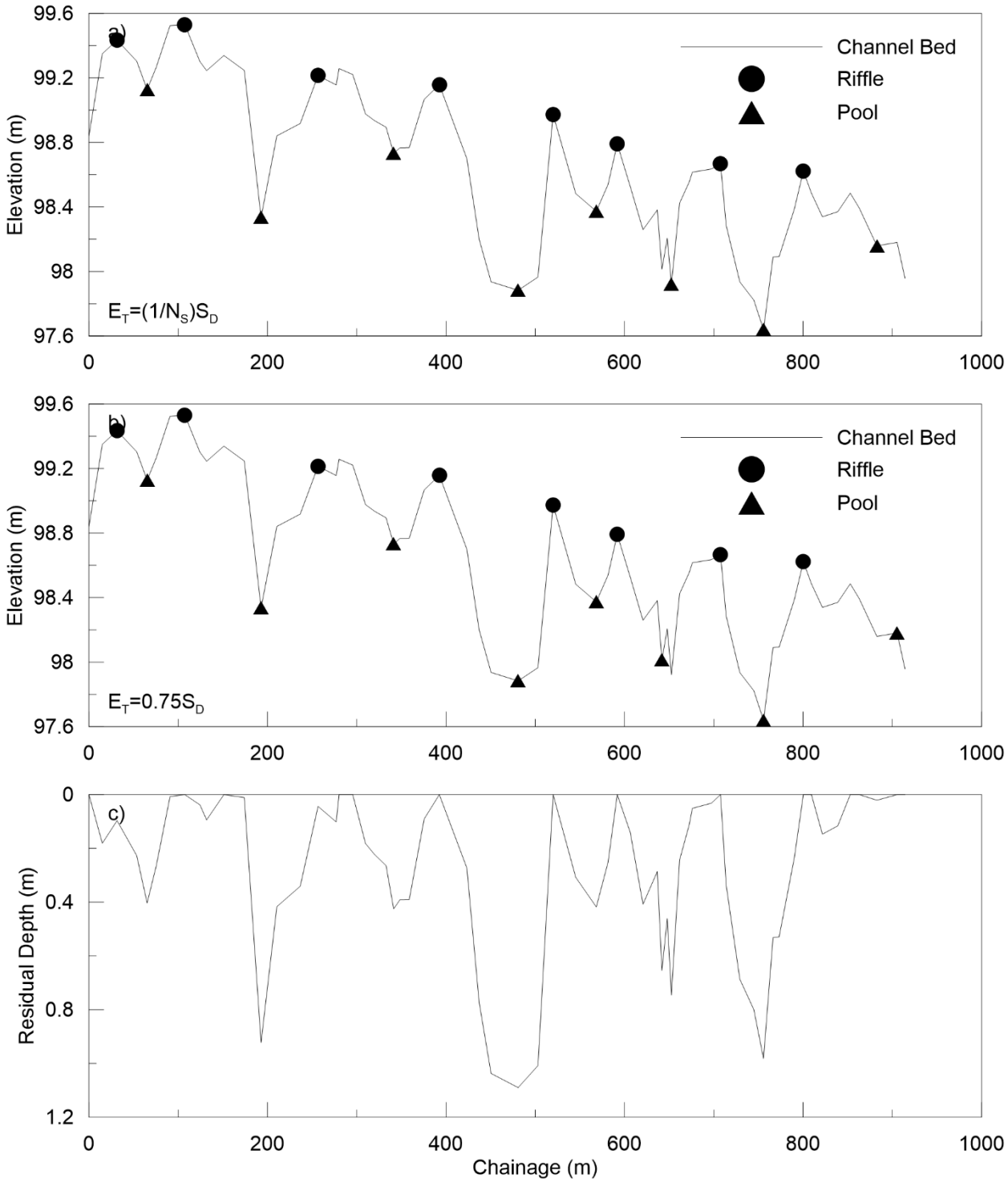

Figure A.16: Longitudinal profile with identified bedforms using bedform differencing with a) $(1/N_S)S_D$ tolerance and b) $0.75S_D$ tolerance and c) residual pool depths for 02HC047.

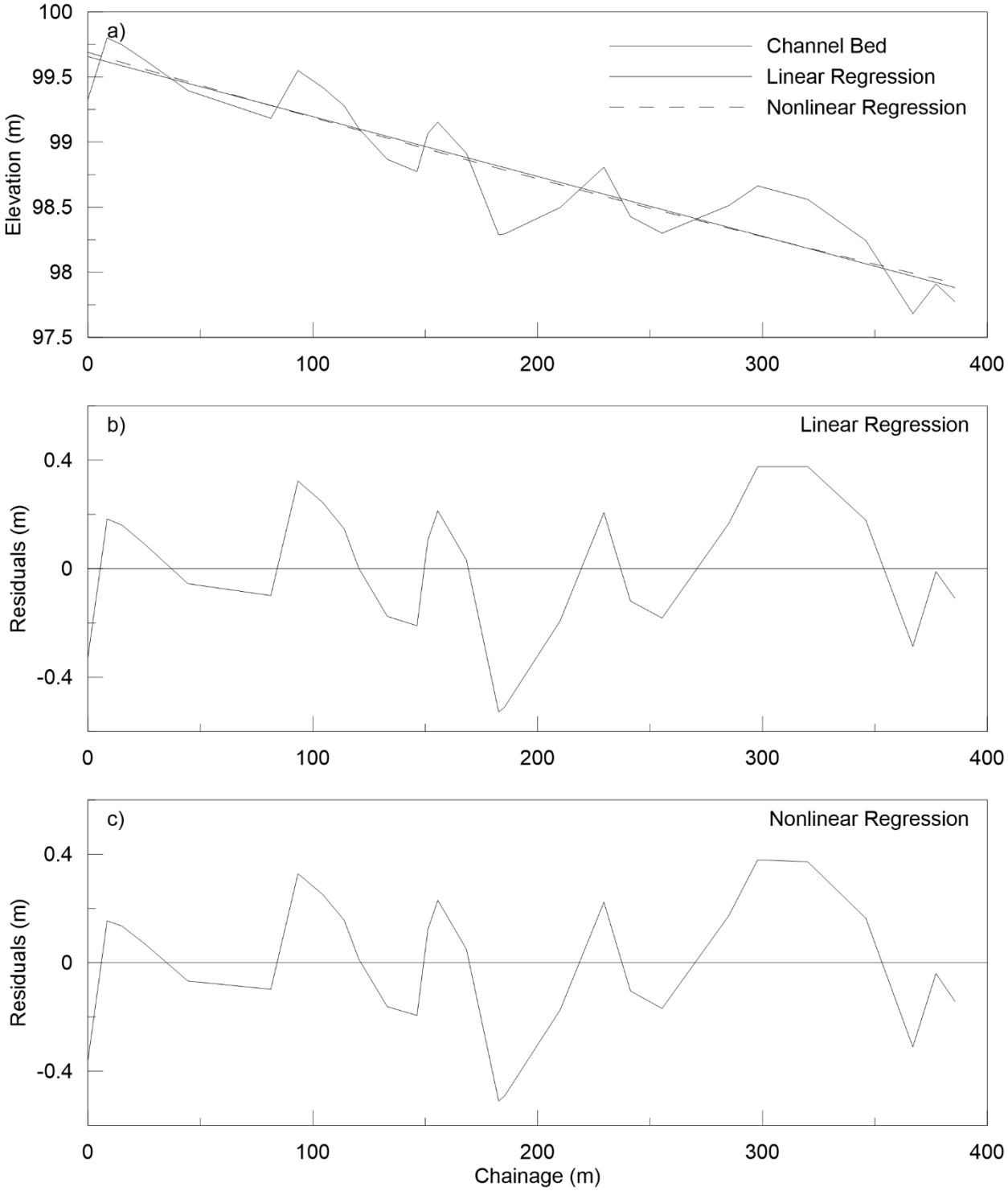

Figure A.17: a) Longitudinal profile with fitted linear and nonlinear regression models, b) residuals from linear regression model and c) residuals from nonlinear regression model for 02ED026.

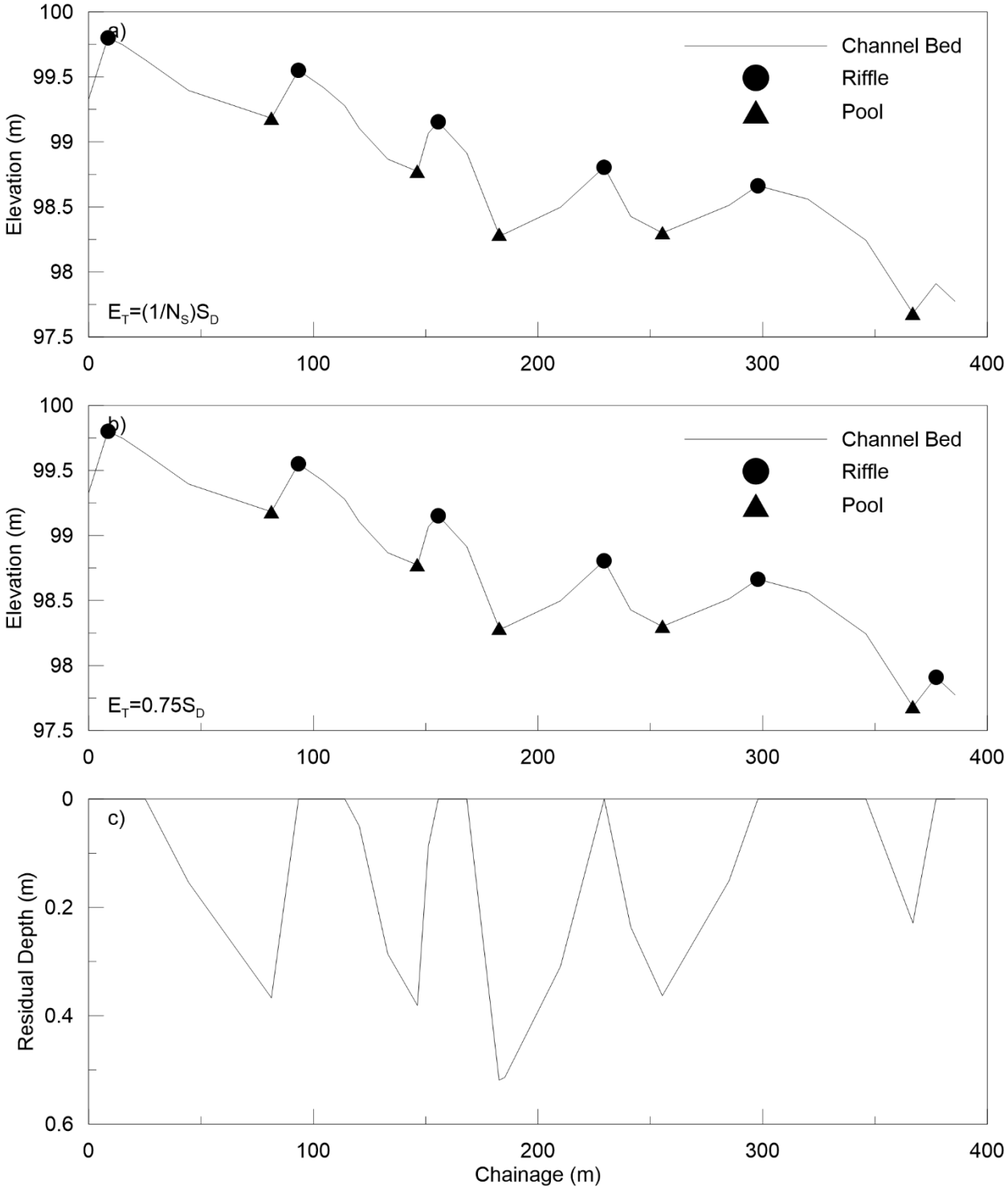

Figure A.18: Longitudinal profile with identified bedforms using bedform differencing with a) $(1/N_S)S_D$ tolerance and b) $0.75S_D$ tolerance and c) residual pool depths for 02ED026.

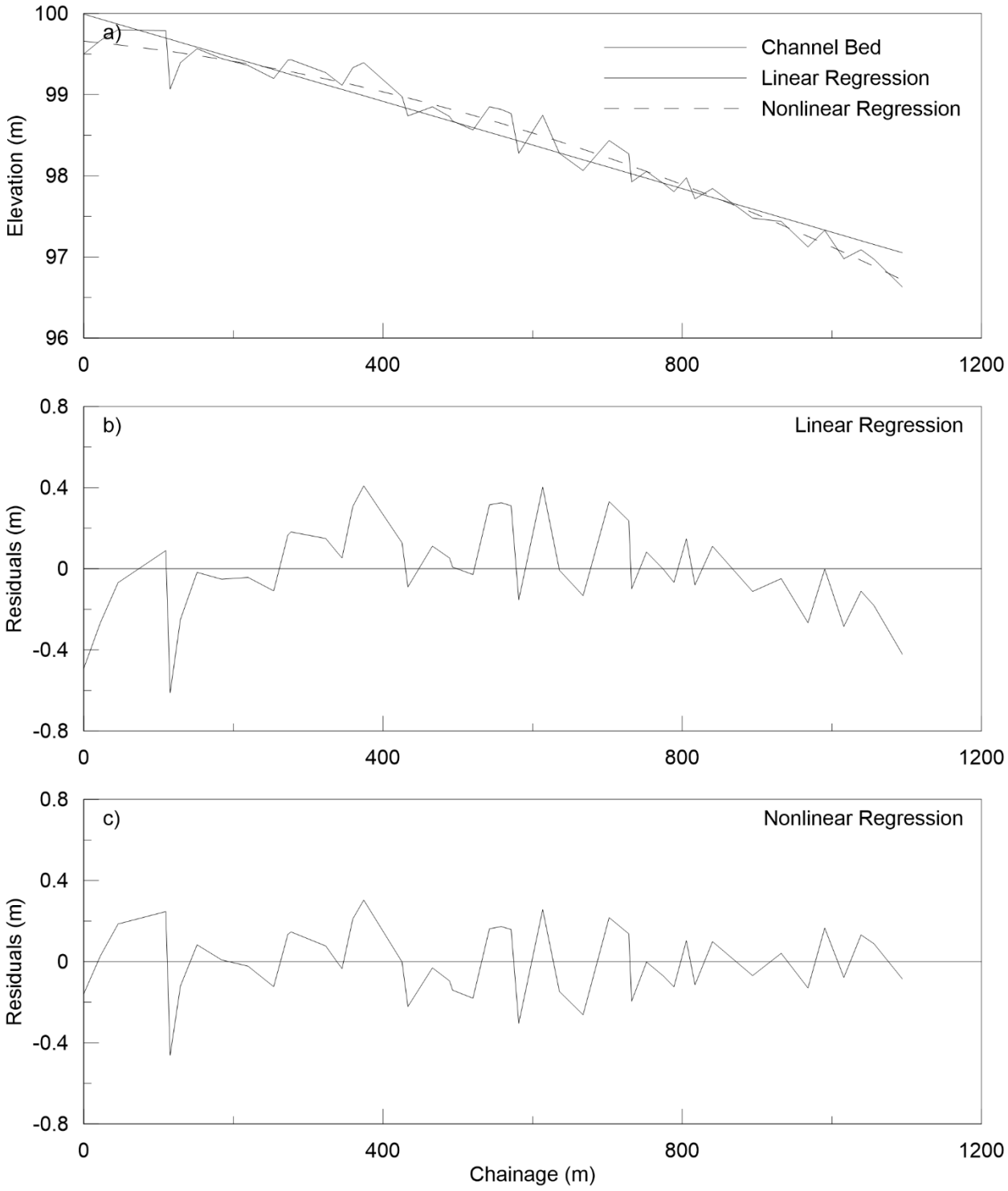

Figure A.19: a) Longitudinal profile with fitted linear and nonlinear regression models, b) residuals from linear regression model and c) residuals from nonlinear regression model for 02FC016.

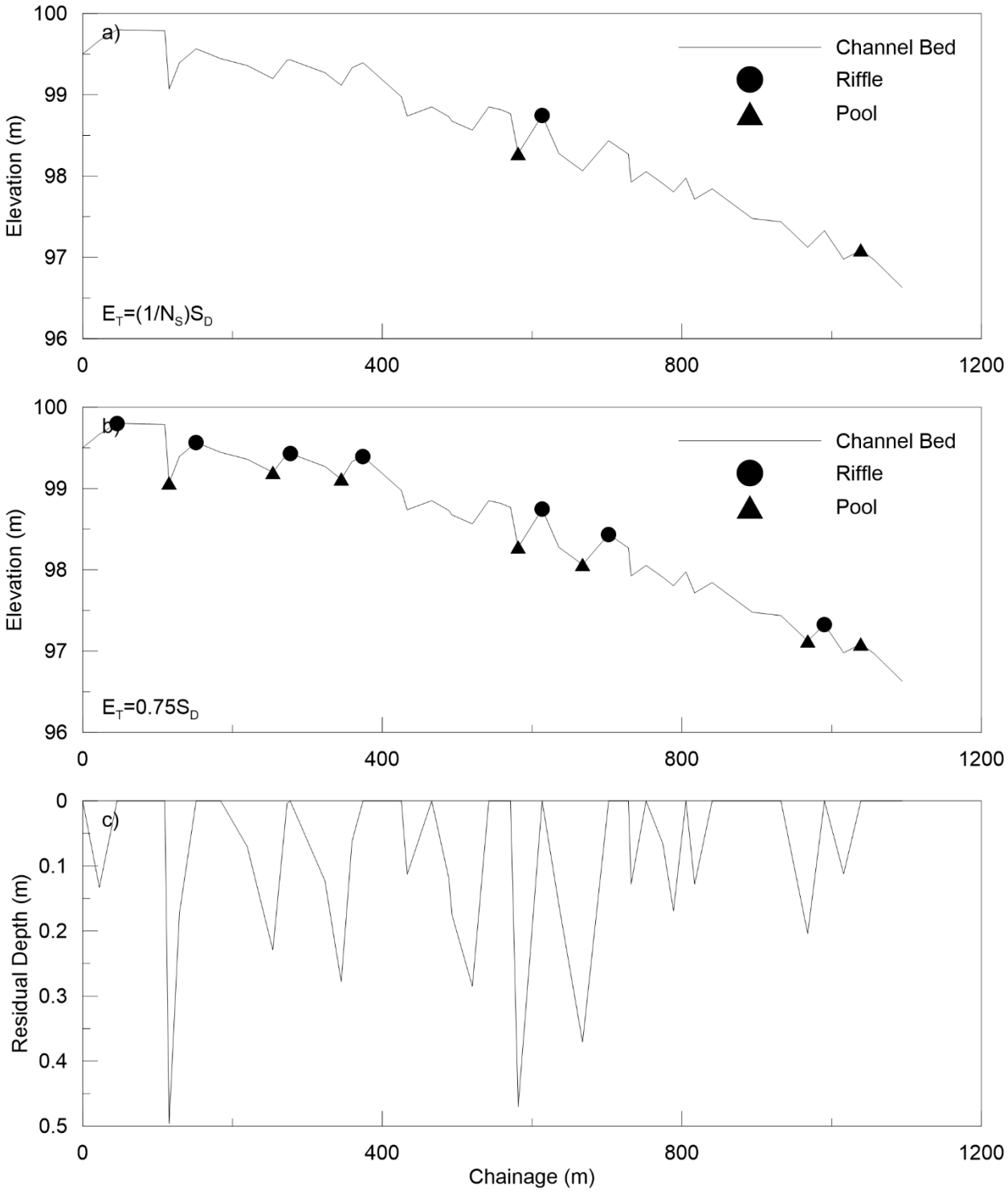

Figure A.20: Longitudinal profile with identified bedforms using bedform differencing with a) $(1/N_S)S_D$ tolerance and b) $0.75S_D$ tolerance and c) residual pool depths for 02FC016.

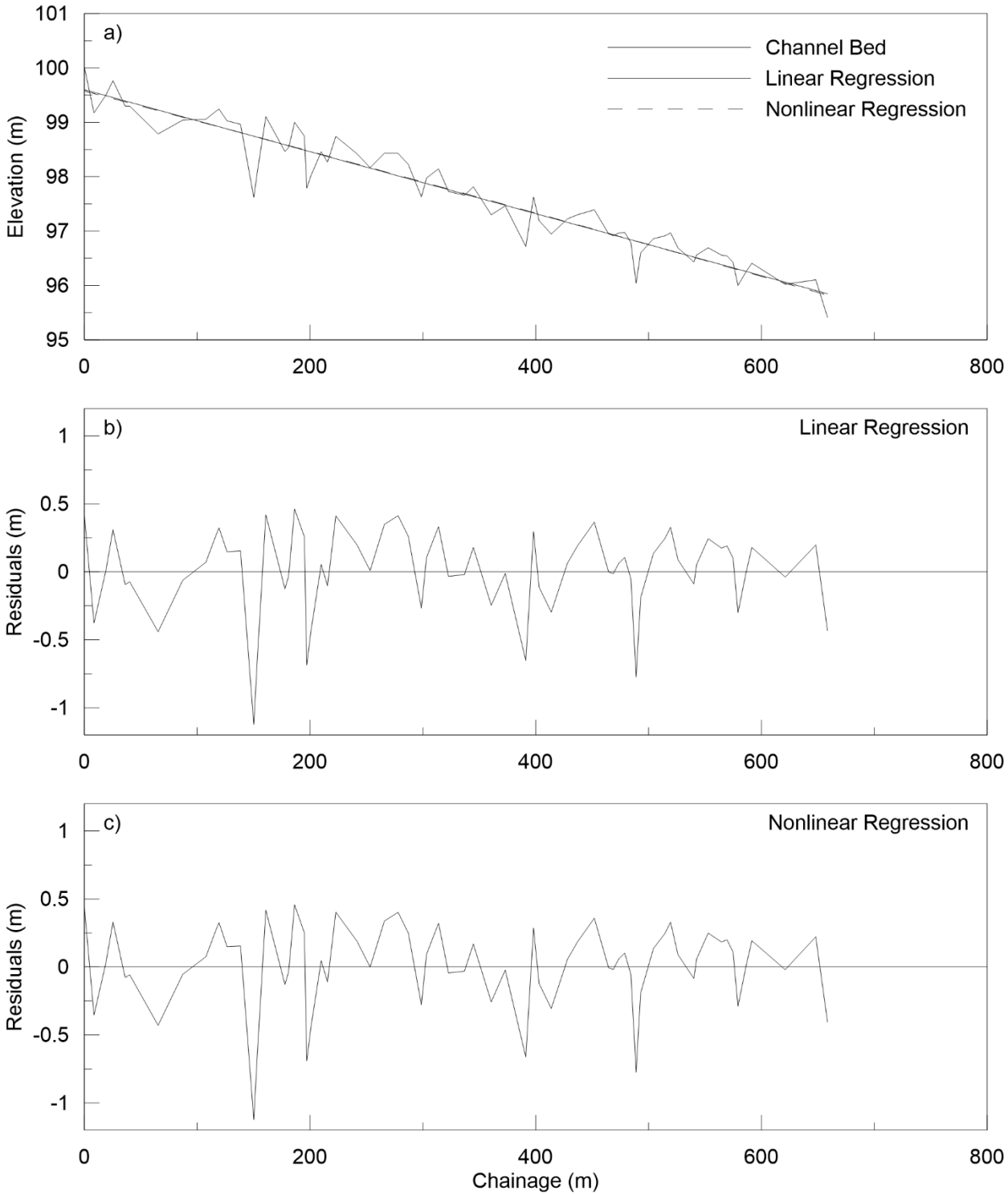

Figure A.21: a) Longitudinal profile with fitted linear and nonlinear regression models, b) residuals from linear regression model and c) residuals from nonlinear regression model for 02ED010.

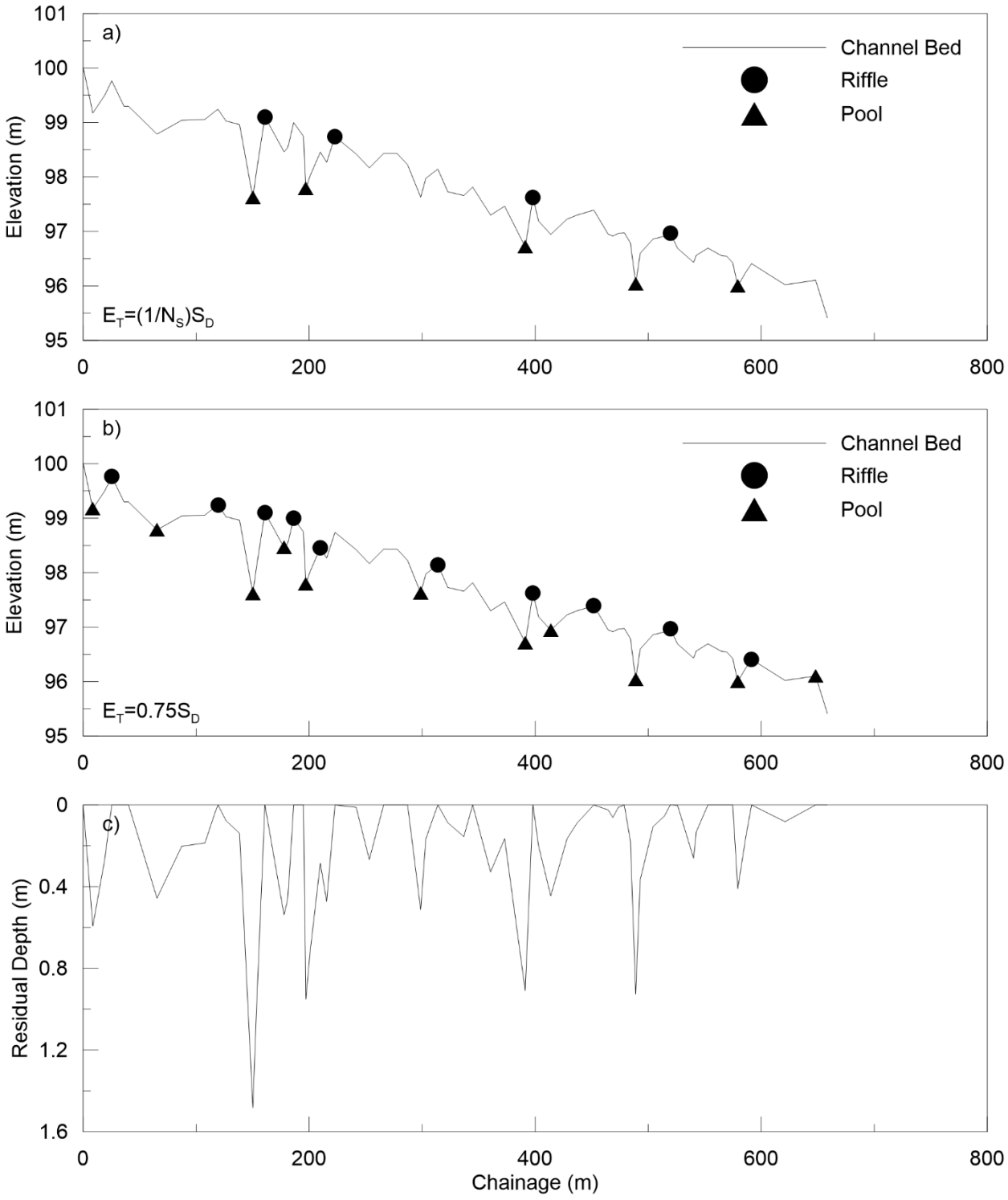

Figure A.22: Longitudinal profile with identified bedforms using bedform differencing with a) $(1/N_S)S_D$ tolerance and b) $0.75S_D$ tolerance and c) residual pool depths for 02ED010.

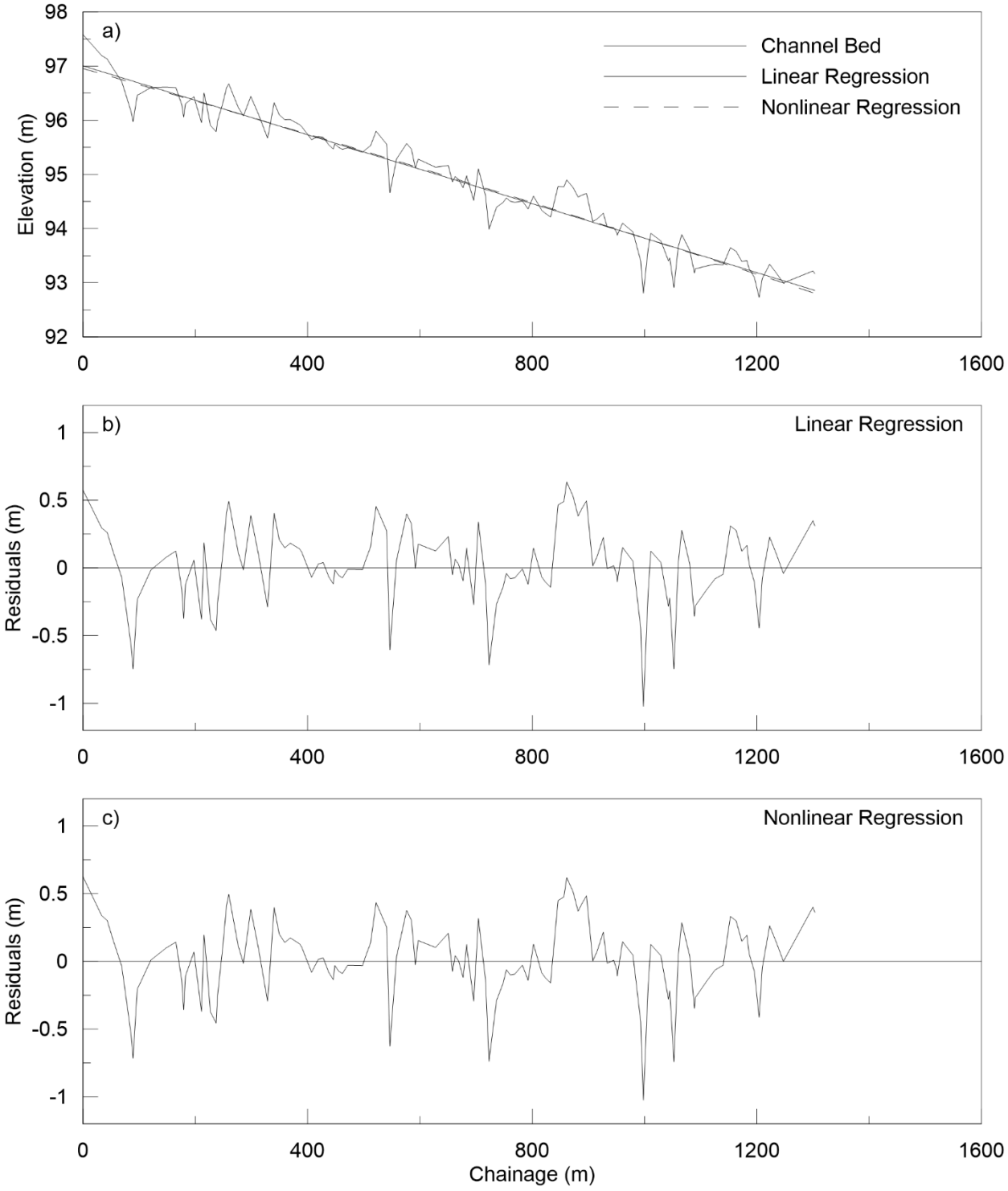

Figure A.23: a) Longitudinal profile with fitted linear and nonlinear regression models, b) residuals from linear regression model and c) residuals from nonlinear regression model for 02HC005.

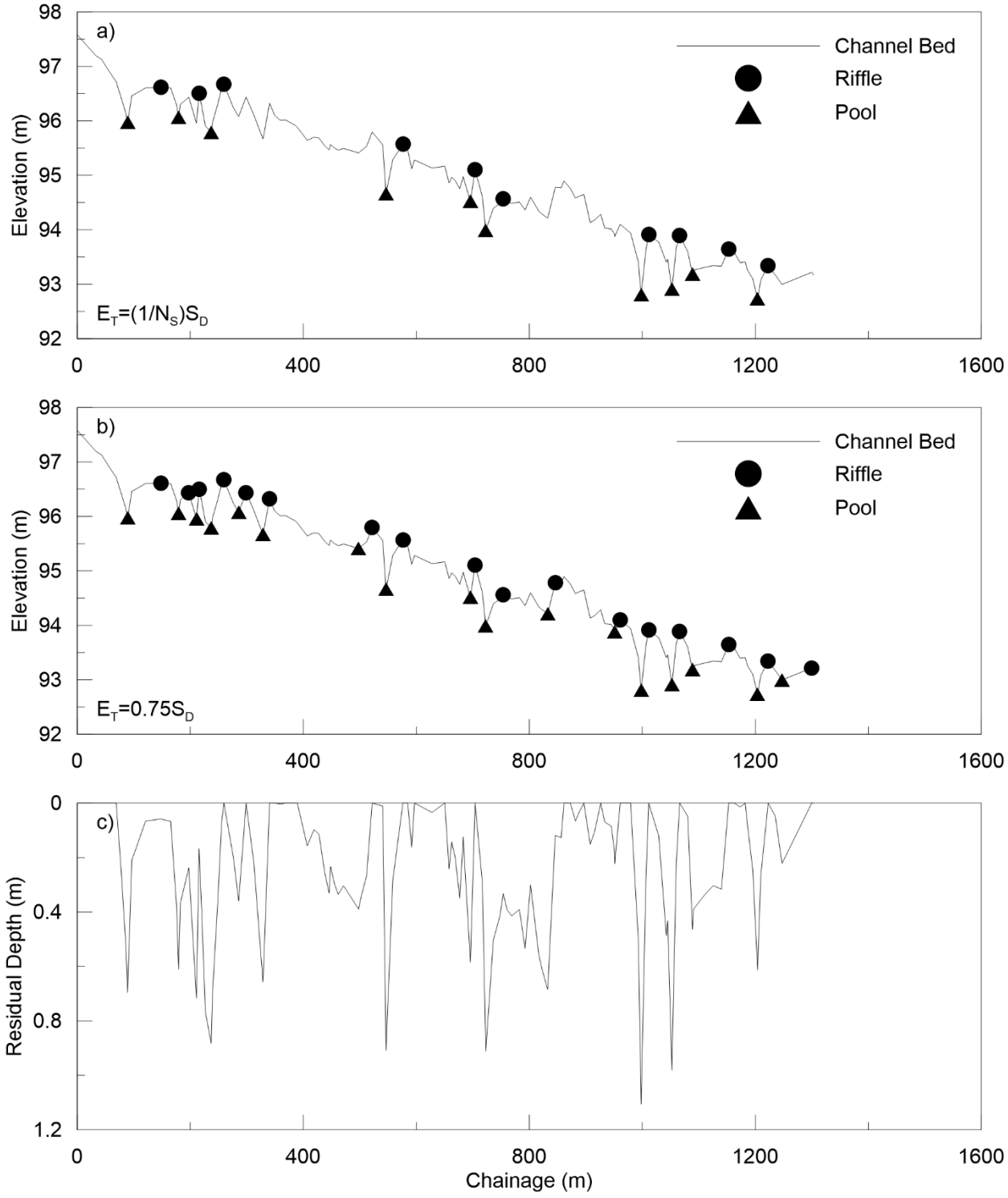

Figure A.24: Longitudinal profile with identified bedforms using bedform differencing with a) $(1/N_S)S_D$ tolerance and b) $0.75S_D$ tolerance and c) residual pool depths for 02HC005.

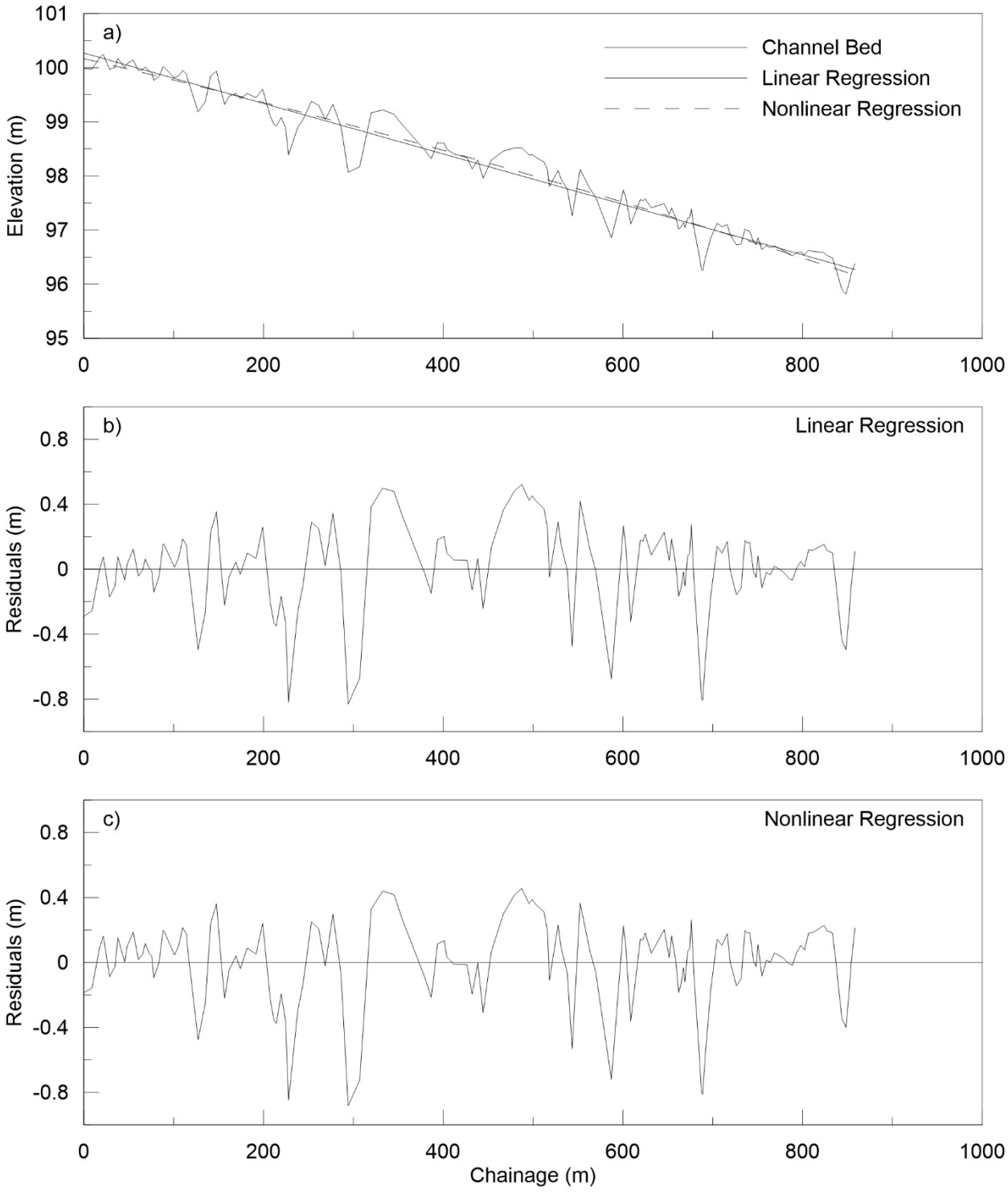

Figure A.25: a) Longitudinal profile with fitted linear and nonlinear regression models, b) residuals from linear regression model and c) residuals from nonlinear regression model for 02HC017.

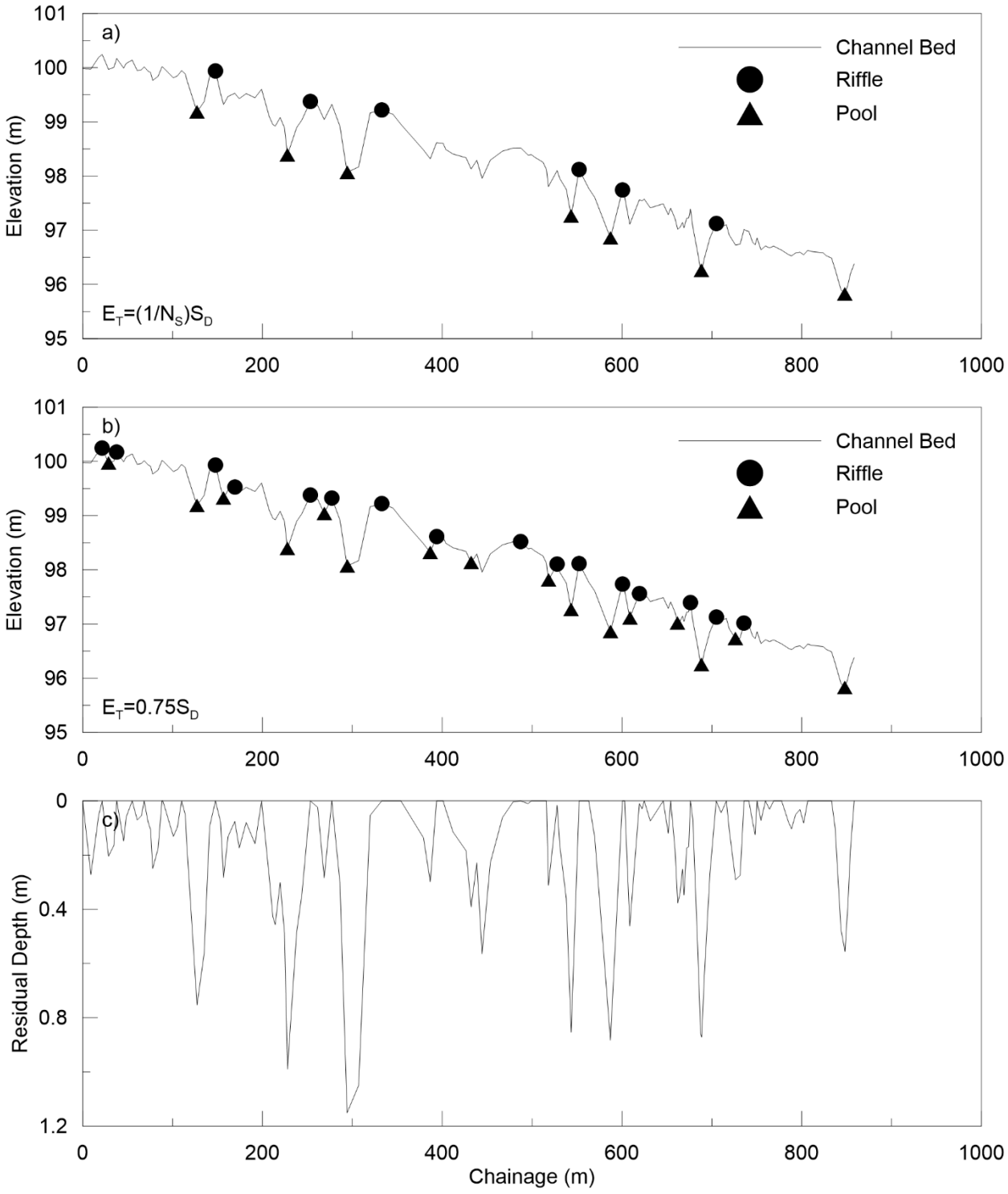

Figure A.26: Longitudinal profile with identified bedforms using bedform differencing with a) $(1/N_S)S_D$ tolerance and b) $0.75S_D$ tolerance and c) residual pool depths for 02HC017.

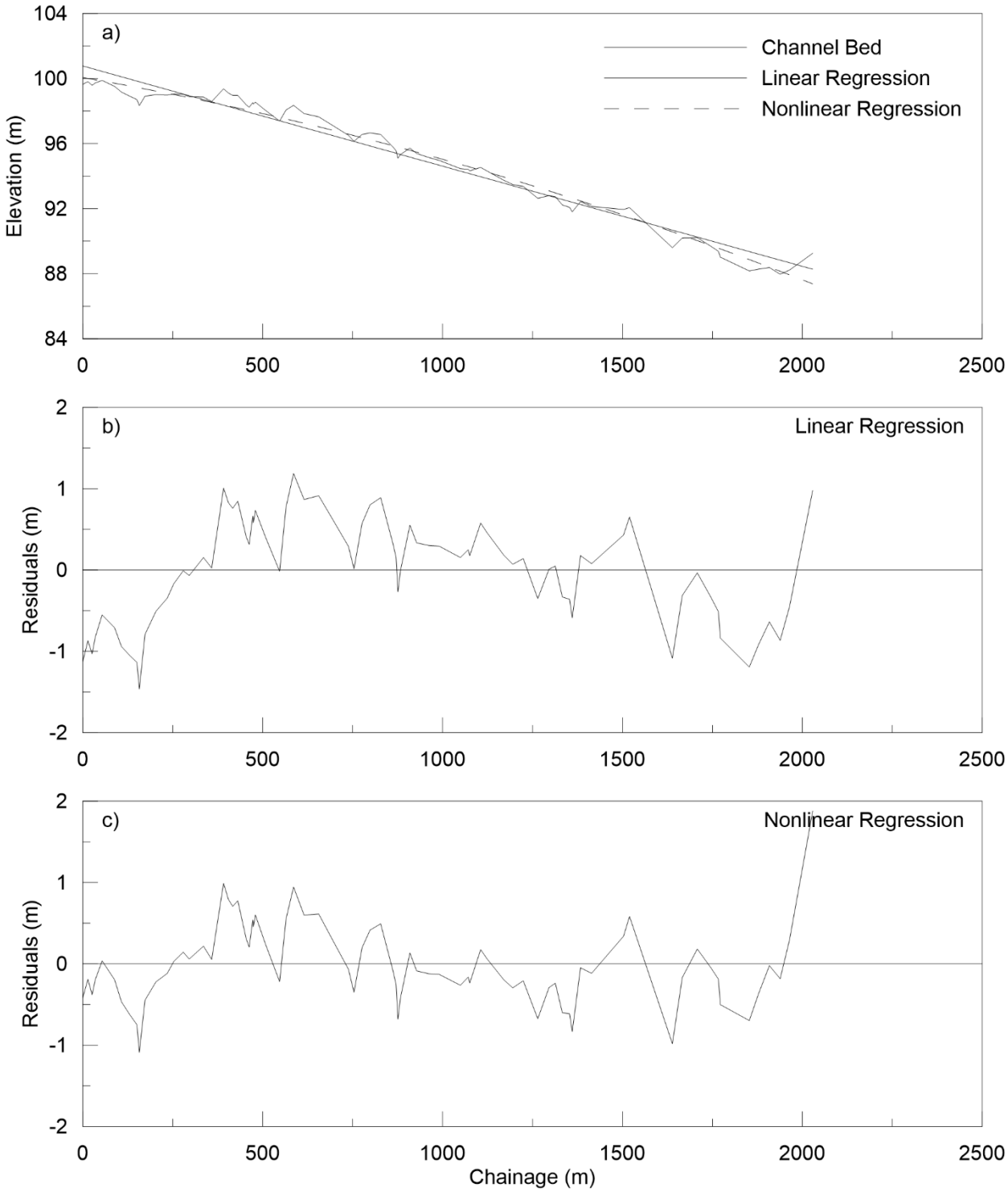

Figure A.27: a) Longitudinal profile with fitted linear and nonlinear regression models, b) residuals from linear regression model and c) residuals from nonlinear regression model for 02HC030.

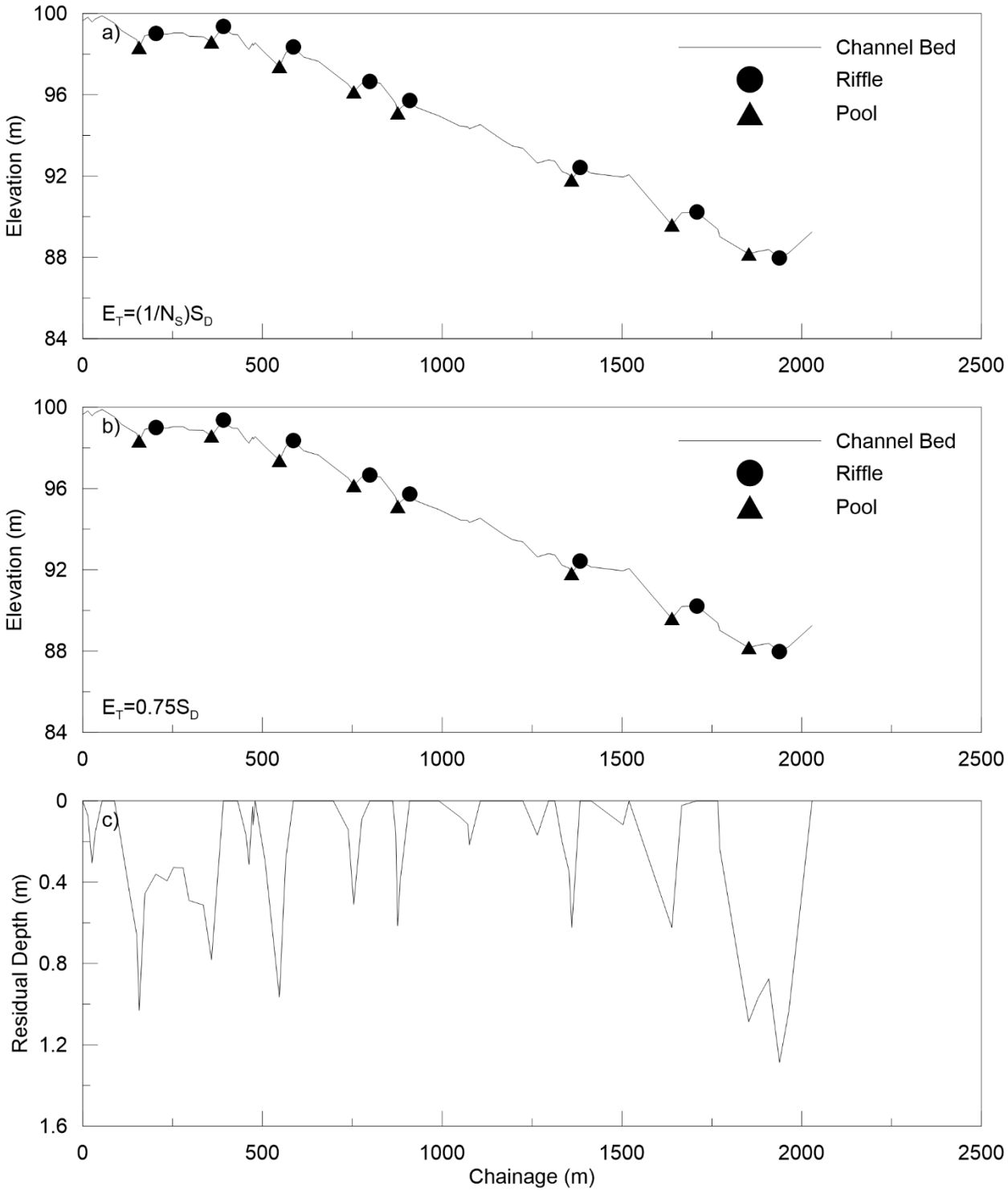

Figure A.28: Longitudinal profile with identified bedforms using bedform differencing with a) $(1/N_S)S_D$ tolerance and b) $0.75S_D$ tolerance and c) residual pool depths for 02HC030.

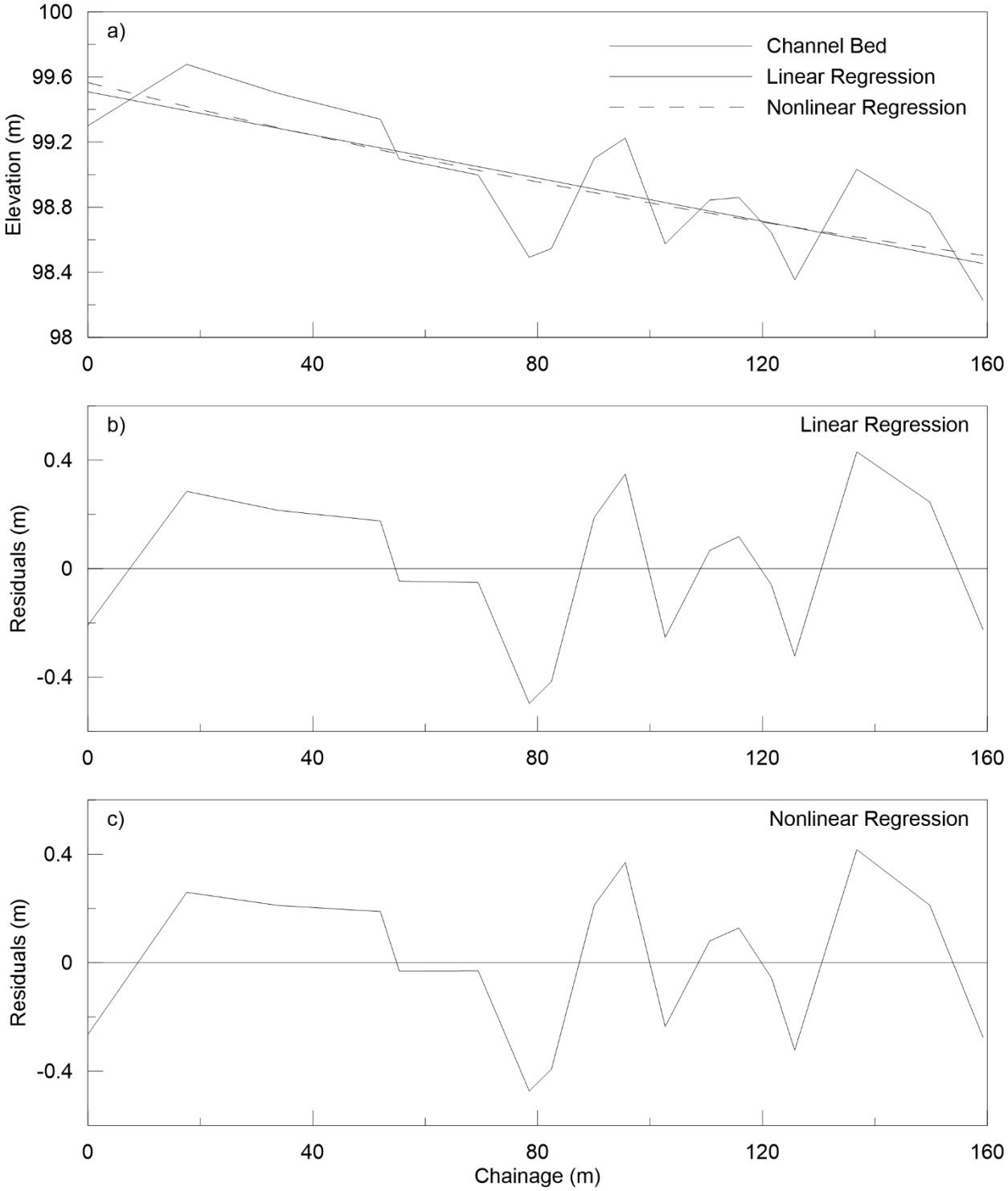

Figure A.29: a) Longitudinal profile with fitted linear and nonlinear regression models, b) residuals from linear regression model and c) residuals from nonlinear regression model for 02HB012.

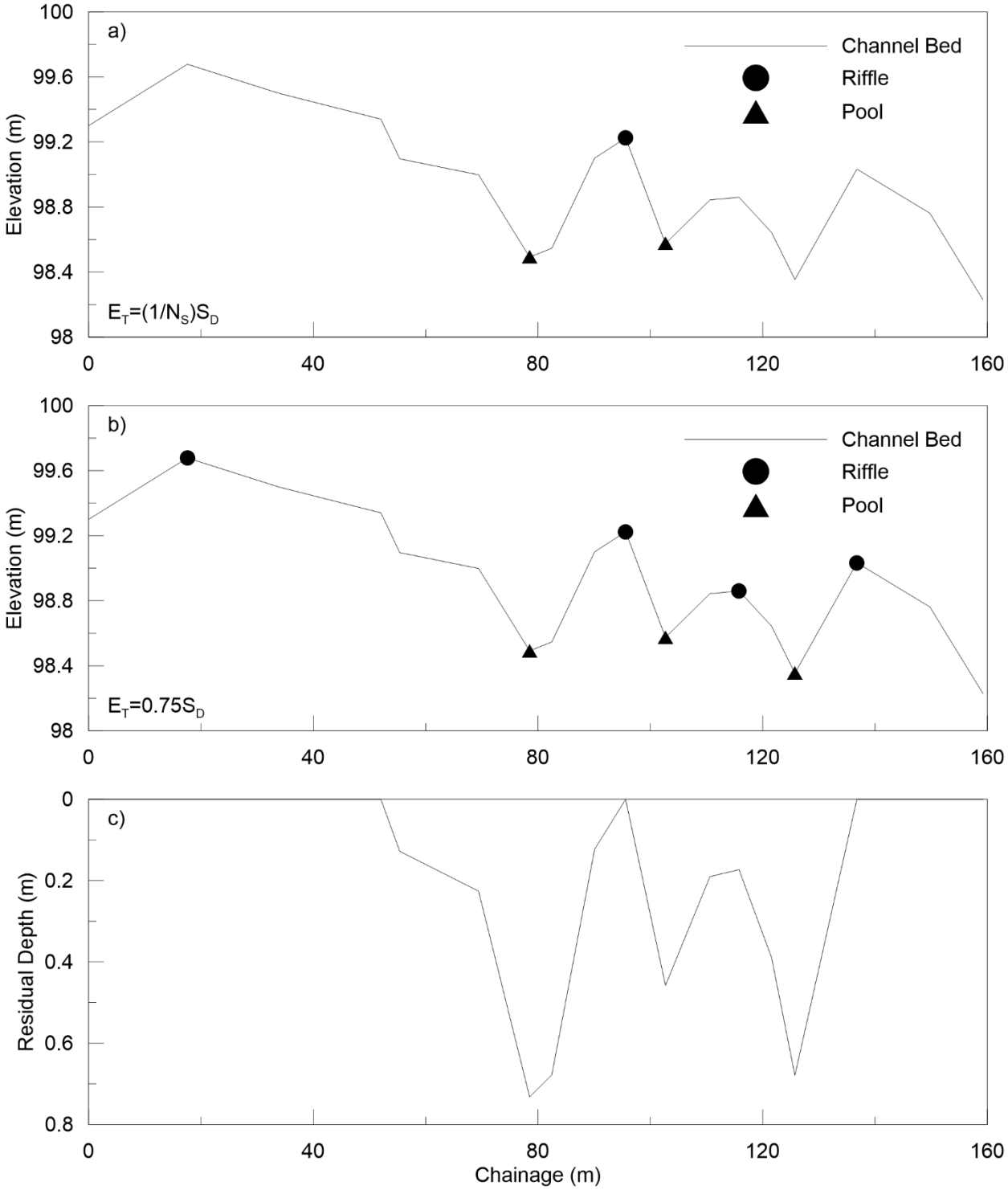

Figure A.30: Longitudinal profile with identified bedforms using bedform differencing with a) $(1/N_S)S_D$ tolerance and b) $0.75S_D$ tolerance and c) residual pool depths for 02HB012.

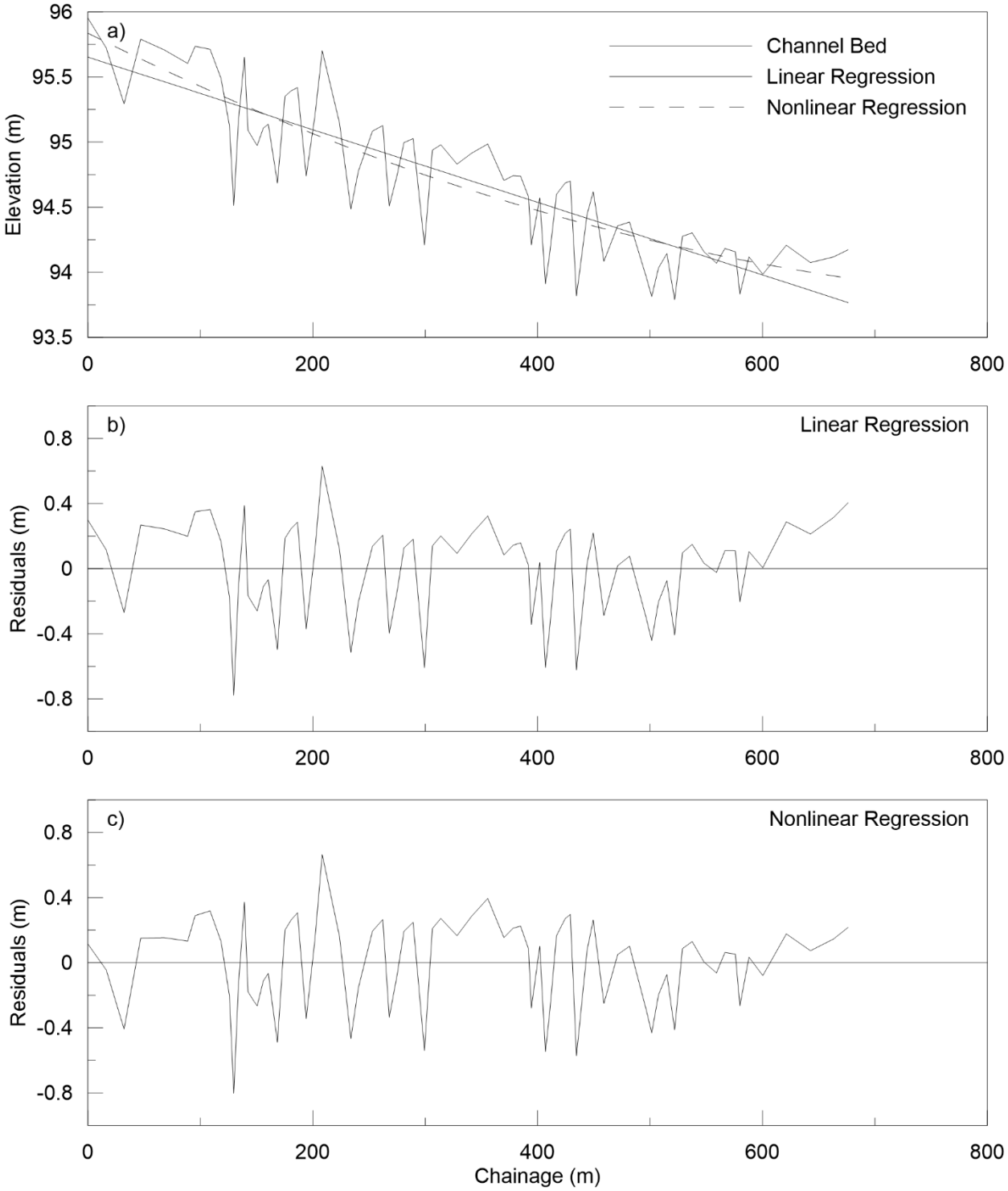

Figure A.31: a) Longitudinal profile with fitted linear and nonlinear regression models, b) residuals from linear regression model and c) residuals from nonlinear regression model for 02HD013.

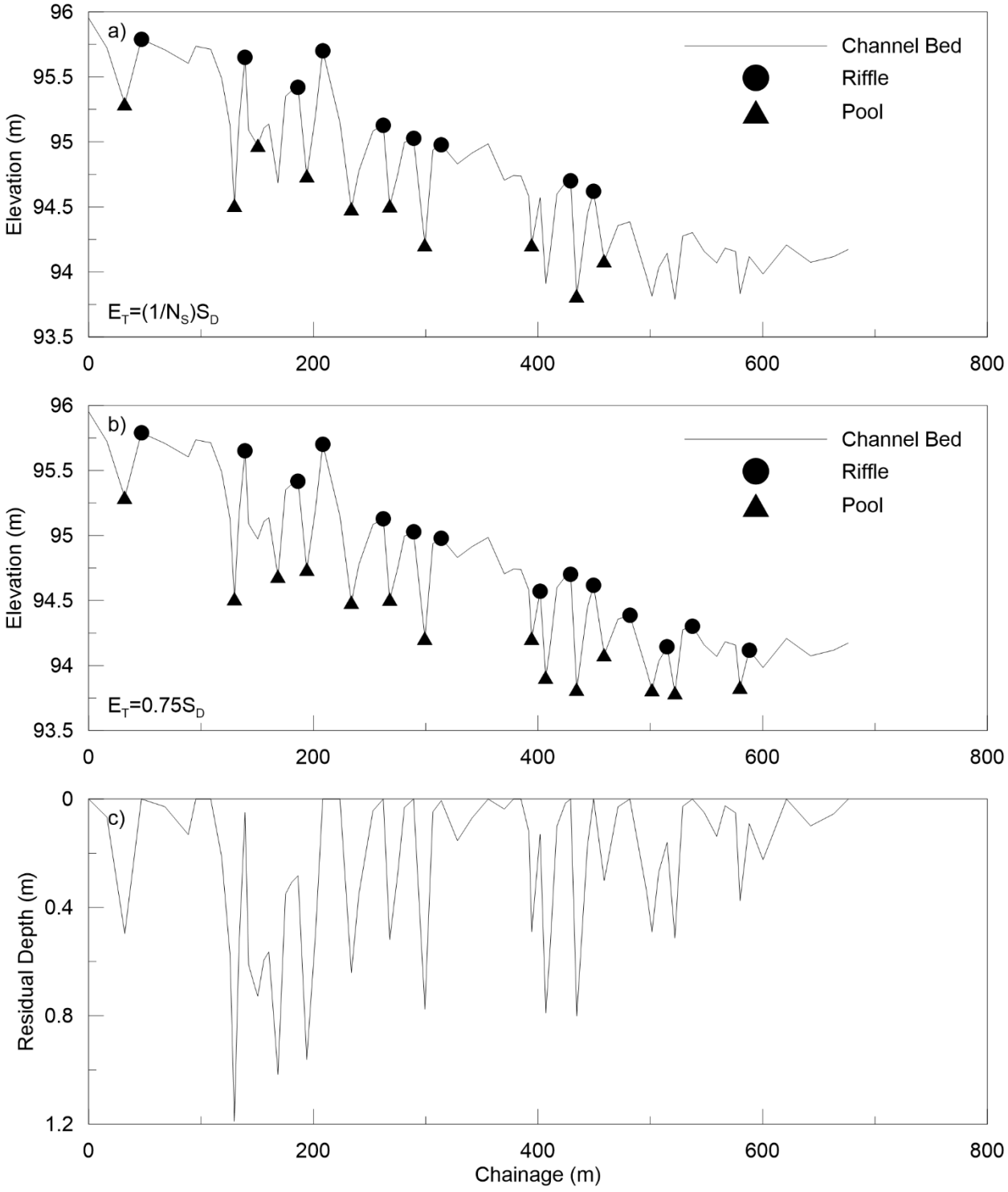

Figure A.32: Longitudinal profile with identified bedforms using bedform differencing with a) $(1/N_S)S_D$ tolerance and b) $0.75S_D$ tolerance and c) residual pool depths for 02HD013.

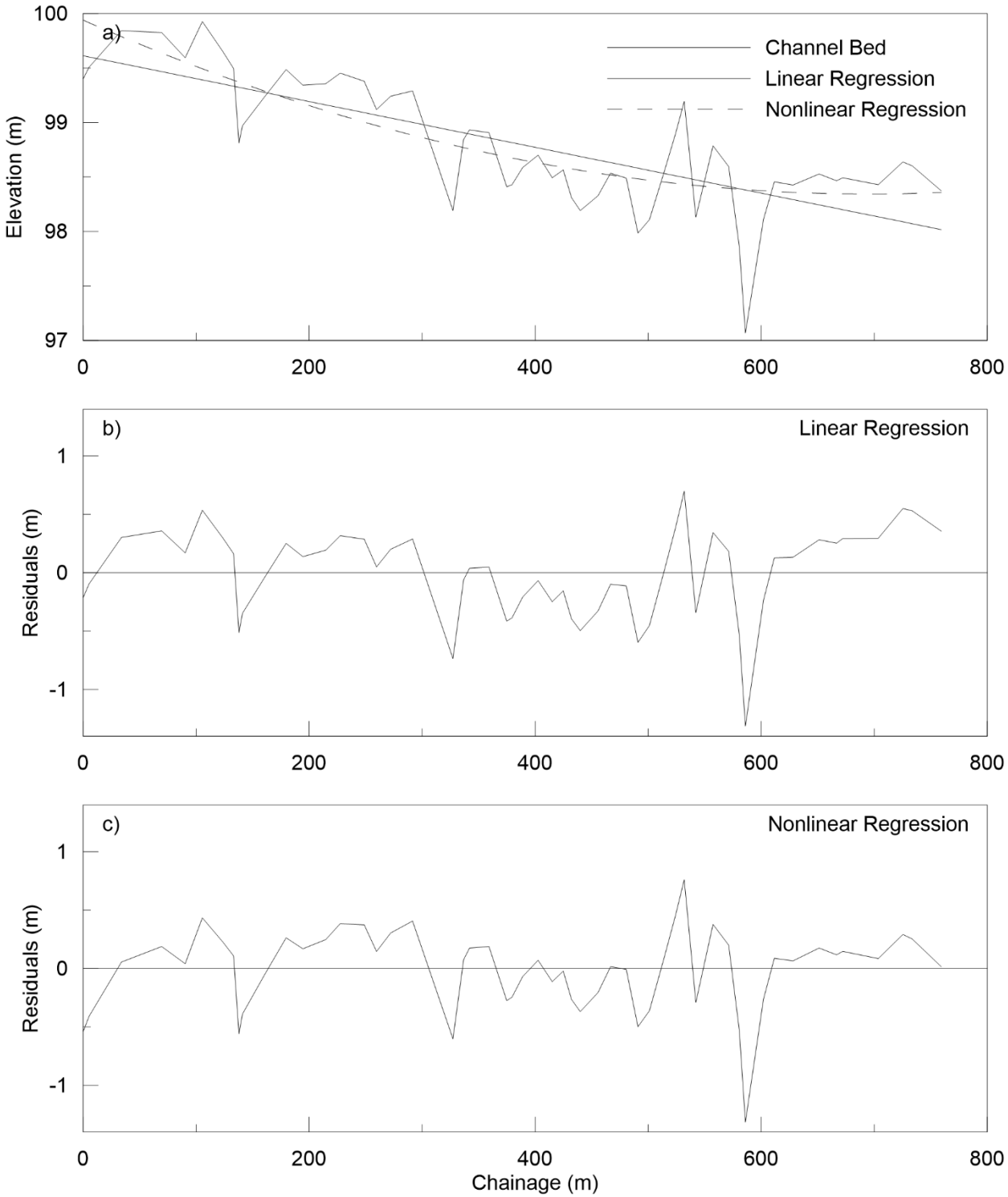

Figure A.33: a) Longitudinal profile with fitted linear and nonlinear regression models, b) residuals from linear regression model and c) residuals from nonlinear regression model for 02HC029.

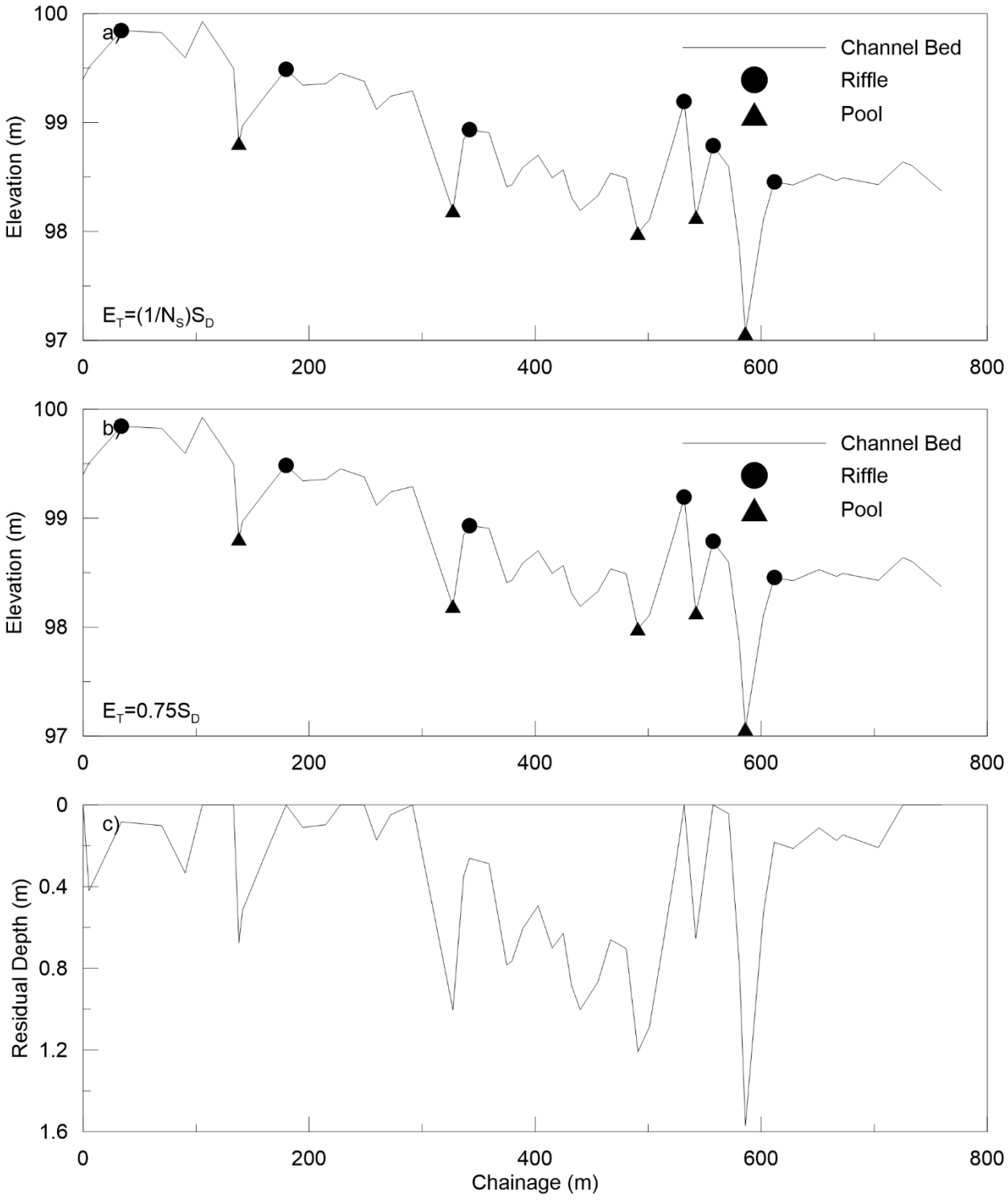

Figure A.34: Longitudinal profile with identified bedforms using bedform differencing with a) $(1/N_S)S_D$ tolerance and b) $0.75S_D$ tolerance and c) residual pool depths for 02HC029.

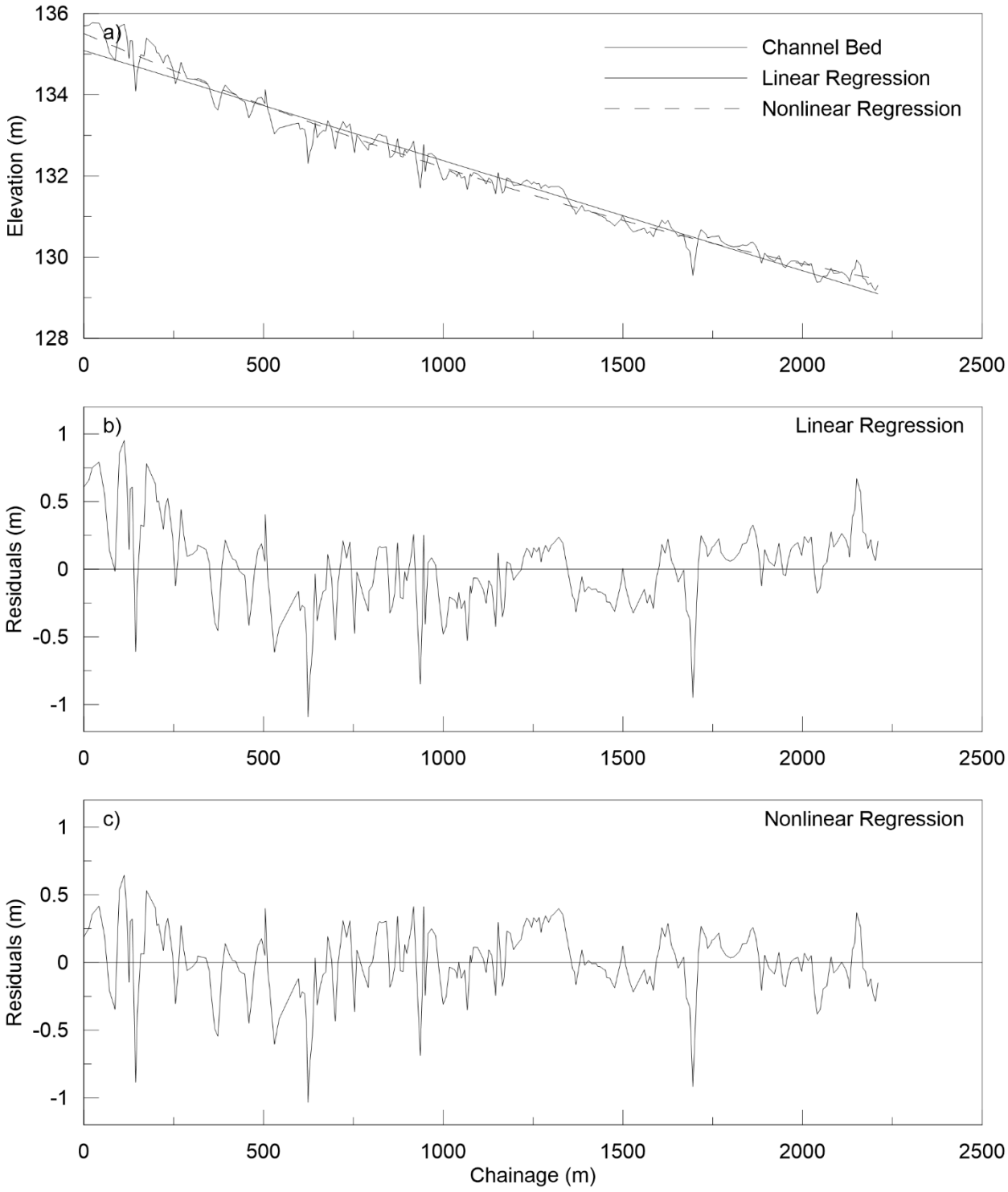

Figure A.35: a) Longitudinal profile with fitted linear and nonlinear regression models, b) residuals from linear regression model and c) residuals from nonlinear regression model for 02HC033.

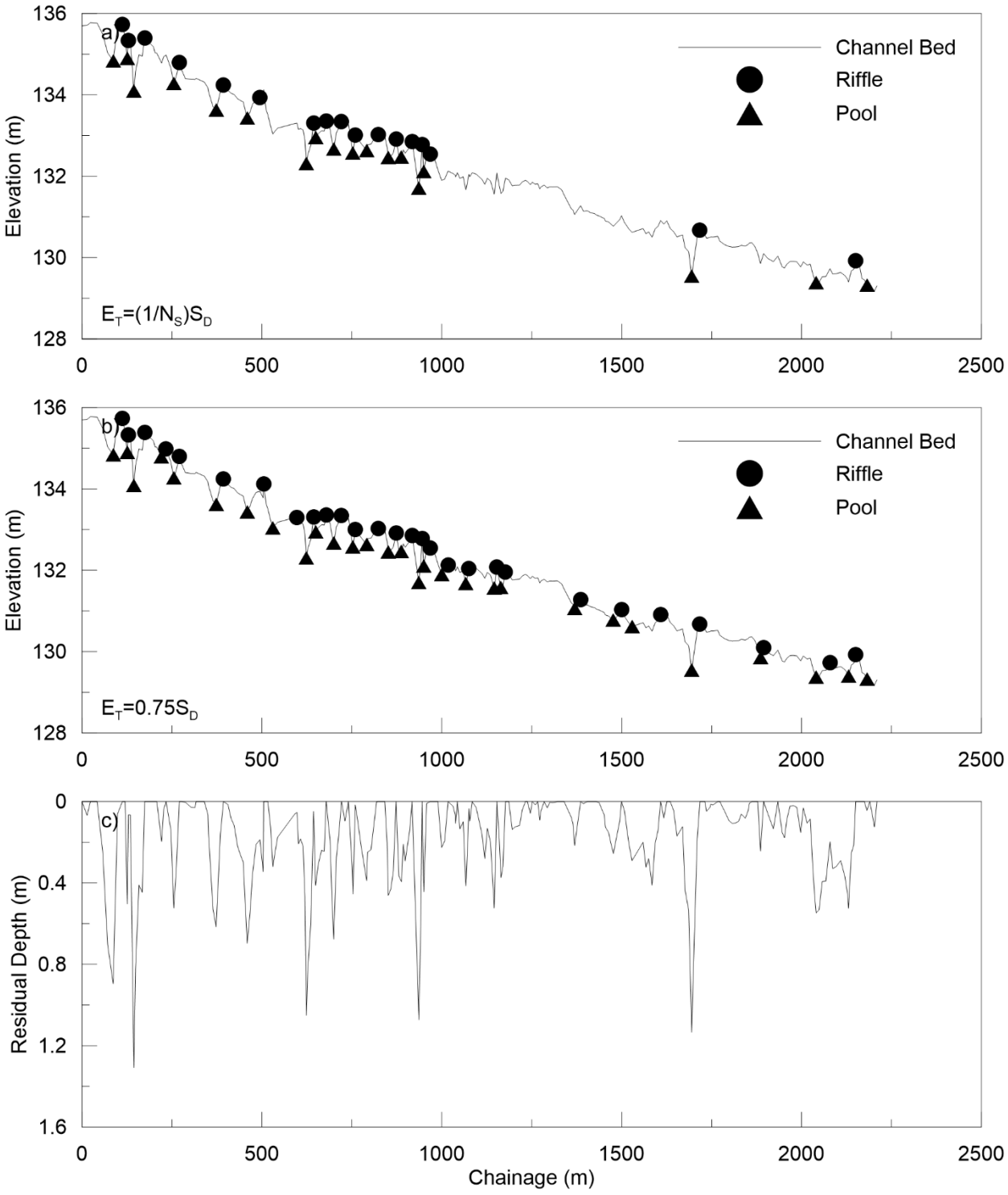

Figure A.36: Longitudinal profile with identified bedforms using bedform differencing with a) $(1/N_S)S_D$ tolerance and b) $0.75S_D$ tolerance and c) residual pool depths for 02HC033.

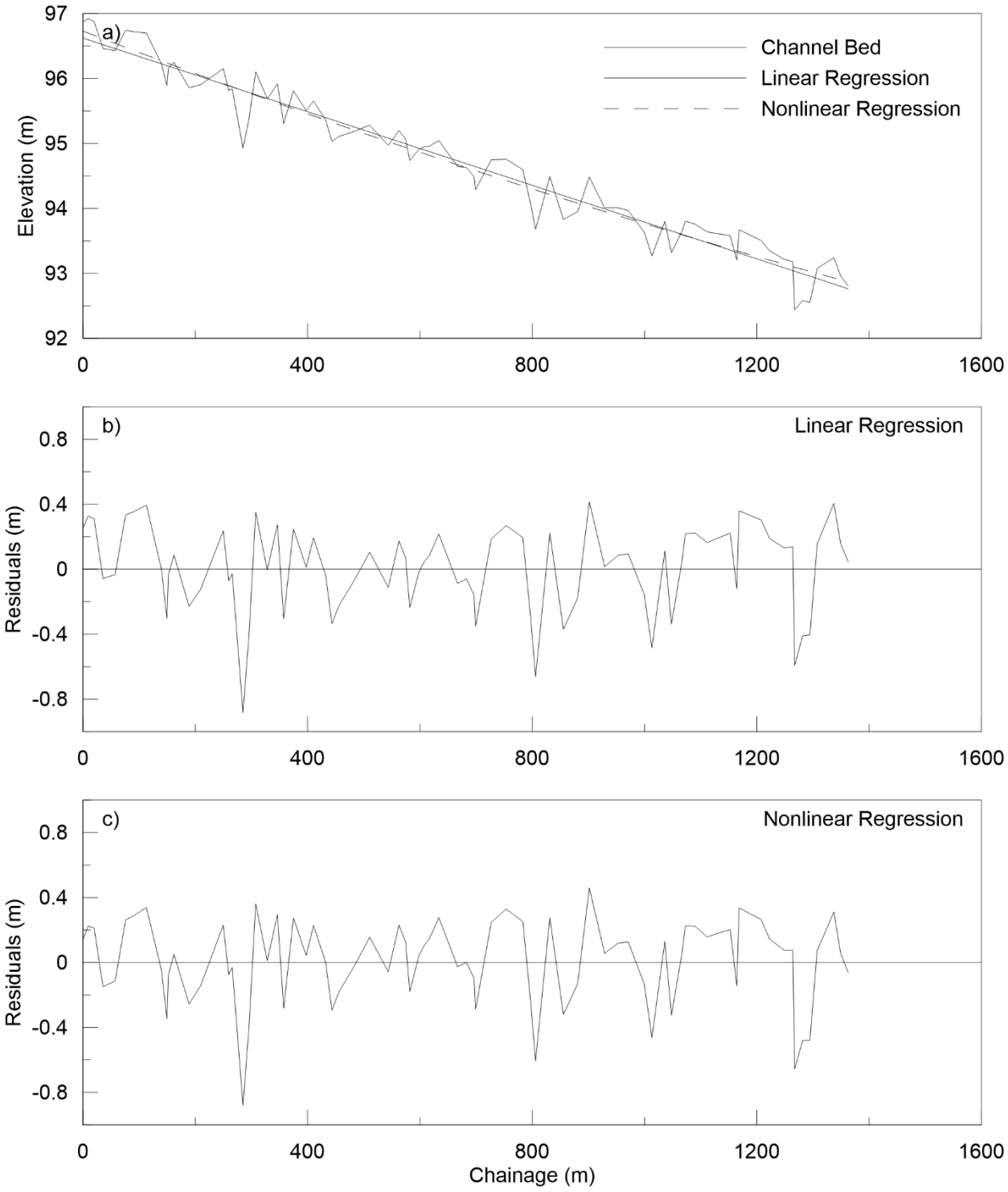

Figure A.37: a) Longitudinal profile with fitted linear and nonlinear regression models, b) residuals from linear regression model and c) residuals from nonlinear regression model for 02HA014.

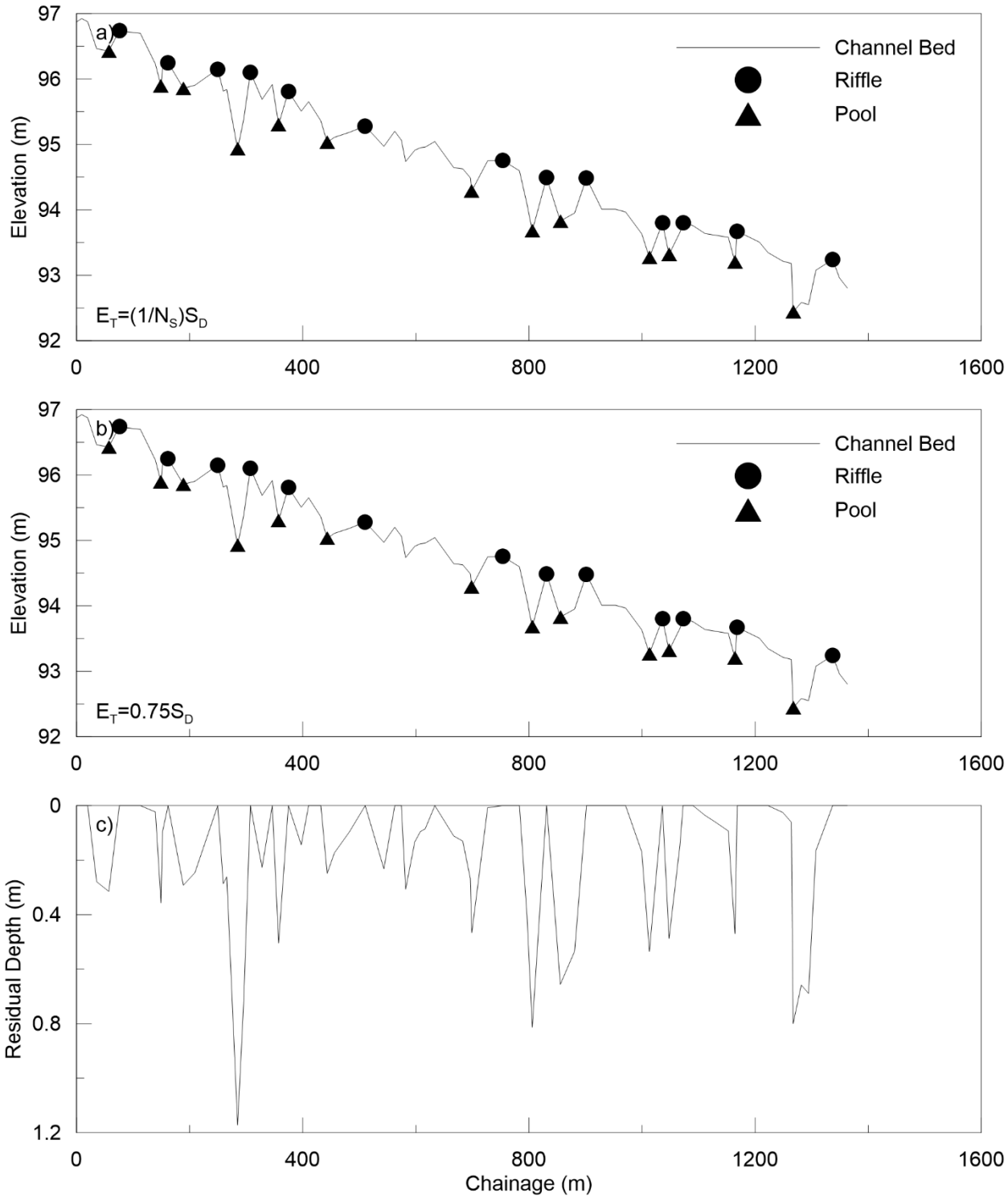

Figure A.38: Longitudinal profile with identified bedforms using bedform differencing with a) $(1/N_S)S_D$ tolerance and b) $0.75S_D$ tolerance and c) residual pool depths for 02HA014.

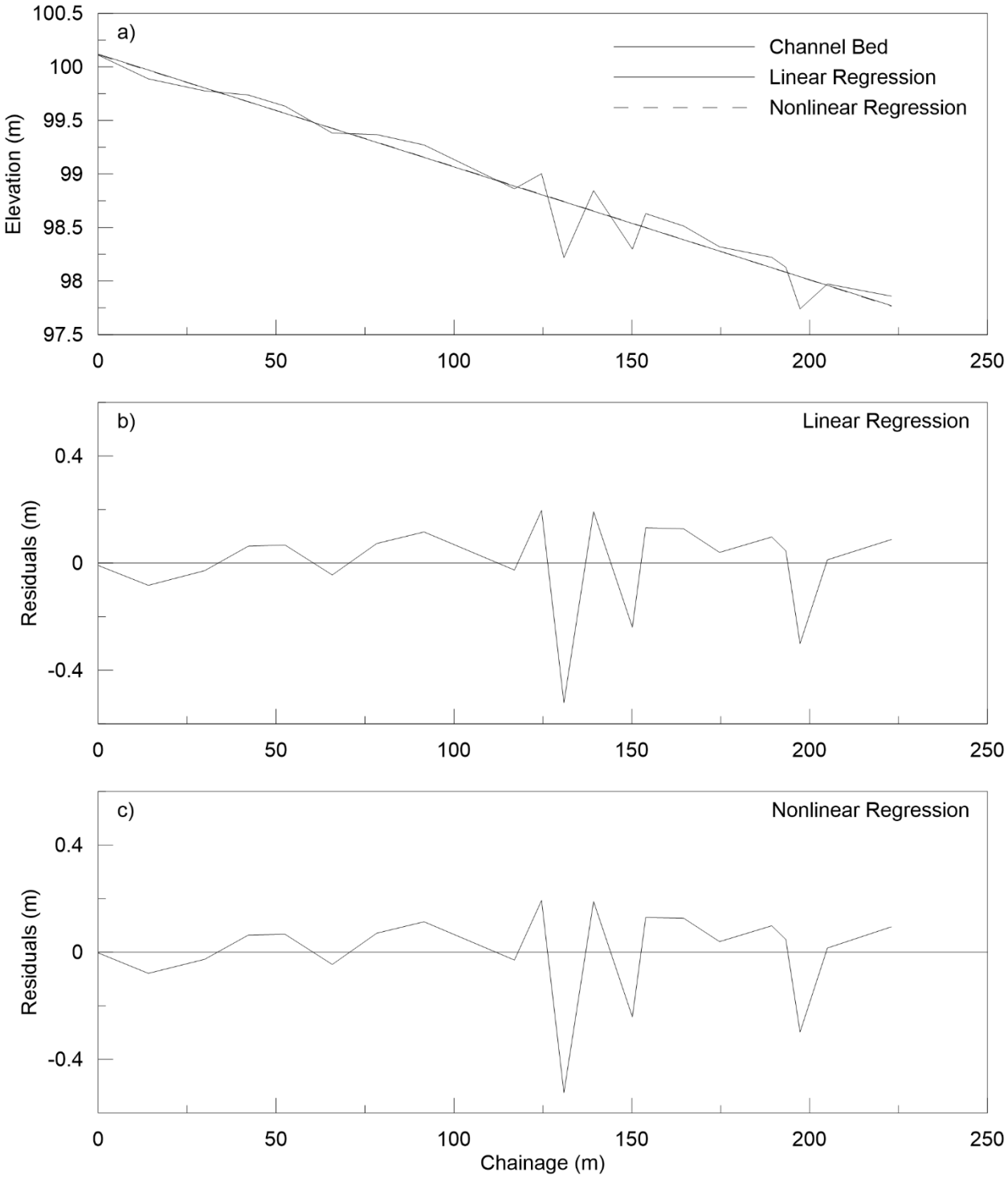

Figure A.39: a) Longitudinal profile with fitted linear and nonlinear regression models, b) residuals from linear regression model and c) residuals from nonlinear regression model for 02HA022.

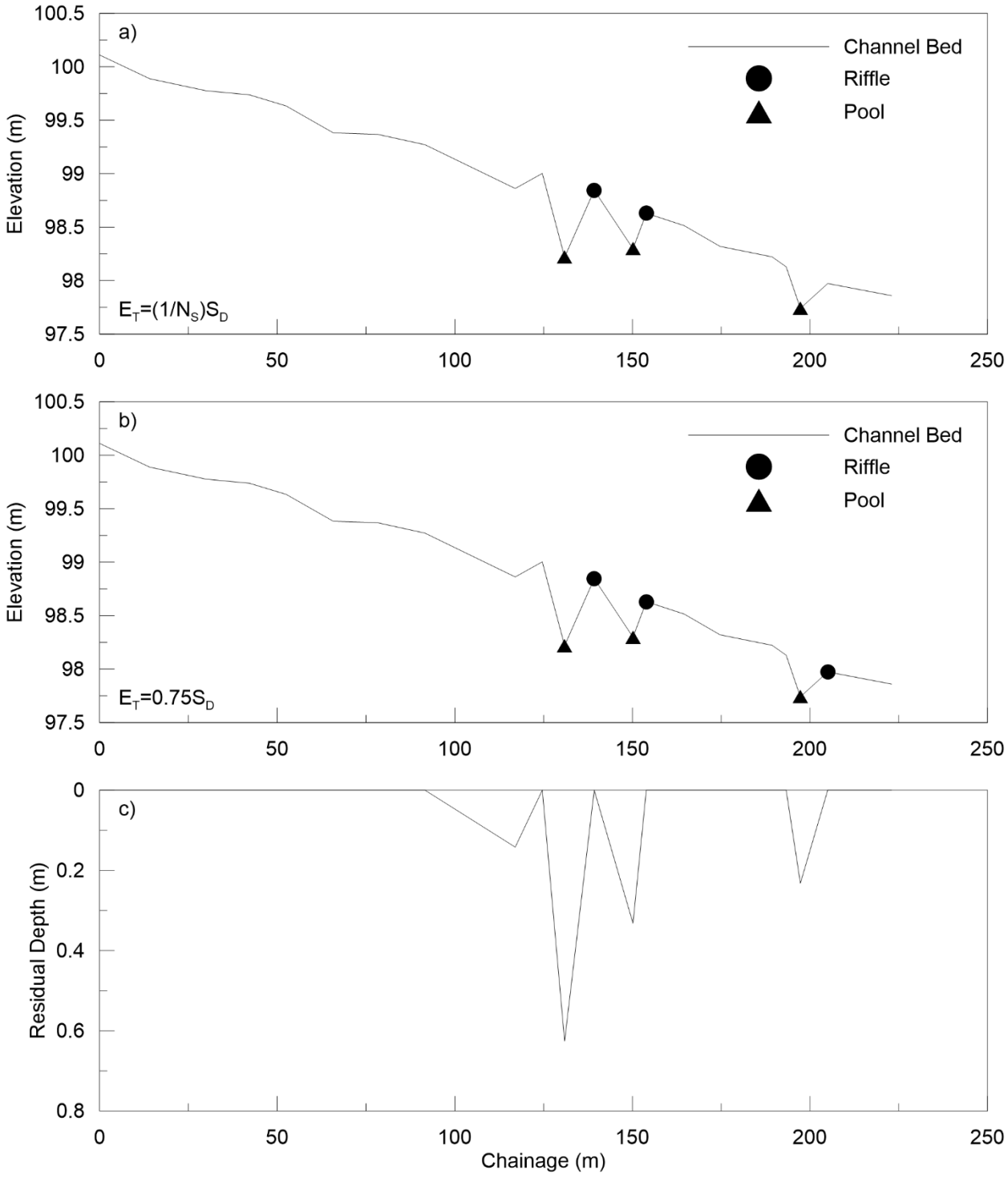

Figure A.40: Longitudinal profile with identified bedforms using bedform differencing with a) $(1/N_S)S_D$ tolerance and b) $0.75S_D$ tolerance and c) residual pool depths for 02HA022.

Appendix B

Additional Results from Chapter 3

Notes: This appendix contains additional results and supporting information from Chapter 2.

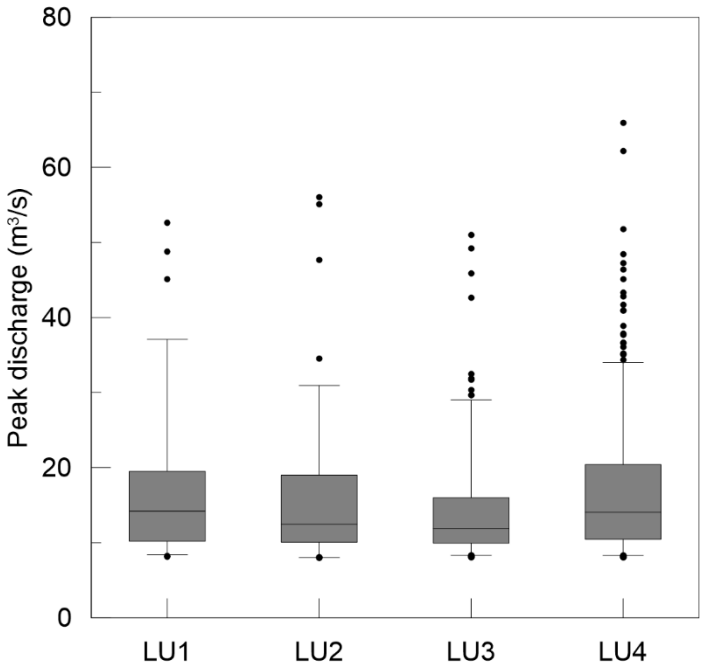

Figure B.1: Distribution of peak discharges for each land-use scenario.

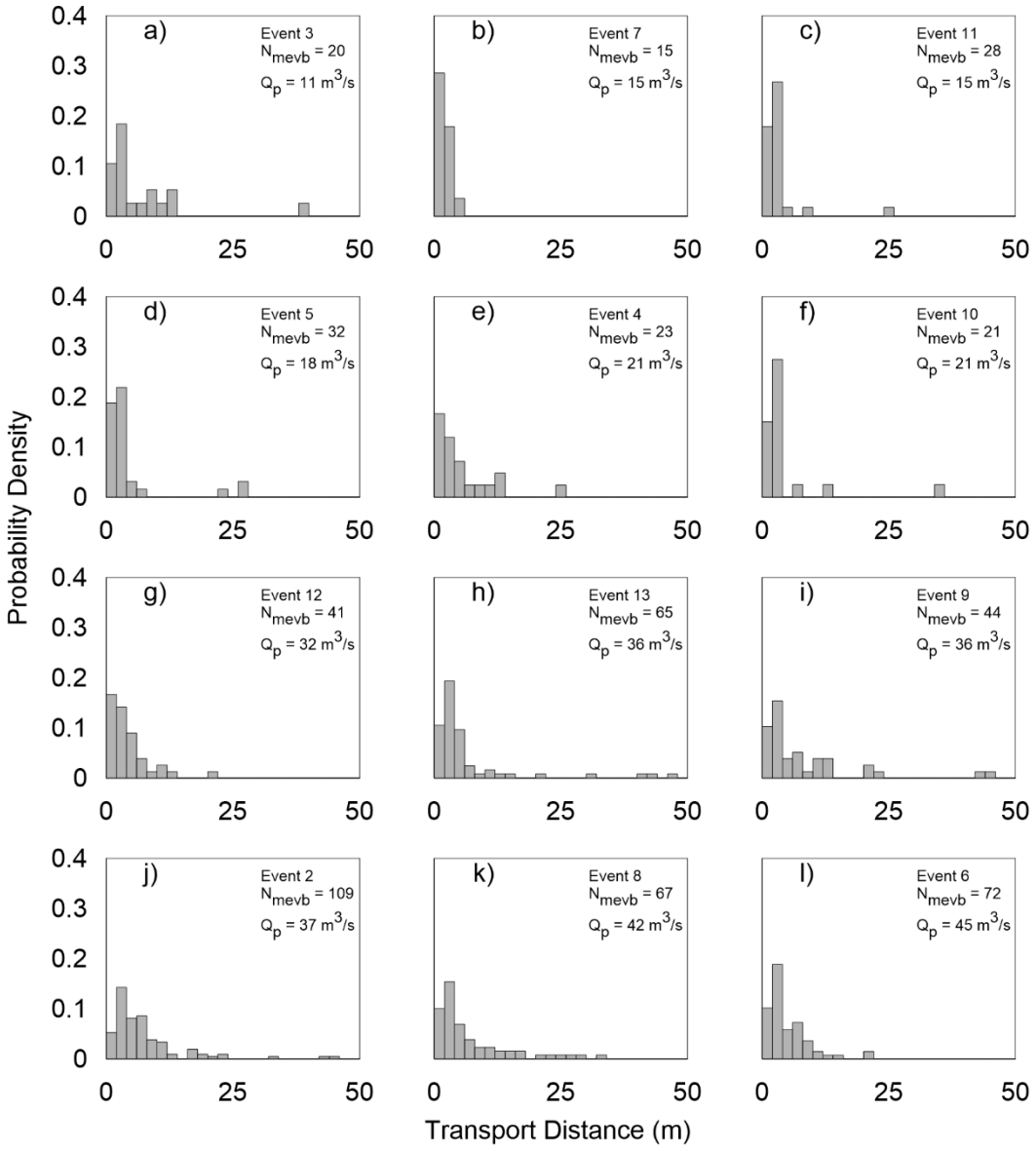

Figure B.2: Tracer transport histograms organized according to peak discharge.

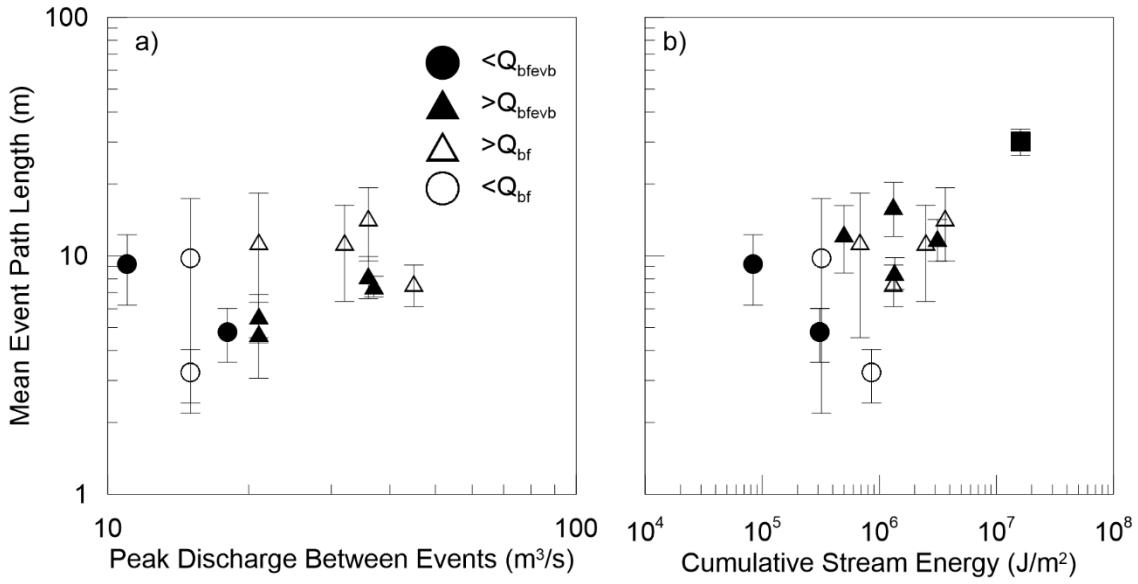

Figure B.3: Mean event path length vs a) peak discharge and b) cumulative stream energy for: event-based tracks (filled) and non event-based tracks (hollow) for both events above and below Q_{bf}. The filled square in b) represents the mean cumulative path length for all events vs. the total cumulative stream energy for the study period. Error bars represent the standard error of the mean.

Table B.1: Temporal land-use characteristics for study watersheds [from *Thompson*, 2013]

Year	% Urban Area	
	Mimico	Etobicoke
1955	10	-
1970	45.1	1.2
1978	54.5	4.8
1995	71.8	16.2
2005	81.5	18.5

	Tracer Survey Date	# of Events >Q_{bf}	# of Events >Q_{thres}	Q_{peak} (m^3/s)	Order of Events >Q_{thres} (m^3/s)	N_f	P_r (%)	N_{fevb}	P_{revb} (%)	N_m	N_{mevb}	P_m (%)	P_{mevb} (%)	L_{mevb} (m)	L_{mevb} Mobile (m)
2011	Nov-25	0	1	12		500	91	500	91	9	9	2	2	0.1	2.8
	Dec-02	1	1	37		490	89	447	81	120	109	24	24	2.9	11.8
2012	Mar-16	0	1	11		468	85	439	80	30	20	6	5	0.4	9.2
	May-09	1	1	21		476	87	427	78	29	23	6	5	0.7	12.4
	Jun-05	0	1	18		483	88	435	79	39	32	8	7	0.4	4.8
	Aug-02	1	3	45	10,18,45	446	81	404	73	81	72	18	18	1.4	7.6
	Aug-15	0	2	15	15,14	474	86	411	75	38	15	8	4	0.4	9.8
	Sep-06	1	1	42		446	81	403	73	80	67	18	17	1.4	8.5
	Sep-13	1	1	36		467	85	399	73	66	44	14	11	1.8	16.2
	Sep-24	1	2	21	21,10	462	84	412	75	36	21	8	5	0.6	11.4
	Nov-15	0	5	15	10,14,15,11,9	377	69	340	62	32	28	8	8	0.3	3.2
2013	Apr-04	1	6	32	32,16,15,12,13,16	326	59	276	50	52	41	16	15	1.7	11.4
	May-31	2	5	36	10,17,21,10,36	404	73	268	49	99	65	25	24	3.5	14.4

Notes: N_f = number of particles found, P_r = percent recovered, N_{fevb} = number found which were also found in the previous track (event-based), P_{revb} = event-based recovery rate, N_m = total number of mobile particles, N_{mevb} = event-based number of mobile particles, P_m = percentage of mobile particles, P_{mevb} = event-based percentage of mobile particles, L_{mevb} = mean transport distance of event-based particles (including immobile particles), L_{mevb} Mobile = mean transport distance of event-based particles (considering only mobile particles). Event-based statistics are based on particles found in two consecutive tracer surveys.

Table B.2: Tracer recovery and mobility statistics for each of the tracer surveys. Also included are number of competent floods, flood magnitude and flood sequence that occurred between sequential tracer surveys.

Appendix C
Additional Results from Chapter 4

Notes: This appendix contains the raw results from all laboratory experiments performed in Chapter 4. Results are shown for each sequential hydrograph, progressing in increasing order from top left to bottom right.

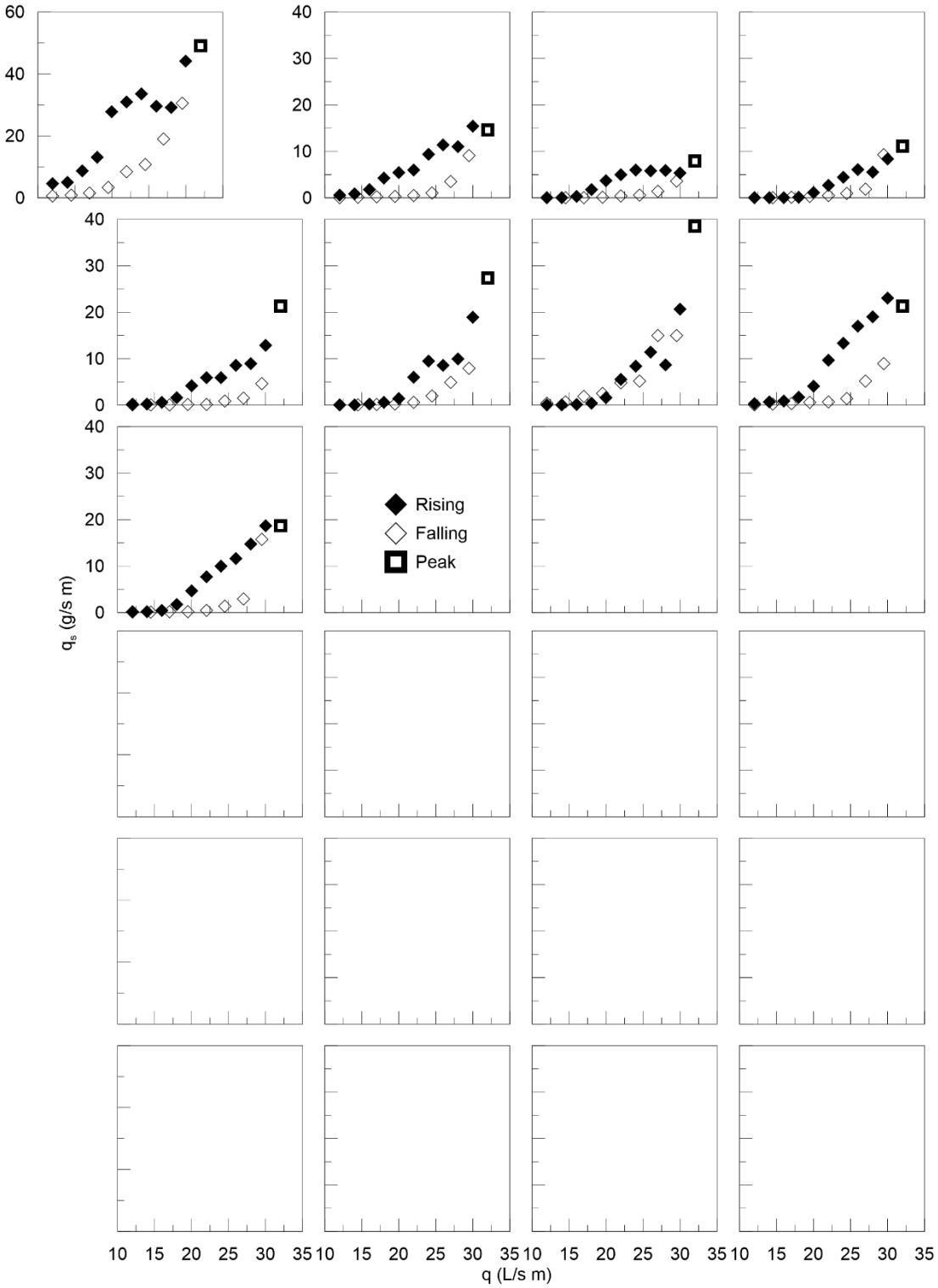

Figure C.1: LU1 phase plots (hydrographs 1 – 9)

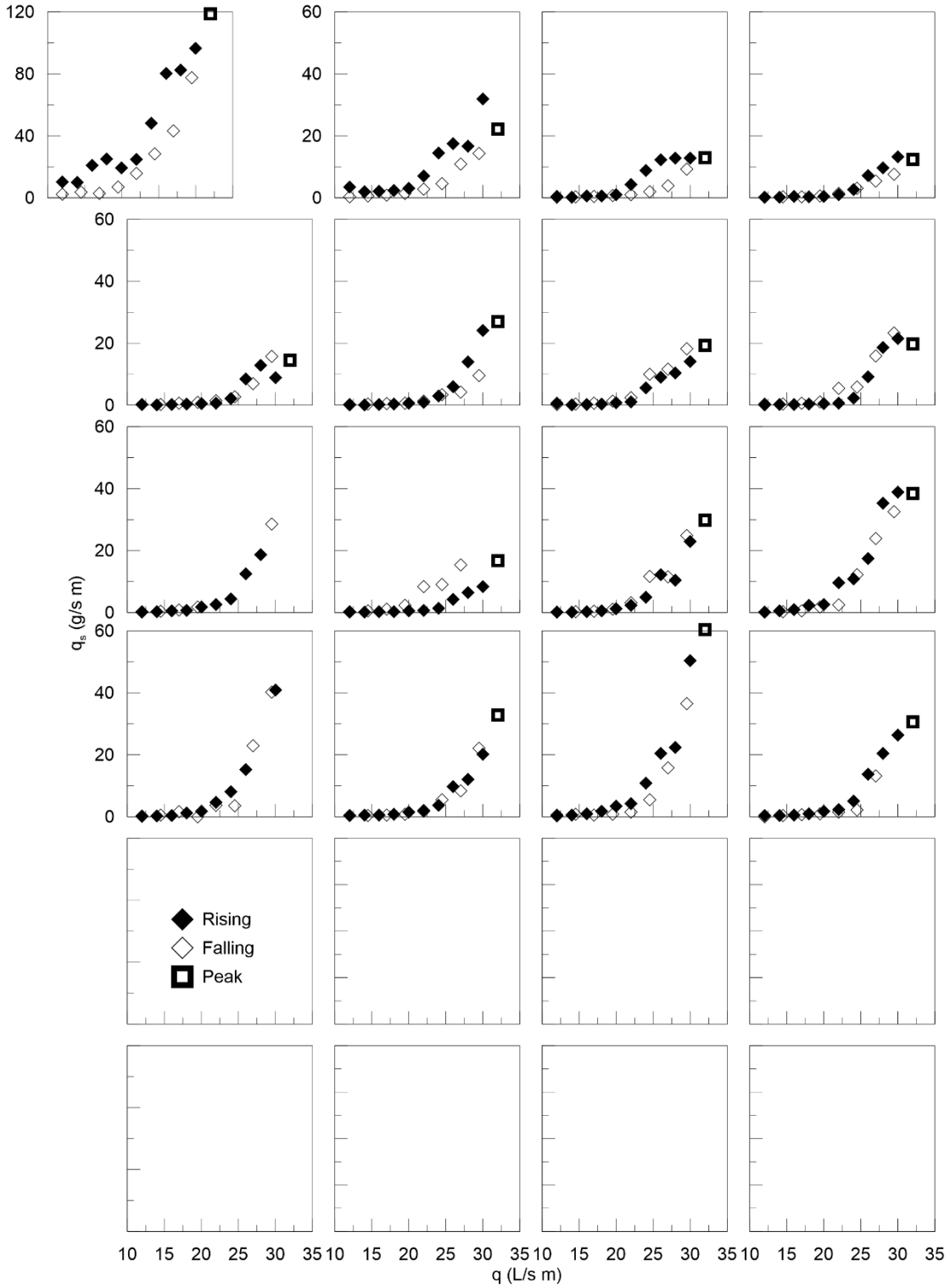

Figure C.2: LU2 phase plots (hydrographs 1 – 16)

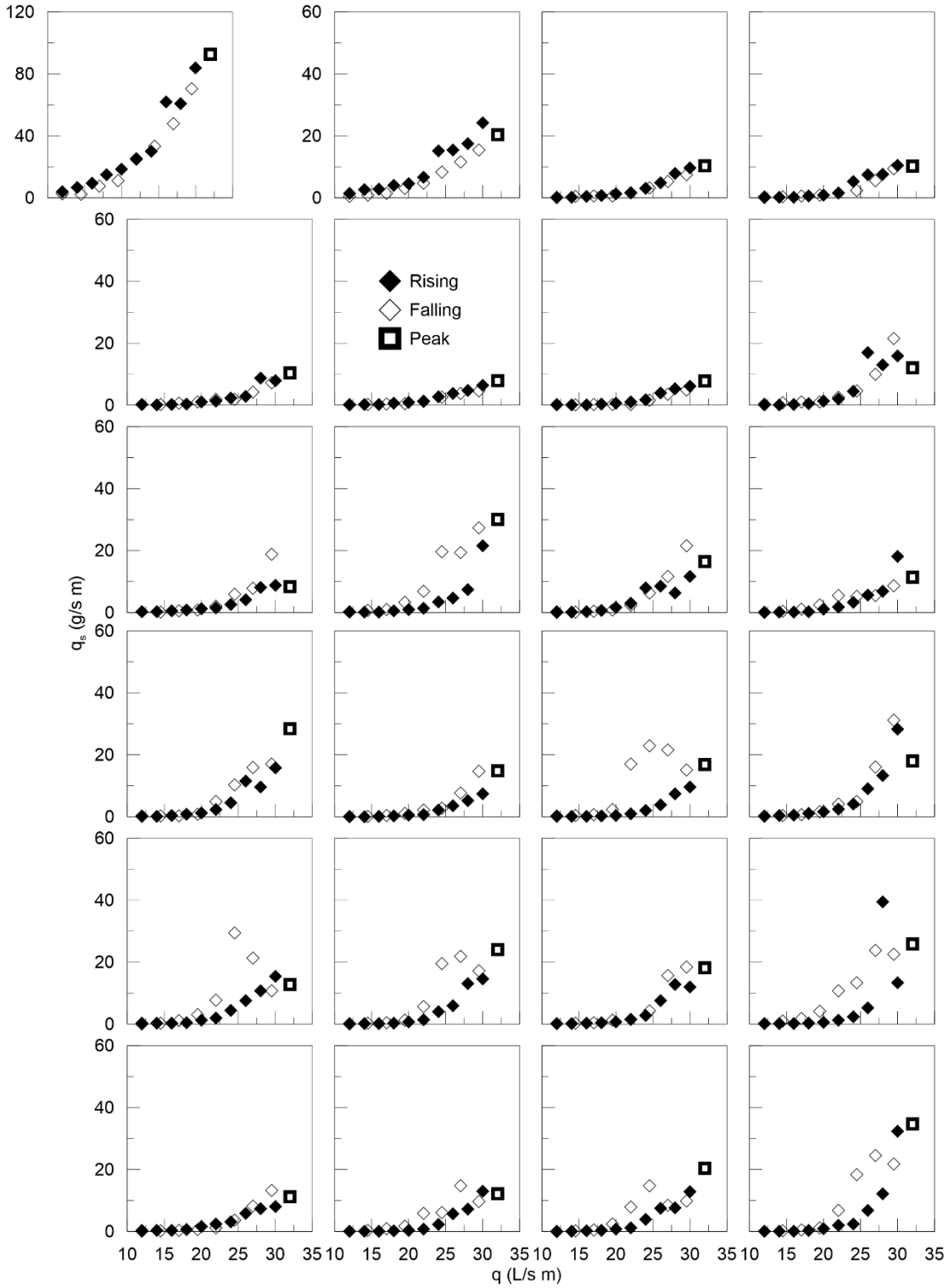

Figure C.3: LU3 phase plots (hydrographs 1 – 24)

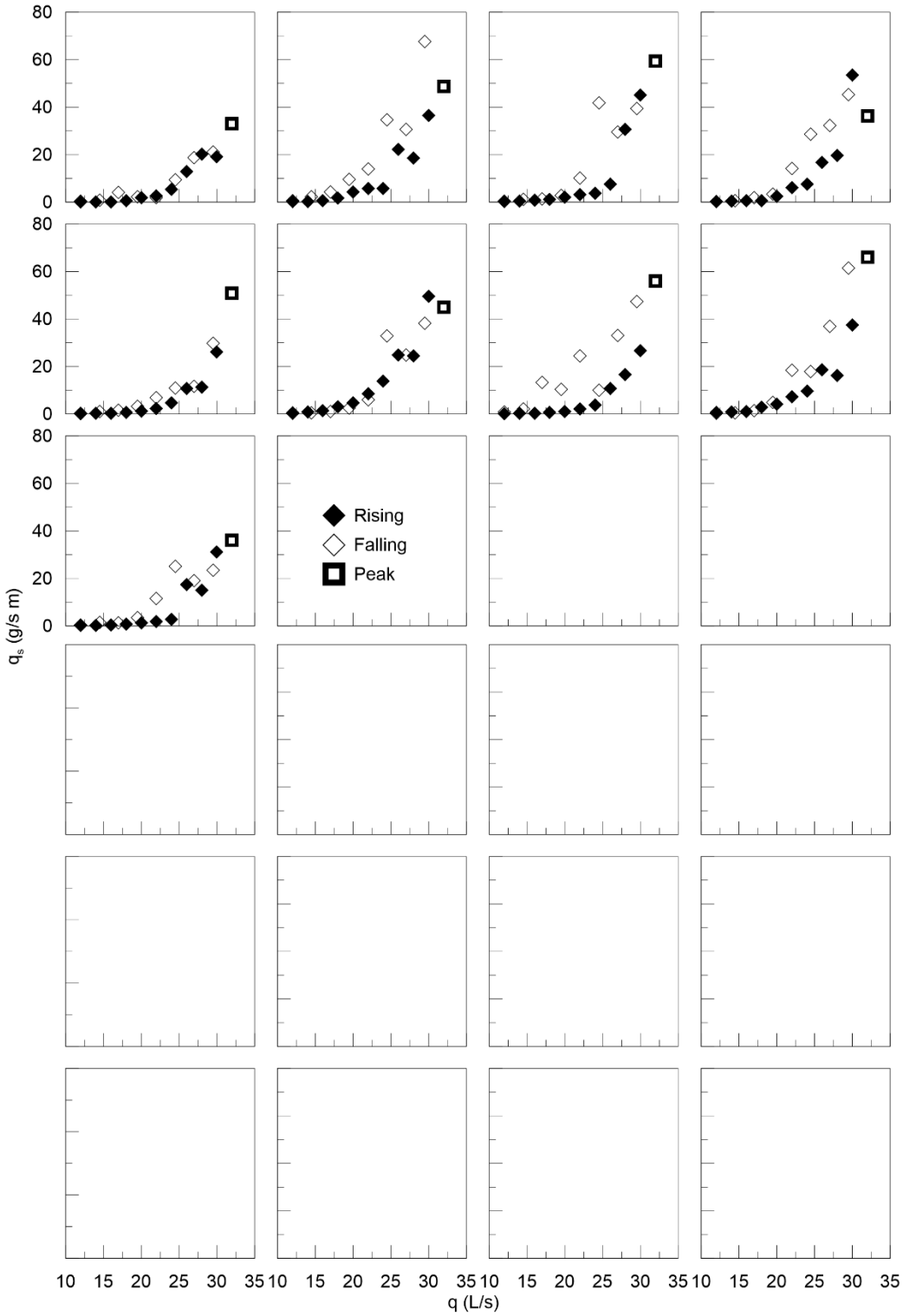

Figure C.4: LU3 phase plots (hydrographs 25 – 33)

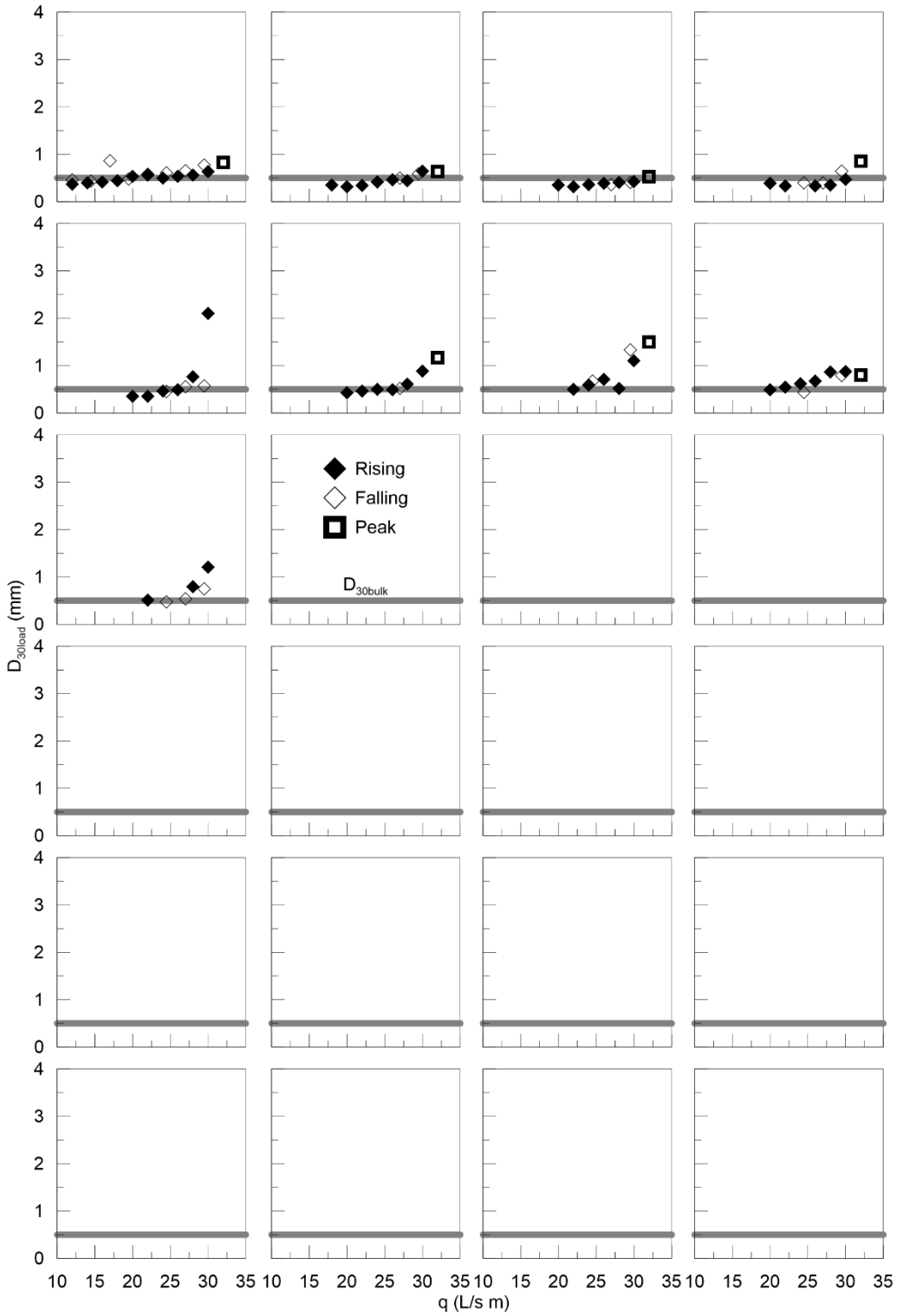

Figure C.5: LU1 *D_{30load}* phase plots (hydrographs 1 – 9)

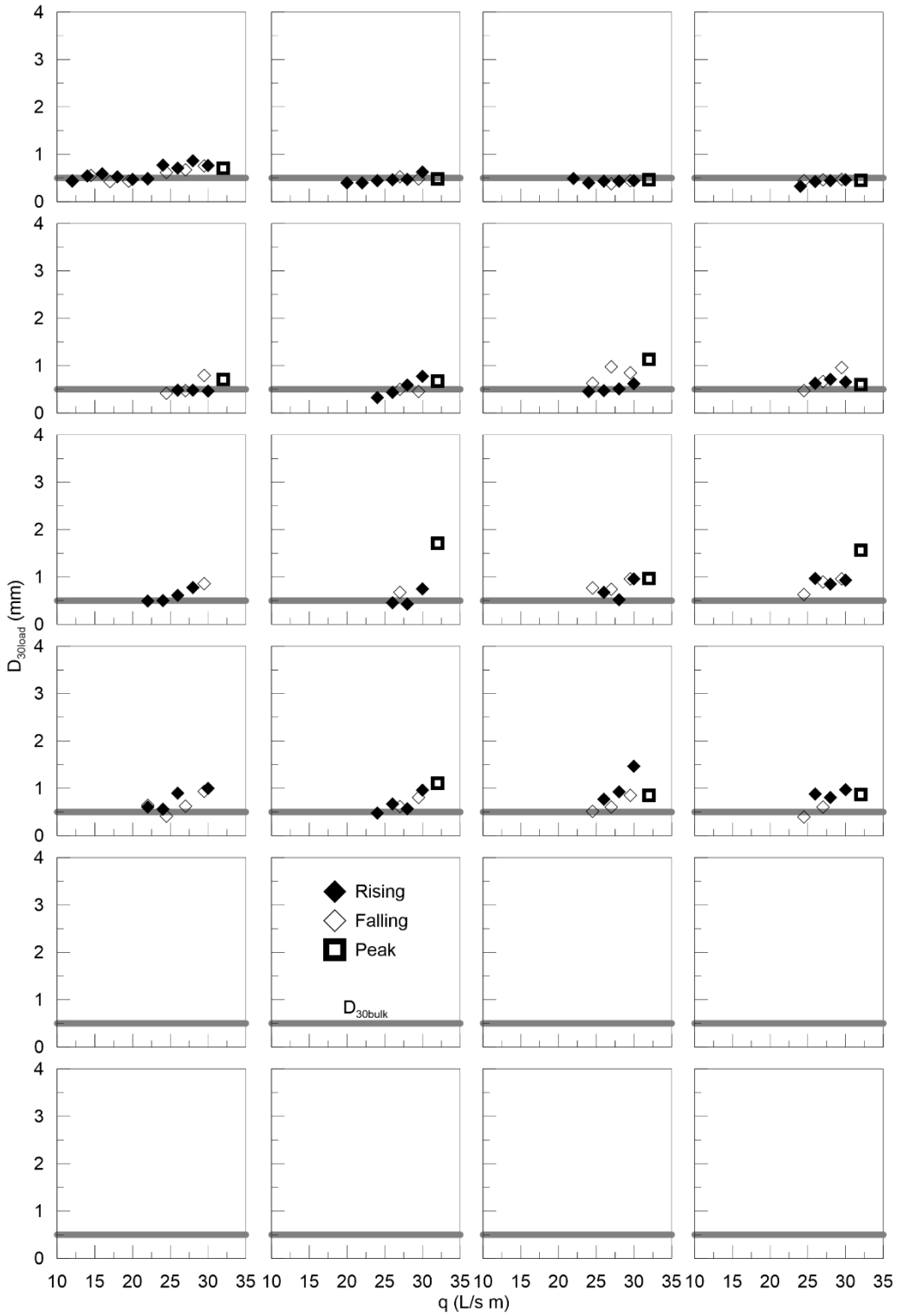

Figure C.6: LU2 *D_{30load}* phase plots (hydrographs 1 – 16)

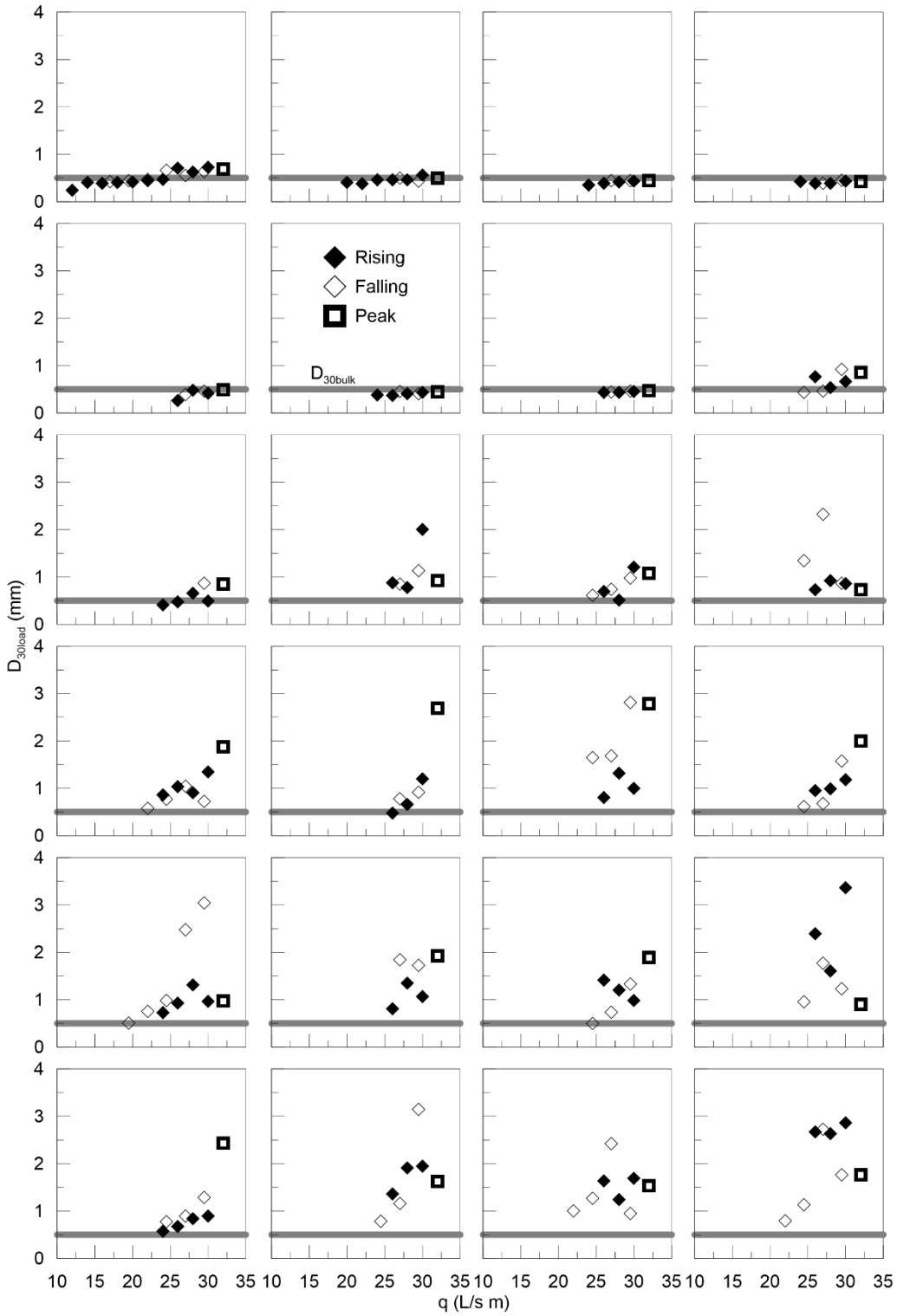

Figure C.7: LU3 *D_{30load}* phase plots (hydrographs 1 – 24)

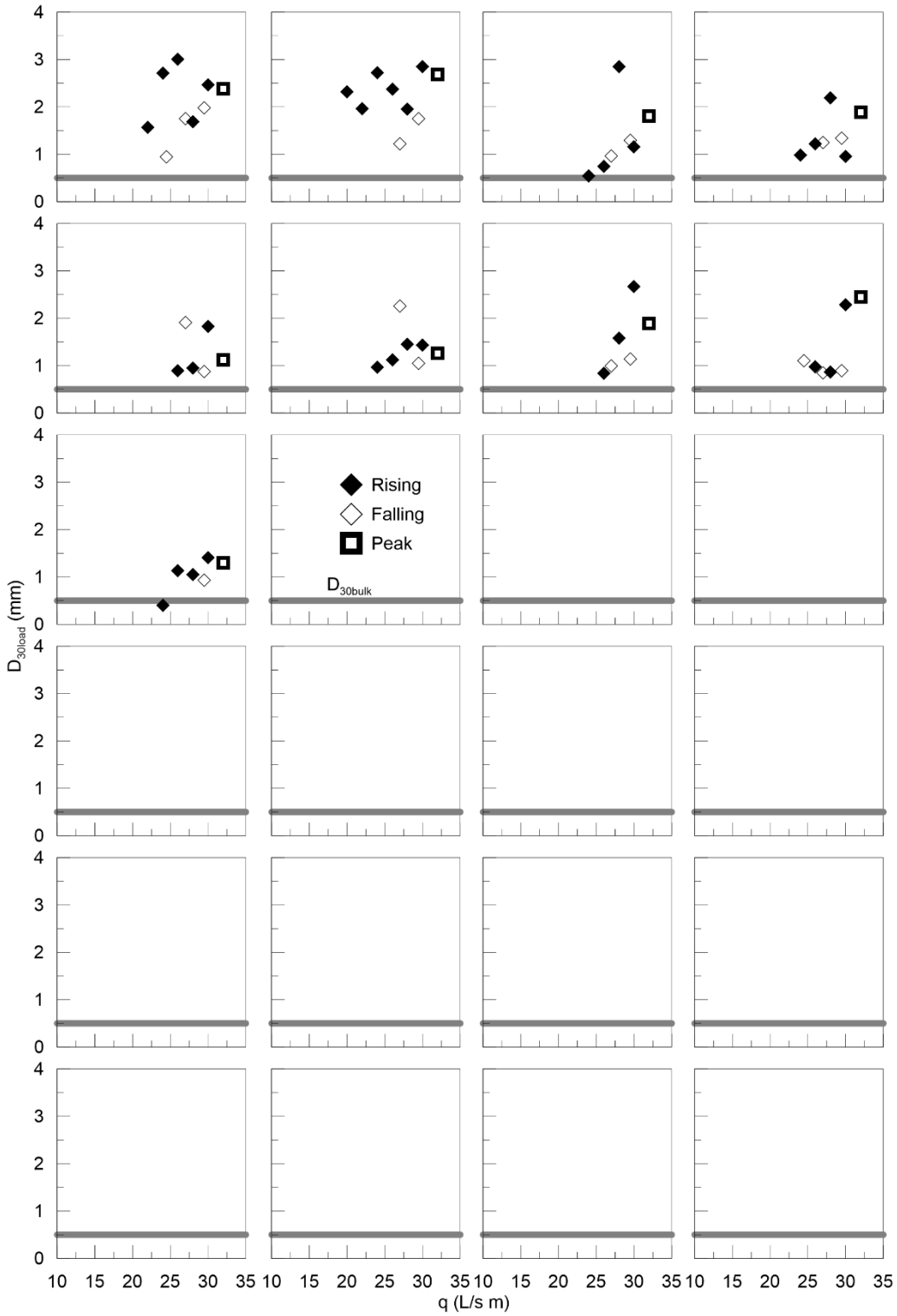

Figure C:8: LU3 D_{30load} phase plots (hydrographs 25 – 33)

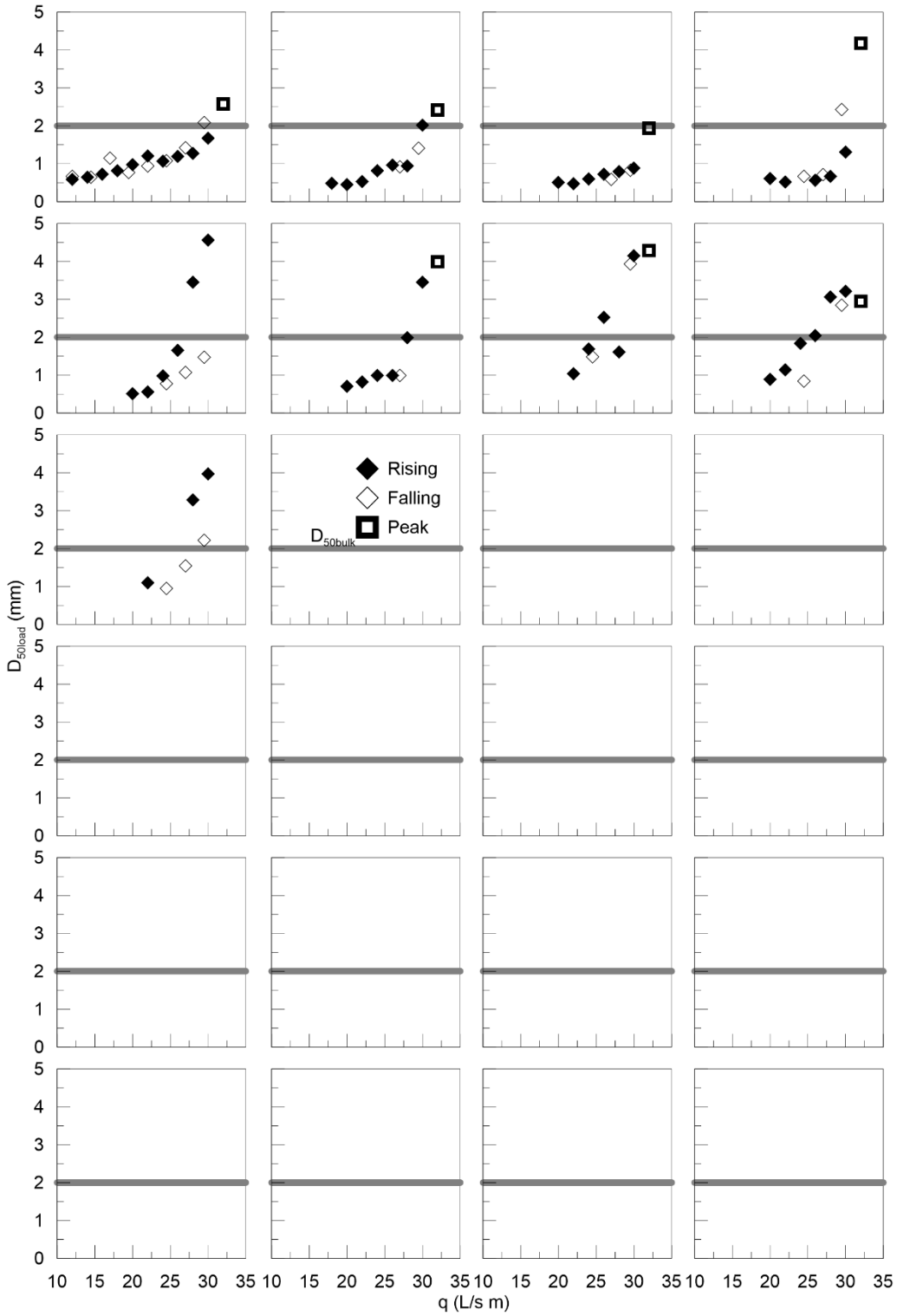

Figure C.9: LU1 *D_{50load}* phase plots (hydrographs 1 – 9)

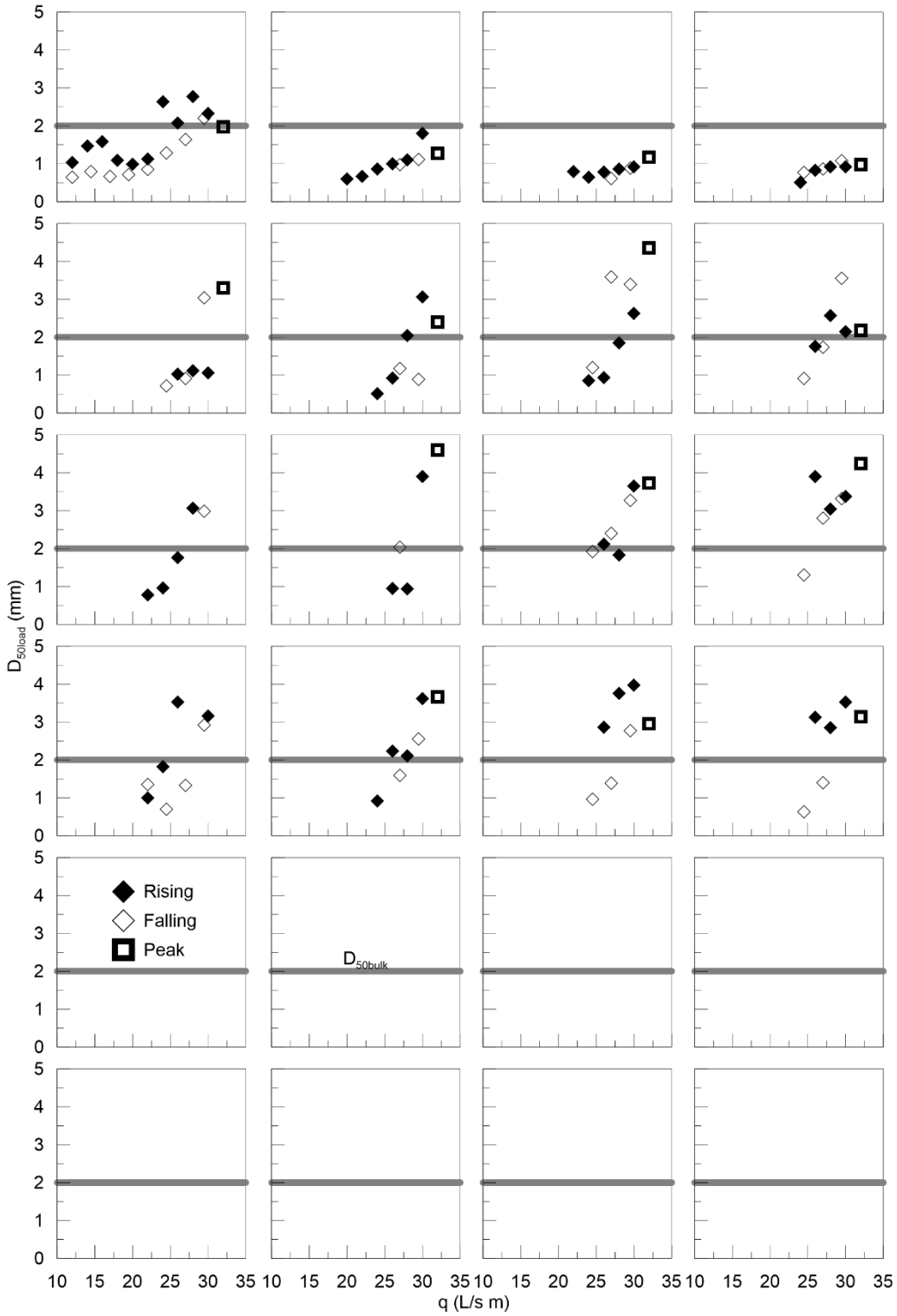

Figure C.10: LU2 D_{50load} phase plots (hydrographs 1 – 16)

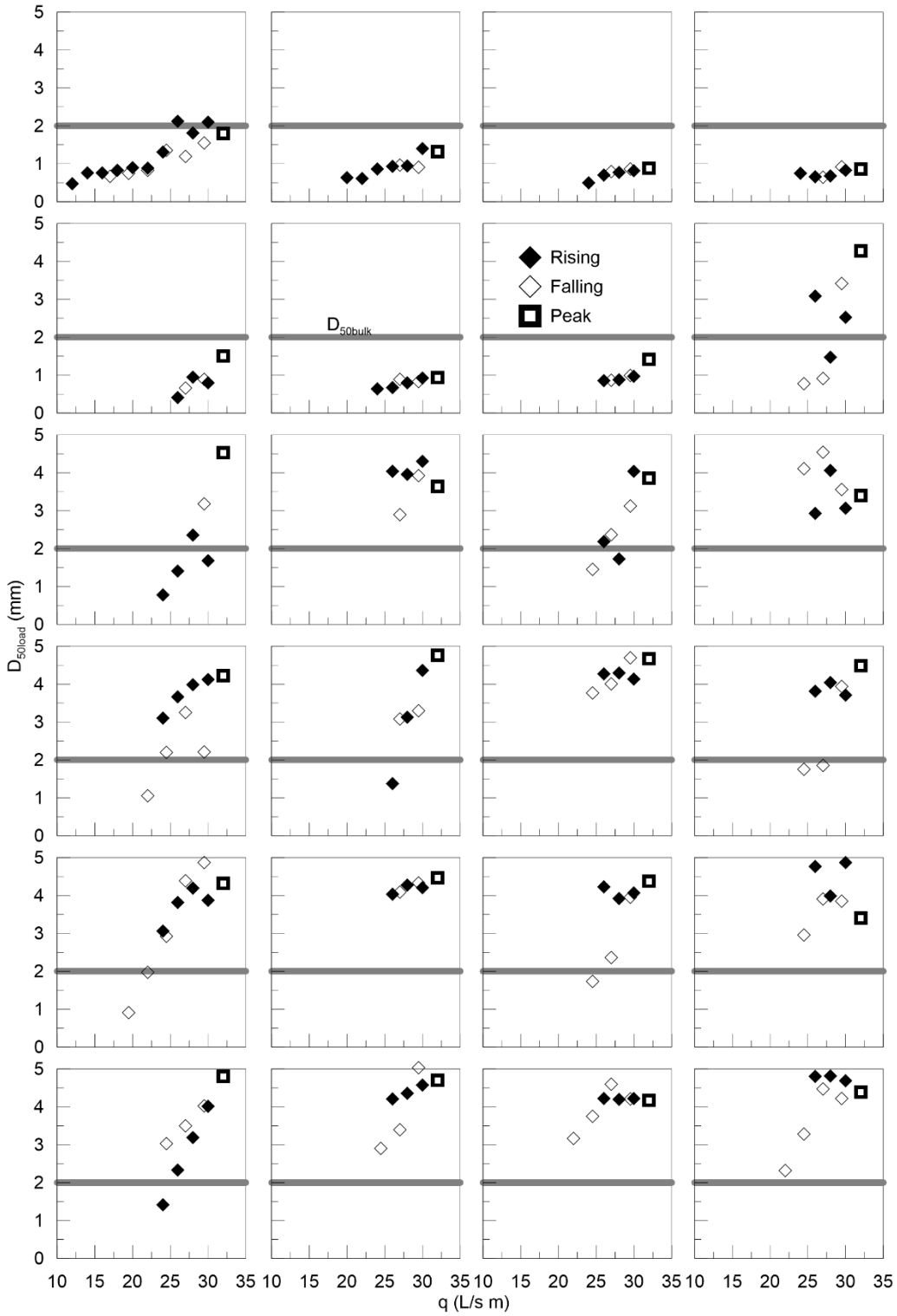

Figure C.11: LU3 D_{50load} phase plots (hydrographs 1 – 24)

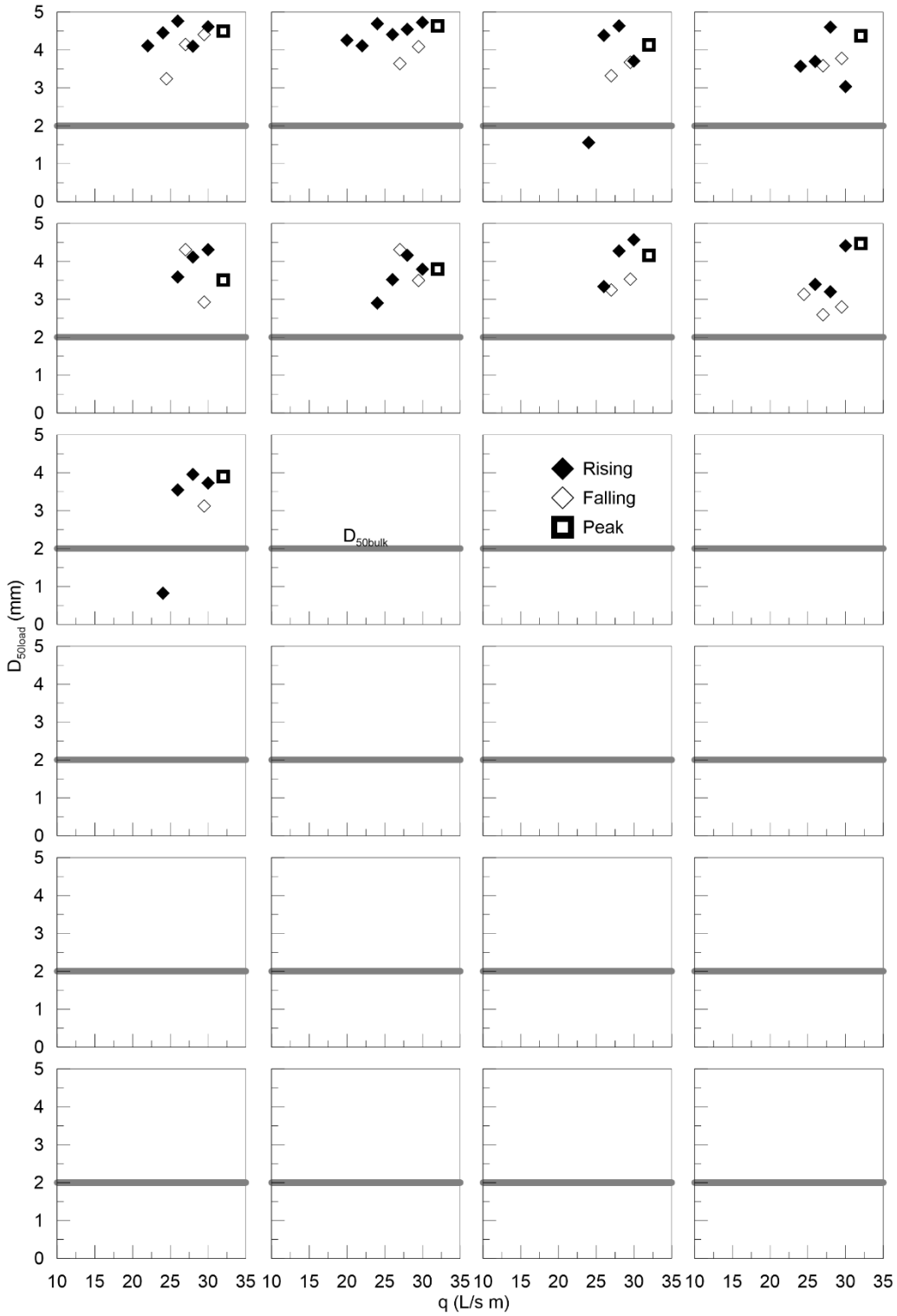

Figure C.12: LU3 D_{50load} phase plots (hydrographs 25 – 33)

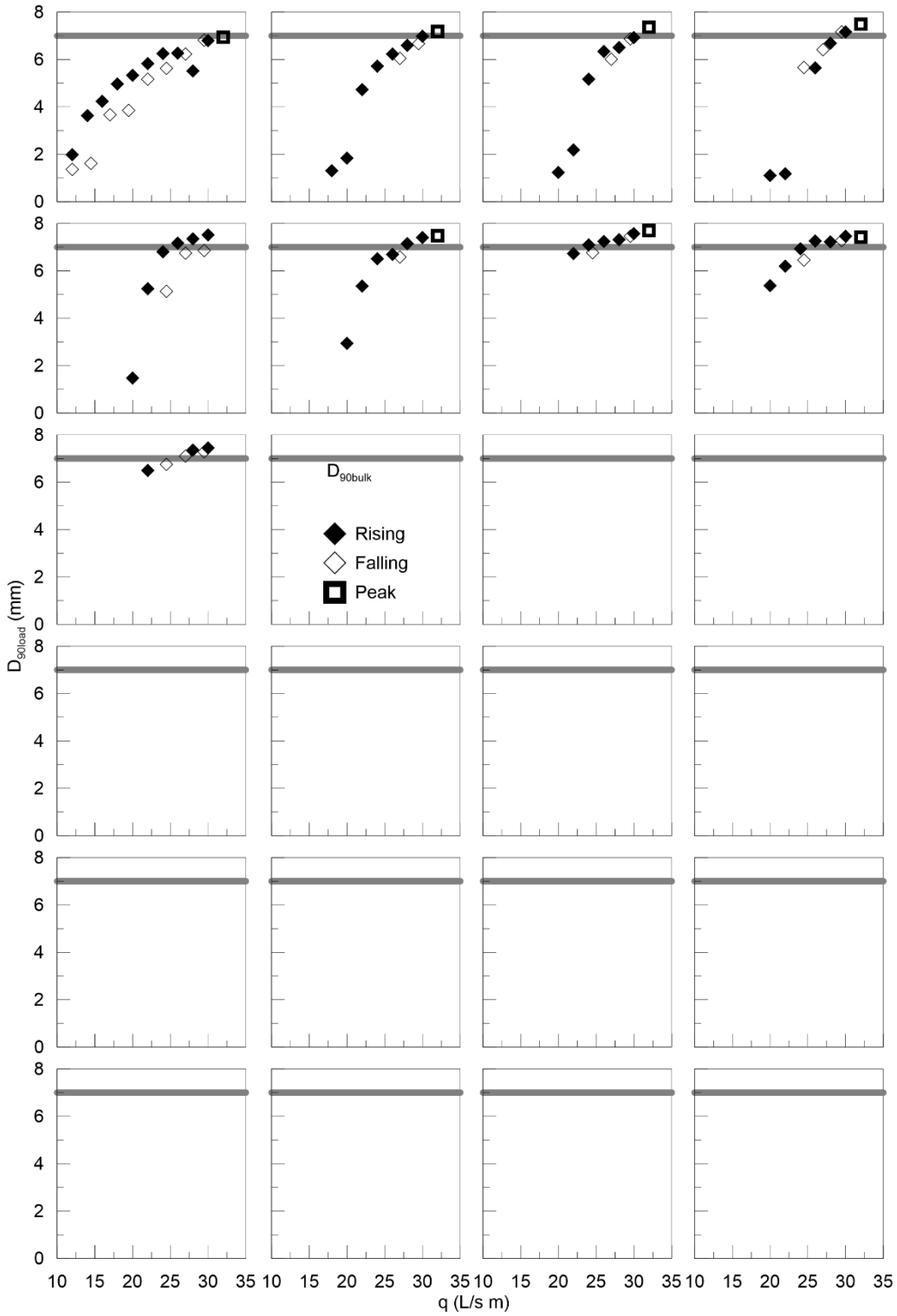

Figure C.13: LU1 D_{90load} phase plots (hydrographs 1 – 9)

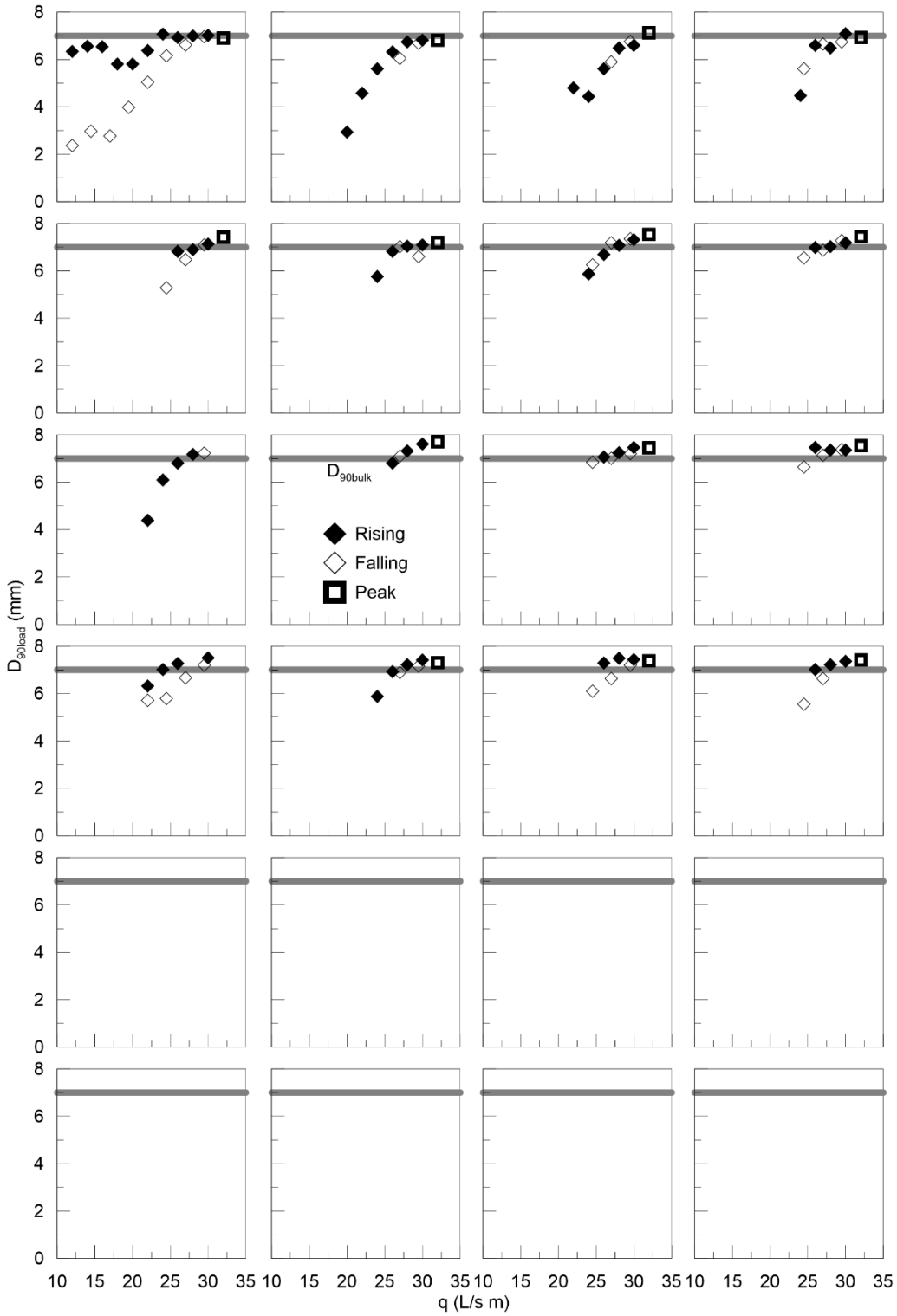

Figure C.14: LU2 D_{90load} phase plots (hydrographs 1 – 16)

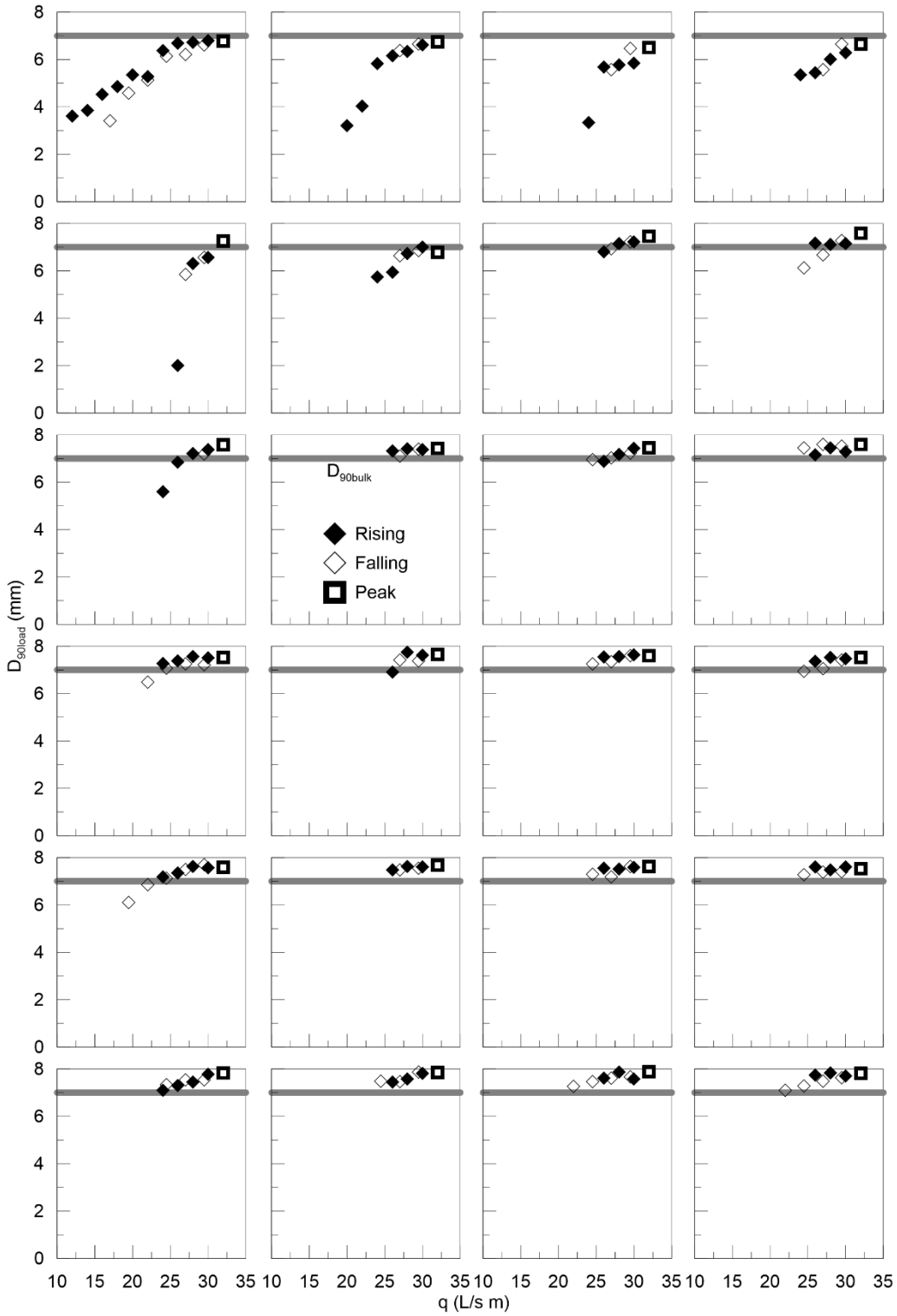

Figure C.15: LU3 D_{90load} phase plots (hydrographs 1 – 24)

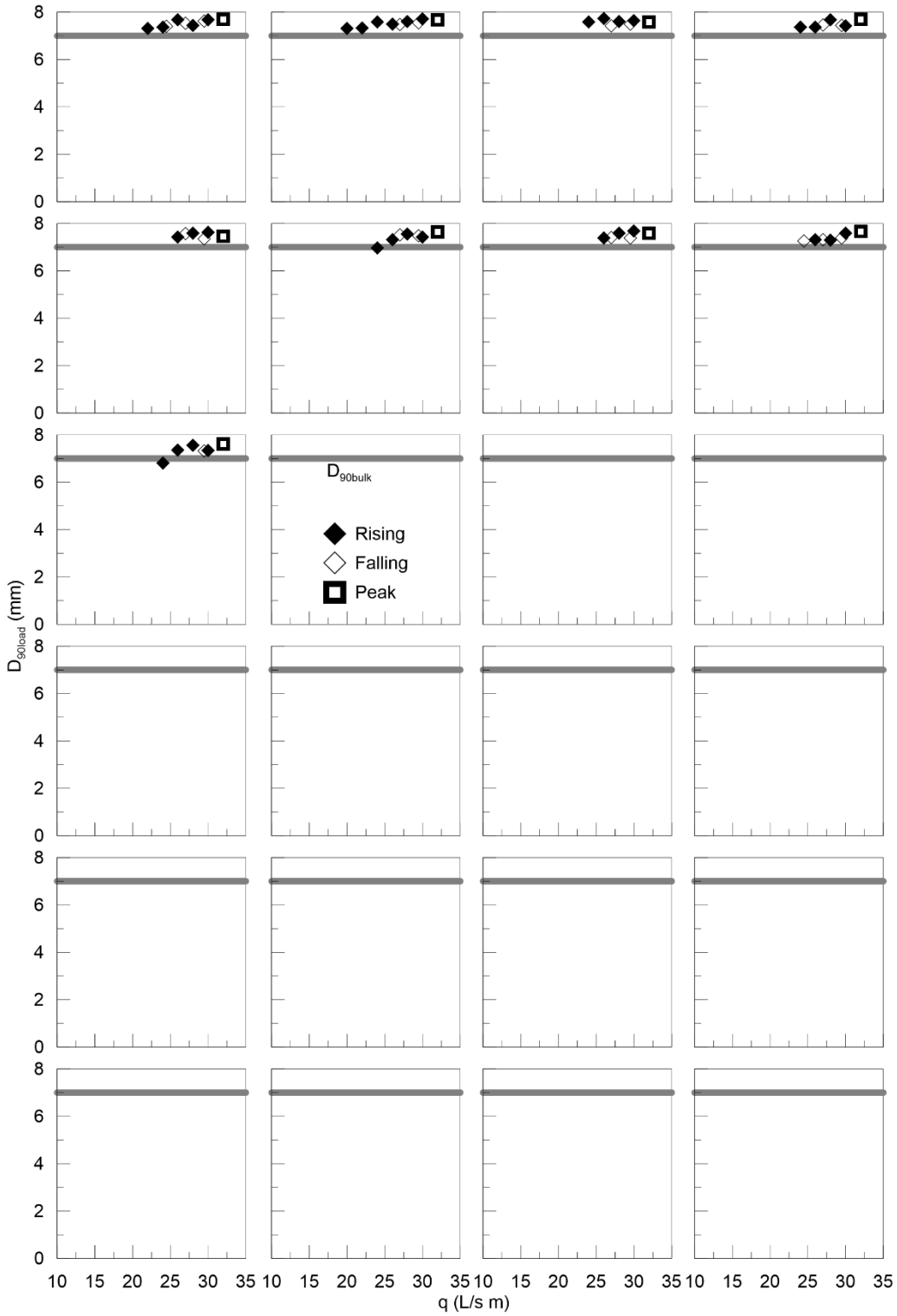

Figure C.16: LU3 D_{90load} phase plots (hydrographs 25 – 33)

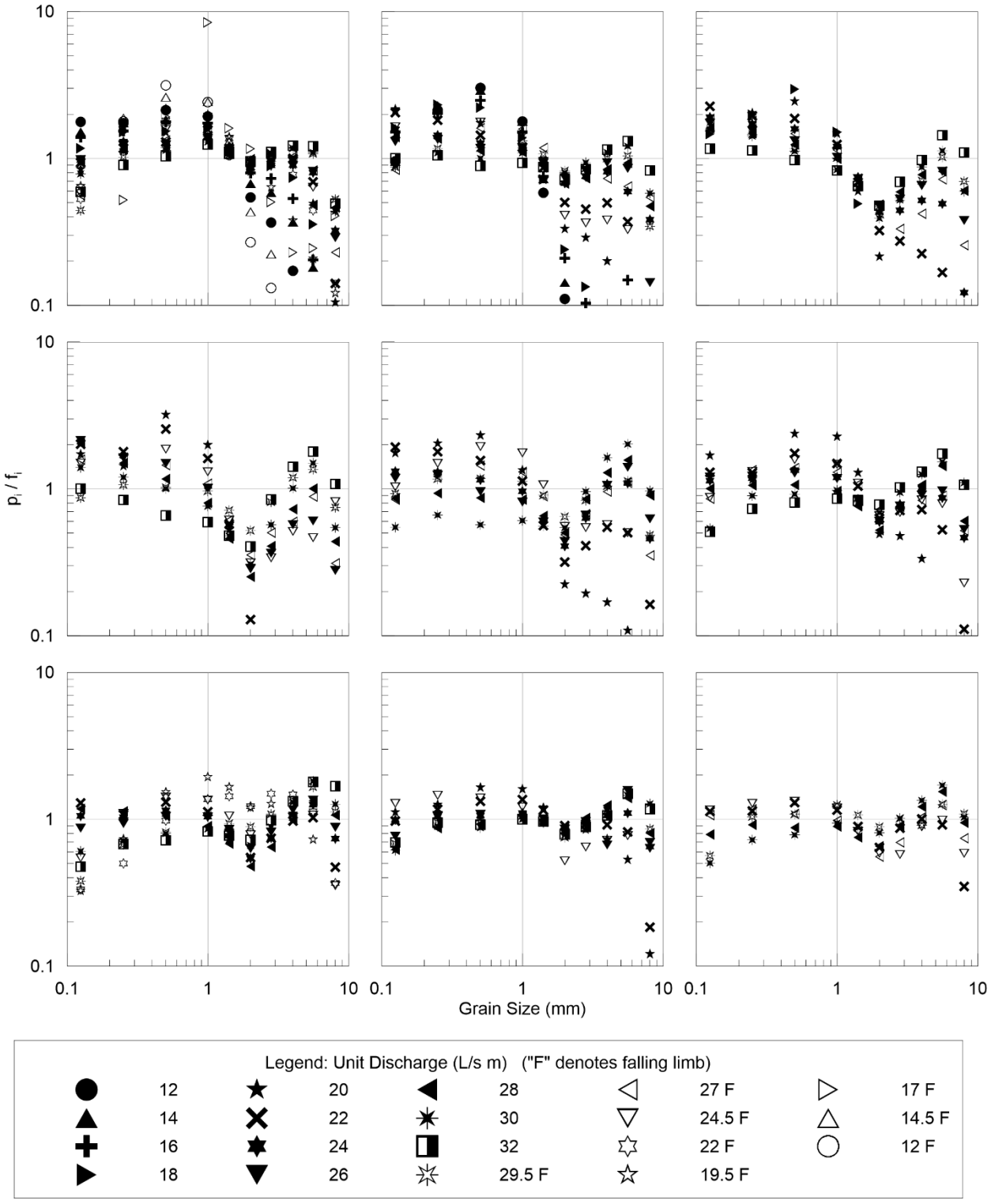

Figure C.17: LU1 Transport ratios (hydrographs 1– 9)

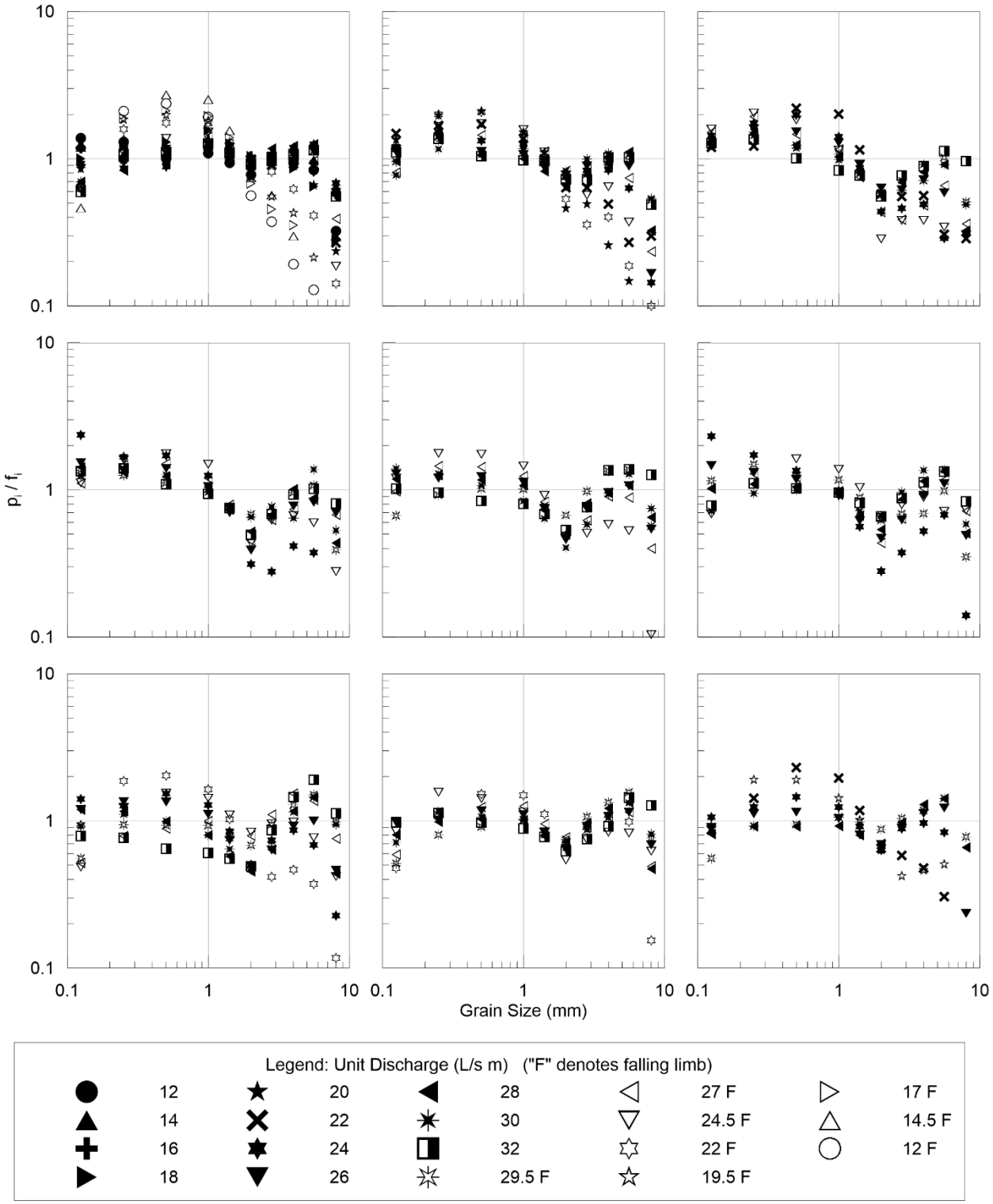

Figure C.18: LU2 Transport ratios (hydrographs 1– 9)

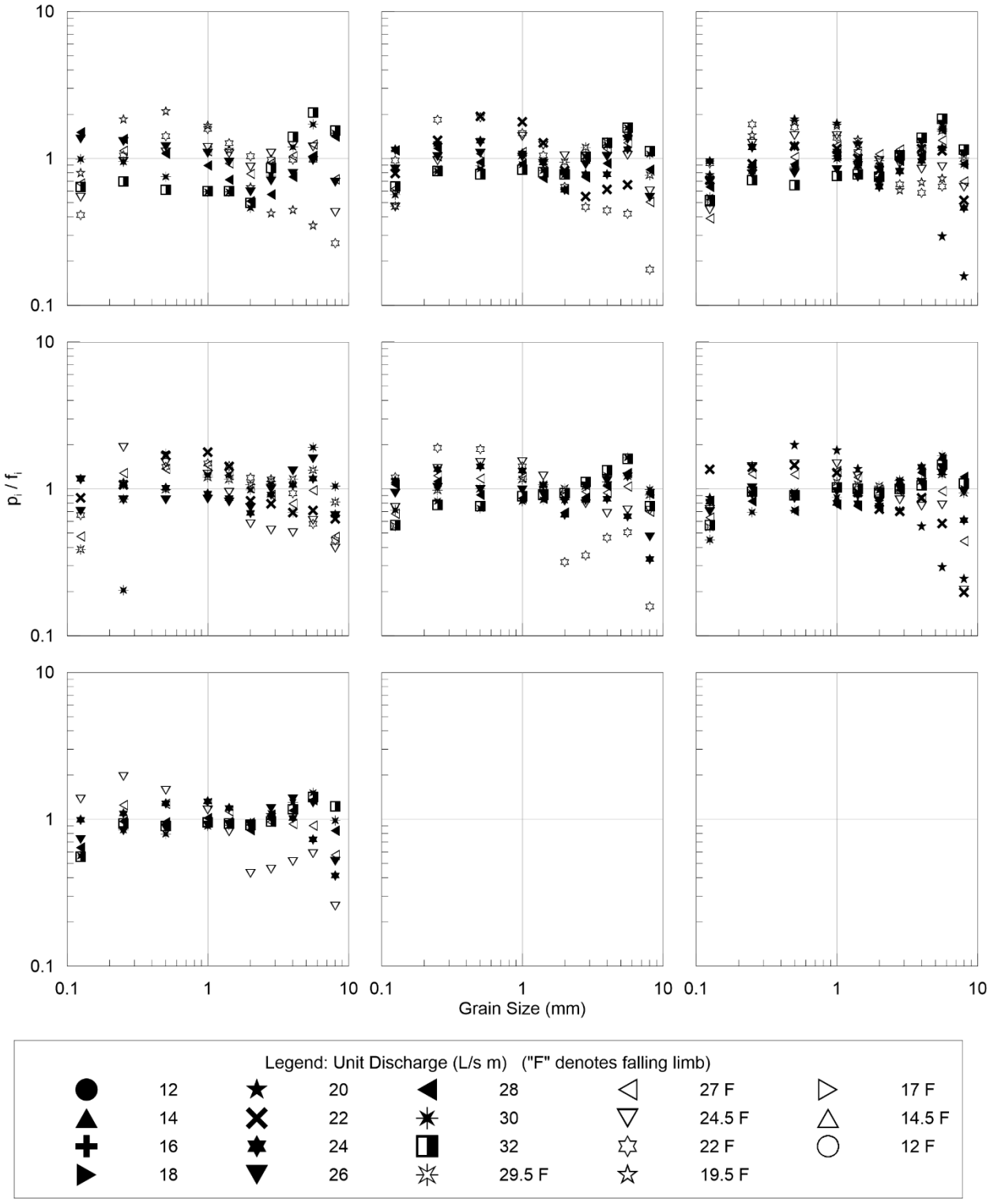

Figure C.19: LU2 Transport ratios (hydrographs 10– 16)

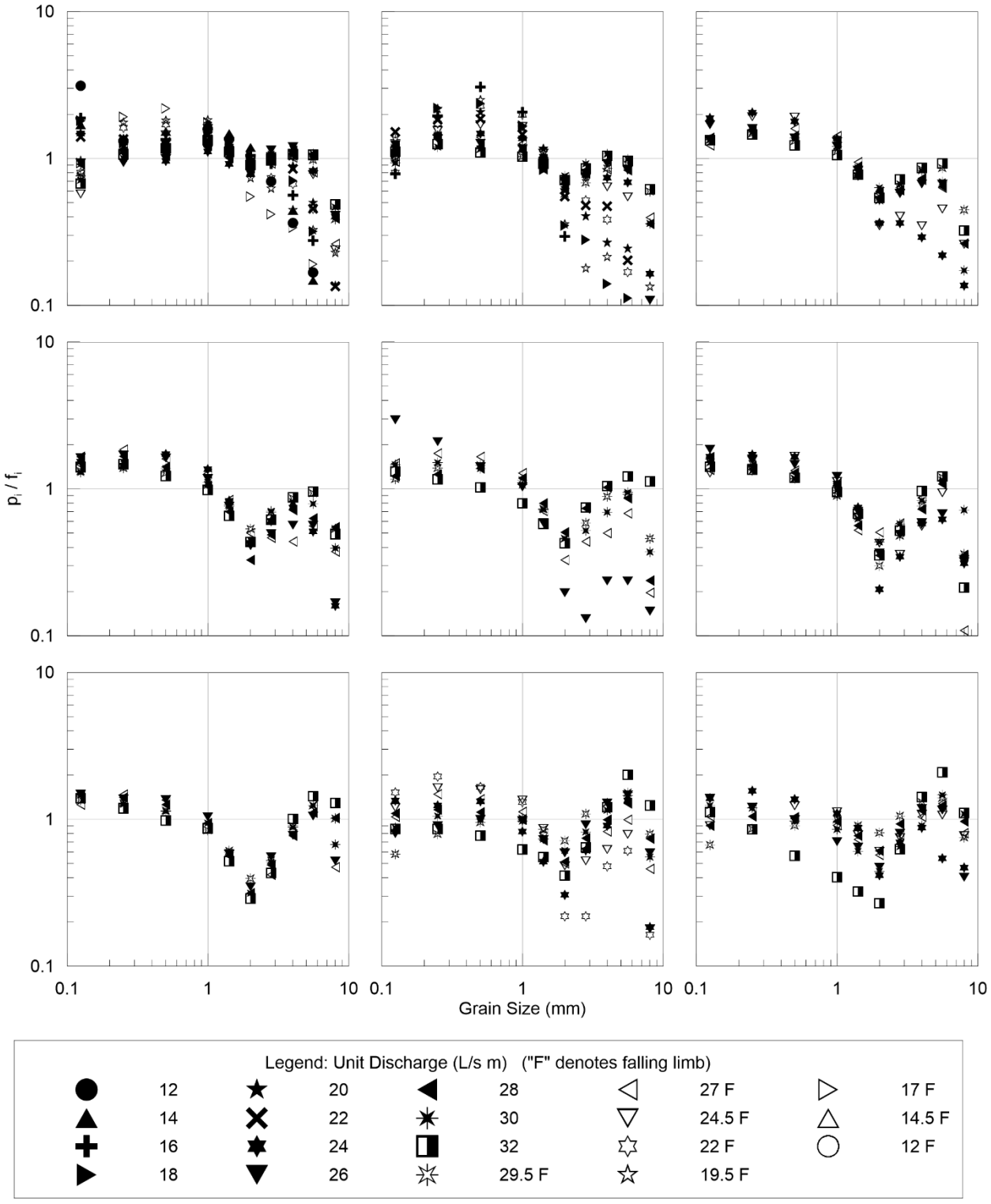

Figure C.20: LU3 Transport ratios (hydrographs 1 – 9)

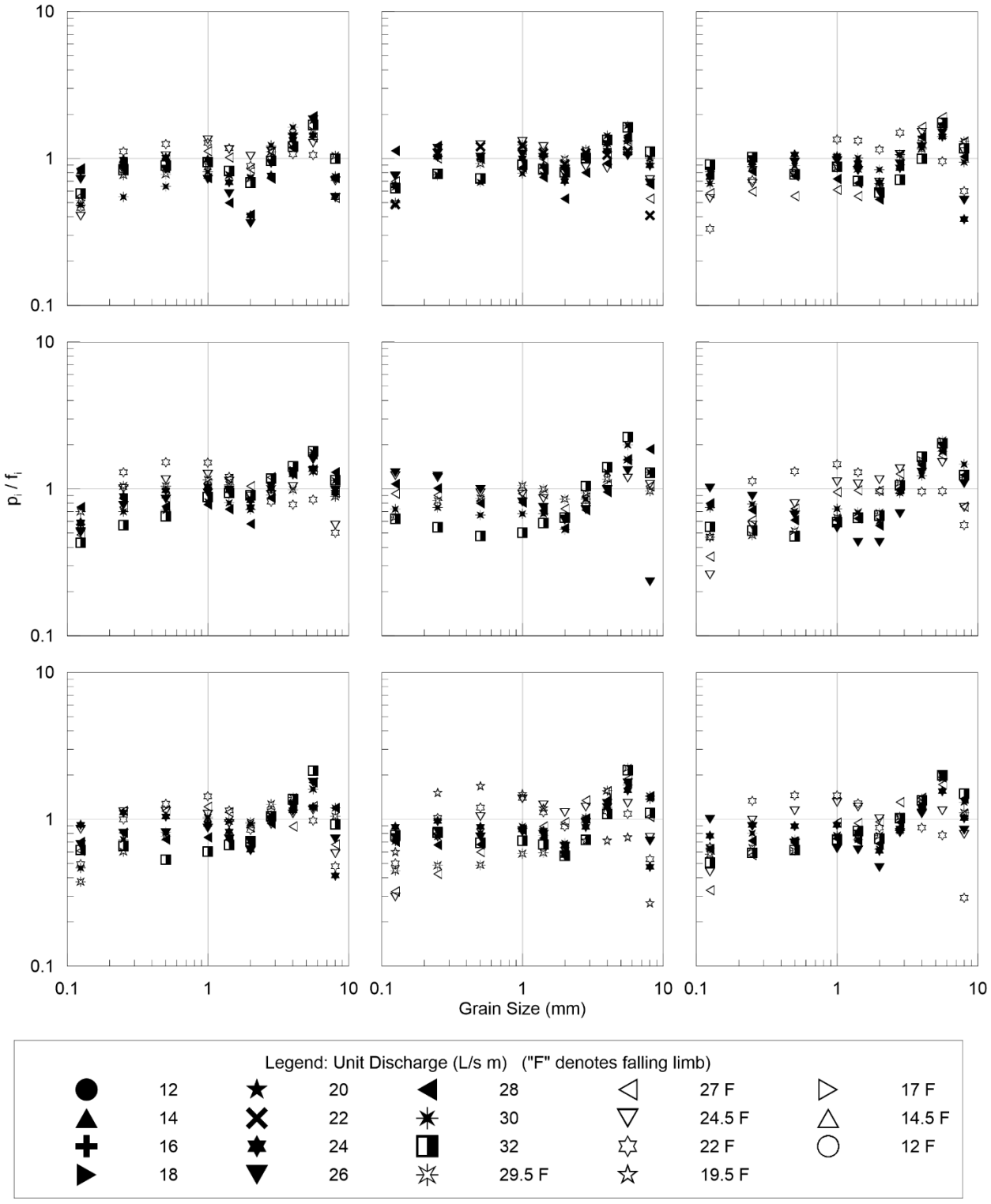

Figure C.21: LU3 Transport ratios (hydrographs 10 – 18)

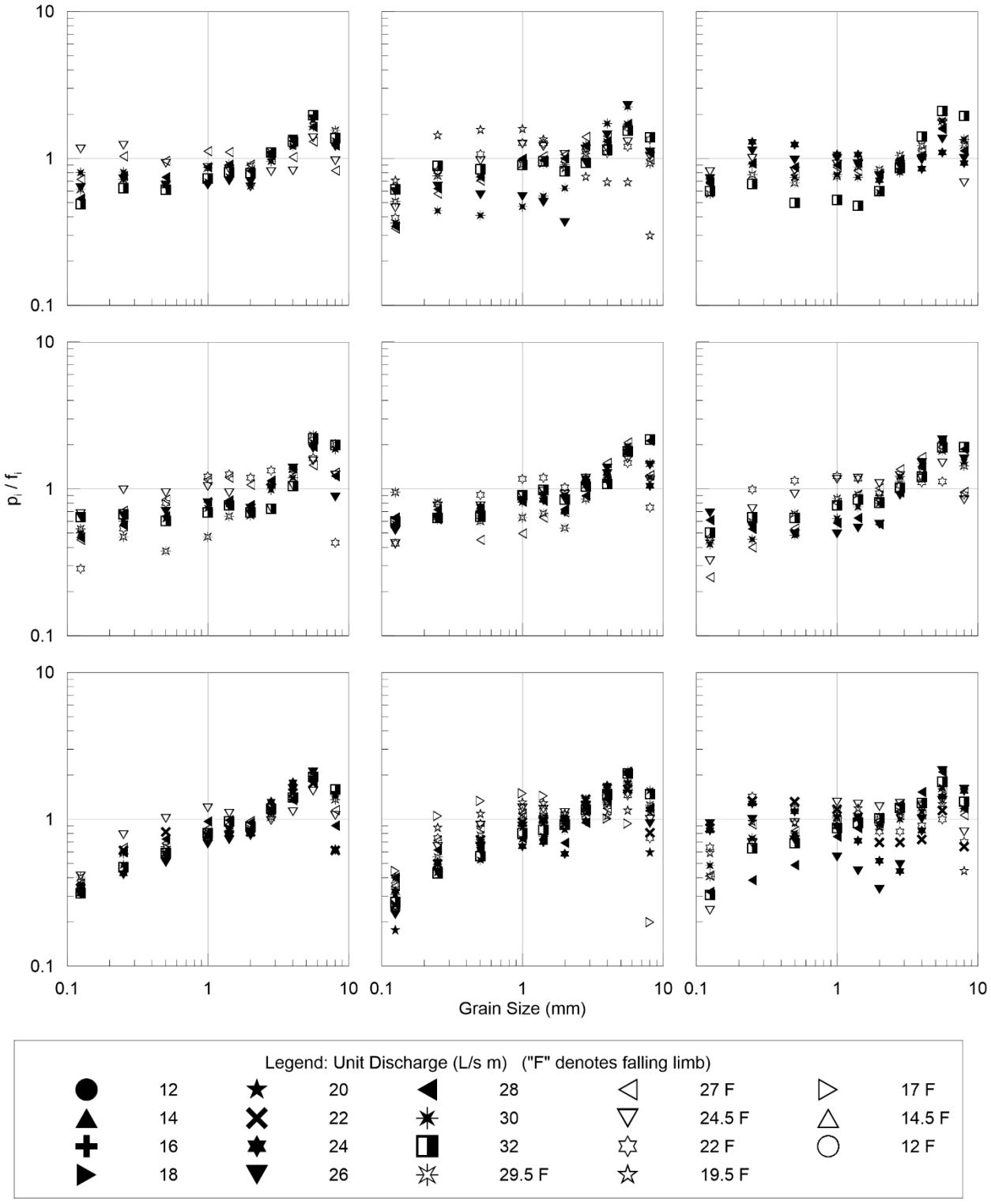

Figure C.22: LU3 Transport ratios (hydrographs 19 – 27)

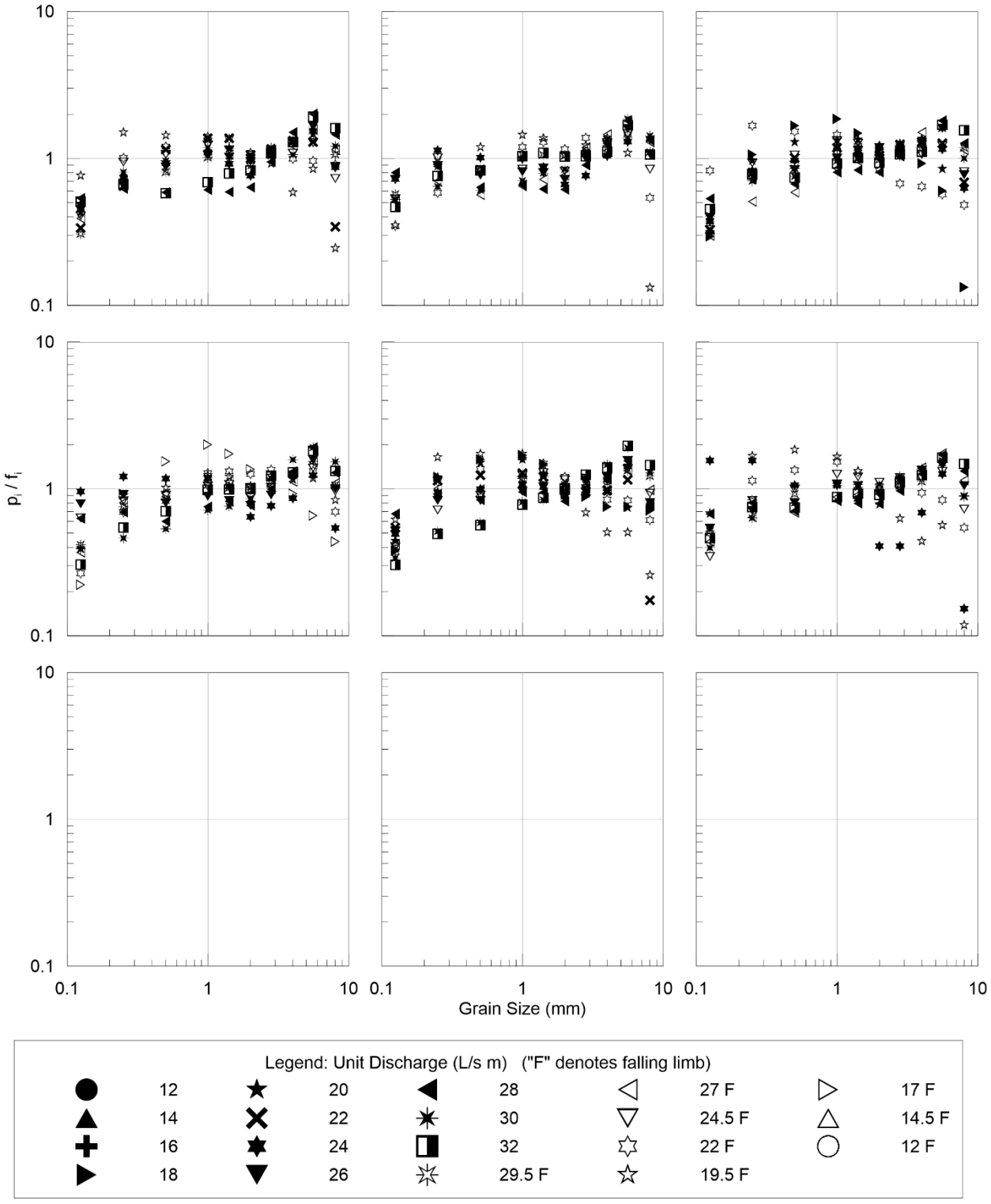

Figure C.23: LU3 Transport ratios (hydrographs 28 – 33)